The University of Nottingham
School of Mechanical, Materials and
Manufacturing Engineering

Finite Element Investigations on the Microstructure of Composite Materials

By Angelo R. Maligno, Laurea

Thesis submitted to The University of Nottingham
for the degree of Doctor of Philosophy
October 2007

Contents

Abstract

This thesis describes the investigation and development of damage modelling for composites materials at their micro-scale (e.g. fibre, matrix).

A damage model for elastic materials, based on a "local" damage approach, has been introduced to predict failure onset and simulate the post-failure behaviour of unidirectional three-dimensional representative volume elements (RVE) or unit cells with hexagonal distribution of the fibres over the cross section. The damage model consists of three parts: an elastic model, a failure criterion and the post-failure behaviour. Modifications of von Mises criteria and Maximum Principal Stress criterion have been considered to evaluate failure in the matrix whilst for the fibre in general the Maximum Principal Stress criterion has been used. The damage model has been implemented into the commercial code ABAQUS with subroutines in FORTRAN (UMAT and USDFLD).

The material properties in the residual stress analyses are considered temperature dependant to simulate the volumetric contraction during the manufacturing process. Hence, the overall residual stress introduced from curing was determined by considering two contributions: volume shrinkage of matrix resin from the crosslink polymerization during isothermal curing and thermal contraction of both resin and fibre as a result of cooling from the curing temperature to room temperature.

Finally, three different typologies of 3D unit cells have been investigated. The first kind of micro-model is based on a symmetric distribution of the fibres and the unit cells have two phases, i.e.: matrix and fibre. The second typology of unit cells is still based on a uniform architecture but

include a three-dimensional interphase between fibre and matrix. As in real composites at their constituent level fibres are randomly distributed. The mutual distance between fibres represents a critical factor for the ultimate mechanical properties of the micro-composites. Hence the last kind of micro-models account for this non-uniform position of fibres within the RVE although they consists of only two phases.

FEM analyses have indicated that predicted damage initiation and evolution are clearly influenced by the presence of residual stresses in all the three different typologies of unit cells analysed. The numerical analyses on the numerical models have proved that, in general, the overall mechanical properties are strongly influenced by the presence of residual stress, fibre volume fraction, fibre distribution and interphasial properties. In particular on transverse tensile loading, residual stresses produces beneficial results in terms of ultimate strength while in the case of longitudinal loading (parallel to the fibres) the matrix, due to the high compressive stress, undergoes a premature failure although.

Acknowledgements

I would like to first thank supervisors, Dr. N.A. Warrior and Prof A. Long whose guidance and patient instruction is deeply appreciated.

Next I'd like to extend my gratitude to the other members of the Polymer Composites Research Group who have offered their time and help over the years and in particular Dr L. Zhao for his precious guidance and advice.

The financial support of EPSRC, the use of departmental facilities of the School of Mechanical, Materials and Manufacturing Engineering of the University of Nottingham are gratefully recognized.

I would also like to thank all my friends and family who have supported and encouraged me throughout this work. Finally, I am thankful to my wife Silvia for her immense patience, her belief in me and her love.

Notation

σ_1	Principal stress
σ_2	Principal stress
σ_3	Principal stress
ε_x	Elastic strain
ε_y	Elastic strain
ε_z	Elastic strain
τ_{xy}	Shear strain in-plane
τ_{xz}	Shear strain through thickness
τ_{yz}	Shear strain through thickness
ν_{xy}	Poisson's ratio in-plane
ν_{xz}	Poisson's ratio through thickness
ν_{yz}	Poisson's ratio through thickness
E_x	Longitudinal Young's modulus (fibre direction)
E_y	Transverse Young's modulus
E_z	Transverse Young's modulus
G_{xy}	Shear modulus in-plane
G_{xz}	Shear modulus through thickness
G_{yz}	Shear modulus through thickness
σ_Y	Yield strength
τ_{max}	Maximum shear stress

d_E Damage factor for Young's moduli

d_G Damage factor for shear moduli

[C] Stiffness matrix

$[S]^{-1}$ Compliance matrix

V^f Fibre volume fraction

α Thermal expansion

Subscripts

x Longitudinal direction (fibre direction)

y Transverse direction

z Transverse direction

C Compressive loading

T Tensile loading

f fibre

m matrix

Chapter 1

Introduction

1.1 Fibre reinforced composite materials

Since the early 1960s, there has been an ever-increasing demand for newer, stronger, stiffer, and yet lighter-weight materials in fields such as aerospace, transportation, and construction. High demands on materials for better overall performance have led to extensive research and development efforts in the field of composite materials. These materials have low specific gravity that makes their properties particularly superior in strength and modulus [1, 2] to many traditional engineering materials such as metals. As a result, these materials are now being utilized in industries that traditionally used metals, and these have become the forefront of research and development activity in many related areas. Composite materials that exist today can be categorized into five major classes, which include ceramic matrix composites (CMCs), metal matrix composites (MMCs), intermetallic matrix composites (IMCs), carbon-carbon composites (CCCs) and polymer matrix composites (PMCs). In this discussion, considerable attention is paid to the latter class of materials (PMCs). There are two important types of polymer matrix composites, short-fibre and continuous-fibre composites. The choice of polymer matrix for such composites can be either a thermoset or a thermoplastic. Continuous-fibre composites that offer the best mechanical properties compared to other fibre-reinforced composites are primarily reinforced with high performance fibres such as carbon, Kevlar or glass. These composites are often utilized in special applications like aircraft components in which the property benefits of the fibres are fully exploited.

The properties of a composite material are strongly influenced by the properties of its constituents and their distribution and also the quality of interactions among them [2, 3]. The most important of all the composite properties are usually the mechanical properties, since

whatever the reason for the choice of a particular composite for some application it must have certain characteristics of shape, rigidity and strength. The mechanical properties of long fibre composites, such as stiffness, can be predicted using several prediction schemes such as the "Rule of Mixtures" and the Halpin-Tsai equations [1, 2].

Continuous fibres offer the highest mechanical properties, and give the possibility of using specific orientations to give the composite directional properties. They are available as lengths of fabric in many different woven, knitted or stitched forms, all of which have different properties, processing characteristics and costs. These include:

- ***Unidirectional*** - almost all the fibres are straight and aligned in one direction. Fabrics may be lightly woven or stitched, or incorporate a binder to maintain their shape.
- ***Biaxial*** - various weave styles have equal quantities of fibres at right-angles. Weaving inevitably involves some crimping of the fibres, resulting in loss of properties that can be attributed, for instance, to the high shear stress and strain due to the local bending effect of the fibres. Shear strain and shear stress have a negative effect especially on the compressive strength. Straightness may be preserved by stitching bundles of fibres.
- ***Multiaxial*** - some specialist weaving techniques can produce triaxial fabrics. Quadriaxial fabrics (with reinforcement at 0°, 90° and 45°) can be produced by stitching.
- ***Random*** - continuous fibres can be combined with a binder and deposited in a random 'swirl' arrangement, primarily for use in resin transfer moulding.

Advantages and disadvantages of composite materials can be briefly summarized

Advantages of Composites:

- Weight saving
- Corrosion resistance
- Long fatigue life

- Manufacturing:
  - reduced parts count (complex geometries can be moulded)
  - novel shapes possible
  - low cost tooling
  - low temperature processing
- Design freedoms:
  - continuous spectrum of properties
  - anisotropic properties possible

Disadvantages of Composites

- High cost of raw materials
- Lack of design standards
- Properties not well characterised
- Low through-thickness tensile and shear strengths
- Sensitivity to stress concentrations
- Dependence of properties on manufacture
- Few mass production processes

1.2 Research aims

Only in the most recent years has the finite element technique together with the high speed and capacity of modern computers made it possible to analyze fibre-reinforced composite in detail. The goal of the present work is to develop numerical micro-models, using the commercial finite element package ABAQUS/Standard, to predict the tensile strength and evaluate the failure, damage onset and its evolution in unidirectional composite materials from the properties of the fibre and matrix.

The micromechanical model considers a unit cell in which fibre and matrix are arranged in a hexagonal cross section array by assuming the repetitive or periodic nature of the fibre and

matrix materials. The unit cell is also a three-dimensional (3D) solid and the size of each unit cell dependents on the fibre volume fraction [3].

The effects of fibre content have been investigated by means of numerical analyses based on the determination of elastic constants of a unidirectional composite using a simple 3D representative volume element (RVE) model with a hexagonal packing array to check the reliability of FE models by comparing numerical results with empirical theories (e.g. Rule of Mixtures, Halpin-Tsai). Further investigations have been performed to study the failure onset and damage evolution on different configurations of unit cells.

In particular unidirectional composites properties, e.g. strength and stiffness, are dependent upon the volume fraction of the fibre and individual properties of the constituent fibre and matrix materials [3]. Particularly the estimation of the damage and failure progression in fibre reinforced composite structures is very complex compared to that of conventional metallic materials. Composite structures may vary their stiffness and strength due to damage accumulation such as matrix cracking and fibre breakage during the loading history of the composite members. In the micromechanical approach, the constituent fibre and matrix materials, and their interaction are distinctively considered to predict the overall behaviour of the composite structural member.

In particular, the present work has been developed in order to simulate progressive failure of UD composites by carrying out numerical analyses on unit cells under different uniaxial load conditions.

Therefore, in order to predict accurately failure and simulate damage, analyses on numerical models have been enhanced with subroutines UMAT and USDFLD in FORTRAN available in ABAQUS/Standard [4] that modify the mechanical behaviour of the component (fibre, matrix) as soon as failure is detected, reducing the elastic properties by introducing an accurate "degradation factor" [5]. The UMAT and USDFLD subroutines allow updating the solution-dependent state variables accordingly to the solution of an analysis. In particular, solution-

dependent state variables can be defined as a function of any other variables appearing in these subroutines and can evolve with the solution of the analysis.

The selection of a proper failure criterion, both for matrix and fibre, represents a very important task of the modelling formulation. In particular in polymers the yield behaviour is sensitive to hydrostatic pressure and as a consequence, the yield stress in tension is different from that in compression [6-8].

For the evaluation of failure within the fibres (E-Glass), it is possible the use of the most common failure theories for isotropic materials such as the von Mises failure criterion, Maximum Principal Stress theory and Maximum Shear Stress theory (Tresca).

This research was especially focused on the evaluation of local distribution and magnitude of residual stresses (introduced during manufacturing process) for different fibre volume fractions and unit cell configurations that will be discussed in the next chapters. Then, subroutines UMAT and USDFLD have been modified to account for the contributions from both the chemical shrinkage of resin and the thermal cooling contraction of fibre and resin. Of interest in this investigation has been the determination of the role that residual stresses play in local damage initiation and evolution in unit cells subjected to uniaxial loading both parallel to the fibres, and transverse in the y and z directions.

1.3 Outline

Chapter-2 represents a review of the relevant research undertaken on micromechanical aspects of composite materials.

This chapter is composed by three main sections. The first section is related to composites materials at their macroscale and describes failure criteria that have been developed to detect failure in real composites. Although this section does not take into account directly the microstructure of composite materials, it describes the difficulties to determine accurately the

mechanical behaviour and ultimate properties of composites. Moreover the section highlights the necessity of a better understanding of the microstructure that strongly influence and determine the overall response of composite material at their macro-level.

The second section describes the main issues related to the micro-modelling techniques in numerical analyses and it is divided into four sub-sections, namely:

1- Review of Literature Related to the Representative Volume Element (RVE)

2 - Review of Literature Review Related to Failure Criteria for Polymers

3 - Review of Literature Related to Damage Modelling

4 - Review of Literature Related to Thermal Residual Stresses

Finally the third section is concerned with the effects of the various actions of the constituents, in particular, the fibre arrangement and the presence of an interphase.

The three-dimensional unit cells adopted in the Finite Element studies required validations. Hence, Chapter-3 covers the preliminary studies that have been carried out in order to determine the elastic constants of the unit cells at different fibre volume fractions. Numerical results have been compared with analytical relationships (e.g. Rule of Mixtures) and/or, if possible, with experimental data available in the literature. The encouraging data obtained by this preliminary study has ensured the capability of the micro-model to describe accurately the mechanical behaviour of micro-composites. An extensive review of the methodologies used to evaluate material properties for the unit cell is also presented in this chapter.

In Chapter-4 the material characteristics and the methodology applied to simulate the residual stress and the damage progression using ABAQUS/Standard is described. As a first approach to numerical investigations a set of numerical analyses has been performed on RVEs with various fibre contents in order to investigate the overall mechanical response of the unit cell under uniaxial tensile loading, with and without residual stresses. The description of this set of studies

is also shown in Chapter-4. Another aspect investigated in this chapter has been the evaluation of different failure theories for polymers to test their capabilities to predict damage onset.

A physical “interphase” can be introduced at the fibre-matrix interface by means of particular procedures (e.g. sizing) on the fibre surface.

An attempt to characterize unit cells with the presence of an interphase with temperature dependant material properties is described in Chapter-5. These numerical studies will be able to predict the effect on the overall mechanical behaviour of composites and more importantly the effect of residual stress arising within the three-dimensional interphase on damage onset and its evolution.

The real distribution of fibres in composite materials at their component level is in general a random arrangement and square and hexagonal arrays represent only an idealization of the micro-structure that, although able to describe accurately the mechanical behaviour of micro-composites, cannot take into account the stochastic effects of inter-fibre spacing on damage onset especially in residual stress analyses.

Hence, non-uniform packing arrays of the unit cell have been investigated in Chapter-6 in order to verify any potential detrimental effect of inter-fibre spacing on failure modality in the numerical micro-models under study.

Results obtained with the residual stress analysis were also compared to data from a non-residual stress analysis used as a benchmark.

Chapter-7 presents the conclusions of the FEM studies on three-dimensional unit cells. This chapter also includes suggestions for future research based on the characterization of composite materials at their constituent level.

Chapter 2

Review of Literature Related to Micro-Modelling of Composite Materials.

2.1 Introduction

The literature review section will describe existing work in the following areas:

- Failure criteria for composite materials at the macroscale.
- RVE modelling.
- Effect of constituents on the mechanical properties of composites.

2.2 Review of Literature Related to Failure Criteria for Composites

Mechanical properties (e.g., strength, damage resistance, stiffness) of composite materials can be improved by tailoring their microstructures. Optimal microstructures of composites, which ensure desired properties of composite materials, can be determined in numerical analyses (e.g. Finite Element Analysis, Boundary Element and Mesh-Free Method,). Hence, for a better understanding of the overall mechanical properties at macroscale and the strong relationship with the micro-properties of composites materials it is worthwhile to briefly summarize the failure criteria that have been developed in order to predict failure onset in real composites.

The most important task of composite design calculation is the strength prediction. The basis for the calculation of composite laminates and structures is the Classical Laminate Theory (CLT). The CLT first looks at unstructured thin laminate plates composed of two or more unidirectional layers (often called plies). These plate elements have no specified dimensions in length and width. Only the thickness, fibre orientation and stacking sequence of its plies are important. This allows the calculation of the laminate's properties as well as its load response to the imposed forces and moments. Structural composite parts can be seen as a composition of these thin laminate plate elements. For simple structural parts (eg. beams, tubes, plates) an exact solution

can be found. Their properties and load response (e.g. bending, stresses, failure, buckling) can be calculated with analytical formulas. The right choice of the failure criterion is crucial. Many different failure criteria for unidirectional plies have been developed over the years. The first published failure criteria were global failure criteria and did not distinguish between different failures modes (Fig.2.1). They were formulated as a single, mathematically simple equation which can be easily adapted to the results of the experiments. Examples for such criteria are Hoffmann, Tsai-Hill and Tsai-Wu [1,9].

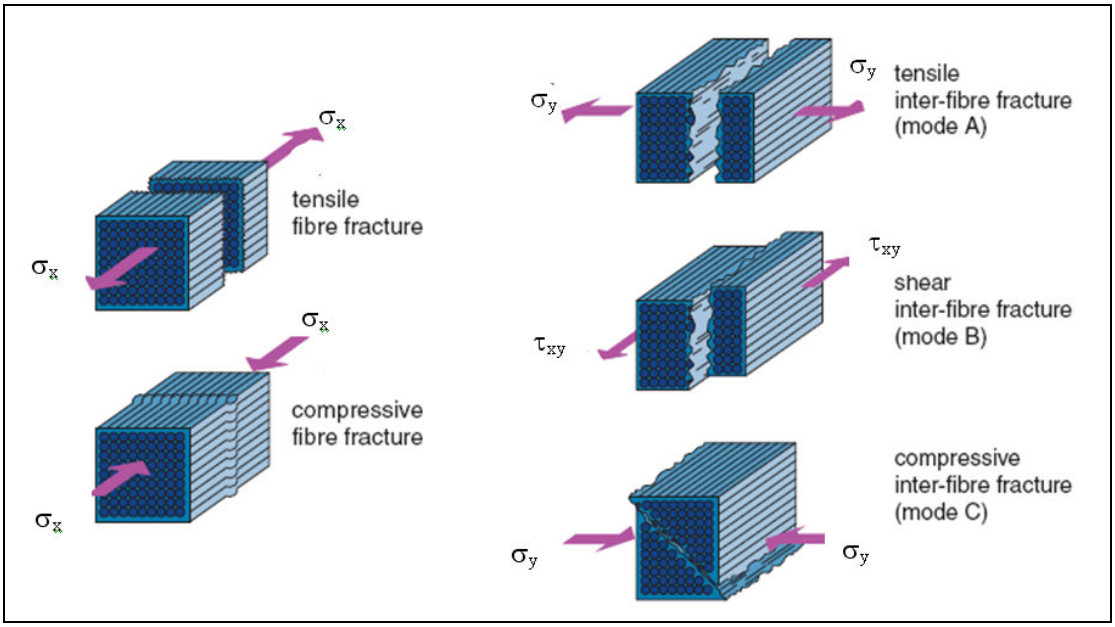

Fig. 2.1 - Fibre failure and inter-fibre failure modes.

A simple stress based failure criteria is the Maximum Stress Criterion for fibre-reinforced composites [9]. This failure criterion states that failure will occur if any of the stresses in the material principal directions exceeds the corresponding ultimate strength. In terms of symbolically expression:

$$\sigma_{xu}^{C} < \sigma_x < \sigma_{xu}^{T}$$

$$\sigma_{yu}^{C} < \sigma_y < \sigma_{yu}^{T}$$

$$\left|\tau_{xy}^{C}\right| < \tau_{xyu}^{S}$$

where the superscript C, T and S corresponding to the compressive, tensile and in-plane shear strength respectively. It should be noted that the Maximum Stress criterion does not consider interaction between stresses in different directions, which may be important in reality.

Zinoviev et al [10, 11] introduced the maximum stress criterion in predicting the failure behaviour of a series of laminates namely: carbon fibre-reinforced epoxy system AS4/3501-6, T300/914C, glass fibre-reinforced epoxy E-glass/LY556, E-glass/MY750. It was found that satisfactory prediction was obtained between the theoretical model and the available experimental data from biaxial tests. For most of the cases, good correlations were found in prediction until final failure. However, in some of the cases i.e. in the case of unidirectional E-glass/LY556 lamina, significant discrepancy was found between experimental and predicted data and it was claimed by the author that the underestimated final failure of the composite was caused by ultimate transverse compressive stresses in one of the unidirectional plies of the composite laminate.

The Maximum Strain Criterion [9] is very similar to the maximum stress criterion, with failure deemed to occur when any strain component in the material principal directions exceeds the corresponding ultimate strain. Mathematically it is expressed as:

$$\sigma_{xu}^{C} < \varepsilon_{x} < \varepsilon_{xu}^{T}$$

$$\varepsilon_{yu}^{C} < \varepsilon_{y} < \varepsilon_{yu}^{T}$$

$$\left|\gamma_{xy}^{C}\right| < \gamma_{xyu}^{S}$$

Similar to the Maximum Stress theory, there is no interaction between the strain components.

As unidirectional composites have directionally dependent strengths, judgment on the cause of failure must be based on all three stress components where the longitudinal strength can be twenty times as high as the transverse and shear strengths. Failure criteria provide the analytical relation for the strength under combined stresses. Most theories are developed to predict first ply failure (FPF), though many laminates can still support load well after FPF so these theories tend to be conservative. However, after FPF, the stiffness of the ply is reduced by either matrix or fibre failures and the strength of the laminate at the same point is evaluated again to see if the laminate can carry an additional load. This ply-by-ply (PBP) analysis progresses until last ply failure (LPF) which would be the ultimate failure of the laminate. Physical observations led to the development of differentiating criteria, which distinguish between fibre failure (FF, or fracture of the fibres) and inter-fibre failure (IFF, fracture of the matrix). Different mathematical formulations are used for the physically different phenomena FF and IFF. Because the effects of the two failure modes and the methods to avoid them are completely different, it is vital for the designer to know which failure is occurring. Examples of such criteria are Hashin and Puck [10, 12].

In contrast to the Maximum Stress and Strain criteria, the Tsai-Hill criterion incorporates the interaction between the three principal failure stresses and combines them into a single expression. Failure will not occur until the following expression reaches unity.

$$\left(\frac{\sigma_x^{\,2}}{\sigma_{xu}^{\,2}} - \frac{\sigma_x \sigma_y}{\sigma_{xu}^{\,2}} + \frac{\sigma_y^{\,2}}{\sigma_{yu}^{\,2}} + \frac{\tau_{xy}^{\,2}}{\tau_{xyu}^{\,2}} \right) = 1$$

The predictions of failure stresses (σ_{xu}, σ_{yu} and $\tau_{xy\mathbf{u}}$) using both Tsai-Hill and Maximum Stress criteria have been evaluated for carbon/epoxy laminae in comparison with experimental data [1].

It was found that the data fits well to the Tsai-Hill curve. However, it does not offer the capability to predict failure modes such as fibre breakage, transverse or shear failure.

The Tsai-Wu failure criterion generally represents a second-order surface in the space with coordinates σ_{xu} , σ_{yu} ,$\boldsymbol{\tau_{xyu}}$ which is in contrast with Maximum Stress theory where the failure envelope is a planar surface with sharp corners and edges. The Tsai-Wu failure criterion is defined by the following expression:

$$\left(F_1\sigma_x + F_1\sigma_y + F_{11}\sigma_x^2 + F_{22}\sigma_y^2 + F_{66}\sigma_{xy}^2 + 2F_{12}\sigma_x\sigma_y\right) = 1$$

Where:

$$F_1 = \left(\frac{1}{\sigma_{xuT}} + \frac{1}{\sigma_{xuC}}\right)$$

$$F_2 = \left(\frac{1}{\sigma_{yuT}} + \frac{1}{\sigma_{yuC}}\right)$$

$$F_{11} = \left(-\frac{1}{\sigma_{xuT}\sigma_{xuC}}\right)$$

$$F_{22} = \left(-\frac{1}{\sigma_{yuT}\sigma_{yuC}}\right)$$

$$F_{66} = \left(\frac{1}{\tau_{xyu}^2}\right)$$

$$F_{12} = F_{12}^{*}\sqrt{F_{11}F_{22}} \quad \text{where } -1 \le F_{12}^{*} \le 1$$

The term F_{12} is usually experimentally determined through conducting a biaxial test, i.e. simultaneous loading in the directions normal and parallel to the fibre. For the prediction of first ply failure, the failure interaction term, F_{12} is the only empirical factor needed for modification. However, an average value of -0.5 is referred to as the generalized model for glass fibre-reinforced and carbon fibre-reinforced composites as indicated in Liu et al [13]. Effect of F_{12}^* has been investigated by Tsai et al [14] where failure envelopes have been drawn for the nominal case (F_{12}^* = -0.5) and two extreme cases (F_{12}^* = -0.1 and -0.9) and good agreement was found with F_{12}^* = -0.5. Whilst sophisticated finite element analysis is necessary in determining the progressive failure of a laminate under non-homogenous stresses, the Tsai-Wu failure criterion provides a good starting point in this case.

The establishment of a failure criterion involves three steps: the formulation of the criterion, the experimental verification and the convincing of future users. A good failure criterion should take the following rules into consideration: (1) it should describe as many different types of materials and loadings as possible; (2) a minimum amount of experimental work should be necessary to determine the criterion's coefficients [15]. It is important to recognize that a failure envelope should be developed using the minimum number of test data points. However, there are geometric and material considerations which will limit the mathematical form of a failure criterion as well as the shape of the corresponding envelope, i.e. a failure envelope must be closed in order to prevent infinite strengths and the envelope must be convex so that unloading from a state of stress will not lead to additional failures. Hence, the ability to predict the strength and deformation of fibre-reinforced composites under complex loadings is of critical importance to designers and users of composite structures. In the ***Failure Criteria in Fibre Reinforced Polymer Composites - The World-Wide Failure Exercise*** [10], the authors have organised and coordinated an international study.

The principal aims of the exercise were to:

- Establish the current level of maturity of theories for predicting the failure response of fibre reinforced polymer laminates.
- Close the knowledge gap between theoreticians and design practitioners in this field.
- Stimulate the composites community into providing design engineers with more robust and accurate failure prediction methods, and the confidence to use them.

The basic plan was to:

- Assemble a comprehensive description of the current, foremost, failure theories for fibre reinforced plastic laminates.
- Compare their predictive capabilities directly with each other.
- Compare their predictive capabilities directly with experimental data.

This exercise has been carried out in three distinct stages referred to as Part A, Part B and Part C. Part A contained detailed descriptions of 14 leading failure theories and predictions by each for a set of test cases. Part B provided a detailed comparison between the theoretical predictions and the experimental results. Part C extends the study to including 4 additional theories that have emerged since the WWFE was first initiated and contains overall conclusions and recommendations. Most of the leading approaches to predicting failure in composites were represented, including theories employing well-known Maximum Stress, Maximum Strain, interactive (Tsai) and mechanistic failure criteria (Puck and Cuntze). Some less widely known methods were also represented (McCartney, Eckold). In response to repeated requests from

industrial users the organisers devised qualitative and quantitative methods of summarising, assessing and ranking the overall performance of the different theories. The qualitative method consisted of comparing the predictions of all of the theories with the experimental results, one test case at a time and noting any 'Fundamental', 'Major' or 'Minor' weaknesses. In the quantitative method the ratio of predicted to measured lamina strengths, laminate initial and final strengths and deformations was calculated for numerous selected combinations of applied loads in all the various test cases. Grades were awarded for each prediction:

- Grade **A** if the prediction was within ±10% of the measured value
- Grade **B** if the prediction was between ±10% and ±50% of the measured value
- Grade **C** if the prediction was below 50% or above 150% of the measured value
- Grade **NA** if no prediction was attempted for that case.

The theories of Zinoviev (Maximum Stress criterion), Bogetti (Maximum Strain criterion), Puck and Cuntze (mechanistic criterion) and Tsai (interactive criterion) showed very good overall performance.

As a result of improvements to his method of post failure analysis, in the light of the experimental results, Tsai further improved his performance in Part B. These five groups together with Sun (L) also formed the top group of theories according to the qualitative method of assessment.

The five leading theories (see above) were explored in greater detail to demonstrate their strengths and weaknesses in predicting various types of structural failure. Recommendations were then derived, as to how the theories can be best utilised to provide safe and economic predictions in a wide range of engineering design applications.

A brief summary of the grades scored by each theory for all the five ranking categories is illustrated in Table 2-1 in which the categories are listed according the number of the A+B grades

achieved . It was noticed that taking Grade A and B scores together, the predictions of a number of theories were within 50% of the experimental results in more than 80% of cases. The full list of theories can be seen in the book *The World-Wide Failure Exercise* [10].

Table 2-1 Summary of the grades scored by each theory [10].

Grade type	A	B	C	NA	A+B
Cuntze-B	59	38	28	0	97
Zinoviev	53	43	29	0	96
Bogetti	51	44	30	0	95
Puck	64	30	31	0	94
Cuntze	62	32	31	0	94
Tsai-B	57	36	32	0	93

The need for careful interpretation of initial failure predictions has been emphasised, and also the necessity to allow for multiple sources of non-linearity (including progressive damage) where a high level of accuracy is sought for certain classes of large deformation and final failure strength predictions. Finally, different aspects requiring further experimental and theoretical investigation has been identified with a specific list of experiments indicating where further tests would be useful to integrate the experimental data employed in the exercise, e.g.:

- Biaxial loading tests on uni-directional lamina to confirm which theoretical predictions are the most realistic at some specific stress ratios.
- Biaxial compression tests to eliminate the influence of buckling that may have resulted in low experimental failure loads for some laminates.
- More tests on initial failure and its significance.

2.3 Review of Literature Related to Micromechanical Modelling

The purpose of this section is to introduce some of the methods used to determine the influence of the mechanical properties of the fibre and matrix on the elastic properties of the composite materials. This area of research, where interest is focused on what is happening at the level of the fibre and matrix, is commonly referred to as micromechanics, primarily to differentiate it from macro-mechanics wherein the stresses and strains within individual layers are generally of interest.

2.3.1 Review of Literature Related to the Representative Volume Element (RVE)

With rapidly growing computational modelling capability, the micromechanical analysis of fibre reinforced composite materials has become an important means of understanding the behaviour of these materials. An appropriately introduced representative unit cell or representative volume element (RVE) is usually the first step into such an analysis. Before a unit cell can be introduced, a common practice is to assume an idealised regular arrangement of the reinforcing fibres in the matrix. Occasionally, regularly packed fibres are obtained in some modern composites. The loading conditions to the material represented by the unit cell can be thermal, mechanical or other types. The prescription of the loads to the unit cell is normally expressed in terms of macroscopic field quantities, such as macroscopic stresses, strains and change in temperature. For unidirectionally fibre reinforced composites, frequently employed idealised fibre-matrix arrangements are square packing (Fig 2.2) and hexagonal packing. They have both been studied extensively, e.g. by several researchers [2, 16-25].

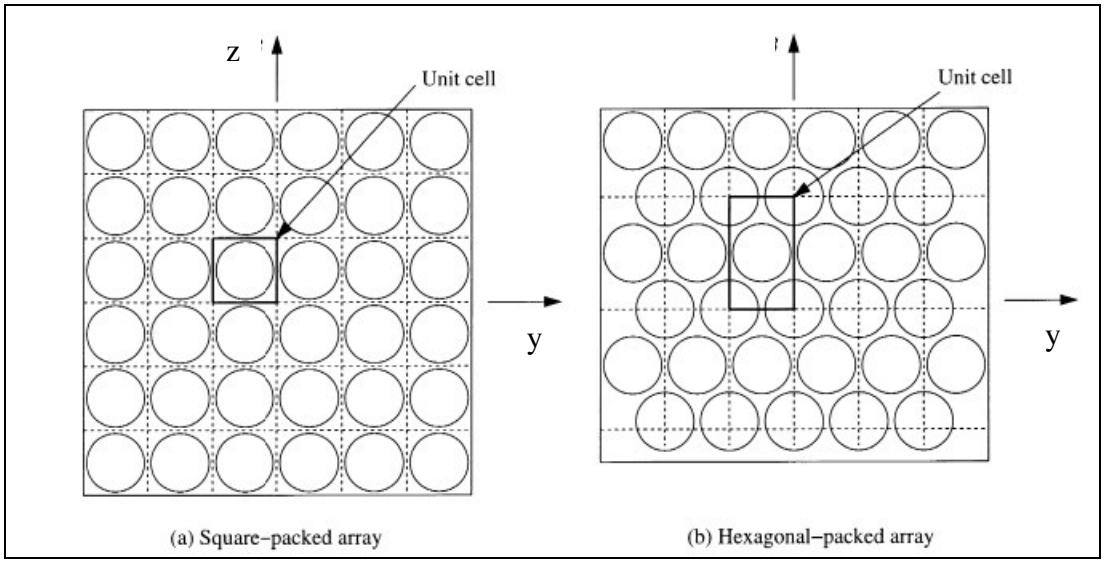

Fig. 2.2 - Unit cells for square- and hexagonally-packed arrays.

When a square layout is assumed, it is relatively easy to define a unit cell and to interpret the symmetries that the system possesses to mechanical boundary conditions of the unit cell for a micromechanical analysis. This is probably why there have been extensive analyses performed with this idealization. On the other hand, the hexagonal layout is less extensively explored, despite the fact that a nearly hexagonal fibre arrangement can be found in some real composites [26].

For UD composites with randomly distributed fibres in the matrix over a cross-section perpendicular to the fibres, there are differences between the two idealisations. An important characteristic of such composites is their transverse isotropy, usually achieved in a statistical sense. It has been shown (Cowin & Mehrabadi 1995) [27] that, although the mathematical proof can be found as early as in Love (1927) [28], a hexagonal layout preserves the transverse isotropy, a statistic feature of the majority of real materials, while, in general, a square layout does not. It is then conceivable that a hexagonal layout is in a more suitable position than a square layout to represent real materials of statistical transverse isotropy [18, 22].

The transverse isotropy achieved through a hexagonal packing, however, is at a price, i.e. the unit cell from it is substantially more sophisticated than that from a square packing. In addition to the

square and hexagonal unit cells introduced through the two packing systems, a cylindrical unit cell (Fig. 2.3) is often used in the literature [2, 17]. In this interpretation it is assumed that the cross-section consists of many concentric cylinders. The inner cylinder of the concentric pair represents the fibre and the outer cylinder represents the matrix. The cylinders are not all the same radius, but the ratio of the radius of the fibre cylinder to the radius of the matrix, or outer, cylinder is the same for all cylinders. Therefore, the fibre volume fraction is the same for each pair of concentric cylinders. As the cylinders become smaller and smaller, more and more volume is filled until, in the limit, the entire cross-section is filled with concentric cylinders.

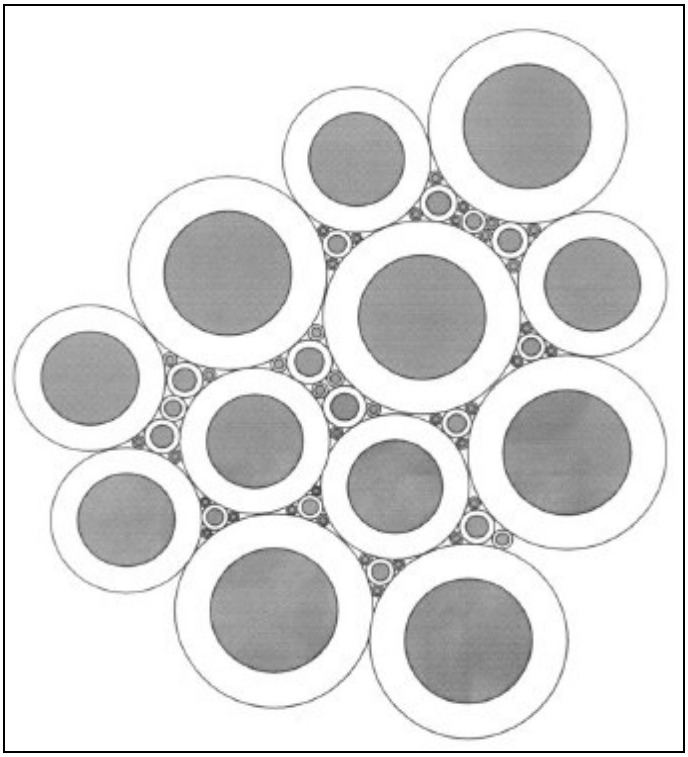

Fig. 2.3 - Alternative interpretation of composite cross-section.

The axisymmetric geometry allows an analytical solution in either an axisymmetric or sinusoidal form in the circumferential direction [18, 22]. In many cases, this model tends to produce good results for predictions of the effective properties of a composite. However, since packed cylinders do not fill the space fully, there is a higher degree of discrepancy between the reality and idealisation than that of the square and hexagonal cells.

Hashin and Rosen [17] included the gaps between cylinders but a rather artificial displacement or stress field must be assumed before an analytical solution is possible. As a result, the obtained distribution of stresses may differ from that from the square or hexagonal cells significantly, especially, in the matrix.

In any of the square and hexagonal packing systems, there are different geometric symmetries as depicted in Fig 2.4. In general, by using different symmetries, different shapes of the unit cells can be obtained, as illustrated by Li [18, 22] in the case of hexagonal packing in unidirectionally fibre reinforced composites.

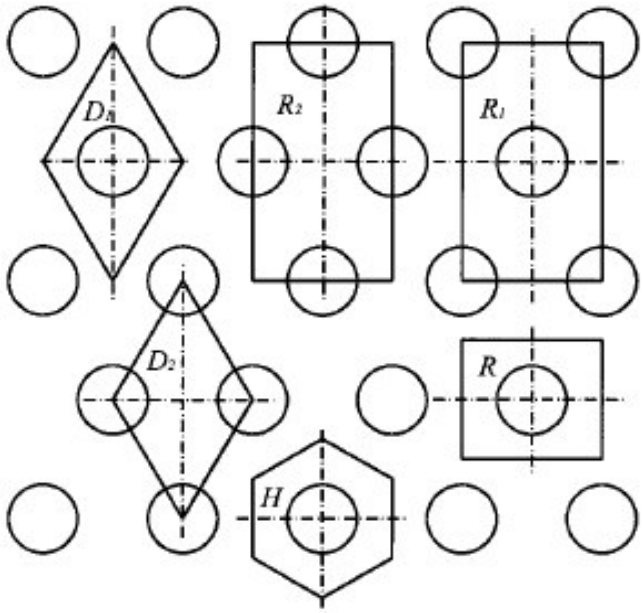

Fig. 2.4 - Different periodical elements for hexagonal packing [18].

However, when one examines a hexagonal layout, the symmetries in it are not as straightforward to interpret to mechanical boundary conditions as those in a square layout. As a result, available analyses made with a hexagonal idealization are not as systematic as with a square layout in the literature. Usually they fall into one of the following categories:

a. Some of the symmetries are interpreted correctly but the existence of the remaining symmetries is not realized [29]. The result is that the size of the unit cell has not been minimized and, therefore, effective use of the unit cell has not been achieved.

b. All the symmetries have been noticed, though vaguely, for some special cases, e.g. under a special loading condition, while a generalization is yet still to be made [30].

c. Some of the symmetry conditions have been interpreted incorrectly to mechanical boundary conditions [31]. This is certainly misleading [18].

In most existing unit cells in the literature, because of the symmetries that have been used, the boundary conditions can only be provided for specific loading conditions, e.g. for a specific macroscopic stress or strain component [18]. As a result, some analyses are restricted to a certain type of loading conditions, such as transverse tension and longitudinal shear [20, 21]. Others have dealt individually with every single component, or a limited combination, of macroscopic stresses or strains [18]. In other words, the macroscopic stresses or strains in an arbitrary combination are not allowed to be applied simultaneously as loads. While it is possible for linear problems to employ a superposition law to obtain the combined effects of such a macroscopic stress or strain state from the results of all the individual cases involved, it may not always be the preferred approach in every application, especially when any form of non-linearity is involved in the problem, in which case, superposition law is not applicable in general. The involvement of reflectional and rotational symmetries when these unit cells are established is responsible for not allowing the arbitrary application of loads because under these types of symmetry transformation, some stress components show symmetric characteristics while others are antisymmetric. The same stress component can be symmetric under one symmetry transformation but antisymmetric under another [18, 22].

Li [18] adopted a systematic approach involving the use of only the translational symmetry transformations. Two typical idealised packing systems have been employed for unidirectionally fibre reinforced composites, square and hexagonal. There are a number of important advantages resulting from this. The unit cells so derived are capable of accommodating fibres of irregular cross-sections and imperfections asymmetrically distributed around fibres such as micro cracks and local debonding in the system, provided the regularity of the packing and imperfections is present. Furthermore, all the unit cells established can be subjected to arbitrary combinations of macroscopic stresses or strains unlike most available unit cells in the literature which can only deal with individual macroscopic stress or strain components. Boundary conditions for these unit cells have been derived from appropriate considerations of the conditions of symmetry transformations.

Applications of macroscopic stresses or strains as the loads to the unit cells have been described in such a way that they can be implemented in a straightforward manner and the effective properties of the composite can be evaluated following a standard procedure. As a result, the unit cells introduced here are all expected to be applicable to non-linear problems of any nature, material and geometry.

For a unidirectionally fibre reinforced composite, it is normally reasonable to assume that the fibres are infinitely long and every cross-section of the composite perpendicular to the fibres is identical. The micromechanical analysis of such a material can then be simplified to a two-dimensional problem in the plane of a cross-section of the composite. In this plane, a mathematical approach, the Voronoi tessellation [31], was adopted by Li [18, 22] to tessellate the domain of interest in the plane with the centres of the fibres being the centres of Voronoi cells. The cells obtained in this way are called Voronoi cells.

A Voronoi cell is bordered by segments perpendicular to and passing the midpoint of the segments connecting the centre of the cell and those of the neighbouring cells (Fig. 2.5).

For regular packing, such as square and hexagonal ones, square and hexagonal cells are obtained as a result of such tessellations. In either case, all the Voronoi cells are identical throughout the plane and any one cell can be reproduced by another through a certain translational symmetry transformation.

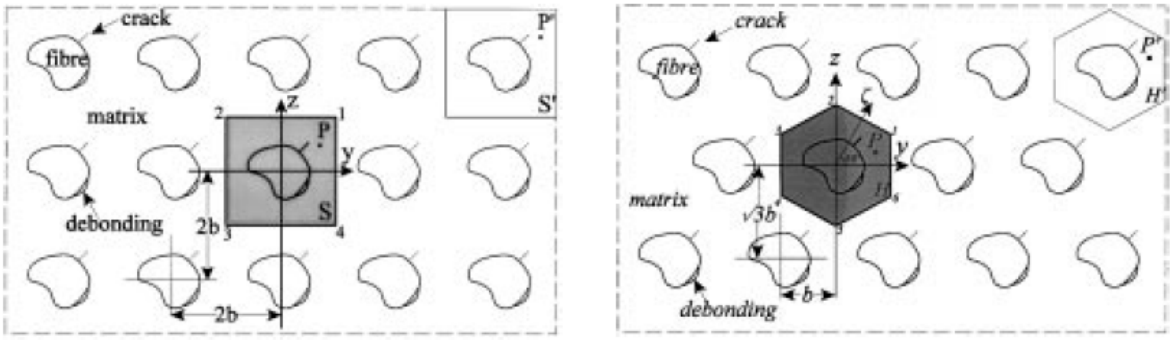

Fig.2.5 - Square (left) and Hexagonal (right) packing and the square unit cell. [18].

Micromechanics has found much success in prediction of the stiffness of unidirectional (UD) fibrous composites. On the other hand, little is known about the ultimate tensile strength, another important mechanical property, of the composite materials. The “Rule of Mixtures” (ROM) is the most widely used analytical approach for estimating the stiffness properties of unidirectional composite materials particularly for elastic behaviour when there is a very strong bond between fibre and matrix. However, as far as failure properties are concerned, the rule of mixtures technique does not predict accurate results due as it does not account for the stress concentration which results from fibre-matrix interactions [33]. A semi-empirical approach namely the Halpin-Tsai relationship is utilised by Crookston [34] in predicting the transverse modulus of a unidirectional composite. Experimental tests have shown that under conditions where all the

stresses are kept low and of short duration, good correlation is obtained with experimental measurements for transverse modulus for long-fibre composites using this approach [35].

Many other models have been developed by researchers [36-39] to predict the mechanical behaviour of unidirectional composite materials.

Most strength theories for fibrous composites have been developed based on macro-mechanical considerations similar to those for isotropic materials, including the Maximum Stress-Strain criteria and the Tsai–Wu theory [40, 41]. Unlike in isotropic cases, extensive experiments including biaxial tests, which may be difficult or expensive to conduct in some cases, have to be performed to determine the strength parameters involved in these macro-mechanical theories whenever they are applied to any composite. Even with the same constituent materials, different composite having different fibre volume fraction still requires similar tests. Another drawback with these theories is that the failure mode cannot be predicted. They are unable to indicate which of the constituent phases initiates the failure of the composite and meanwhile how rich the strength of the other phase is. Several micromechanics based attempts to the ultimate strength of fibrous composites have been made [42, 43]. However, they were focused mainly on the micro-structural failure mechanisms and were developed by pre-assuming a priori deformation modes.

Huang proposed in [38] a set of simple micromechanical formulae for the ultimate tensile strengths of the unidirectional fibrous composites under individual uniaxial loads. The failure prediction of the composites is based on understanding for the stress states in the constituent materials without any pre-assumed deformation mode. Only the material properties of the constituent fibre and matrix as well as fibre volume fraction are required to apply these formulae.

Wilczyński and Lewiński [36,37] presented an algorithm that has been used for determining the elastic properties of a unidirectional polymeric fibrous composite with isotropic reinforcement such as glass fibre as well as orthotropic reinforcement, typically carbon, polyethylene or aramid fibres. The algorithm consists of a cylindrical cell of unit radius and length representing a regular

structure of continuous, parallel, elastic and isotropic fibres (in a hexagonal array) embedded in an isotropic elastic matrix. Initial research work [36] covered analysis on isotropic reinforcement while later analysis [37] permits not only for isotropic reinforcement but also the more complicated case of orthotropic reinforcement with carbon fibres. The approach presented is able to obtain all five elastic constants for unidirectional, continuous-fibre composite (E_x, E_y, G_{xy}, υ_{xy} and υ_{yz}) as well as the stress concentrations on the boundary of the phases with good accuracy in comparison with experimental results, and is sufficiently simple to be utilised on a Personal Computer. However, other authors [44, 45] found that transverse modulus predicted from a square unit cell is closer to the experimental results.

The prediction of the transverse modulus (E_y) of unidirectional fibre composites is of great importance not only because the transverse modulus itself is one important property of engineering materials but also because it is used as an elastic constant in predicting the stiffness of general laminates or the off-axis stiffness of unidirectional laminates [46] and the stiffness of short-fibre reinforced composites [47, 48]. There is large body of work on models that predict the transverse modulus of unidirectional fibre composites in terms of the properties of the constituents.

The models can be classified into two categories according to whether the transverse composite modulus depends on fibre aspect ratio. Most of the existing models assumed that the transverse composite modulus (E_y) was independent of fibre length-to-diameter ratio.

The inverse Rule-of-Mixtures (iRoM) equation [46] for E_y was derived by assuming that the fibres have a rectangular cross-section and employing the Rules-of-Mixtures for the strains of the composite and its constituents. The iRoM equation was modified by considering the constitutive relations of the constituents [31]. The advantage of the two models is that they are simple in form and thus convenient to use, but they were not satisfactorily applied to experimental results [46].

The Halpin-Tsai equation was derived using a semi-empirical approach [49-51]. The Halpin-Tsai equation has been widely cited in the literature because it provides a fairly good prediction of E_y for continuous fibre composites.

Shaffer [52] derived two equations for the transverse composite modulus using the mechanics of materials method. One of these equations is applicable when fibre volume fraction is less than 68% and the other when fibre volume fraction is greater than 68%. The results obtained from these equations predict values lower than the results evaluated from experiments.

Tsai [53] studied the problem of parallel elastic cylindrical inclusions in an elastic matrix and derived upper and lower bounds for E_y by interchanging the role of fibre and matrix in the potential energy theorem. Since the bounds are far apart, Tsai hypothesized that the transverse composite modulus lies somewhere between the two bounds. Hashin and Rosen [17] considered both hexagonal and random arrays of fibres. They used potential and complementary energy theorems to derive two bounds for E_y. The bounds obtained by Hashin and Rosen are much improved. Numerical solution techniques have also been used to evaluate the transverse composite modulus. Adams and Doner [21] used the finite difference method to predict the transverse modulus of continuous fibre composites.

The above models are only suitable for continuous fibre composites since they neglected the effect of fibre aspect ratio. Some other models evaluated the effect of fibre aspect ratio.

Yun Fu et [54] proposed a new micromechanical model for predicting the transverse modulus of unidirectional continuous and discontinuous fibre composites. This model is based on modelling a composite with a regular array of volume elements and constructing a stress pattern based on simple averaging procedures in the direction transverse to the fibre axis for a representative volume element. The predictions of the model are compared with existing experimental results for various fibre/matrix systems and very good agreement was found. This model has advantages over other existing models not only because the effects of fibre aspect ratio, inter-fibre spacing

and fibre end gap are taken into account and the expression for the transverse modulus of composites is simple in form but also because the present model gives precise predictions of the transverse composite modulus (Fig.2.6).

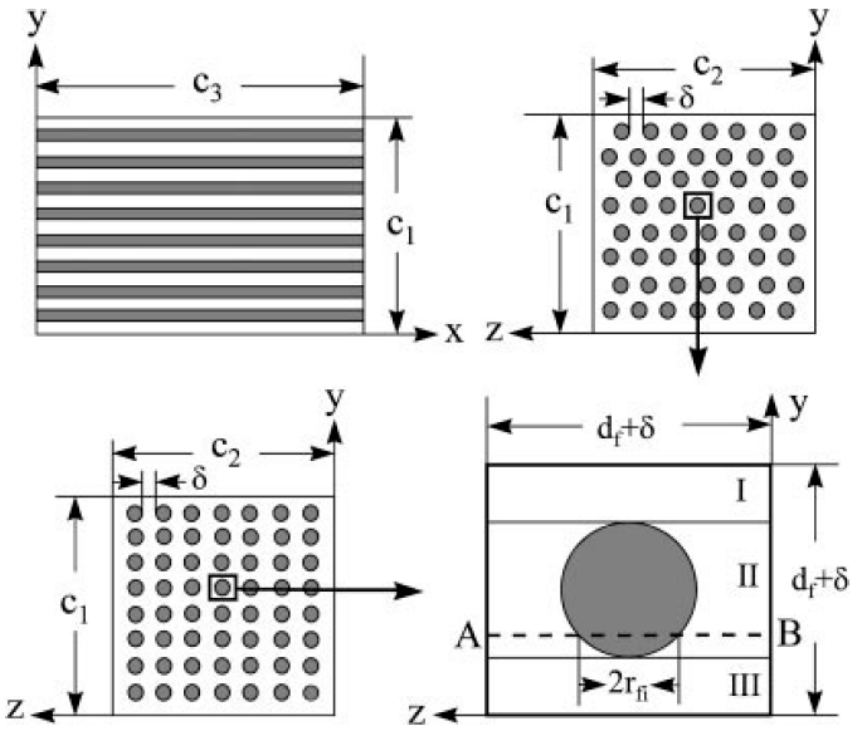

Fig. 2.6 - Schematic drawing of continuous fibre composites and a corresponding simple representative volume element. [54].

Several theoretical models have been proposed for the prediction of composite properties from those of the constituent fibre and matrix. Among the elastic constants predicted by these models, the longitudinal modulus and Poisson's ratio show good agreement with experiments and can be approximated by the simple Rule of Mixtures. The predictions for the other elastic constants, however, show significant scatter and depend upon the assumed geometrical model of the composite. Experimental determination of the unidirectional composite moduli is difficult, especially when it involves determining the longitudinal and transverse shear moduli. Thus, numerical techniques like finite element methods are needed to verify the feasibility of the models. Numerical methods to estimate composite properties usually involve analysis of a

representative volume element (RVE) corresponding to a periodic fibre packing sequence. Several papers exist in the literature where the RVE is analysed to determine composite moduli. These analyses present few issues that need to be examined.

Firstly, the correct RVE corresponding to the assumed fibre distribution must be isolated. This has not always been done correctly. For example, Shi et a1 [55] modelled a hexagonal distribution of short fibres by a RVE that actually represents a square array fibre distribution [3]. Secondly, correct boundary conditions need to be applied to the chosen RVE to model different loading situations. Proper consideration must be given to the periodicity and symmetry of the model in arriving at the correct boundary conditions. Under longitudinal and transverse normal loading, a typical RVE can deform in such a way that it remains a right parallelepiped, i.e. plane sections remain plane. This has been correctly modelled by several researchers [21, 56, and 57]. However, many researchers, modelling longitudinal and transverse shear loading, have made incorrect assumptions about the deformed shape of the RVE.

Naik [58] and Brockenbrough et al. [57] modelled transverse shear loading assuming that the deformed boundary of the RVE remained plane (no distortion). Caruso [59] also made a similar assumption about the deformed shape under transverse shear loading and noted that 'the finite element predictions for G_{23} are not very reliable in view of the difficulty associated with simulating the respective boundary conditions'.

In their work, Sun and Vaidya [3] show that the assumptions made by many researchers are incorrect applying the appropriate constraints on the RVE for various loading conditions, such that they simulate the actual deformation within the composite and relating the non-homogeneous stress and strain fields within the RVE to the average stresses and strains by using Gauss theorem and strain energy equivalence principles.

Evaluation of sensitivities for transversely isotropic [60,61] unidirectional composites to a number of material and geometric parameters using two-dimensional, generalised plane strain elements within an implicit FE code (ABAQUS/Standard) has been proposed by Crookston et al [60]. This method enables quick determination of the significance of each input parameter before a series of time consuming and computationally expensive three-dimensional analyses of textile composite repeating unit cells is conducted. The input parameters addressed in the analysis included fibre modulus, matrix modulus, matrix failure stress, the amount of fibres, the tow aspect ratio and the tow shape. The effect on the transverse modulus and failure strength of the composite was examined for each of the input parameters. It was found that the number of fibres enclosed within the tow region of a unit cell had great influence on the transverse behaviour of the unit cell. Conversely, the fibre modulus which is believed to have significant effect in the longitudinal direction was proven to have the least effect on the modulus and failure behaviour of the unit cell in the direction perpendicular to the fibre.

Micro-mechanical interaction of fibre and matrix is the key to understanding the mechanical behaviour of composite materials. By modelling the fibre-reinforced material at the micro-mechanics level the mechanical response can be understood and improved. Also, understanding the complex micro-mechanical response is important for studying load transfer among fibres and the effect of fibre waviness. As the fibres are being melt-spun, the cross-section of the generated fibre may be non-circular or wavy. Also, there may not be perfect bonding between the fibre and matrix.

Chati and Mitra [62] investigated composite elastic constants at a macroscopic level and the stress distribution at interfaces for a given volume fraction of fibre by using in their work the Boundary Element Method (BEM). The effects of waviness or “crenulations” and debonding have also been studied. In this work it is assumed that the binder and the fibre materials are

linearly elastic, isotropic and homogeneous. However, due to the fibre placement, the reinforced material is anisotropic.

Even Eischen and Torquato [63] have applied the BEM for the determination of effective elastic moduli of composite materials taking into account an idealized hexagonal array of infinitely long fibres. A variety of inclusions either stiffer or weaker than the matrix and, a wide range of volume fractions of fibres have been examined. The main difference between Eischen and Torquato' s work and Chati and Mitra's work is that their model is purely two-dimensional, whereas Chati and Mitra's model is three-dimensional for a transversely isotropic material.

Taliercio et al [39] developed a numerical model based on the "homogenization theory" (the term homogenization usually qualifies the passage from the micro to the macro-scale) to describe the macroscopic mechanical response of unidirectional long-fibre composites with strain-softening matrix, subjected to stresses acting in any plane transverse to the fibres. The matrix brittleness is more significant in comparison to the fibres in this plane since the strengthening effect of the fibres is negligible. This method is applicable to any macroscopic stress conditions provided that a 3D finite element model with suitable boundary conditions. The main results of these analyses showed that the macroscopic tensile strengths of a brittle-matrix composite are much lower than both the strength of a ductile-matrix composite and the strength of the unreinforced matrix.

De Kok [44] has created a representative unit cell model for glass fibre reinforced epoxy based on a two-dimensional generalized plane strain finite element model in which meshes are based on square and hexagonal arrays. The fibre and matrix were attached with coinciding nodes and perfect fibre-matrix bonding was assumed. By changing the material properties of the circular layers at the fibre-matrix interface from fibre to matrix or vice versa, a range of fibre volume fractions could be obtained from the geometric model. The transverse elasticity and failure

behaviour of the unit cell has been examined and it is found that using von Mises failure criterion, a good agreement is found between failure strain results from the model and experiments. A similar yet simplified version of the representative volume element (RVE) from De Kok has been generated using plane strain elements. It is believed that the differences in local stresses caused by the use of plane strain (through-thickness strain is neglected) rather than generalized plane strain (permits through-thickness strain) are expected to be small [64, 65].

Unidirectional glass-reinforced plastics (GFRP) show poor mechanical performances in the transverse (90°) direction. This drawback limits use of such materials in many structural applications. Indeed, transverse failure of composite plies can lead to an important loss of stiffness of the structure, to a decrease of fatigue strength. Despite efforts made by material scientists during the last decade to improve performance of laminates, transverse failure strain and stress of composites remain much lower than ultimate properties of un-reinforced polymers. As a matter of fact, transverse failure strains of glass/epoxy or glass/polyester composites are usually close to 0.5% [66, 67]. Many experimental and theoretical studies have been performed in order to find the origin of composites' transverse brittleness or to propose technological solutions to solve the problem [66–70]. Briancon et al [68] observed in situ plastic strain of the matrix during transverse loading of unidirectional glass/epoxy composites. Plastic strains in the matrix were revealed by distortions of micro-grids settled on specimen surface.

Using this technique, the authors showed that plastic strain is localised near the tip of micro-cracks and is limited by the nearest fibres which prevent its further extension. This feature gives a first explanation for the overall brittle transverse behaviour of the material. In another study, Asp et al [69] showed that epoxy resins submitted to a triaxial state of stress exhibit values of failure stress very close to those observed for unidirectional composites in transverse tension. They

concluded that the triaxial stress state in the polymer matrix is mainly responsible for transverse brittleness of laminates.

More advanced analyses have also been performed [64]. They are generally based on the determination of stress field distribution by means of analytical or numerical models. Failure criteria allow the evaluation of maximum admissible strain in the polymer matrix or in the interfacial areas. Using finite elements calculations, Asp et al [64] studied the stress distribution in an ideal composite constituted by a square array of fibres. These authors employed a failure criterion based on the dilatation energy which accounts for the influence of stress triaxiality on the matrix behaviour. They found that transverse failure mechanism of laminates is governed by the storage moduli of the constituents, by the glass fibre content, and eventually by the presence of an interphase. The model also predicted an increase of failure stress and strain when incorporating a soft rubbery interphase between fibre and matrix. The analysis performed by De Kok et al [44] using finite element calculations showed that high local strains take place in the matrix at low global strain of the composite. Application of von Mises yield criterion pointed out that local strains are concentrated in thin bands near fibre/matrix interface. The authors also suggested that a rubbery interphase allows the plastic strain to extend in the matrix and promotes an increase of the overall strain of the composite. De Buhan and Taliercio [70] proposed an analytical approach based on the concept of homogenisation in periodic media. The model describes the failure behaviour of laminates taking into account a debonding criterion for the fibre/matrix interface.

Experimental and theoretical studies have therefore pointed out several factors responsible for the transverse brittleness of laminates: (i) high localisation of plastic strain in the matrix which is confined by surrounding fibres; (ii) triaxial state of stress in the polymer; and (iii) probable insufficient level of adhesion at fibre/matrix interface leading to premature debonding. Since local plastic strain of the matrix and interfacial adhesion are influent parameters on the transverse

properties of composites, two ways have been investigated in order to improve the performance of laminates: a) increasing the ductility of the matrix; b) optimising the fibre surface treatments. Influence of fibre surface treatments on transverse properties of composites is a matter of discussion. Several studies have provided contradictory results on the subject. Tryson and Kardos [71] found that coating fibres with a reactive elastomer (flexible epoxy) leads to a 67% increase of transverse failure stress and strain for unidirectional glass/epoxy composites. According to these authors, such a phenomenon is related to a modification of the stress field and to a relief of residual stresses near the rubbery interphase. On the contrary, Podgaiz et al. [72] and Gatward et al. [73] observed a decrease of transverse failure strain and stress when coating glass fibres with elastomer sizing (flexible epoxy or polyvinyl). They suggested that the low tensile strength of elastomers and a poor level of adhesion between the rubbery interphase and the epoxy matrix could be responsible for the poor performance of such composites. According to these authors, tensile strength of the interface/interphase is a crucial parameter for transverse properties of composites.

Benzarti et al. [66] investigated the effects of fibre surface treatments on transverse mechanical behaviour of unidirectional glass/epoxy composites. Model composite plates were processed by filament winding using glass fibres coated with different sizing changing by their epoxy functionality and their reactivity towards the matrix.

In the first part of their study, transverse tension and micro-indentation characterisations were performed in order to correlate the ultimate behaviour of the composite with interfacial properties. Experiments revealed that the most reactive sizing promote the highest interfacial strength and also increase ultimate properties of laminates in transverse tension. This feature was attributed to the high crosslink density of the polymer network in interfacial areas.

In the second part the authors carried out finite element calculations in order to evaluate local strain and stress concentration in a composite submitted to transverse tension conditions

establishing the general trend for the evolution of composite failure strain as a function of interfacial strength. The modelling showed that a transition of the composite failure mode occurs at a global strain of 1.15%, from an adhesive rupture at the fibre/matrix interface to a cohesive rupture in the matrix. In the domain of adhesive rupture, the value of the composite failure strain appeared to be directly governed by the interfacial strength. Therefore, improving interfacial strength by use of fibre sizing with high epoxy functionality could constitute an interesting way to reduce transverse brittleness of composite structures.

2.3.2 Review of Literature Review Related to Failure Criteria for Polymers

The development of polymers for use as matrix materials in composites has generally been driven by the desire to achieve high yield stress and toughness as well as good adhesion with fibres. Although these properties are desirable and generally lead to improved composite performance, it is important to realize that the local stress state in the matrix within a composite can induce behaviour which may not be reflected in these properties. The response of polymers to the mechanical loading is very complex. For example, the stress state plays a considerable role in the material failure. Tests under all possible stress combinations cannot be provided [6, 7], therefore, for the prediction of their strength, it is necessary to use a failure criterion obtained on the basis of general performance information about the material. In addition, it is important to consider the effects of the strain rate and temperature, since they have a significant influence on the yield and failure behaviour of polymers. For isotropic engineering polymers, these effects were examined in [6, 7, 74-76].

On the contrary most metals, the deformation and the failure stress of polymers are greatly affected by the hydrostatic pressure, as shown by the difference observed between the stress-strain curves in uniaxial tension and uniaxial compression [6, 77]. This effect also leads to a

pressure dependence of the yield and failure stresses. The effect of hydrostatic pressure on the yield behaviour of polymers was demonstrated experimentally by several authors [77-81]. In contrast to metals, for polymers, the yield stress is often assumed to be equal to the maximum stress in the stress-strain curve [6]. The general effect of hydrostatic pressure on the mechanical properties of polymers consists in increased yield and failure stresses. The one-parameter yield criteria, such as the Tresca and von Mises criteria, represent the polymer behaviour inadequately because they cannot describe the dependence of the yield and failure stresses on the hydrostatic part of the stress tensor. Several criteria have been proposed to predict the yield and failure of polymers subjected to static multi-axial loading. Two modifications of the Tresca and von Mises criteria are often used [64, 81-83]. According to the first one, using the maximum shear stress or the hydrostatic stress, respectively, a linear function of the hydrostatic pressure was introduced [6,7]. A pressure-modified von Mises criterion predicting a nonlinear dependence of the yield stress on the hydrostatic pressure was applied to polymers [64, 84-86]. In the three-dimensional space of principal stresses, the modified Tresca surface is an irregular hexagonal pyramid, and the two modified von Mises criteria are a cone and a paraboloid (Fig.2.7), respectively. Another criterion, used for polymers is the Mohr–Coulomb criterion [87, 88]. It predicts that the critical stress can occur in any plane and depends linearly on the normal stress in the plane. The experimental investigations have shown that the criteria based on a linear dependence of the yield stress on the hydrostatic pressure afford a good description of polymer behaviour mainly under low pressures [6, 81-83]. The experimental results show that the yield and failure stresses first grow linearly with this pressure and then, at higher pressures, the growth rate decreases [6].

In commercially produced composites with high fibre volume fractions it is inevitable that fibres are distributed unevenly and that clusters of fibres as well as resin-rich areas exist. In such conditions the local stress states will vary between nearly shear dominated to nearly hydrostatic.

The same given matrix will thus be predisposed to different deformation and failure modes in different regions of the composite. In most studies of glassy polymers, the shear-driven yielding has been emphasised with attention being given to the associated influence of hydrostatic stress.

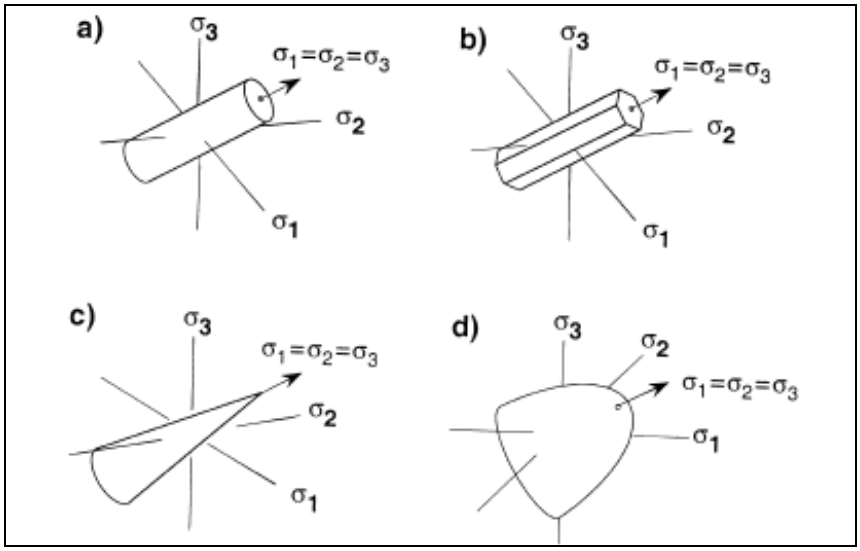

Fig. 2.7 - Failure surfaces in the principal stress space, coaxial with the hydrostatic axis σ_o ($\sigma_1 = \sigma_2 = \sigma_3$) (a) von Mises; (b) Tresca; (c) Coulomb; (d) Mohr [88].

Several yield criteria for this purpose have been proposed [88]. These criteria usually predict the effect of hydrostatic compression on the yield stress satisfactorily but do less well when hydrostatic tension is applied. Also, the consideration of the yield stress reduction alone cannot explain the observed fact that although the strain to failure in uniaxial tension for matrix materials ranges from 1.5 to 70%, the strain to failure in transverse tension of unidirectional fibre composites typically varies between 0.2 and 0.9% [1, 64, 67].

A part of the explanation could lie in fibre/matrix debonding which may occur at low strains. However, as demonstrated in a [64, 69] the triaxial stress state can reduce the strain to failure of epoxies to within the observed failure strains in transverse tension of composites.

Yield and failure criteria for epoxies subjected to different stress states were examined by Asp et al. [69]. In particular, the authors examined three epoxy systems of interest as composite matrix materials for their yielding and failure behaviour under uniaxial, biaxial and triaxial stress states.

Yield criteria applicable to glassy polymers, i.e. accounting for the hydrostatic stress effect on the deviatoric stress to yielding, were assessed. It was evaluated that under stress states resembling those in matrix constrained between fibres, e.g. equi-biaxial and equi-triaxial tension, yielding is suppressed while brittle failure, presumably caused by crack growth from cavitation, occurs. Therefore the critical dilatational strain energy density was proposed as criterion of failure.

Perez and Pavan [82] tested three amorphous polymers, polymethyl methacrylate, polystyrene and polycarbonate in uniaxial tension, uniaxial compression, plane strain compression and simple shear, over a range of temperatures. In each test, the yield point was precisely determined via residual strain measurements after unloading. With the yield stresses determined for these four different stress states, two pressure dependent shear yield criteria, i.e, the modified Von Mises and the modified Tresca criteria, were checked and compared. It was shown that (i) in each case (material, temperature, initial ageing state), the yield locus is satisfactorily described by either one or the other of the two criteria, and (ii) each criterion can be associated with a specific deformation mode (either homogeneous or localized in shear bands). As for the temperature dependence of the yield stress sensitivity to the hydrostatic pressure, it appears to be related to the glass transition temperature (T_g) and more precisely to the α and β relaxations. Finally, the pressure dependence of the yield stress was explained as being due to two effects: (i) the influence of pressure on molecular motions leading to yielding and (ii) the influence of pressure on the micro-structural state.

By assuming that the failure condition is time and temperature-independent and the strength of polymers is a function of the stress state, the failure condition can be expressed as:

$$f(\sigma_{ij}, k_1, k_2, ...) = 0 \qquad (2\text{-}1)$$

where σ_{ij} are the components of the stress tensor and k_1, k_2 , ... are material constants. The failure condition defines a failure limit of the material under a complex stress state. For isotropic materials, the stress components in Eq. (1) can be replaced by a set of isotropic arguments, for instance, the principal stresses σ_1, σ_2 , and σ_3 :

$$f(\sigma_1, \sigma_2, \sigma_3, k_1, k_2 , ...) = 0 \tag{2-2}$$

In discussing failure conditions, very useful is the geometrical representation of a stress state in the three-dimensional space of principal stresses σ_i (i = 1, 2, 3). Each point with coordinates σ_1, σ_2 , and σ_3 can also be described by the coordinates ξ, η and θ, where ξ is the hydrostatic coordinate with $\sigma_1 = \sigma_2 = \sigma_3$, whereas η and θ are the polar coordinates in a deviatoric plane ξ= const. The coordinates ξ, η and θ, can be expressed in terms of σ_i as follows:

$$\xi = \frac{1}{\sqrt{3}}(\sigma_1 + \sigma_2 + \sigma_3),$$

$$\eta = \frac{1}{\sqrt{3}}\sqrt{(\sigma_1 - \sigma_2)^2 + (\sigma_2 - \sigma_3)^2 + (\sigma_3 - \sigma_1)^2}, \tag{2-3}$$

$$\tan\theta = \frac{2\sigma_2 - \sigma_1 - \sigma_3}{\sqrt{3}(\sigma_1 - \sigma_3)}, \quad -30^\circ \le \theta \le 30^\circ.$$

Therefore, the failure condition results in the relationship

$$f(\xi, \eta, \theta, k_1, k_2 , ...) = 0 \tag{2-4}$$

The form of the failure surface can be determined from experimental data. Numerous tests with polymers show that the failure surface in the space of principal stresses is axisymmetric relative

to the hydrostatic axis, therefore, it is possible to reduce the number of coordinates to two, ξ and η so that the failure condition can be written in the form:

$$f(\xi, \eta, k_1, k_2, ...) = 0 \tag{2-5}$$

Altenbach [6, 7] proposed a new static failure criterion for isotropic polymers with different strengths in tension and compression based on exponential dependence between the mean stress and the von Mises equivalent stress.

The authors assumed an exponential dependence between ξ and η:

$$f = \eta + (\eta + k)\exp\left(\frac{\xi}{\xi_0} - 1\right) - k = 0, \tag{2-6}$$

where k and ξ_0 are material parameters. The two material parameters introduced can be determined by two simple tests, the uniaxial tension and compression. This failure criterion allows a geometrical interpretation. In the space of principal stresses, it defines a smooth, convex rotational surface open in the direction of hydrostatic pressure. It is convenient to represent this surface in two characteristic sections. The intersections of the failure surface with the deviatoric planes ξ=const are circumferences, Fig. 2.8a. A meridional section is shown in Fig.2.8b. It can be noticed as a pure hydrostatic pressure cannot cause failure. The constant k is the limit value of η, since from $\xi \rightarrow -\infty$ it follows that

$$\exp\left(\frac{\xi}{\xi_0} - 1\right) \approx 0, \quad \text{or} \quad \eta \approx k.$$

Hence, the constant ξ_0 defines the vertex of the surface. The locus of the criterion is nearly conical for low hydrostatic pressures and tends to a cylindrical form if an increased hydrostatic pressure is applied.

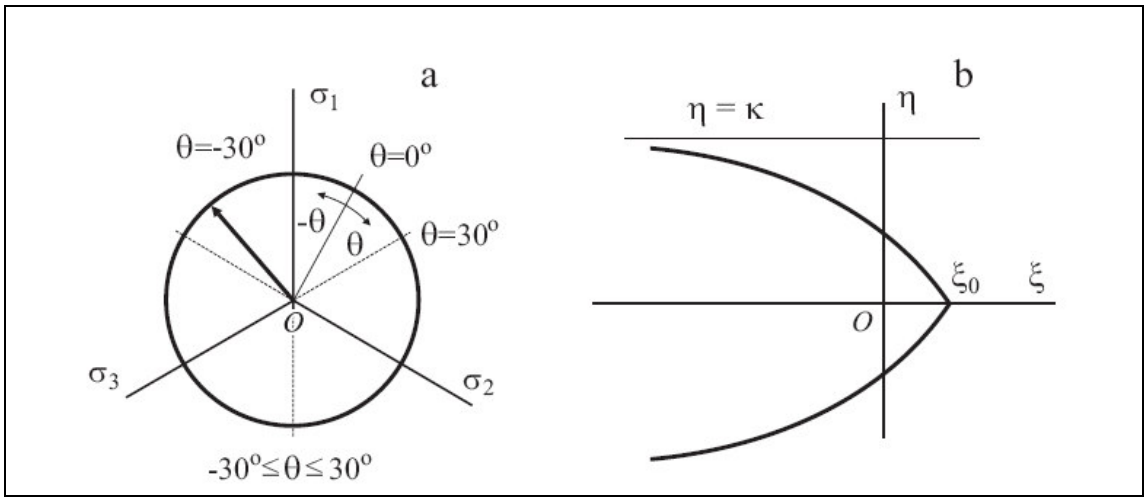

Fig. 2.8 - Representation of the failure surface: a) deviatoric plane and b) meridional plane (η-ξ plane).

The validity of the criterion was demonstrated by experimental strength data taken from the literature for several polymers in the case of superimposed hydrostatic pressure. A limitation in the use of this failure criterion is that for practical application it is necessary to determine experimentally the material parameters.

Bigoni and Piccolroaz [89] proposed a new yield/damage function for modelling the inelastic behaviour of a broad class of pressure-sensitive, frictional, ductile and brittle-cohesive materials. The yield function allows the possibility of describing a transition between the shape of a yield surface typical of a class of materials to that typical of another class of materials.

This is a fundamental key to model the behaviour of materials which become cohesive during hardening (so that the shape of the yield surface evolves from that typical of a granular material to that typical of a dense material), or which decrease cohesion due to damage accumulation. The proposed yield function was shown to agree with a variety of experimental data relative to soil, concrete, rock, metallic and composite powders, metallic foams, porous metals, and polymers. The yield function represents a single, convex and smooth surface in stress space approaching as limit situations well-known criteria and the extreme limits of convexity in the deviatoric plane. The yield function is therefore a generalization of several criteria, including von Mises, Drucker–

Prager, Tresca, modified Tresca, Coulomb–Mohr, modified Cam-clay, and concerning the deviatoric section, Rankine and Ottosen.

Theocaris [90] reconsidered existing failure criteria for isotropic bodies compared with modern versions taking into account either the influence of the strength differential effect or the influence of the internal dilation of the materials on yielding and therefore the contribution of the hydrostatic component of stress in failure. Modern criteria are expressed by quadric polynomials whose coefficients constitute convenient terms of the failure tensor of the material which for the isotropic body is defined by the respective failure stresses in simple tension and compression.

Among the different expressions for the respective failure tensor polynomial of a material the paraboloid of revolution failure locus is the most convenient, since it fulfils the requirements of invariancy relative to any reference coordinate system, it is flexible and yields a unique solution for each loading path while it is unambiguously defined in the stress space. Furthermore, it is in conformity with basic physical laws and the extensive experience that the hydrostatic stress constitutes a safe loading path for the material. Experimental evidence with all varieties of isotropic materials corroborates the theory upon which the criterion is based. Finally, the authors presented a failure criterion, based on void coalescence mechanisms inside the material, which also takes into consideration the influence of internal dilation of the material and therefore it depends on the hydrostatic component of stresses. This criterion is an improvement of the Gurson-McClintock [91-92] criterion which permits a judicial determination of the coefficients of the respective quadric polynomial expressing it, since it belongs to the broad family of criteria based on energy principles.

The Gurson-McClintock failure model [91, 92], based on a description of failure void nucleation and coalescence for the initiation and propagation of cracks in a material, is expressed by a yield

condition, which is based on an upper-bound rigid-plastic solution for spherically symmetric deformations, applied around a spherical inclusion.

This condition is expressed by:

$$\sigma^2_e + 2\, q_1 f\, \sigma_m^2\, ch(q_2\sigma_{hh}/2\sigma_m) - (1+ q_3\, f^2)\, \sigma_m^2 = 0$$

where σ_e is, as usual, the macroscopic effective von Mises stress, given by

$$\sigma^2_e = \tfrac{1}{2}\, s_{ij}\, s_{ij}$$

with s_{ij} the deviatoric components of stresses, whereas $\sigma_{hh}/3$ is the hydrostatic stress. While Gurson assumed values for the constants $\boldsymbol{q_i}$ (i = 1, 2, 3) given by $q_1 = q_2 = q_3 = 1$, it was found [38,43] that a better fitting of results can be achieved, when the influence of neighbouring voids to a central pair of voids is considered, for periodically arranged cylindrical voids in a matrix. If this influence is taken into account in a continuum model without initial voids, these constants should take the values:

$q_1 = 1.5$;

$q_2 = 1.0$

$q_3 = q^2_1 = 2.25$.

Moreover, σ_m is the equivalent tensile flow stress, representing the actual macroscopic stress state in the voided matrix material, disregarding local stress concentrations, and f is the current void volume-fraction.

2.3.3 Review of Literature Related to Damage Modelling

The damage and failure progress in laminated fibrous composite structures is very complicated compared to that of conventional metallic materials. Composite structures may vary their stiffness and strength due to damage accumulation such as matrix cracking and fibre breakage during the loading history of the composite members.

The study of composite materials and structures can be undertaken from two different approaches: micro-mechanical, meso-mechanical and macro-mechanical approaches. In the micro-mechanical approach, the constituent fibre and matrix materials, and their interaction are distinctively considered to predict the overall behaviour of the composite structural member. The damage and failure in fibrous composites are modelled at the fibre and matrix level. In the macro-mechanical approach, the properties of the constituent fibre and matrix materials are averaged to produce a set of pseudo-homogeneous properties for the composite structural member. The macro-mechanical approach does not consider the distinctive modelling of the fibre and matrix materials. The damage and failure of composite structures are examined based on smeared composite stresses and strains. The macro-mechanical approach has the advantage of requiring less detailed modelling than the micromechanical approach. However, the micromechanical approach provides more physical information, e.g. failure of fibre and matrix, as well as load transfer between the two. As a result, a micromechanics model is developed for analyses of laminated, fibrous composite structures. In particular, the strength and stiffness degradation of laminated fibrous composites is analyzed as damage and failure progress.

Micromechanics studies related to continuous fibre reinforced composites deal with detailed micromechanical analyses of fibres and surrounding matrix. These studies model a single fibre or a small number of fibres to predict effective composite stiffness properties, composite strength properties and damage evolution of micro-cracks. While some studies derive analytical solutions, most of the studies use finite element analyses. These investigations show a detailed account of the effects of fibre and matrix properties, fibre-matrix interaction and neighbouring fibre-fibre

interaction on the effective composite material properties of stiffness and strength. Furthermore, a partial fibre-matrix interface debonding as well as local micromechanical cracks, e.g. matrix cracking and fibre breakage are studied to determine their effects on the effective composite material properties.

The importance of the numerical simulation is partly due to the difficulty in conducting tests with special configurations or observing the occurrence of internal damages at different loading levels. This simulation is usually carried out through the use of the finite element method. The analytical models used to represent these materials are either homogenous [93, 94], or heterogeneous in nature. The use of the first type is limited to the macroscopic mechanical evaluation. While the second type, which includes two-dimensional [95] and three-dimensional models [96–99], is dedicated to the microscopic mechanical evaluation. A two-dimensional model is acceptable when plane stress and strain conditions are imposed. However, these conditions are not fulfilled when we deal with structures such as woven composites. For such structures, a three-dimensional modelling becomes necessary, and has been investigated by many researchers. There are numerous papers on the numerical simulation of woven fabric composites, which are limited within linear characteristics such as elastic moduli and initial failure [96–99]. In existing research, only geometric non-linearity was considered without stiffness reduction caused by damage [99], or all damaged stiffness were assumed to be zero [100]. A few non-linear analyses have employed an anisotropic damaged constitutive equation corresponding to its modes [5, 101–103]. As their anisotropic damage model has been based on only experimental knowledge, some questions remain about the selection of reduced components and the determination of reduced values. Therefore, it is required to establish a theoretical anisotropic damaged constitutive equation and finite element analysis considering damage modes for woven fabric composites.

Zako et al [104], developed a theoretical anisotropic damaged constitutive equation based on damage mechanics, and employed it to reveal damage mechanisms for unidirectional fibre reinforced composite materials [105,106]. In a more recent paper Zako et al [107] proposed a non-linear finite element analysis based on the previous results. The utility of the new formulation was proven through its application onto a plain woven fabric composite. The authors employed a three dimensional heterogeneous FE model, which consists of fibres and matrix. Fibres and matrix were treated macroscopically as anisotropic and isotropic homogeneous bodies, respectively. The fibres were arranged unidirectionally within lamina of the composite laminates, but they were in the form of fibre bundles in textile composites. For the fibres, one or more damage modes, such as fibre breaking and transverse cracking, can take place [108]. These modes affect strongly the mechanical behaviour of the structure. An anisotropic damage model for fibres and an isotropic damage model for matrix were utilized by Zako et al [107] to simulate the microscopic damage propagation and thus to characterize the damage modes. Since in general failure criteria can not indicate the type of damage mode, which affects strongly the mechanical behaviour of composites, the damage modes of fibres was classified into four types as shown in Fig. 2.9(a). The axes L, T, and Z (x, y, z in the present work) mean the principal coordinates of orthotropic material, and they correspond to fibre and transverse directions, respectively. According to the local orientation of the fibres, the material coordinates are defined for each element and by calculating the corresponding stress-to-strength ratios for the different modes, the authors deduced that the damage mode that takes place is the one in which the stress-to-strength ratio has the maximum value. Moreover in order to characterize each one of the damage modes, the authors adopted the Murakami's damage tensor [22], which is defined by the following equation:

$$\boldsymbol{D} = \sum_i D_i n_i \otimes n_i \qquad (i = L, T, Z)$$

D_i and n_i are the principal value and principal unit vector of the damage tensor. In matrix form, this is expressed as follows:

$$[D] = \begin{bmatrix} D_L & 0 & 0 \\ 0 & D_T & 0 \\ 0 & 0 & D_Z \end{bmatrix}$$

The characteristics of anisotropic damage model for fibre bundle are depicted in Fig. 2.9(b).

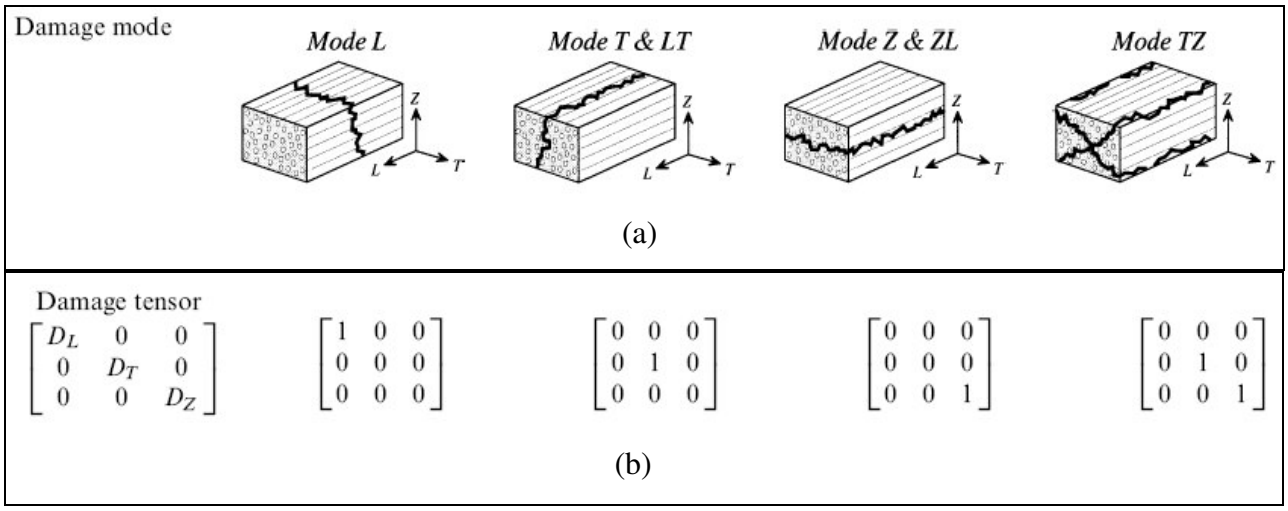

Fig. 2.9 - Characteristics of anisotropic damage model for fibre bundle [107].

Bakuckas et al [110] in their research presented the concept of micromechanical-anisotropic continuum approach to study the mechanistic damage growth at the micro-structural level in centre-cracked unidirectional composite specimens. The methodology developed was incorporated into a displacement-based finite element program to form the Micromechanics Analysis and Damage Growth In Composites (MADGIC) code. One of the unique features of this code is that in simulating the damage growth in the form of propagating cracks, the crack paths need not be selected *a priori.* Damage growth or crack path generation capabilities, were introduced by a node splitting and nodal force relaxation algorithm. Prediction of fibre breakage, matrix cracking and fibre-matrix debonding was accomplished by determining the sequence and direction of node splitting through the employment of appropriate failure criteria. Depending on the location of a node, only certain types of splitting mechanisms may occur. All the nodes must

be classified according to their locations in the composite medium so that failure criteria can be applied appropriately. In Fig.2.10 is shown schematically a state of damage in a unidirectional composite and six possible classes of nodes.

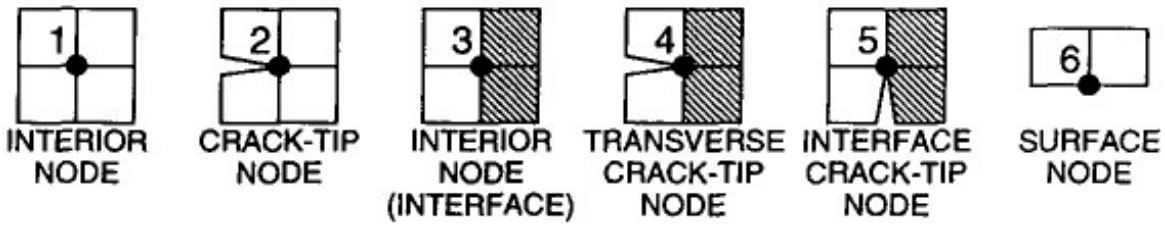

Fig.2.10 - Schematics of node classes.

Due to the modular structure of the MADGIC code, any failure criterion can be readily implemented for each of the different constituents. Only the maximum normal stress and maximum shear stress failure criteria were used in the study. In addition, an incremental flow theory with isotropic hardening has been incorporated in the code to account for matrix plastic deformation when analyzing damage growth in metal matrix composites.

Tabiei et al [111] suggested a micro-mechanical material model of woven fabric composite materials to simulate the progressive failure. The quarter sub-cell of the representative volume cell (RVC) depicted in Fig. 2.11 is divided in many blocks.

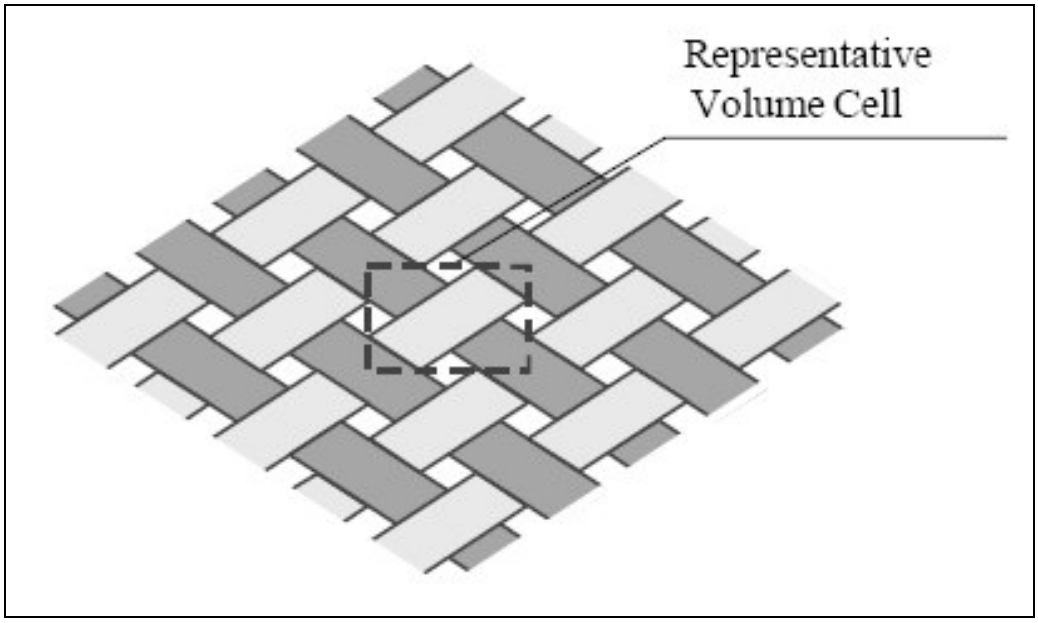

Fig. 2.11 - Woven composite interlacing pattern [111].

Micro-mechanical failure criteria for each constituent material in the block and corresponding stiffness degradation were adopted there. The material shear non-linearity described by Hahn and Tsai is included in the model. The material models of woven fabric composites described by the researchers are suitable for non-linear finite element failure analysis of composite structures, but because of the high degree of RVC discretization, they are computationally inefficient to be applied in explicit finite element codes. The authors developed a computationally efficient and simplified micro-mechanical model of woven fabric composite materials [112] to predict their elastic properties. The advantage of the model is the lack of RVC discretization and good elastic property prediction. The choice of the RVC is intended to account for geometrical non-linearity a simple and efficient technique for fibre reorientation was incorporated in the model [113, 114]. The failure criteria and stiffness degradation scheme is adopted almost entirely from Blackketter et al [5]. The isotropic matrix material in each sub-cell is checked for failure by testing the maximum of the principal stresses:

$$\text{if } \max\{\sigma_{\mathrm{I}}^{\mathrm{m}}, \sigma_{\mathrm{II}}^{\mathrm{m}}, \sigma_{\mathrm{III}}^{\mathrm{m}}\} > X_{\mathrm{m}} \text{ then } d_E = 0.01, \quad d_{fG} = 0.20,$$

where X_m is the tensile strength of the matrix, d_E and d_{fG} are the discount factors. The failure criteria and the degradation scheme for the yarn material are illustrated in Table 2-2.

Table 2-2 Failure criteria and degradation scheme for yarn material [112]

Failure mode	Failure condition	Discount coefficients				
		d_2	d_3	d_{f4}	d_{f5}	d_{f6}
Longitudinal tension	$c_t\sigma_1^y > X_t$	Fiber breakage—ultimate failure				
Longitudinal compression	$-c_c\sigma_1^y > X_c$	Fiber breakage—ultimate failure				
Transverse tension, 2-direction	$\sigma_2^y > Y_t$	0.01	1.00	0.20	1.00	0.20
Transverse compression, 2-direction	$-\sigma_2^y > Y_c$	0.01	1.00	0.20	1.00	0.20
Transverse tension, 3-direction	$\sigma_3^y > Y_t$	1.00	0.01	0.20	1.00	0.20
Transverse compression, 3-direction	$-\sigma_3^y > Y_c$	1.00	0.01	0.20	1.00	0.20
Longitudinal shear, 12-plane	$\lvert\sigma_4^y\rvert > S_l$	0.01	1.00	0.01	1.00	1.00
Transverse shear, 23-plane	$\lvert\sigma_5^y\rvert > S_t$	0.01	0.01	0.01	0.01	0.01
Longitudinal shear, 31-plane	$\lvert\sigma_6^y\rvert > S_l$	1.00	0.01	1.00	1.00	0.01

The failure in the axial direction of the yarn leads to fibre breakage. This kind of failure is considered as an ultimate failure of the composite material.

Kwon et al presented [115] a simplified micromechanics model to predict the effective composite behaviour, as well as to study the damage evolution for composite structures.

The micromechanical model considers a unit cell composed of four subcells by assuming the repetitive or periodic nature of the fibre and matrix materials. One subcell represents the fibre and three subcells represent the matrix material. The unit cell is a three-dimensional solid, the rectangular parallelepiped. As shown in Fig. 2.12, the unit cell models a quarter of a fibre embedded in a matrix material because of symmetry.

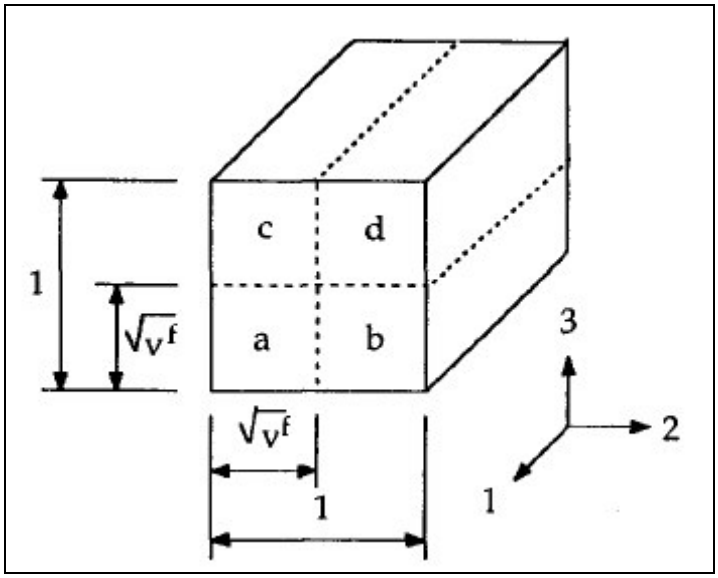

Fig. 2.12 - A unit cell made of subcells (a-fibre; b, c and d-matrix) [115].
(1-, 2-, 3-directions are respectively *x*-, *y*-, *z*-directions in the present work).

The unit cell has dimensions of unity. The size of each subcell is dependent on the fibre volume fraction.

Incorporating this micromechanical model into a finite element analysis program for composite structures provided the following sequence of calculations:

(1) Compute the effective material property matrix of the fibrous composite from the fibre and matrix material properties, and the fibre volume fraction using the present micromechanics model.

(2) Find the nodal displacements from the finite element analysis of the composite structure using the effective material property matrix. For a laminated structure, the effective material property matrix should be transformed according to the rotation of the axes of each layer.

(3) Compute the composite strains from the displacements.

(4) Compute the fibre and matrix strains from the composite strains.

(5) Determine the fibre and matrix stresses from the fibre and matrix strains using their constitutive equations.

(6) Calculate the composite stresses from the fibre and matrix stresses.

(7) If necessary, calculate the residual force vector from the composite stresses for iterations.

The micromechanical damage and failure process was considered based on the fibre and matrix stress level, because the fibre and matrix stresses are computed explicitly. Once failure criteria are satisfied, the material property of the fibre or matrix is degraded to induce stress unloading at the failure location. For matrix cracking, the matrix property is degraded while the fibre property is degraded for fibre.

The effect of waviness in the fibre yarns were investigated by Ismar et al in [116]. Considering the fibre bundle arrangement to be periodical, the unit cell of Fig. 2.13 can be used to characterize a two-dimensional woven composite.

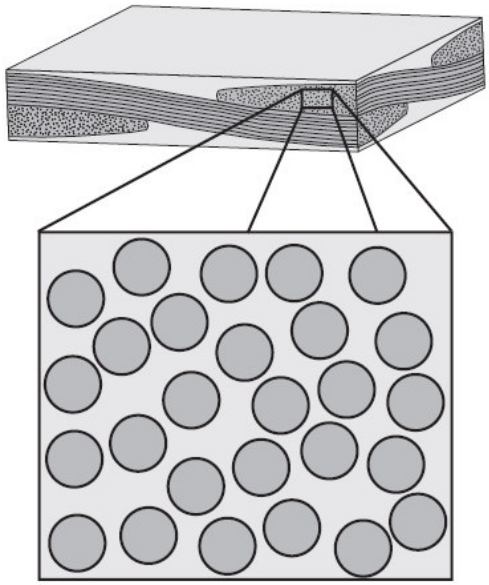

Fig. 2.13 - The built-up of the fibre bundles.

The damage behaviour of the fibre bundles strongly depends on the loading situation. The Fig. 2.14 shows a fibre bundle in different basic loading situations.

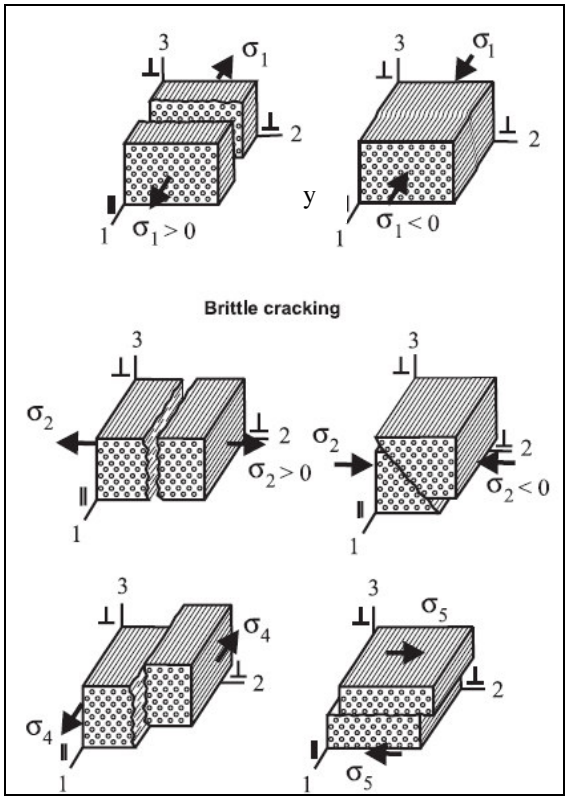

Fig. 2.14 - Damage behaviour in fibre bundles [116].
(1-, 2-, 3-directions are respectively *x*-, *y*-, *z*-directions in the present work).

The linear elastic behaviour of the fibre bundles under tensile loading in fibre direction ends because of crack initiation in the matrix and fibre-matrix debonding. At higher stresses multiple fibre breaking occurs and causes the end of the load bearing capacity of the fibre bundles. Considering the fibre bundles as homogeneous on the yarn scale these micromechanical damage events (matrix cracking, fibre breaking and debonding) result in a reduction of the elastic coefficients of the fibre bundles. Primarily the Young's modulus E_x, the Poisson's ratios ν_{xy}, ν_{xz} and the moduli of shear G_{xy}, G_{xz} are reduced by these events.

Because of symmetry, the material behaviour perpendicular to the fibre direction can be considered to remain isotropic during progressive loading: $\nu_{xy} = \nu_{xz}$ and $G_{xy} = G_{xz}$. In order to describe the damage behaviour of the fibre bundles parallel to the fibre direction the authors used three damage variables D_E, $D_{\nu,}$ D_G to increase the material degradation of the fibre bundle in the

fibre direction. By using damage variables the authors were able to describe the nonlinear behaviour of the fibre bundles in the fibre direction, while the commonly used fracture criteria only distinguish between total integrity and total fracture of the structure regarded.

2.3.4 Review of Literature Related to Thermal Residual Stresses

Most composites are made at an elevated temperature: as the thermal expansion coefficients of the fibres generally do not match those of the matrix, thermal residual stresses will be generated in both the fibres and the matrix when the composite cools down to room-working temperature. While these residual stresses essentially do not affect the composite stiffness, they do influence the composite strength. The amount of influence depends on the temperature variation and on the thermal–mechanical properties of the constituent materials. It is, thus, necessary to incorporate the thermal residual stresses into the composite strength formulae. Several attempts have been made in the past to understand thermal load effects on composite behaviours.

Schapery [117] obtained explicit expressions for the overall thermal expansion coefficients based on the thermo-elastic extreme principle, using only the constituent thermal-elastic properties and the fibre volume fraction. The Schapery's formulae are known to be sufficiently accurate, especially for the longitudinal thermal expansion coefficient of the composite [118]. However, the Schapery's results can also be obtained upon an assumption of free-transverse stresses [46]. Therefore, Schapery's formulae are less accurate for thermal stress analyses. In [118] Huang incorporated these thermal residual stresses into isothermal strength formulae of a unidirectional composite described in [51].

The fabrication process of fibre-reinforced polymer matrix composite materials requires a high temperature curing procedure.

A typical curing process consists of two steps:

(1) isothermal curing at an elevated temperature during which the polymer shrinks as a result of the purely chemical reaction (polymerisation) and builds up stiffness while the reinforcement remains unchanged;

(2) thermal cooling from the curing temperature to room temperature during which both polymer and reinforcement contract but by different amount and in addition the polymer may change its stiffness significantly.

Chemical shrinkage and thermal cooling contraction of polymer resin are constrained by the surrounding fibre reinforcement, which inevitably results in the development of residual stresses both at the fibre/matrix interface and inside the bulk resin and fibre. Therefore, cure residual stress is contributed by the chemical shrinkage of the curing resin and the thermal cooling contraction of the resin and fibre system. Shrinkage stress is a direct result of volume changes of polymer matrix that occur during the polymerization process and will depend on the chemical nature of the material and the curing procedure. During curing, the polymer can go through two main transitions: gelation and vitrification. Gelation corresponds to the formation of molecular networks and vitrification occurs when the glass transition temperature T_g of the polymer reaches the curing temperature. If the material is isothermally cured above the glass transition temperature, only gelation will occur. When the material is cured below the glass transition temperature, it will first gelate and then vitrify. The gelation process results in an equilibrium elastic modulus, whereas vitrification is associated with the transition from a rubbery modulus to a glassy modulus. The change in elastic modulus associated with gelation and vitrification, together with the volume contraction of the polymer, is the dominant factor in the occurrence of the shrinkage stress [120]. Thermal cooling stress arises from the mismatch in the coefficients of thermal expansion of the fibre and matrix. During cooling, both constituents contract but the full contraction of the matrix is constrained as a consequence of being bonded to the fibre. On the

other hand, the fibre is not only shortened by its own thermal contraction, but is also compressed by the constrained contraction of the matrix. As a result, residual compressive stresses are induced in the fibre. At the same time, the matrix is constrained by the fibre from full contraction, and as a result, is stressed in tension. The magnitude of these stresses will depend on the properties of the fibre and resin system including the thermal expansion coefficient α, Poisson's ratio ν and elastic modulus *E*.

The resulting stresses are sufficient to initiate fracture within the matrix immediately around the fibre [1, 2]. Therefore, it is important to determine the current state of the residual stresses and their effects on the behaviour of the composite when subsequently subjected to multi-axial mechanical loading. After curing and cooling of the composite, the matrix is subject to a triaxial residual stress state [119]. The resulting thermal residual stresses are of compressive nature in the fibre and tensile nature in the matrix [120].

Numerous methods have been developed to determine the residual stresses in polymer-matrix composites both experimentally and analytically. In general, experimental methods fall into two categories, namely destructive and non-destructive methods. Destructive methods, such as hole-drilling [121], sectioning/cutting [122] and first-ply failure test [123], require the specimen to be destroyed during testing and therefore cannot be used for *in-situ* measurements. Non-destructive tests include warpage/curvature measurements [124], the cure-reference method [119] and techniques using embedded sensors (strain gauges, fibre optics or crystalline materials) with an X-ray or neutron diffraction method [125, 126].

As far as analytical methods are concerned, residual stresses in composites are generally studied on the macro and meso/micro levels. On the macro-level, classical laminate theory is generally used and gives predictions at the ply level [127-129]. On the meso/micro-level, a Representative Volume Element (RVE) or unit cell which represents the meso/microscopic periodic structure of

the laminate is constructed and the analysis is often carried out using a numerical procedure such as the finite element method [130-132].

Three dimensional finite element models have been employed to study the influence of residual stresses on shear response of the composites [35, 36]. More recently, a finite element micro-mechanical based model has been developed to investigate the off-axis behaviour of unidirectional composites [37]. This model is general and can be used for any combination of normal and shear loading with residual stresses.

Analytical approaches include methods based on the Self-Consistent Model (SCM) of Hill [25], extension of the Eshelby's equivalent inclusion technique [27], Vanishing Fibre Diameter (VFD) model of Dvorak [30], Concentric Cylinder Models [28, 31] and Aboudi's Method of Cells [33]. The effects of thermal residual stresses on mechanical behaviour of the composite materials have also been extensively studied by Nimmer [133] and Wisnom [25]. They examined the transverse behaviour of high temperature composites in the presence of thermally induced residual stress fields and found that the presence of residual stresses is beneficial for the transverse behaviour of composites with low interfacial strength due to the generation of compressive residual stresses at the interface of the fibre and matrix, for example, positive hoop stresses around the reinforcing fibre may augment the pull-out energy dissipation and thus increase toughness [133].

Residual stress and strain fields at the fibre-matrix or tow level can be predicted from the meso/microscopic unit cell model. The formation of residual stresses, especially the tensile stress in the matrix, is generally detrimental in the production of polymer-matrix composite parts, since the stress can be high enough to initiate material damage before loading such as interface debonding and matrix micro-cracking as shown in Fig. 2.15 [134, 135].

The initial damage can reduce the stiffness and the strength of the material, as well as acting as sites for environmental degradation and nucleation of macro-cracks. Therefore, any analytical or experimental study involving damage and fracture mechanics of composites should take into account residual stresses if they exist. For glass fibre epoxy resin model composites, Fiedler et al showed that the thermal residual stresses can be calculated by finite element analysis (FEA) using the actual temperature dependent stiffness of the resin [136].

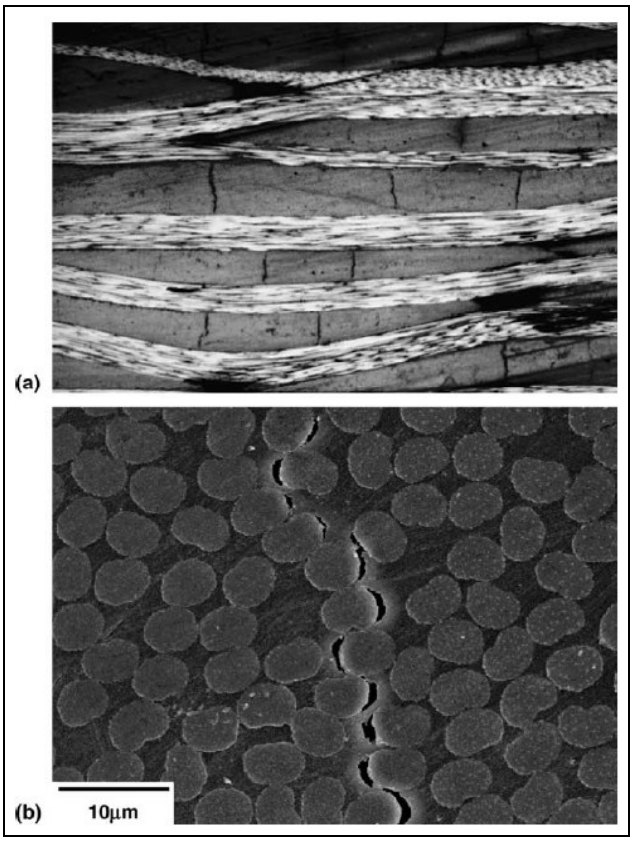

Fig. 2.15- Transverse tow micro-cracks in a woven graphite fibre polyimide composite. Individual tow micro-crack from (a), fibre/matrix debonding [134].

Asp et al [64] showed by a FEA study that the thermal residual stress strongly reduces the ultimate strength of transversely loaded unidirectional (UD) composites. When load is applied to the fibre-reinforced composite the triaxial stresses in the matrix increase. Both the polymer matrix and the fibres cannot behave as they would individually as bulk materials, and the difference in the Poisson's ratios causes a triaxial stress state reducing the maximum bearable

load. In recent studies [64, 69], it was shown that yield criteria are applicable to glassy polymers under uniaxial, biaxial and triaxial loading if the hydrostatic stress effect is accounted for. Also it was found that for UD composites yielding is suppressed while a brittle failure due to crack growth occurs. Fiedler et al also demonstrated that the parabolic Mohr failure criterion is suitable to describe the experimentally observed macroscopic yield and fracture behaviour of epoxy resin [88, 137]. The residual stresses depending on the local fibre distribution can improve or reduce the local ultimate transverse strength of the composite [137].

2.4 Review of Literature Related to the Constituents

Clearly unidirectional composite materials are seen to have a highly anisotropic properties with excellent stiffness and strength in the fibre direction and rather poor properties in the transverse direction due to high heterogeneity of composites. Moreover in all loading directions, the macroscopic behaviour is influenced by phenomena occurring at microscale. In the longitudinal and in the transverse direction, the stress transfer from the polymer matrix to the fibre determines the overall mechanical behaviour. Especially under longitudinal loading the failure mode is influenced by the strength of fibre/matrix adhesion. Hence, a better understanding of mechanical behaviour of composites at macroscale can only be achieved with a study of a more realistic microstructure.

In fact, the matrix undergoes micro-structural modifications in the vicinity of the fibres due to local changes of chemical and physical processes such as crystallisation and cross-linking. The region of the matrix affected by the presence of fibres referred to as the interphase region highly affects the mechanical behaviour of polymer composites. It has also been shown [1] that the nature of the fibre surface can affect the curing kinetics and cross-link density of nearby matrix. As shown by Gao et al [138,139] the local microstructure can be appropriately engineered by various fibre surface treatments, causing property differences between the interphase region and

the bulk matrix. The authors [138, 139] conducted a comparative study of the fibre sized topography and modulus as well as the local mechanical property variation by using tapping mode phase imaging and nano-indentation tests based on the atomic force microscope (AFM). Their results demonstrate that the nature of the interphase within a thickness less than 1μm is able to modify the overall mechanical response of three-phase composites.

Kobayashi et al [140] showed that initial microscopic damages, such as transverse cracks, can be suppressed when a tough and flexible fibre/matrix interphase is applied to the composites hence, as a result, the durability of composites is improved, since transverse crack causes other severe damage, such as delamination and/or filament breakage. In order to suppress microscopic damages in the composites the authors [140] also developed a method to fabricate epoxy-based woven fabric composites with a flexible interphase. It was demonstrated that strength and maximum strain increased with interphase content. The reason is that the microscopic damaged zones, which cause local stress concentration in warp fibre bundles, were suppressed by the flexible interphase. Moreover first cracking strains were delayed and crack densities became smaller in laminates containing the interphase.

Tanoglu et al [141] used a novel experimental technique (dynamic micro-debonding technique) to test and characterize the interphases of various sized E-glass-fibre/epoxy-amine systems at displacement rates in the range 230±2450 μm/s. A schematic of the test configuration is shown in Fig. 2.16.

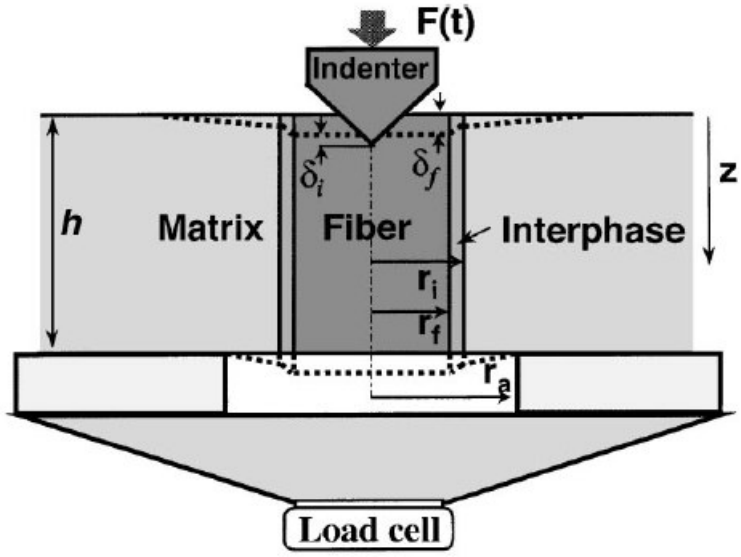

Fig.2.16 - Schematic of test configuration and the micro-debonding process [141].

For this technique, a new apparatus called the dynamic interphase-loading apparatus (DILA) was designed utilizing the fast expansion capability of piezoelectric actuators. This method enables one to quantify the interphase strength and the energy absorption due to debonding and frictional sliding over a wide range of loading rate. The loading rate achieved using DILA was about three orders of magnitude faster than the rates reported in the literature using traditional methods.

The authors performed a case study based on a typical glass/epoxy composite subjected to ballistic impact to determine the significance of the interphase-related micro damage modes in absorbing the impact energy. These results showed that the energy absorbing capability and the shear strength of the fibre/matrix interphase is affected by the properties of the interphase and the loading rate. In summary, the authors concluded, an interphase that has lower strength may better contribute to energy absorption, while an interphase with higher strength is needed for structural integrity and environmental durability.

An elaborated research was developed by Matzenmiller et al [142] based on the generalised method of cells (GMC) to quantify the overall effective properties of the composite with an elastic interphase region of finite thickness. This method is based on the analytical homogenisation scheme of the cells method where the in situ properties of the interphase are determined from the effective properties of the composite and the parameters for the bulk material of the individual phases. The GMC allows the modeling of arbitrary shaped inclusions in a matrix. Therefore, the interphase region, comprising the material adjacent to the bond, may by taken into account as a thin layer of subcells between the fibre and the matrix phase. A comparison between a GMC and FEM models is shown in Fig. 2.17.

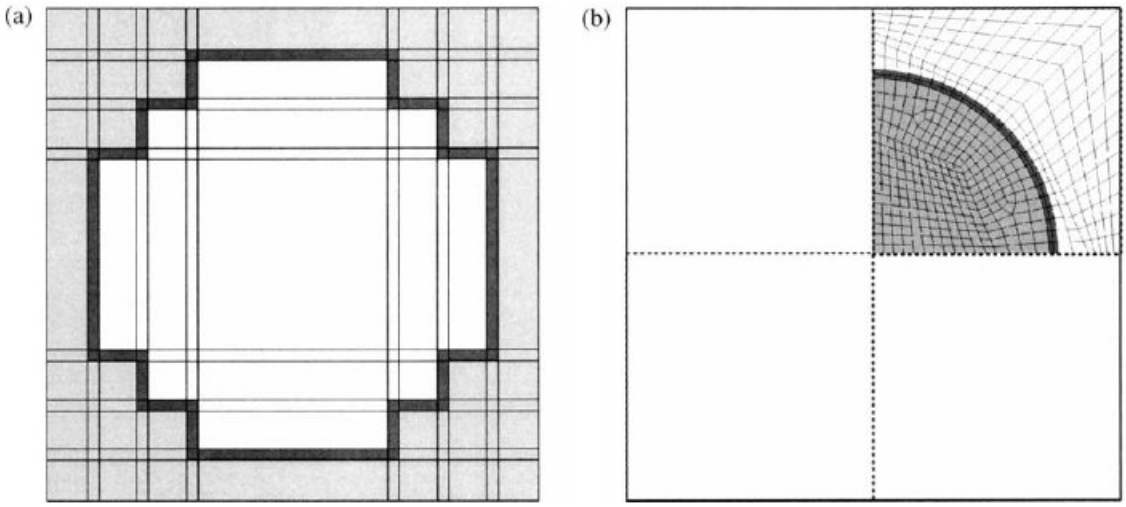

Fig. 2.17 - RVE with interphase modelled by (a) GMC and (b) FEM [6].

The inverse determination of the interphase properties from the effective material moduli requires the detailed knowledge of the microscopic structure of the composite. With the results of the inverse identification for the interphase properties it is possible to evaluate the mechanical effect of the various manufacturing influences on the interphase characteristics. Although the interphase parameters were successfully identified by the authors from the experimental data for most composites with various chemical treatment of the fiber surface, the numerical results are still not

satisfying in all cases. In fact, numerical analyses showed that the interfacial properties are unrealistically high for the fibre-matrix-interphase systems if a transverse isotropic material model is assumed for the calculation of the overall composite behaviour.

In the recent past, using a finite elements analysis, Asp et al. [8, 143] studied the stress distribution in an ideal composite constituted by a square array of fibres. These researchers employed a failure criterion based on the dilatation energy which accounts for the influence of stress triaxiality on the matrix behaviour. The dilatational (volumetric) energy density for a linear elastic material is given by:

$$U_v = \frac{1-2\nu}{6E}(\sigma_1 + \sigma_2 + \sigma_3)^2$$

where σ_1, σ_2, and σ_3 are the principal stresses, and ν and **E** are the Poisson's ratio and Young's modulus, respectively. The authors demonstrated that transverse failure mechanism of laminates is governed by the storage moduli of the constituents, by the glass fibre content, and eventually by the presence of an interphase. The model also predicted an increase of failure stress and strain when incorporating a soft rubbery interphase between fibre and matrix. Especially under longitudinal loading the failure mode is influenced by the strength of the fibre/matrix adhesion.

Podgaiz et al [144] observed a decrease of transverse failure strain and stress when coating glass fibres with elastomer sizings (flexible epoxy or polyvinyl). They suggested that the low tensile strength of elastomers and a poor level of adhesion between the rubbery interphase and the epoxy matrix could be responsible for the poor performance of such composites. According to the authors, tensile strength of the interface/interphase is a crucial parameter for transverse properties of composites. More recently Benzarti et al [145] performed an investigation on effects of fibre surface treatments on transverse mechanical behaviour of unidirectional glass/epoxy composites. Model composite plates were processed by filament winding using glass fibres coated with

different sizings changing by their epoxy functionality and their reactivity towards the matrix. Experiments (transverse tension and micro-indentation characterisations) revealed that the most reactive sizings promote the highest interfacial strength and also increase ultimate properties of laminates in transverse tension. This feature was attributed to the high crosslink density of the polymer network in interfacial areas. The authors also carried out finite element calculations in order to evaluate local strain and stress concentration in a composite submitted to transverse tension conditions. The numerical modelling showed that a transition of the composite failure mode occurs at a global strain of 1.15%, from an adhesive rupture at the fibre/matrix interface to a cohesive rupture in the matrix. In the domain of adhesive rupture, the value of the composite failure strain appeared to be directly governed by the interfacial strength. These authors found therefore that improving interfacial strength by use of fibre sizings with high epoxy functionality could constitute an interesting way to reduce transverse brittleness of composite structures.

Foley [146] by means of a technique utilizing the indenting capabilities of the atomic force microscope (AFM) evaluated the local changes in material response of polymer composite systems near the fibre–matrix interface for two model composite systems at both room temperature and elevated temperatures. Eventually these authors compared the AFM indentation results with finite element model predictions to gain a fundamental understanding of the influence that the interphase properties have on the measured responses. They found good agreement between the finite element model predictions and the AFM measured results for all cases studied. The finite element results confirmed that the interphase region for an unsized graphite fibre is too small (relative to the physical size of the indentation probe) to conduct realistic characterization. However, the sized fibre case has an interphase region sufficiently large to obtain useful measurements. The finite element model was finally used to identify the effects

of interphase region size on the potential usefulness of the AFM as a viable interphase characterization method.

Effects of residual stress on damage were investigated by Aghdam [147]. These researchers developed a three-dimensional finite element micromechanical model to study effects of thermal residual stress, fibre coating and interface bonding on the transverse behaviour of a unidirectional SiC/Ti–6Al–4V metal matrix composite (MMC). The model includes three phases, i.e. the fibre, coating and matrix, and two distinct interfaces, one between the fibre and coating and the other between coating and matrix. The model was employed to investigate effects of various bonding levels of the interfaces on the initiation of damage during transverse loading of the composite system. Moreover the authors adopted two different failure criteria, which are combinations of normal and shear stresses across the interfaces in order to predict the failure of the fibre/coating and coating/matrix interfaces. It was shown that any interface fails as soon as the stress level reaches the interfacial strength.

Wang [148] presented an extension of the work by Mogilevskaya and Crouch [149] to model micromechanical behaviour and macroscopic properties of fibre-reinforced composites with radially graded interphases. The approach is based on the numerical solution of a complex boundary integral equation in which the boundary parameters are expressed in terms of complex Fourier series. All the integration can be done analytically and thus the method allows for accurate calculation of the elastic fields anywhere within the material, including inside the fibres and interphases. Explicit expressions for the effective elastic constants can be obtained from general relations between the average stresses and strains. The interphase layer for each inclusion was modelled by the authors with a system of thin bands with different properties that are constant for each band but vary from band to band to provide the piece-wise constant

approximation of the function that governs the gradation of the interphase material. In the numerical implementation, each radially graded interphase j has been discretized into a series of n_j concentric layers characterized by homogeneous elastic properties (Fig. 2.18).

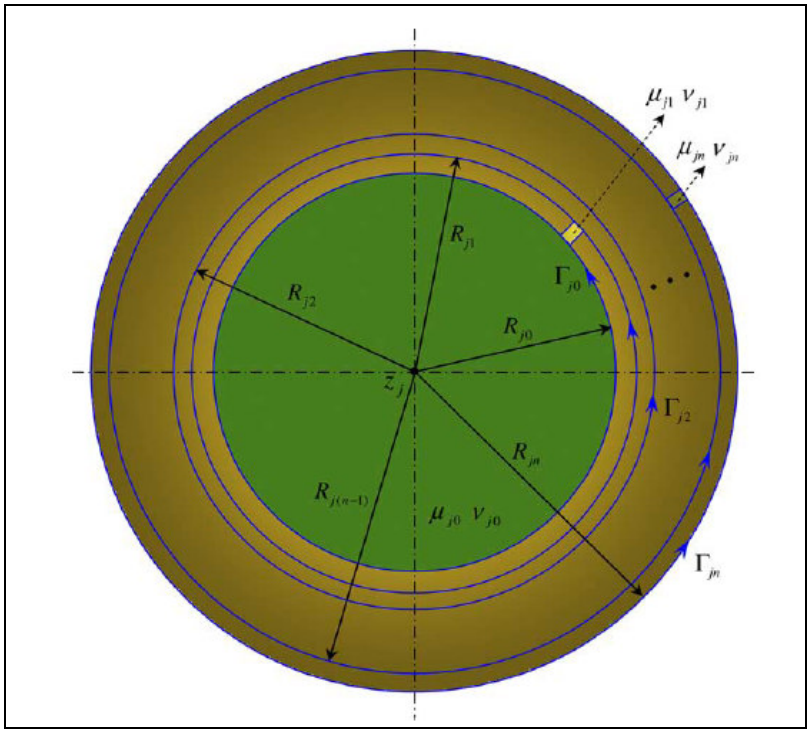

Fig. 2.18 - Discretization of a radially graded interphase into n-layered homogeneous interphases [148].

The authors proved that this approach show high generality and versatility for large number of fibres with arbitrary sizes, locations and elastic properties and especially for the micro-scale the method allows for accurate calculation of the elastic fields anywhere within the material, including inside the fibres and interphases. Moreover the interphases can also have arbitrary thickness and elastic properties.

Fisher et al [150] investigated the mechanical property predictions for a three-phase visco-elastic (VE) composite by the use of two micromechanical models: the original Mori–Tanaka (MT) method and an extension of the Mori–Tanaka (MT) solution developed by Benveniste [151] to

treat fibres with interphase regions. Whilst MT method does not model the geometry of an annular interphase region surrounding the fibre inclusion, but treats the fibre and interphase regions as separate, physically distinct regions as shown in Fig. 2.19, the Benveniste model maintains the proper fibre-interphase-matrix geometry as shown in Fig. 2.20. It utilizes a related auxiliary problem (i.e. a single fibre-interphase inclusion within an infinite matrix material) to find the stress-concentration tensors relating an applied far-field stress to the phase-averaged stresses of the included (fibre and interphase) phases.

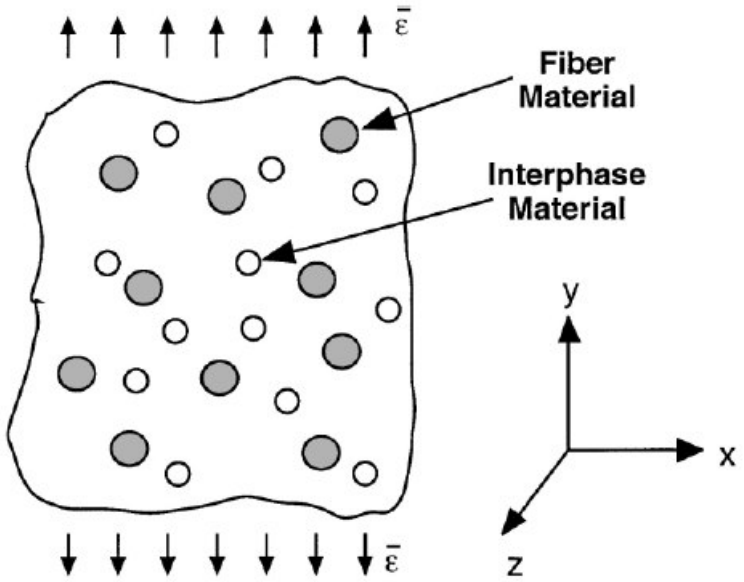

Fig. 2.19 - Interphase modeled as a distinct inclusion region for the Mori–Tanaka method.

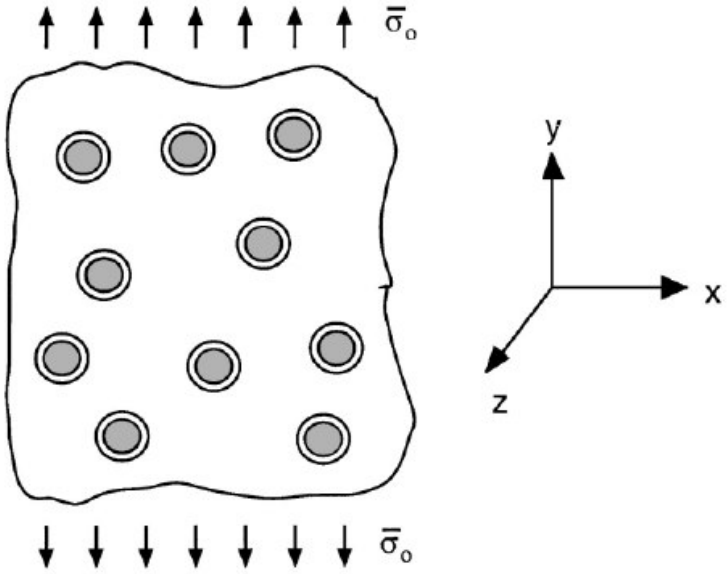

Fig. 2.20 - Three phase composite model for the Benveniste solution.

The main goal of their research was principally to optimize composite properties through engineered interphases and to measure the interphase mechanical properties through experimental tests,

The several case studies performed in this research were used to compare the composite moduli predicted by each of these methods, highlighting the role of the interphase. Although the authors proved that the MT method, in general, provides a reliable micromechanical approximation of the viscoelastic behaviour of the composite; however, the micromechanical methods only provide an order-of-magnitude approximation for the effective moduli. Moreover the FEA results suggest that the interphase plays a large role in determining the overall behaviour of the composite.

Another factor that strongly influences the material micromechanical properties is related to the distribution of the fibres over the cross-section in real composites.

In a unidirectional composite at micro level fibres are embedded in the matrix material parallel to the longitudinal direction. In the transverse cross-section (perpendicular to the fibre direction) a random distribution of fibres exists and generates transverse isotropic properties. To model the fibre distribution in the transverse plane, the simplest idealization for analytical or numerical approaches is to adopt for example a hexagonal or a square array of fibre packing geometry. These packing geometries assume a uniform distribution and periodic packing of the fibres and are greatly convenient in numerical modelling since representative elements of a limited size can be used. Moreover the boundary conditions for both analytical and numerical analyses can be constructed in a simple way [22].

As in UD composites fibres arrangement in the matrix over the transverse cross section is generally at random, a more realistic response on a local as well as a global level can be obtained by taking into account a non-uniform packing geometry. In micromechanical finite element analyses of UD composites of fibres distributed at random over the transverse cross-section using 'unit cells', boundary conditions for such 'RVEs' can no longer be prescribed precisely due to the lack of symmetry about the boundary. Wongsto and Li [152], studied the effects of incorrectly prescribed boundary conditions for such RVEs on the predicted behaviour of the composite represented by the 'unit cells'. The decaying characteristics of such effects far from the boundary, accordingly to the Saint Venant's principle, have been examined. A decay length has been found to amount to a couple of times of the centre-to-centre fibre spacing. Using the decay length obtained, analyses have been made to UD composites in which fibres are really distributed at random over the transverse cross-section. Although, the prescribed uniform normal displacement along the boundary represents an incorrect boundary condition, correct deformation and stress distribution can be obtained from a sub-domain of the unit cell away from the boundary by a number of times of average fibre spacing.

Aghdam and Dezhsetan [153] extended the geometry of the Simplified Unit Cell (SUC) model, to study effects of random fibre arrangement on the mechanical and thermal characterizations of unidirectional composites to predict the behaviour of a fibrous composite subjected to thermal and mechanical, normal and shear, loading .

Fang and Liu [154] examined the effects of different cross-sectional geometry, such as the fibre shape (circular, square and lozenge), size and random fibres distribution on the transverse elastic and plastic deformation of the metal-matrix composites with specific randomly distributed, aligned continuous fibres. Numerical results showed that the overall transverse plastic flow of the composites is rather sensitive to the fibre geometric parameters while the elastic properties exhibit a much lower sensitivity to the fibre distribution.

Bulsara [155] performed a systematic study of a multi fibres RVE size appropriate for characterizing initiation of damage under a tensile load normal to fibres in a unidirectional ceramic-matrix composite. In this case, the damage initiation process showed little sensitivity to the radial distribution of fibres in the cross-section when a tensile load normal to fibres was applied. However, significant dependence on the fibre distribution was found when thermally-induced damage was considered.

Gusev et al [156] used a combination of numerical and experimental techniques to study the fibre packing and elastic properties of a transversely random unidirectional glass/epoxy composite. They showed that measured and numerical results were in excellent agreement and moreover randomness of the composite microstructure had a significant influence on the transverse composite elastic constants while the effect of fibre diameter distribution was small and unimportant. A comparison between analytical approaches and finite element analyses (FEA) for varying fibre distributions, ranging from single fibre unit cells to complex cells was performed by Rossol et al. [157] on metal matrix composites. Analysis of micro-fields showed that the main

cause for deviation from the equistrain rule of mixtures is a stiffening effect of matrix confinement when surrounded by touching fibres arranged as ‘‘rings’’ (Fig. 2.21).

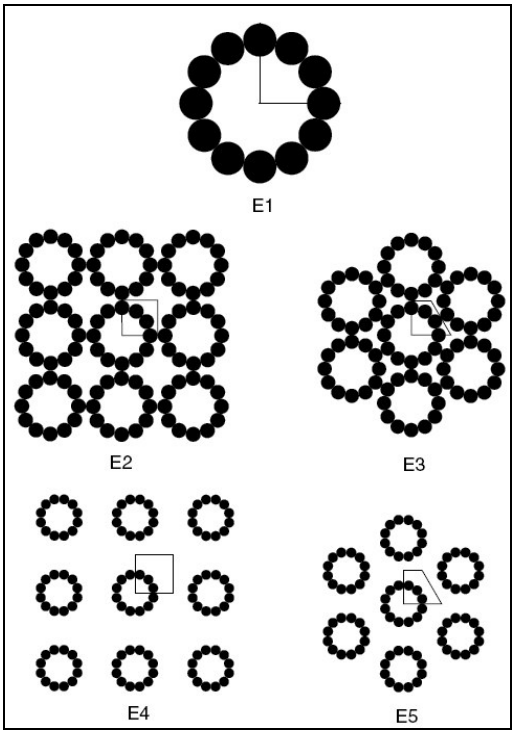

Fig. 2.21 - Artificial arrangements of fibres forming rings. The frame designates the unit cell for FEA. E1: Single ring of 12 fibres confining the matrix. E2: Periodic cubic arrangement of E1. E3: Periodic hexagonal arrangement of E1. E4: Periodic cubic arrangement of E1, but fibre rings are distant. E5: Periodic hexagonal arrangement of E1, but fibre rings are distant. In cells E2–E5 the matrix is both inside the fibre rings as well as in between them [157].

The Boundary Element Technique (BEM) and the embedded cell approach (ECA) were adopted by Knight et al [158] to investigate the micromechanical response of fibre-reinforced materials. The geometrical structures examined (multi-fibre RVE) were formed by uniformly spaced fibre arrangements (square and hexagonal array) and randomly placed fibres within the matrix. Non-periodic arrangements give rise to higher local stresses, and the magnitudes of these stress concentrations have a strong dependence on the ligament length (distance between the two neighbouring fibres that have a common high-stress region), and to a lesser extent on the angle relative to the applied load (angle between a plane containing the two fibre centres and the applied load).

In the analysis of materials with random heterogeneous microstructure the assumption is often made that material behaviour can be represented by homogenized or effective properties. While this assumption yields accurate results for the bulk behaviour of composite materials, it ignores the effects of the random microstructure. The spatial variations in these microstructures can focus, initiate and propagate localized non-linear behaviour, subsequent damage and failure. Baxter et al [159] used a computational method, moving window micromechanics (MW), to capture microstructural detail and characterize the variability of the local and global elastic response and to generate material property fields characterizing the non-linear behaviour of random materials under plastic yielding. The basis of the moving-window technique is a digitized image of the material microstructure in which the phases are visually distinguishable i.e., the greyscale level of each pixel can be used to designate it as one or the other of the phases of the composite (Fig. 2.22).

Digital images of material microstructure describe the microstructure and a local micromechanical analysis was used to generate spatially varying material property fields. The strengths of this approach are that the material property fields can be consistently developed from digital images of real microstructures, they are easy to import into finite element models (FE) using regular grids, and their statistical characterizations can provide the basis for simulations further characterizing stochastic response.

Fig.2.22 - Sample fibre-reinforced composite material.
Fibres are white, matrix is black [159].

The use of a locally non uniform unit cell (Fig. 2.24) accounting for inhomogeneous fibre distribution but still able to preserve the convenience of RVE when applying the boundary conditions have been adopted by Zhang et al [160, 161]. These studies have been performed in order to investigate the transverse creep behaviour of UD reinforced glass-fibre composites with unsaturated polyester in which the matrix shows a non-linear viscoelastic constitutive behaviour. The new geometries seem to be more suitable than the traditionally used regular packing geometries in fact they displayed good agreement with experimental data and moreover reveal a detailed stress and strain distribution and redistribution over time on a local level.

Generally, inhomogeneous coefficient of thermal expansion (CTE) and stiffness of the matrix and fibre cause microscopic internal residual stresses even in unidirectional composites. In order to investigate the effect of fibre arrays on such residual thermal stresses at the fibre–matrix interface in a unidirectional lamina, three different fibre arrays with various fibre volume fractions (FVF) were considered by Jin et al [162]: square and hexagonal regular arrays, and a random array, as illustrated in Fig 2.23. The generation of the RVE for the random fibre array

follows the same procedure described in the authors' previous work [163]. The RVEs are generated for various FVFs ranging from 0.1 to 0.6. When FVF is 0.6, the RVE for the random fibre array contains about 200 non-overlapped fibres. In order to simulate a sufficiently large number of fibres without computational difficulties in modelling and analyzing, ten sets of RVEs for each FVF were constructed using the same procedure.

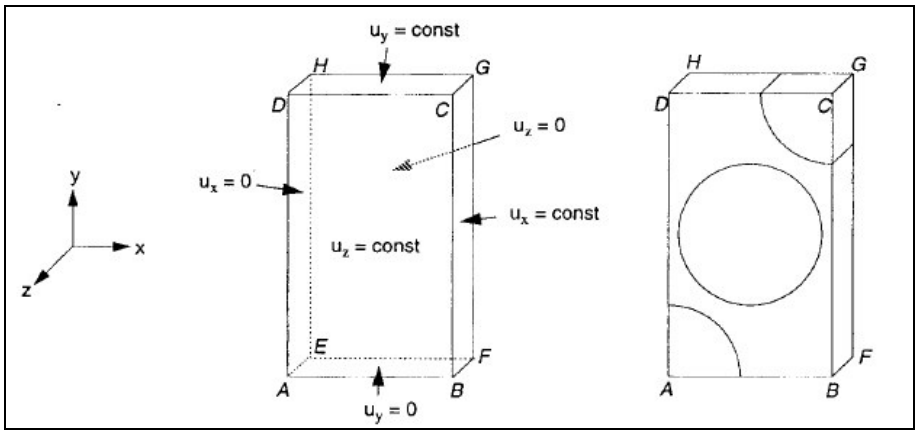

Fig 2.23 - Boundary conditions for the non-locally uniform unit cell [160].

The generated RVEs were statistically verified using the nearest neighbour distribution function and the radial distribution function [163–165], showing that the simulated RVEs have a statistically equivalent spatial distribution and represent the real microstructure of the composite. A three-dimensional finite element analysis was performed to analyze the residual thermal stresses within the given RVEs, as shown in Fig. 2.24.

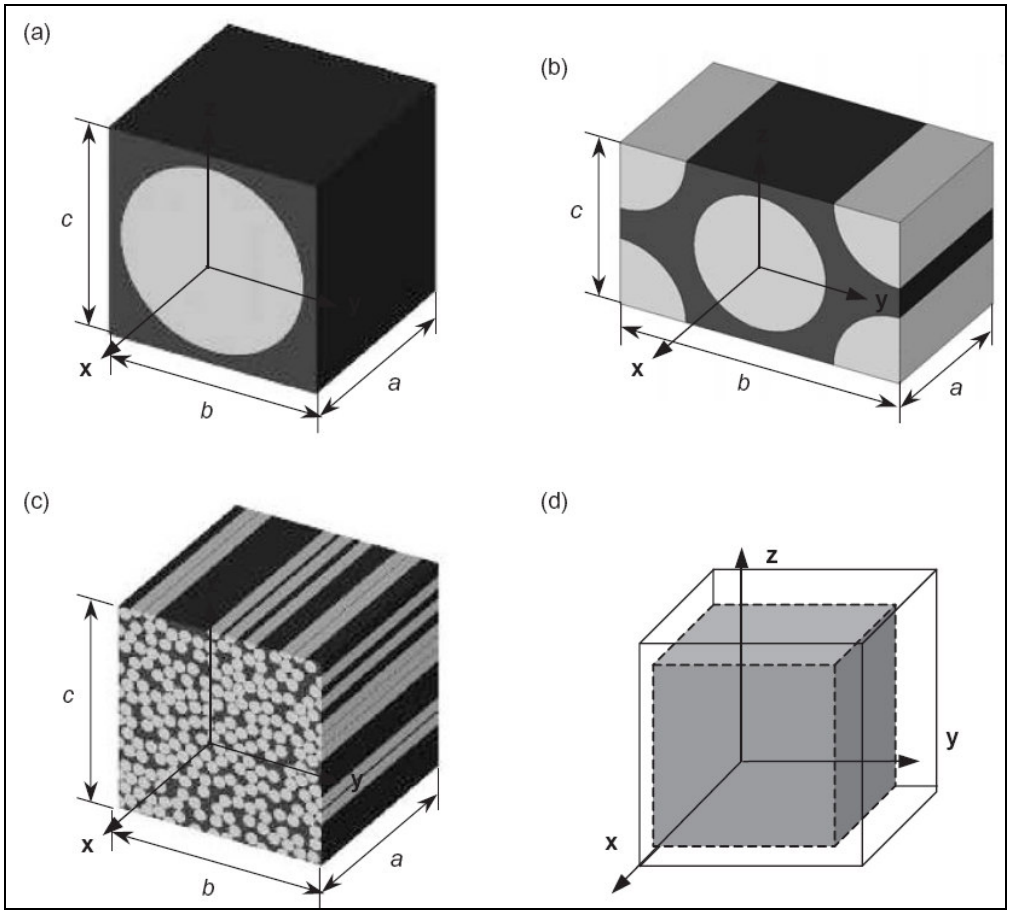

Fig. 2.24 - Representative volume elements of regular and random fibre arrays, and mechanical boundary conditions: (a) square array; (b) hexagonal array; (c) random array and (d) deformed shape after thermal loading [162].

2.5 Conclusion

Published work in the field of composite mechanical properties prediction at the microscale has been reviewed. The unidirectional reinforced unit cell has been identified as the basic building block for the overall mechanical composite properties. Various micromechanical methods to determine the elastic behaviour of composite materials have been discussed, in addition to those for failure under uniaxial loading. Published methods to determine the failure onset and to simulate the damage evolution in unidirectional RVEs or more complex geometries of composites materials at the microscale have been also discussed in detail. This review also

includes numerous methods which have been developed to determine the effects of residual stresses in polymer-matrix composites.

This review highlights the need for a purely predictive numerical model that incorporates the effects of residual stress within the micromechanics based damage model. In particular the damage model in this work has been “designed” to detect the local failure onset and damage propagation in three-dimensional unit cells as shown in Chapter-4.

Although extensive research has been done to describe numerically the damage propagation in composite materials and the effect of residual stresses, it has been noted that all the numerical investigations have been based on two-dimensional (2D) models. These models, which are in general assumed in a plane stress or plane strain state, unfortunately are unable to represent realistically the triaxial stress state that arises in real composites during the manufacturing process. In addition, the fibres in the 2D unit cell are also assumed to have a regular distribution over the cross-section while, in real composites, the fibres are randomly distributed within the unit cell.

It has been noted that recently few authors have developed more advanced numerical 3D models. Nevertheless, the purpose of these investigations concerned with the effects of non-symmetric RVEs on the overall mechanical properties and/or the distribution of residual stress in 3D numerical models. No damage model has been applied to determine the effect of residual stresses and the irregular packing array of the fibres on failure. A possible methodology to estimate the mechanical response of non-symmetric unit cells and the influence of the fibre position on failure is presented in Chaper-6 of this thesis.

Published work in the field of the micromechanics of composite materials has also proved that the presence of a 3D interphase influences drastically the mechanical behaviour of composite materials. Experimental research has been performed to determine the final characteristics of the interphase. These data have been used by several authors to develop various methods in order to study the influence of a third phase on the overall mechanical behaviour of composites. Nevertheless, none of the published studies have adopted a 3D unit cell for the numerical analyses, no damage models have been implemented in numerical codes and the effects of thermal residual stresses have been always neglected. A potential way to determine the mechanical response of unit cell with a 3D interphase has been suggested in Chapter-5 of this thesis.

Chapter 3

Micromechanical Stiffness

3.1 Introduction

Unidirectional (UD) composites are those which have all fibres aligned in a single direction. The properties of such composites vary significantly with direction. A unidirectional composite with a hexagonal array of fibres can be transversely isotropic because the properties are the same along any plane which is normal to the fibre direction. The stiffness and strength of a unidirectional composite are anisotropic properties since they vary with orientations. The stiffness of unidirectional composites in the fibre direction is usually dominated by the fibre properties while the strength in the transverse direction is dominated by the matrix properties. Since the strength of a unidirectional composite under transverse tension is much smaller than under longitudinal tension, transverse tensile loading is believed to be the critical loading of unidirectional composite materials.

One of the basic requirements in the mechanics of composite materials is to determine the effective elastic properties. Experimental determination of the moduli of unidirectional composites is difficult, especially when it involves determining the longitudinal shear and transverse shear moduli. Thus, numerical techniques like the finite element method are needed to calculate these shear moduli. Numerical methods to calculate composite material properties usually involve analysis of a representative volume element (RVE) [3, 22], corresponding to a periodic fibre packing sequence.

There are a few issues that need to be verified carefully when carrying out such analyses. Firstly, the correct RVE corresponding to the assumed fibre distribution must be isolated. Secondly, correct boundary conditions need to be applied to the chosen RVE to model different loading

situations. Proper consideration must be given to the periodicity and symmetry of the model in arriving at the correct boundary condition.

In the present work, the procedure for predicting the elastic constants of the composite from the RVE is established for a micromechanical three-dimensional finite element analysis. The finite-element calculations are made at a specific volume fraction because the geometry of the regions of the finite-element mesh that represent the fibre and matrix differ from one volume fraction to the next and, therefore, each volume fraction study requires a separate analysis. The finite-element calculations are for hexagonal array cross-section models (Fig. 3.1). The unit cell for the hexagonal array is shown in Fig. 3.2. To be noted in these figures that the *x*-axis is aligned with the fibre direction, and the *y*- and *z*-axes are perpendicular to the fibres.

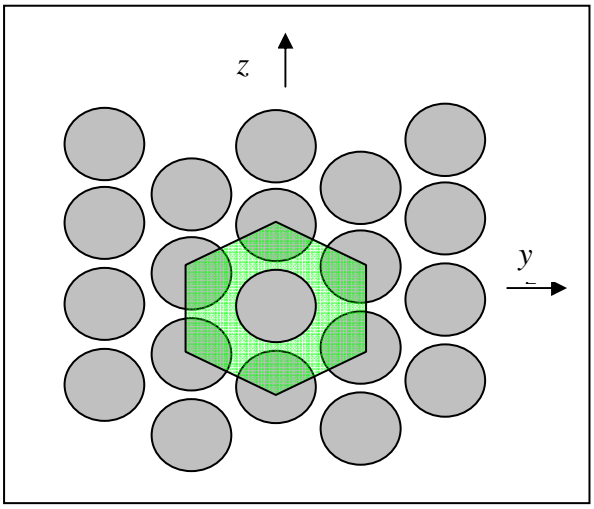

Fig. 3.1 - Cross-section idealization (hexagonal array) for micromechanics studies.

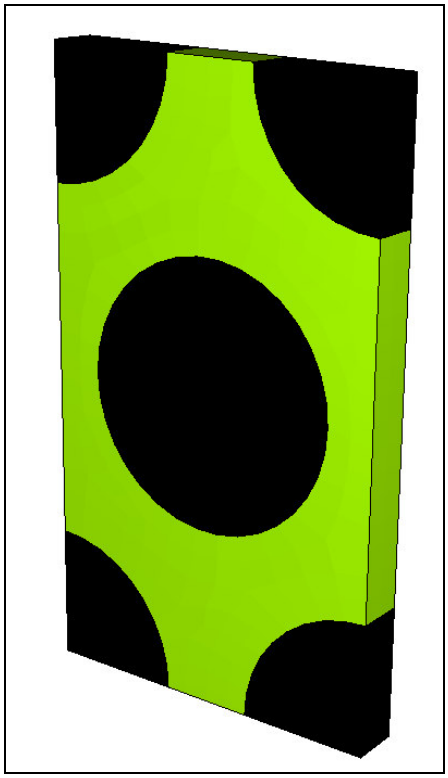

Fig. 3.2 - Details of 3D unit cell for hexagonally-packed array.

In the present study the following assumptions are made:

- The composite is: Macroscopically homogeneous

  Linearly elastic

  Macroscopically transversely isotropic

  Initially stress free (no thermal stress)

- The fibres are: Homogeneous

  Linearly elastic

  Isotropic

  Regularly spaced

  Perfectly aligned

- The matrix is: Homogeneous

  Linearly elastic

Isotropic

The material stiffness parameters are easily obtained from Hooke's law. In the numerical examples, both the fibre and the matrix are taken as an isotropic material. The composite can be assumed transversely isotropic with straight fibres [166].

The strain–stress relations for such a material can be written as [2]:

$$\begin{Bmatrix} \varepsilon_x \\ \varepsilon_y \\ \varepsilon_z \\ \gamma_{yz} \\ \gamma_{xz} \\ \gamma_{xy} \end{Bmatrix} = \begin{bmatrix} S_{11} & S_{12} & S_{13} & 0 & 0 & 0 \\ S_{12} & S_{22} & S_{23} & 0 & 0 & 0 \\ S_{13} & S_{23} & S_{33} & 0 & 0 & 0 \\ 0 & 0 & 0 & S_{44} & 0 & 0 \\ 0 & 0 & 0 & 0 & S_{55} & 0 \\ 0 & 0 & 0 & 0 & 0 & S_{66} \end{bmatrix} \begin{Bmatrix} \sigma_x \\ \sigma_y \\ \sigma_z \\ \tau_{yz} \\ \tau_{xz} \\ \tau_{xy} \end{Bmatrix} \tag{3-1}$$

in which

$S_{11}= 1/E_x$ $S_{12}= - \nu_{xy}/E_x$ $S_{13}= - \nu_{xz}/E_x$

$S_{22}= 1/ E_y$ $S_{23}= - \nu_{yz}/E_y$ $S_{33}= 1/E_z$

$S_{44}= 1/ G_{yz}$ $S_{55}= 1/ G_{xz}$ $S_{66}= 1/ G_{xy}$

Since the material is said to be transversely isotropic in the *y*-*z* plane the number of elastic constants required for the three-dimensional relation is five as $\mathbf{E_z = E_y}$, $\mathbf{G_{xz} = G_{xy}}$, and $\boldsymbol{\nu_{xz} = \nu_{xy}}$ [2].

The relations of Equation (3-1) become:

$$\begin{Bmatrix} \varepsilon_x \\ \varepsilon_y \\ \varepsilon_z \\ \gamma_{yz} \\ \gamma_{xz} \\ \gamma_{xy} \end{Bmatrix} = \begin{bmatrix} S_{11} & S_{12} & S_{12} & 0 & 0 & 0 \\ S_{12} & S_{12} & S_{23} & 0 & 0 & 0 \\ S_{12} & S_{23} & S_{22} & 0 & 0 & 0 \\ 0 & 0 & 0 & 2(S_{22} - S_{33}) & 0 & 0 \\ 0 & 0 & 0 & 0 & S_{66} & 0 \\ 0 & 0 & 0 & 0 & 0 & S_{66} \end{bmatrix} \begin{Bmatrix} \sigma_x \\ \sigma_y \\ \sigma_z \\ \tau_{yz} \\ \tau_{xz} \\ \tau_{xy} \end{Bmatrix} \tag{3-2}$$

in which

$S_{12} = - \nu_{xy}/E_x = S_{yx} = - \nu_{yx}/E_y$

Mechanical and thermal properties of typical glass fibre and epoxy matrix are summarized in Table 3-1.

Table 3-1 - Mechanical properties of fibre and matrix

Material properties	**E-Glass**	*Epoxy*
Longitudinal modulus, $\mathbf{E_x}$ (GPa)	76	4
Transverse modulus, $\mathbf{E_y}$ (GPa)	76	4
Poisson's ratio, $\boldsymbol{\nu}$	0.2	0.35
Shear modulus**, G** (GPa)	29.9	1.46

3.2 FEM Procedures

The aim of this work was, the determination of elastic properties in a 3D unidirectional unit cell in which fibres are arranged in periodic array in order to asses the reliability these micromodels. Most of the unit cells investigated in the past literature are related to two-dimensional unit cells. Unlike two-dimensional unit cells, 3D unit cells undergo a contraction in both two directions (e.g. *y*-direction and *z*-direction) if loaded in the third direction (*x*-direction). Thus this leads to a triaxial deformation.

Moreover finite element results could be affected by the elements size in the mesh. Hence it was necessary to evaluate the micromodels and their meshes under different loading condition to verify that, although they undergo a triaxial deformation, elements in the mesh retain a adequate aspect-ratio to avoid erroneous results.

The procedure to assess the validity of these micro-models was performed by determining elastic properties of a RVE and by comparing numerical results with analytical and/or possibly experimental data available in the literature.

The package used for the analyses was ABAQUS/Standard version 6.3. The mesh was built using initially C3D8elements (8-node linear brick) and C3D20 (20-node linear brick) elements for a better accuracy [92] both available in ABAQUS/Standard version 6.3. All these types of element are three-dimensional continuum elements and allow stress and displacement analysis.

The FE analyses were carried out at different volume fractions and in particular the following fibre volume fractions were taken into account: *0.50, 0.55, 0.60, 0.65, 0.70, 0.75, 0.70, 0.75, 0.80 and 0.85*.

The number of element depends on the fibre volume fraction and the types of element used in the mesh. In general, the number of element ranges from circa 17000 to more than 40000 for solid brick elements.

3.3 Axial stiffness - Longitudinal Modulus E_x

The simplest treatment of the elastic behaviour of unidirectional long fibres composites is based on the premises that the material can be considered as if it were composed of parallel slabs as shown in Fig.3.3 and Fig.3.4 of the two constituents perfectly bonded together, with relative thicknesses in proportion to the fibre and matrix volume fraction. The two slabs are forced to have the same lengths parallel to the bonded interfaces. Hence if the stress is applied in the

direction of the fibres alignment (*x*-direction in Fig.3.2), then the constituents (fibre and matrix) exhibits exactly the same strain:

Under these circumstances it is possible to derive an analytical expression for the Young's modulus E_x:

$$E_x = E_f V^f + E_m V^m \tag{3-3}$$

This equation can be rearranged in the following form:

$$E_x = E_f V^f + E_m (1 - V^f) \tag{3-4}$$

where E_f ,V^f , E_m ,V^m are the fibre and matrix Young's modulus and volume fractions respectively.

This equation is known as the "Rules of Mixture" [1, 2] and indicates that the composite stiffness is a weighted mean between the moduli of matrix and fibre and E_x depends only upon the fibre volume fraction.

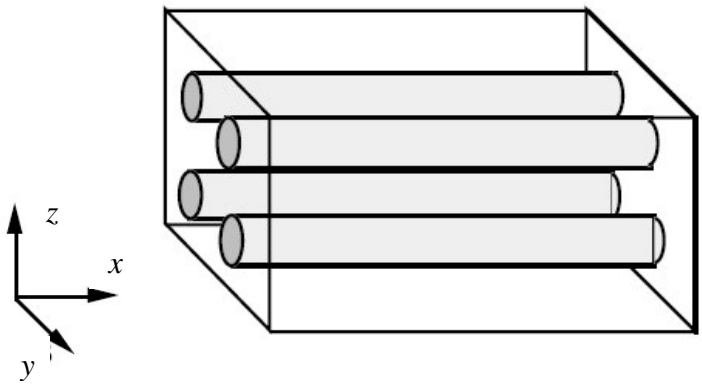

Fig. 3.3 - Ideal Unidirectional RVE

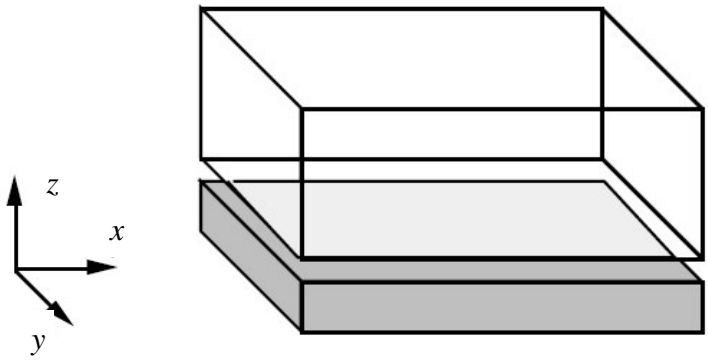

Fig. 3.4 - Slab configuration

To carry out the numerical analyses the unit cell used in the analysis is shown in Fig. 3.2.

Only a quadrant of the original RVE (Fig.3.5) is modelled since there are two axes of symmetry in this problem.

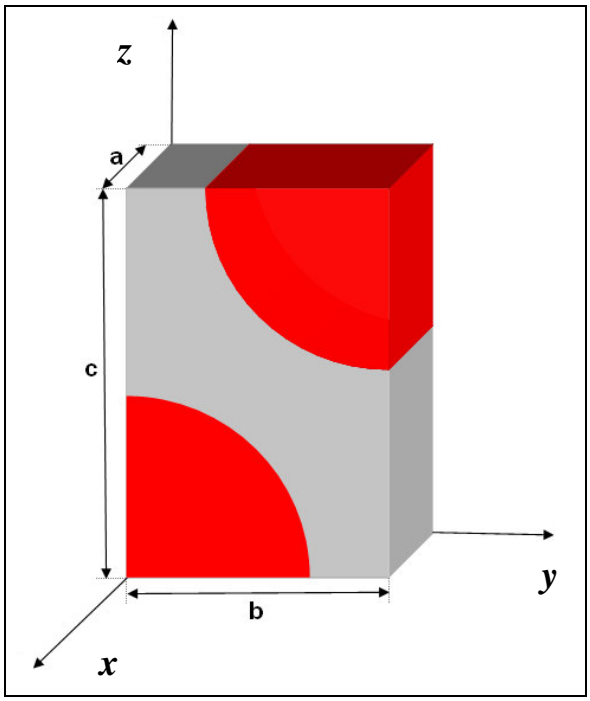

Fig.3.5 - ¼ RVE of the hexagonal array packing.

Axial loading is modelled by a displacement acting on the plane yz at x = ***a.*** For such loading conditions, the boundaries of the RVE also correspond to lines of symmetry. Thus, normal displacements of the boundaries of the quadrant are restricted to those that cause the boundary to

displace only parallel to the original boundary. The displacement constraints applied to the finite element model are:

$\boldsymbol{u_x}$ (0,y,z) = 0

$\boldsymbol{u_x}$ (a,y,z) = constant = 5.0E-05 [mm]

$\boldsymbol{u_y}$ (x,0,z) = 0

$\boldsymbol{u_y}$ (x,b,z) = constant = $\boldsymbol{\delta_y}$

$\boldsymbol{u_z}$ (x,y,0) = 0

$\boldsymbol{u_z}$ (x,y,c) = constant = $\boldsymbol{\delta_z}$

Due to Poisson's ratio effects, nodes placed in y = b, z = c undergo a displacement of $\boldsymbol{\delta_y}$ and $\boldsymbol{\delta_z}$. The comparisons for the results of Equation (3-4) for the composite extensional modulus in the fibre direction E_x and the finite element calculations at several volume fractions are shown in Fig. 3.6. The hexagonal finite-element array gives practically identical results to the rule of mixtures shown in equation (3-3). The linear dependence of E_x on fibre volume fraction is demonstrated and, as expected, the modulus increases whilst increasing the fibre volume fraction.

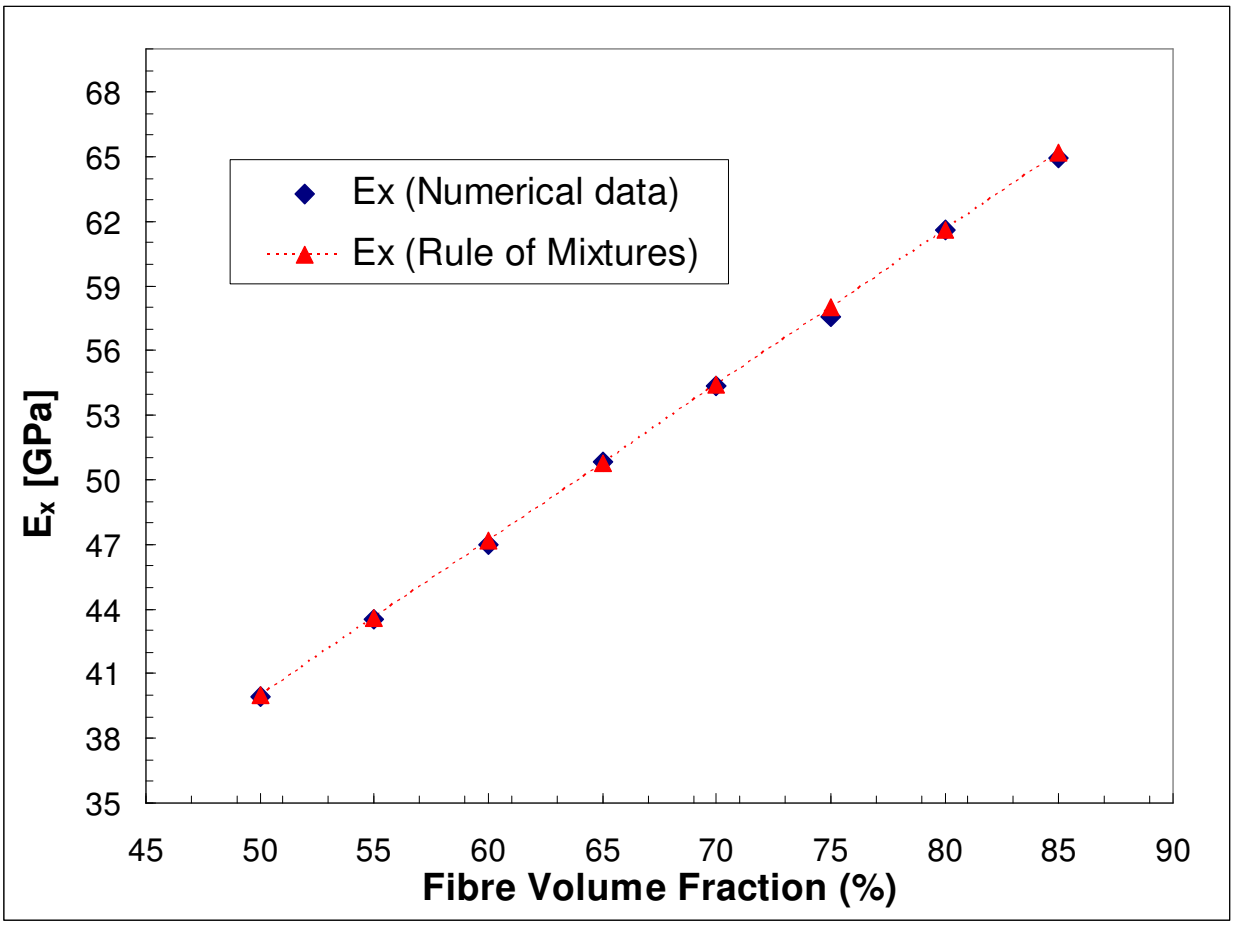

Fig. 3.6 - Comparison of numerical data and rule of mixtures data for composite modulus E_x.

3.4 Transverse Stiffnes –Elastic Moduli E_y and E_z

The analytical prediction of the transverse stiffness in unidirectional composite appears more difficult than the axial case. Although the system can be still represented by the "slab model" depicted in Fig. 3.4, this simplified model shows a serious drawback. In the unit cell in Fig. 3.5, the *y*- and the *z*-directions appear to be transverse to the fibres. In the slab model in Fig. 3.4 the transverse directions are not identical and in particular the *z*-direction is now equivalent to the axial direction while in the micromodels investigated, due the periodic distribution of the fibres over the cross-section (hexagonal packing array), the stiffness in the *z*-direction and *y*-direction are supposed to be the same. Thus, to avoid this drawback, the same analytical solution to evaluate E_y has been adopted to calculate E_z.

The expression derived from the conventional approach of the slab model that in the case of transverse loading is also called the “equal stress model”.

The relation derived from the slab model approach is [1]:

$$\frac{1}{E_y} = \left(\frac{1}{E_f}\right) V^f + \left(\frac{1}{E_m}\right)\left(1 - V^f\right) \tag{5}$$

This is the Rule of Mixtures relation for E_y. Comparing equation (3-5) with the expression for E_x in equation (3-4), it is seen that it relates the reciprocal of the extensional moduli with the volume fraction rather than the moduli themselves. This expression is similar to the expression for the equivalent stiffness of a pair of springs in series.

The non-uniform distribution of stress and strain during transverse loading implies that the simple equal stress model appears to be inadequate to evaluate the transverse elastic properties and more in detail the slab model gives an underestimate value of the Young’s modulus.

The most successful empirical expression to obtain more accurate estimates of E_y (and E_z) has been proposed by Halpin-Tsai in 1967 [1, 2]. Although it is not base on a rigorous theory of elasticity it takes into account the enhanced capability of fibre load bearing, relative to the equal stress model.

The relation for the transverse stiffness is:

$$\frac{E_y}{E_m} = \frac{1 + \Psi \eta f}{1 + \eta f} \tag{3-6}$$

in which η is:

$$\eta = \frac{\gamma - 1}{\gamma + \Psi}$$

and γ is:

$$\gamma = \frac{E_f}{E_m}$$

ψ is a measure of fibre reinforcement of the composite material and is dependent on fibre geometry, packing geometry, and loading conditions. Obtaining accurate values for ψ is the most difficult part of using the Halpin-Tsai equations. The expression (3-6) gives the correct values in the limits of f =0 and f =1 (f is the fibre content) and in general shows a good agreement with experimental data over the complete range of fibre volume fraction.

The value of ψ is then an adjustable parameter and its magnitude is generally of the order of unity [81].

Approximations for ψ are [2]:

- Circular fibres in square array (excellent results for V_f~0.55)

  $\psi = 2$ for E_y

  $\psi = 1$ for G_{xy}

- Square fibres in square array (good results for V_f<=0.9)

  $\psi = 2$ for E_y

  $\psi = 1$ for G_{xy}

- Rectangular cross section in diamond array (good results for V_f<=0.9)

  $\psi = 2a/b$ for E_y

  $\psi = 1.73\log(a/b)$ for G_{xy}

Where a = width of fibre, and b = thickness of fibre

In the present work (hexagonal packing array) a good agreement between numerical and analytical (Halpin-Tsai) results have been reached by considering a value of ψ = 1 for the evaluation of the elastic moduli E_y and E_z.

To study the other basic composite elastic properties, the unit cell of Fig. 3.5 must be loaded differently. To consider the composite extensional moduli perpendicular to the fibres, E_y (E_z) the load illustrated in Fig. 3.7 is used. A displacement in the *y*-direction (*z*-direction) has been applied to the unit cell in Fig. 3.5 and it was still assumed that the fibre and matrix are perfectly bonded together.

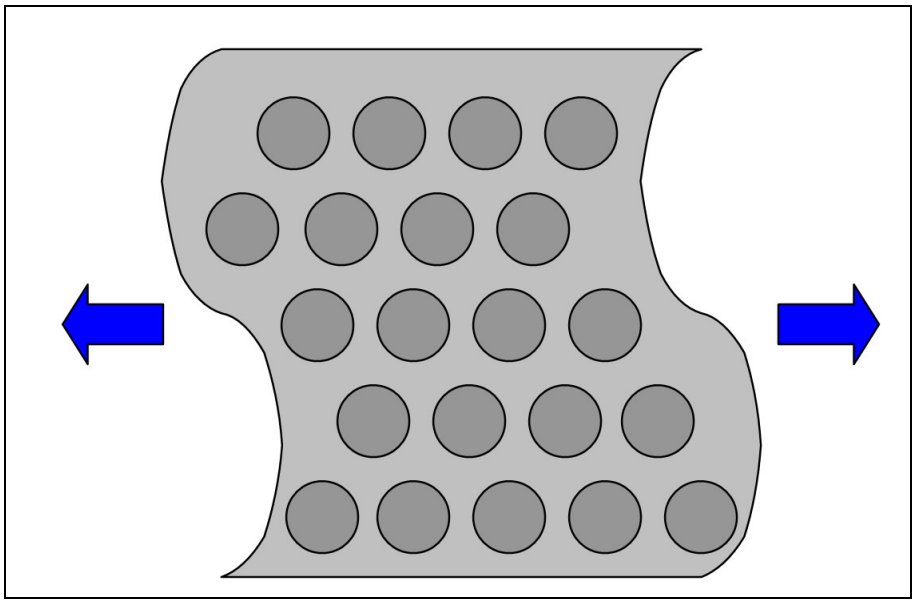

Fig. 3.7 - Cross-section subjected to transverse load.

Transverse loading is modelled by a displacement acting on the plane *xz* in $y = \boldsymbol{b}$ in order to evaluate E_y and on the plane *xy* in $z = \boldsymbol{c}$ for E_z.

Again, normal displacements of the boundaries of the quadrant are restricted to those that cause the boundary to displace only parallel to the original boundary. The displacement constraints applied to the finite element models are:

- **to determine $\mathbf{E_y}$**

$\boldsymbol{u_x}$ (0,y,z) = 0

$\boldsymbol{u_x}$ (a,y,z) = constant = $\boldsymbol{\delta_x}$

$\boldsymbol{u_y}$ (x,0,z) = 0

$\boldsymbol{u_y}$ (x,b,z) = $\boldsymbol{\delta_y}$ =5.0E-05 [mm]

$\boldsymbol{u_z}$ (x,y,0) = 0

$\boldsymbol{u_z}$ (x,y,c) = constant = $\boldsymbol{\delta_z}$

- **to determine E_z**

$\boldsymbol{u_x}$ (0,y,z) = 0

$\boldsymbol{u_x}$ (a,y,z) = constant = $\boldsymbol{\delta_x}$

$\boldsymbol{u_y}$ (x,0,z) = 0

$\boldsymbol{u_y}$ (x,b,z) = constant = $\boldsymbol{\delta_y}$

$\boldsymbol{u_z}$ (x,y,0) = 0

$\boldsymbol{u_z}$ (x,y,c) = $\boldsymbol{\delta_z}$ = 5.0E-05 [mm]

The first step of the research was to determine the values of E_y and E_z from the numerical analyses. Finite element results are shown in Fig. 3.8 and as expected, on the assumption that the composite is macroscopically transversely isotropic the values obtained for the whole unit cells investigated are perfectly coincident.

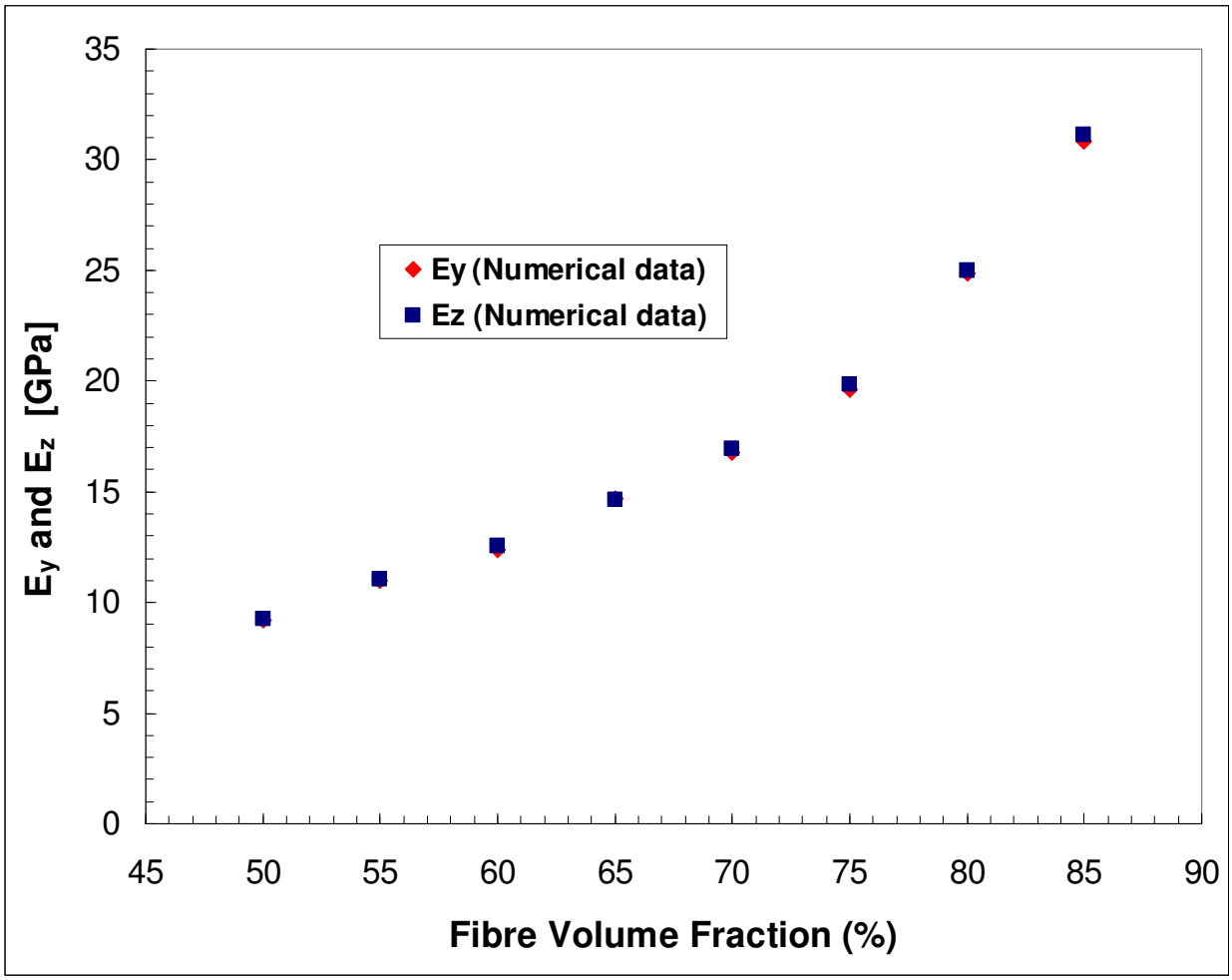

Fig.3.8 - Comparison of numerical results for the transverse Young's modulus E_y and E_z.

The Rule of mixtures model, the Halpin-Tsai equation and data from the finite-element calculations are compared in Fig. 3.9.

A comparison with numerical results for E_z also shows a good agreement between Halpin-Tsai and finite element values.

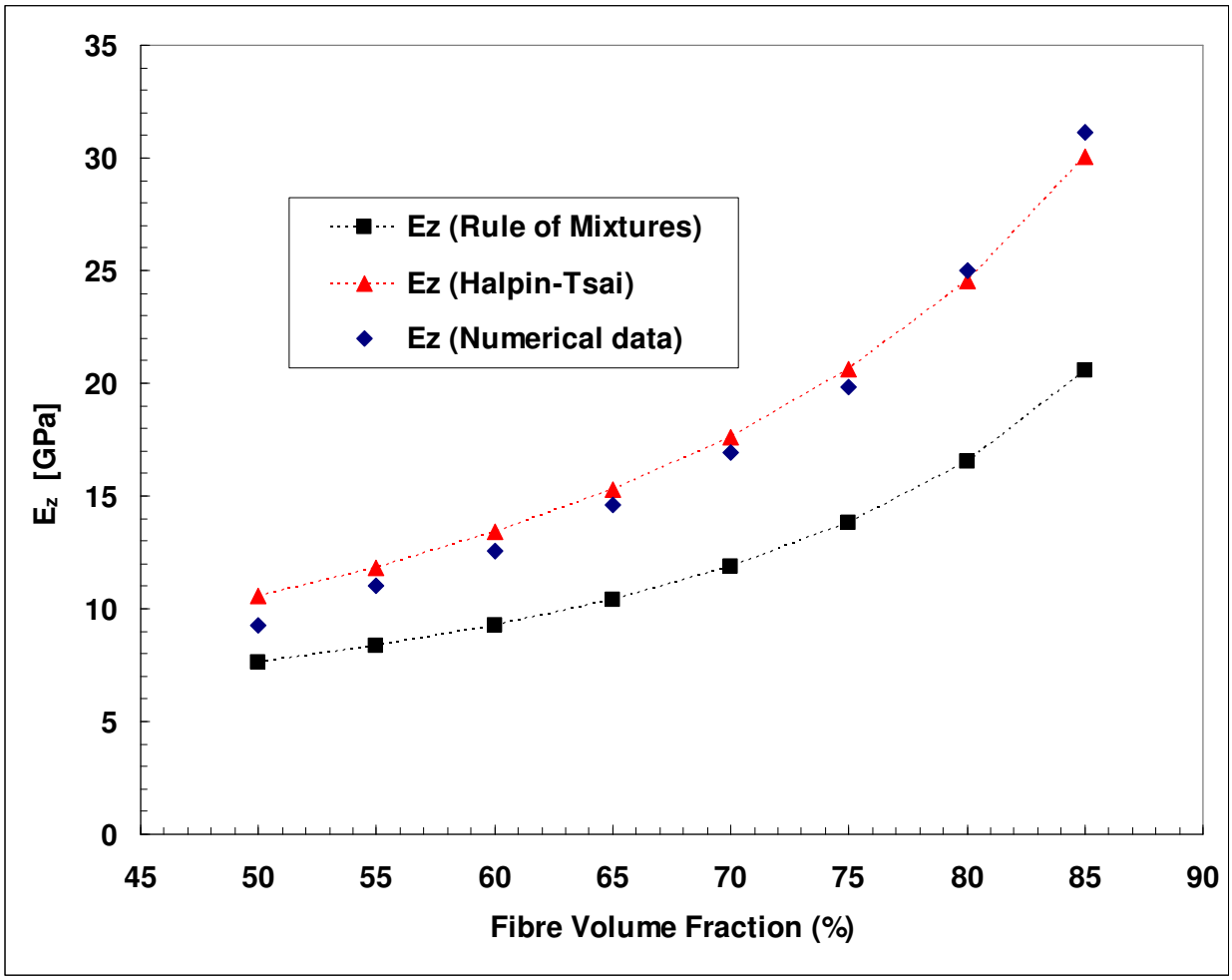

Fig. 3.9 - Comparison of finite-elements data, rule of mixtures and Halpin-Tsai results for composite moduli E_z.

3.5 Shear Stiffness

The shear moduli of unidirectional composite materials can be estimated in a similar way to the axial and transverse stiffness using the simplified slab model. It is worthwhile to understand the conventions used to identify shear stress and shear strain. The shear stress is conventionally designated with τ_{ij} ($i \neq j$) and τ_{ij} refers to a stress acting in the i-direction on a plane with a normal in the j-direction. In a similar way the shear strain γ_{ij} can be considered as a rotation of the j-axis towards the i-axis.

The transverse modulus G_{ij} is the ratio of $\boldsymbol{\tau_{ij}}$ over $\boldsymbol{\gamma_{ij}}$.

In unidirectional composite materials since the *y*-direction and *z*-direction are equivalent it follows that there are only two shear moduli because $G_{xy}=G_{yx}=G_{xz}=G_{zx}\neq G_{yz}=G_{zy}$

For the shear modulus G_{yz} and G_{xy}, a semi-empirical expression has been developed by Halpin and Tsai:

$$\frac{G_{xy}}{G_m} = \frac{1+\Psi\eta f}{1+\eta f} \tag{3-7}$$

in which η is:

$$\eta = \frac{\gamma - 1}{\gamma + \Psi}$$

and γ is:

$$\gamma = \frac{G_f}{G_m}$$

Where, G_f and G_m are the shear moduli for the fibre and the matrix. In the present work the best agreement between numerical and analytical results (Halpin-Tsai) have been reached by considering a value of $\psi = 2$ for the elastic modulus G_{xy} and $\psi = 1$ for the elastic modulus G_{yz}. The Halpin-Tsai relation represents a greatly good approximation to the shear moduli and in particular it approaches closer values related to the axial shear modulus G_{xy}

3.5.1 Shear Modulus G_{yz}

The stress and strain fields in a composite under a transverse shear loading are independent of the axial coordinate (***x***-direction) and are functions of ***y***-direction and ***z***-direction only. The RVE adopted in the numerical analyses to determine the shear moduli for a hexagonal array micromodel is shown in Fig. 3.2.

Many researchers modelled transverse shear by assigning equal and opposite displacements to the faces normal to $y = \boldsymbol{b}$ and $z = \mathbf{c}$ and assuming the deformed unit cell to remain a parallelogram with straight edges. This is an overly restrictive constraint [3]. The deformed shape needs only to satisfy periodicity and symmetry conditions without necessarily remaining a parallelogram in the deformed configuration.

To calculate the shear modulus G_{yz} the boundary conditions applied to the "full" unit cell depicted in Fig.3.2 are described with the help of Fig. 3.10:

$\boldsymbol{u}_y$ (-b, z) = $\boldsymbol{u}_y$ (b, z)

$\boldsymbol{u}_y$ (y, -c) = $\boldsymbol{u}_y$ (y, c)

$\boldsymbol{u}_z$ (-b, z) = $\boldsymbol{u}_z$ (b, z)

$\boldsymbol{u}_z$ (y, -c) = $\boldsymbol{u}_z$ (y, c)

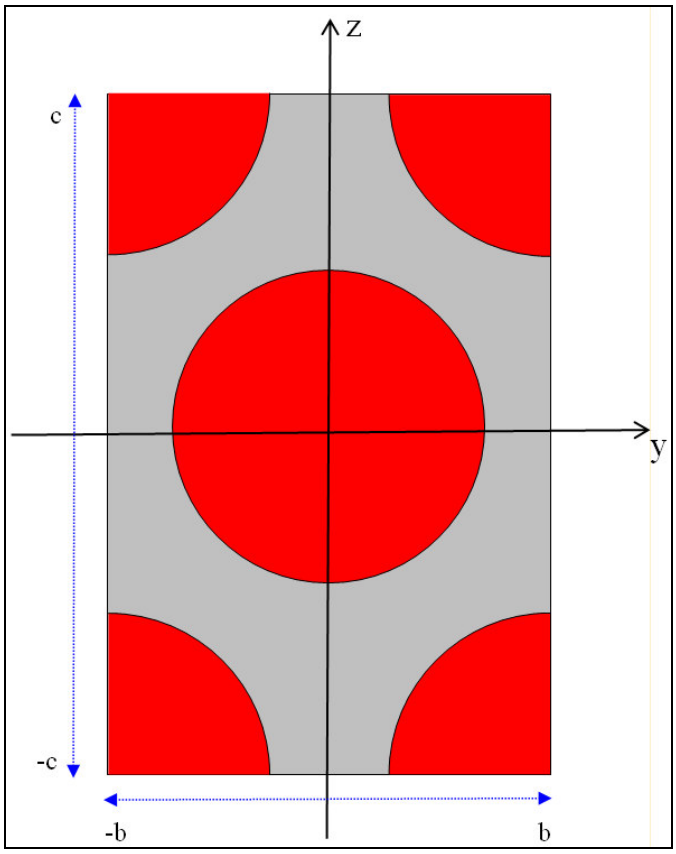

Fig. 3.10 – Details of an RVE for hexagonally-packed array.

A further constraint is that the boundaries of the RVE undergo constant lateral displacement as depicted in Fig.3.11:

$\boldsymbol{\varepsilon_{zz}}\ (\pm b, z) = 0 \quad \text{or} \quad \boldsymbol{u_z}\ (\pm b, z) = \delta_z$

$\boldsymbol{\varepsilon_{yy}}\ (y, \pm c) = 0 \quad \text{or} \quad \boldsymbol{u_y}\ (y, \pm c) = \delta_y$

Since correspondent nodes in opposite faces are forced to displace in the same way, a simple program in FORTRAN has been written to number properly the nodes on the LEFT face (nodes at y = -b) and RIGHT face (nodes at y = b), TOP face (nodes at z = c) and BOTTOM face (nodes at z = -c) and match up with each other correctly and then degrees of freedom of the correspondent nodes are repeated.

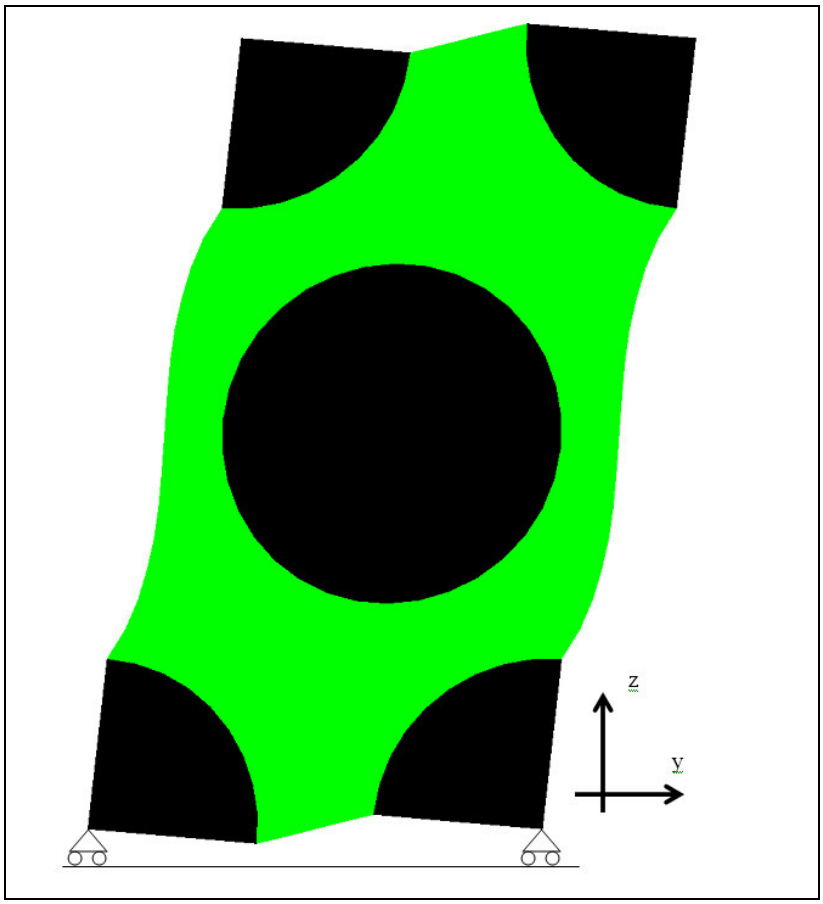

Fig. 3.11 - RVE under transverse shear loading to evaluate G_{yz}.

To simulate transverse shear loading, a displacement of 50E-05 mm is applied to each node of the TOP surface of the RVE (Fig. 3.11) in the *y*-direction.

The bottom corners are placed at $\delta_z = 0$ on rollers to eliminate rigid body displacement.

3.5.2 Shear Modulus G_{xy}

Similar boundary conditions have been applied to evaluate G_{xy}. Since the fibres are much stiffer than the matrix, they should exhibit a different shear strain, hence it is incorrect to assume that $\gamma_{xy}^{matrix} \neq \gamma_{xy}^{fibre}$. The strain field in a composite subjected to longitudinal loading is two-dimensional in nature and it is independent of the axial coordinate (x coordinate). To impose this constraint in the RVE, the FRONT face (nodes at $x = a$) and REAR face (nodes at $x = 0$) faces of the RVE are required to undergo identical displacement. In particular nodes on the FRONT face and REAR face with the same *y* and *z* coordinates are constrained to have the same displacements in all three directions. Thus, for the RVE shown in Fig. 3.2 and Fig. 3.10:

$\boldsymbol{u_x}$ (0, y, z) = $\boldsymbol{u_x}$ (a, y, z)

$\boldsymbol{u_y}$ (0, y, z) = $\boldsymbol{u_y}$ (a, y, z)

$\boldsymbol{u_z}$ (0, y, z) = $\boldsymbol{u_z}$ (a, y, z)

From symmetry conditions, the additional constraints on the RVE are:

$\boldsymbol{u_x}$ (x, 0, z) = 0

$\boldsymbol{u_x}$ (x, b, z) = δ_x = 50E-05 [mm]

$\boldsymbol{u_y}$ (x, 0, z) = 0

$\boldsymbol{u_y}$ (x, b, z) = 0

u_z (x, 0, z) = 0

u_z (x, c, z) = 0

Deformed shapes of unit cells under shear loading applied to evaluate G_{xy} are depicted in Fig. 3. 12 and Fig. 3.13

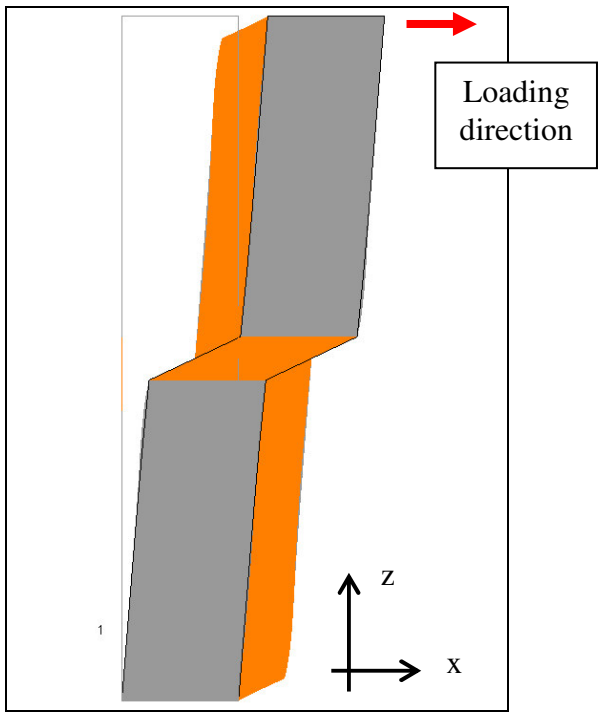

Fig. 3.12 - RVE under transverse shear loading to evaluate G_{xy}.

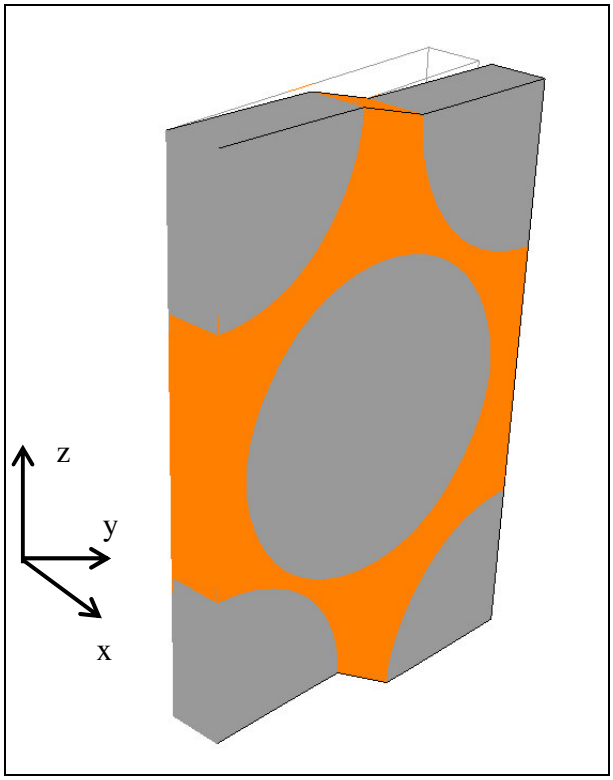

Fig. 3.13 – 3D view of the RVE under transverse shear loading to evaluate G_{xy}.

A comparison between numerical calculations for the shear moduli G_{xy} and G_{yz} (Fig.3.14) shows that their values are rather close to each other, with G_{xy} slightly greater in magnitude.

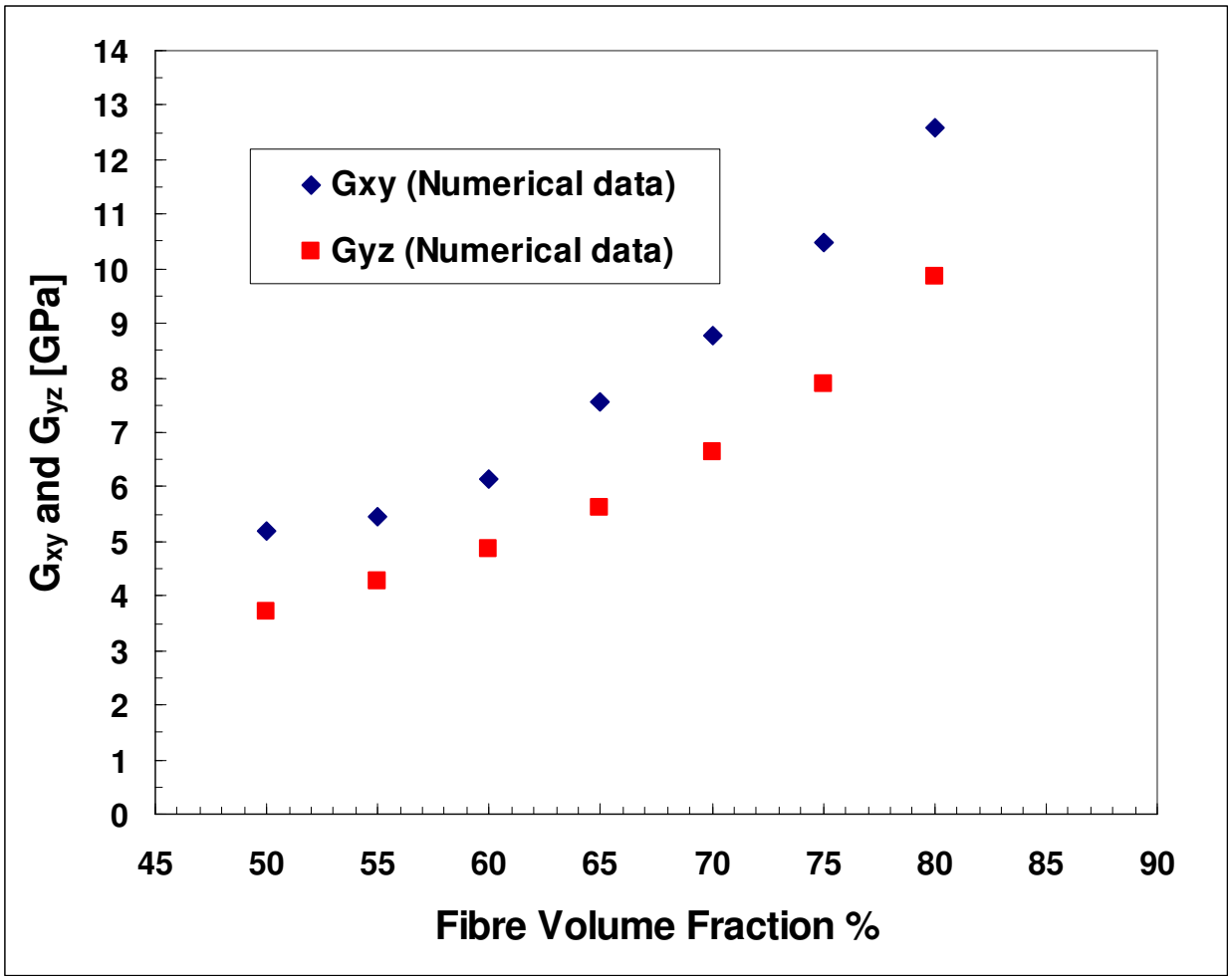

Fig.3.14 – Numerical results for Modulus G_{xy} and G_{yz}.

In Fig. 3.15 and Fig 3.16 results obtained by means of the Halpin-Tsai have been compared to the numerical calculations. Although the shear modulus G_{yz} appears to be slightly overestimated, especially at lower fibre volume fraction, by the Halpin-Tsai expression compared to the numerical data the differences can be considered in a reasonable range in magnitude and agree with data in the literature for similar materials [1].

In particular a better agreement can be seen in Fig 3.16 that displays the comparison between FEM values and data from the semi-empirical equation. In general differences in the results for G_{xy} are within the range of 3%.

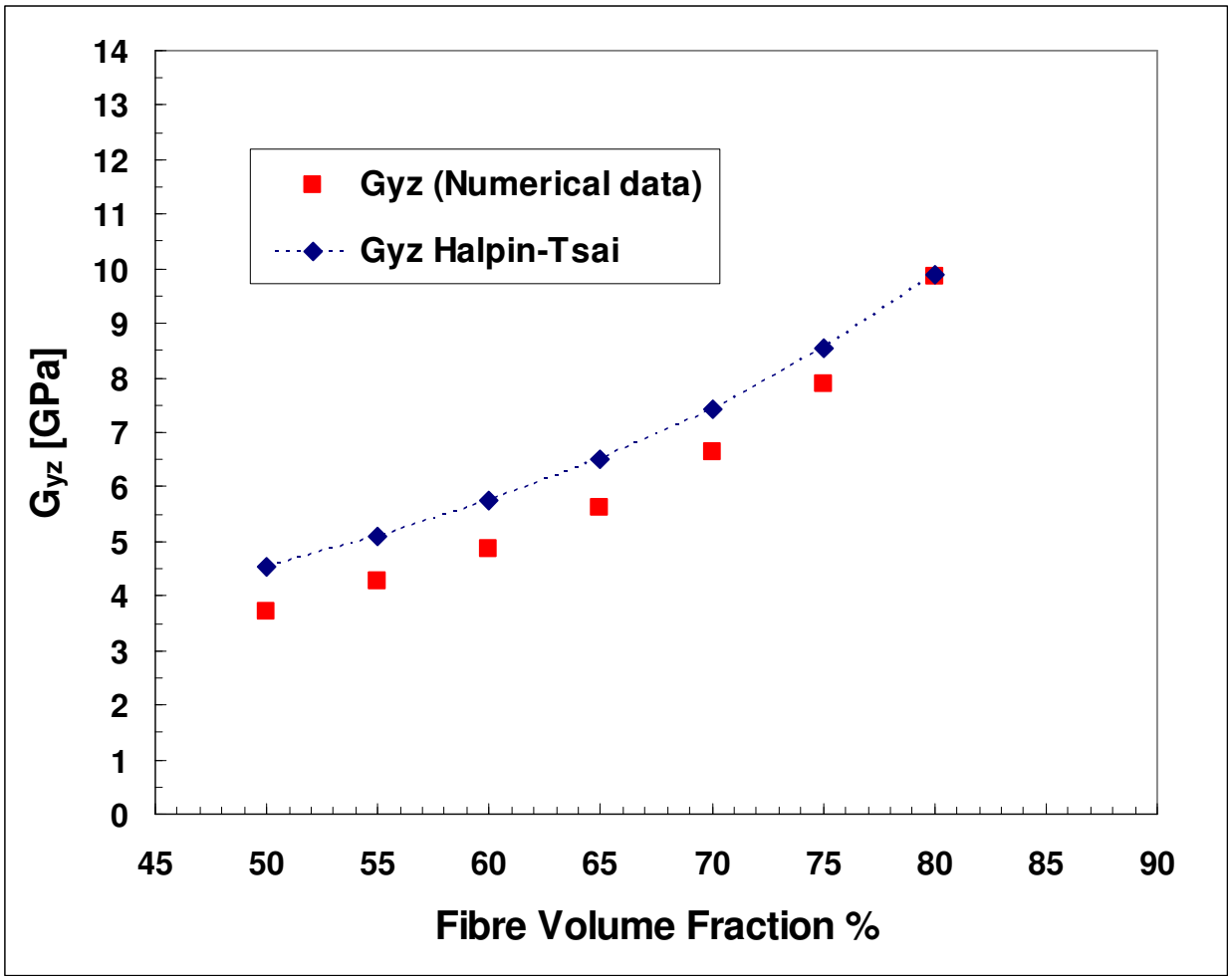

Fig. 3.15 – Comparison of finite-elements data and Halpin-Tsai results for composite moduli G_{yz}.

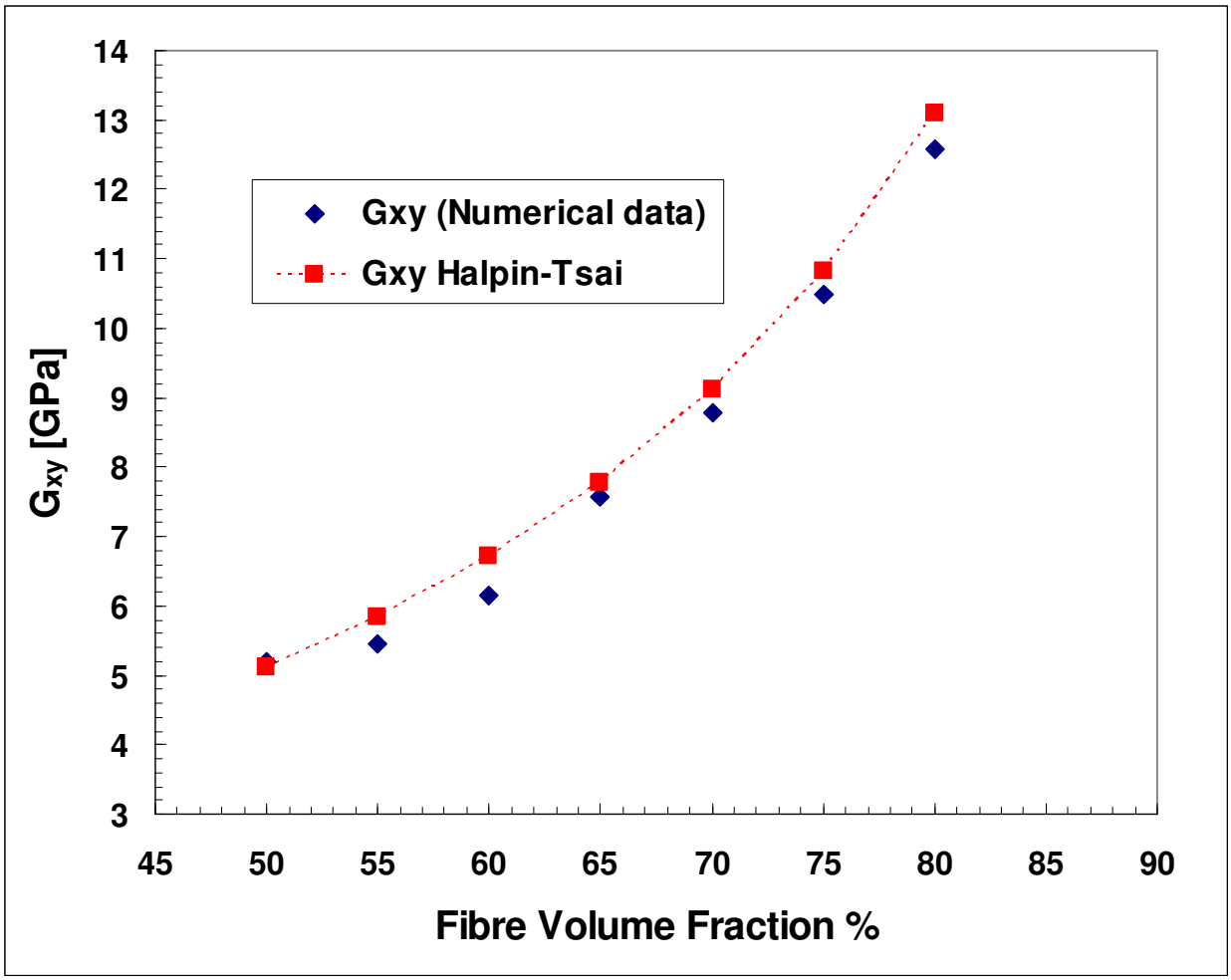

Fig. 3.16 – Comparison of finite-elements data and Halpin-Tsai results for composite moduli G_{xy}.

3.6 Poisson contraction effects

The Poisson's ratio ν_{ij} describes the contraction in the *j*-direction if the stress is applied on the *i*-direction. The Poisson's ratio can be defined with the following equation:

$$\nu_{ij} = -\frac{\varepsilon_j}{\varepsilon_i}$$

For unidirectional composite materials there are three different Poisson's ratios. Unfortunately the evaluation of Poisson's ratio values on the basis of the idealised slab model presents several difficulties due to the greater degree to which the contraction of the two constituents, fibre and matrix, must match if compared with the real structure of unidirectional composite materials.

Although three different Poisson's ratios can be estimated reliable results can only be obtained for the case of ν_{xy} assuming an equal strain of the two constituents. Thus in this case the Poisson's ratio of the constituents can be evaluated individually and summed. Then a simple Rules of Mixtures can be applied because of the equal strain assumption is accurate for the axial loading parallel to the fibres in unidirectional composites. As far as the other two Poisson's ratios, simple expressions have been developed in order to evaluate their values but in general they lead to not reliable results if compared to experimental data. In particular the Poisson's ratio ν_{yx} has been estimated to be lower than ν_{xy} because on applying a transverse load, the fibres offer a stiff resistance to axial contraction. Hence a more pronounced transverse contraction is expected leading to a higher value of ν_{yz}.

3.6.1 Poisson's Ratio ν_{xy}

By examining the overall contraction of the unit cell in Fig. 3.17, an expression for the composite major Poisson's ratio can be derived. The major Poisson's ratio for the composite is defined as minus the ratio of strain in the y-direction divided by the strain in the *x*-direction when only the stress $\boldsymbol{\sigma_x}$ is applied, namely:

$$\nu_{xy} = -\frac{\varepsilon_y}{\varepsilon_x} = \nu_{xz} = -\frac{\varepsilon_z}{\varepsilon_x} \tag{3-8}$$

where $\boldsymbol{\sigma_x} \neq 0$; all other applied stresses = 0

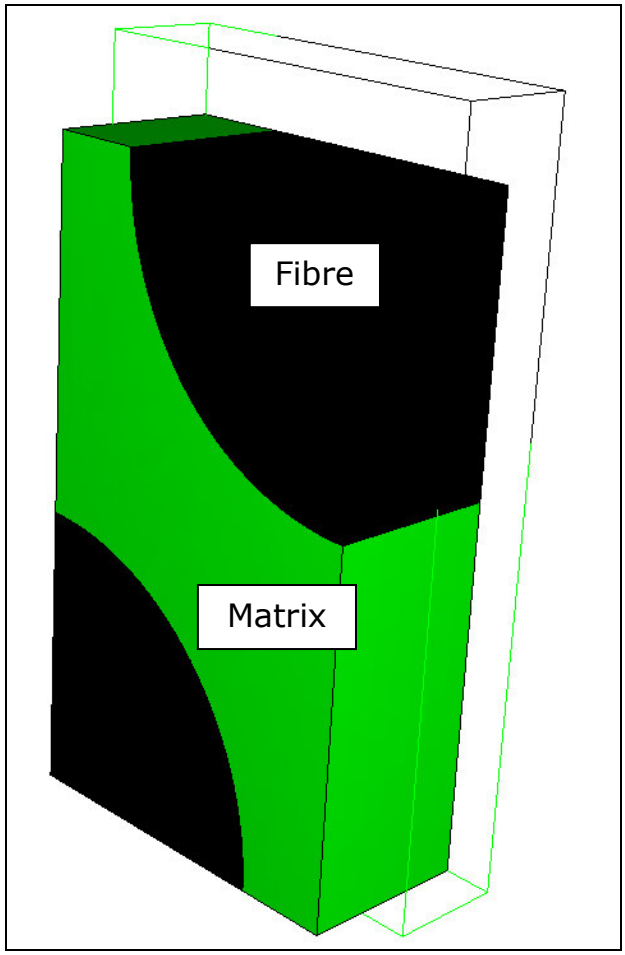

Fig.3.17 - Deformations of fibre and matrix..

The Rule of Mixtures expression for the composite Poisson's ratio is similar in form to the expression for E_1 [81, 90] and it can be formulated with the following equation:

$$\nu_{xy} = \nu_{xy}^{f} V^{f} + \nu_{xy}^{m}(1 - V^{f}) \tag{3-9}$$

where V^f is the fibre volume fraction, ν_{xy}^{f} and ν_{xy}^{m} are the Poisson's ratios for the fibre and the matrix.

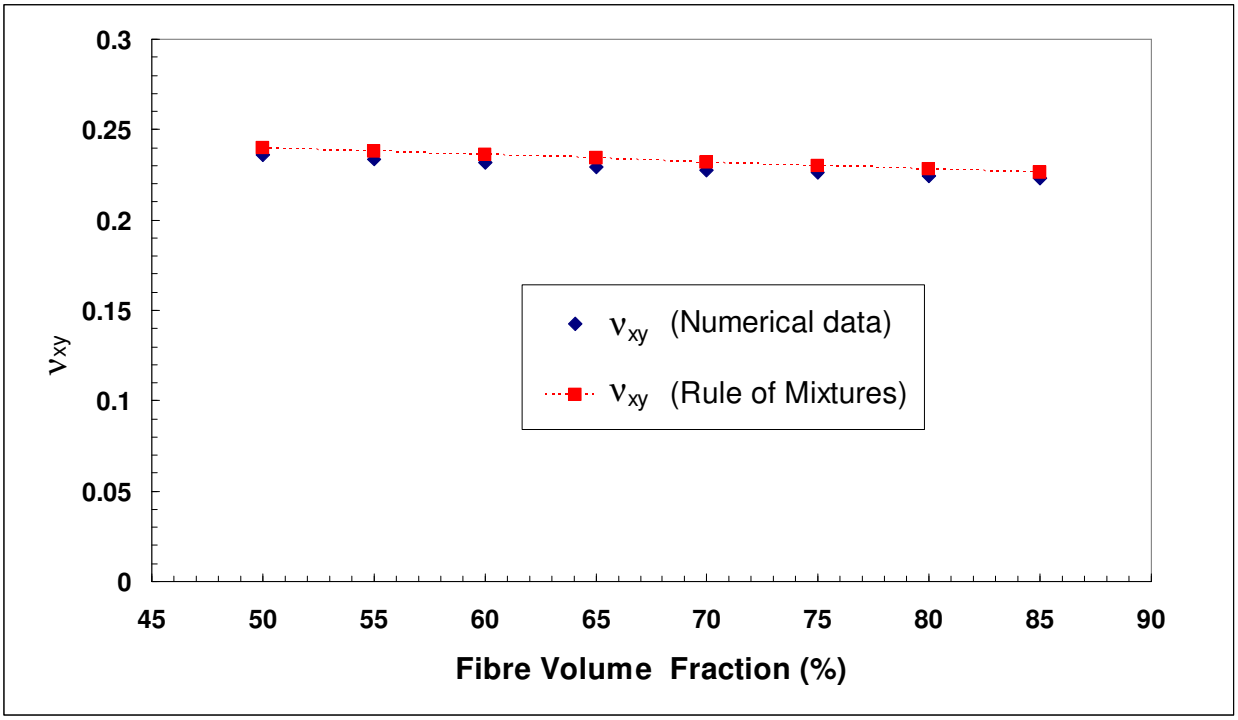

Fig. 3.18 - Comparison of finite element data and rule of mixtures results for composite Poisson's ratio $\mathbf{v}_{xy}$.

The comparison for the composite major Poisson's ratio $\mathbf{v}_{xy}$ from Equation (3-5) is presented in Fig. 3.18. Curves in Fig.3.18 displays that analytical and numerical results are in perfect agreement although data from the Rules of Mixtures are slightly higher than the finite-element results (in general less than 1.0%) .

3.6.2 Poisson's Ratio $\mathbf{v}_{yz}$

The Poisson's ratio ν_{yz} describes the contraction in the *z*-direction on applying loads in the *y*-direction. Although no analytical formulas have been applied to compare with numerical results it is worthwhile to show finite element results for several fibre volume fractions (Fig. 3.19 and Fig.3.20).

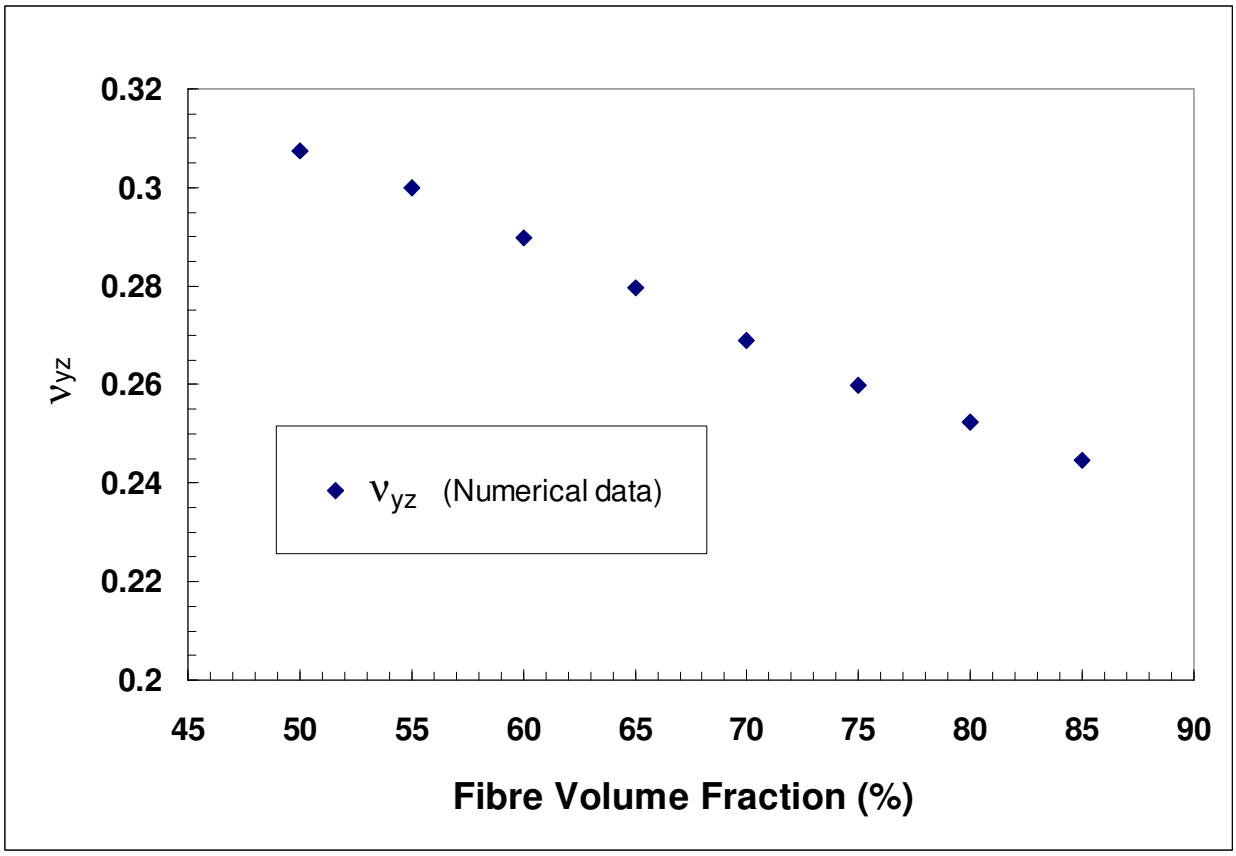

Fig. 3.19 - Poisson's ratio ν_{yz}.

As expected, ν_{yz} appears to be higher than ν_{xy} and, the comparison between the two Poisson's ratios shows that Poisson's ratios ν_{xy} are less sensitive to the fibre volume fraction. In particular, the values of ν_{xy} are quite close to the bulk E-glass Poisson's ratio (Table 3-1) especially at higher fibre volume fraction. On the contrary, ν_{yz} is strongly dependent from the fibre volume fraction and, its values approaches the Poisson's ratio for the bulk epoxy resin at lower values of the fibre volume fraction (Table 3-1). In fact, at high fibre volume fractions the fibres in the micromodel are almost in contact (in hexagonal packing array the fibre volume fraction is ~90%). Then the fibres represent an obstacle to the transverse contraction leading to a "stiffer" overall response in the composite.

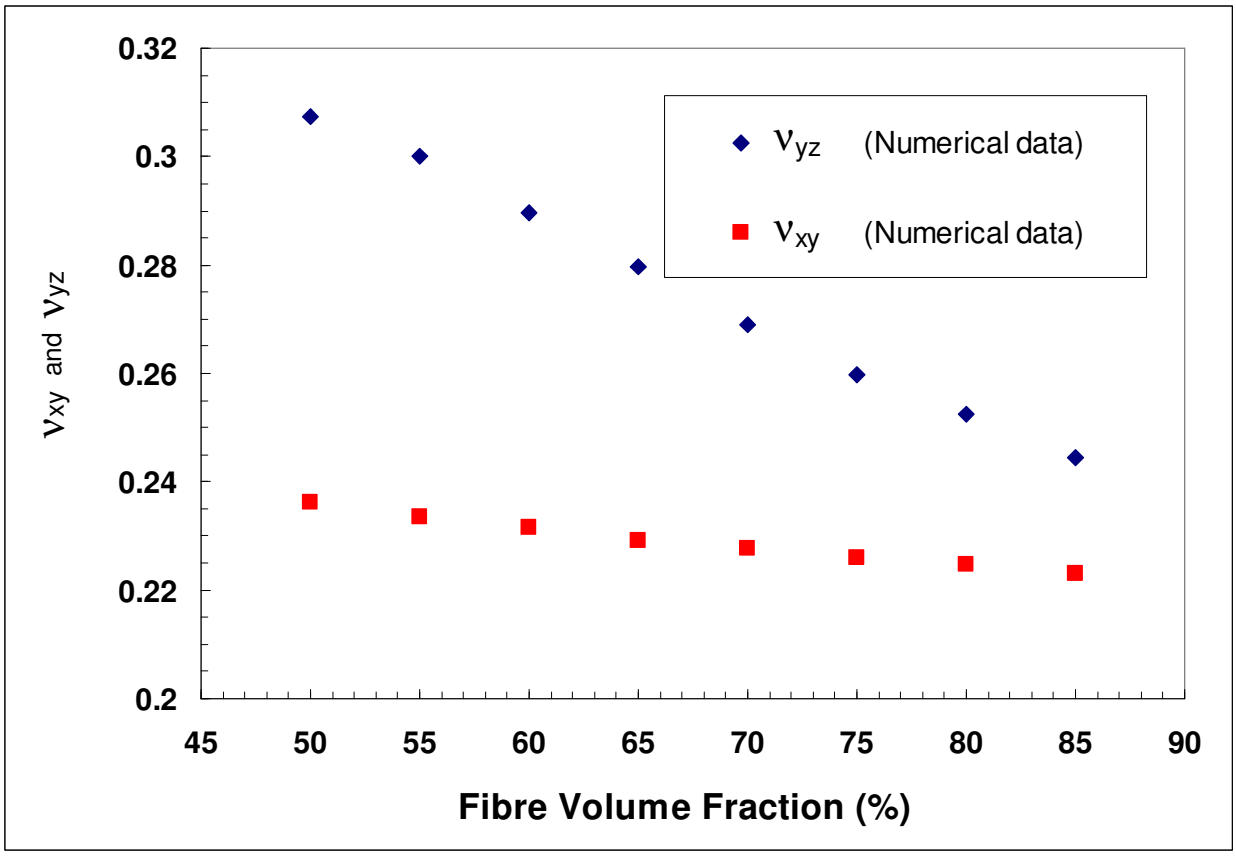

Fig. 3.20 – Comparison between Poisson's ratio ν_{xy} and Poisson's ratio ν_{yz}

3.7 Conclusion

The appropriate constraints on the RVE under various loadings have been determined from symmetry and periodicity conditions obtaining a nearly complete set of elastic constants for a three-dimensional unidirectional composite. The transverse elastic moduli are exactly coincident showing a proper symmetry in the micromodel. The elastic moduli obtained from the analysis for the hexagonal array also have been compared with analytical results employed in this exercise namely the Rules of Mixtures and the Halpin-Tsai semi-empirical expression. When possible, numerical results have been compared with experimental results available in the literature. The 3D micromodels have displayed a surprising uniformity with the analytical models and an adequate equality with experimental data.

As all the micromodels have show their capability to predict reliable mechanical properties it will be possible to implement them with a micromechanics damage model in order to predict failure with and without thermal residual stresses. Moreover since the matrix behaves differently in tension and compression it will be interesting to evaluate how different failure criteria (energy and strain based) predict damage in the composites at their microscale.

Chapter 4

Micromechanical Strength

4.1 Introduction

A modified micromechanics based damage model similar to the Blackketter model [5] has been applied by Zhao et al [170] to investigate the effects of thermal residual stresses in a two-dimensional (2D) unit cell in which fibres are distributed over the cross-section in a square packing array. Uniaxial and biaxial loading conditions applied on the 2D square unit cell shown that the overall response is strongly influenced by the presence of residual stress. Although under uniaxial transverse loading the effects of residual stresses are in general beneficial on the contrary on applying a biaxial transverse loading the overall mechanical response seems to undergo detrimental effects.

The main goal of this part of research is to apply uniaxial loading (axial and transverse) on 3D unit cells that represents more realistically the behaviour of composites materials by taking into account the tri-axial stress state arising during the manufacturing process. In order to achieve this goal a subroutine in FORTRAN as been developed to simulate the temperature-dependent material properties of matrix and fibres. The effect of residual stress has been evaluated for different unit cells with different fibre volume fractions and numerical results have been compared with the numerical values obtained in absence of thermal stresses.

Finally, since the epoxy matrices show a different mechanical behaviour in tension and compression, as a further exercise, the reliability to predict failure and simulate damage within the matrix of different failure criteria has also been accounted for. Three different failure criteria have been adopted for our purposes. The first two failure criteria are strain based and they the Maximum Principal Stress criterion that is used in combination with the Tresca failure criteria.

The third criterion used to predict failure in the matrix is a modification by Raghava of the well know von Mises criterion. This criterion includes the hydrostatic dependency of the epoxy matrix.

Composites properties, e.g. strength and stiffness, are dependent upon the volume fraction of the fibre and individual properties of the constituent fibre and matrix materials. Particularly the estimation of the damage and failure progress in fibre reinforced composite structures is very complicated compared to that of conventional metallic materials. Composite structures may vary their stiffness and strength due to damage accumulation such as matrix cracking and fibre breakage during the loading history of the composite members. In the micromechanical approach, the constituent fibre and matrix materials, and their interaction are distinctively considered to predict the overall behaviour of the composite structural member.. The present work has been developed in order to simulate progressive failure of an UD composite with a hexagonal array cross-section by carrying out micromechanical finite element analyses on a unit cell under different uniaxial load conditions. The advantage of the micromechanical model is that the stresses can be associated and related to each constituent (fibre and matrix). Therefore, failure can be identified in each of these constituents and a proper degradation model can be modelled. Also, different fibre volume fractions can be taken into account by varying the geometry of the unit cell.

Here, the micromechanical model considers a unit cell in which fibre and matrix are assumed to be perfectly bonded to the fibres throughout the analysis, with fibres arranged in a hexagonal cross section array (Fig. 4.1) by assuming the repetitive or periodic nature of the fibre and matrix materials. The unit cell is a three-dimensional solid and the geometry of each unit cell depends on the fibre volume fraction [22].

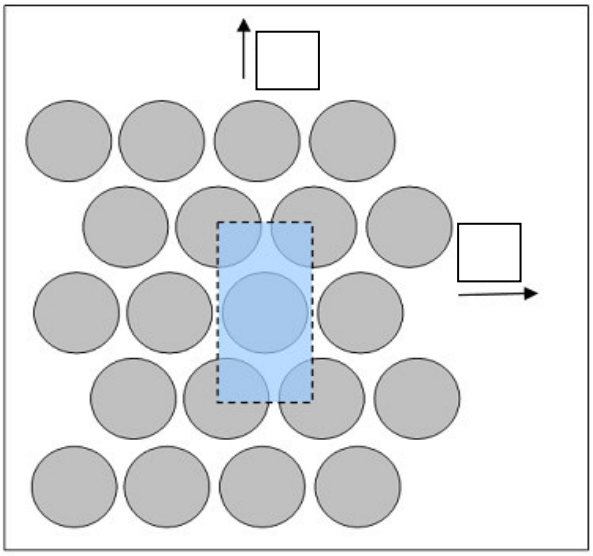

Fig. 4.1 – Cross sectiononal idealization (hexagonal packing array) in micromechanics studies. Detail of the RVE.

The micromechanical unit cell models are constructed depending on the type of load applied after curing. The entire RVE is displayed in Fig. 4.1, but for longitudinal and transverse tensile loading, due to the symmetry, a quarter of the unit cell (Fig. 4.2) can be considered.

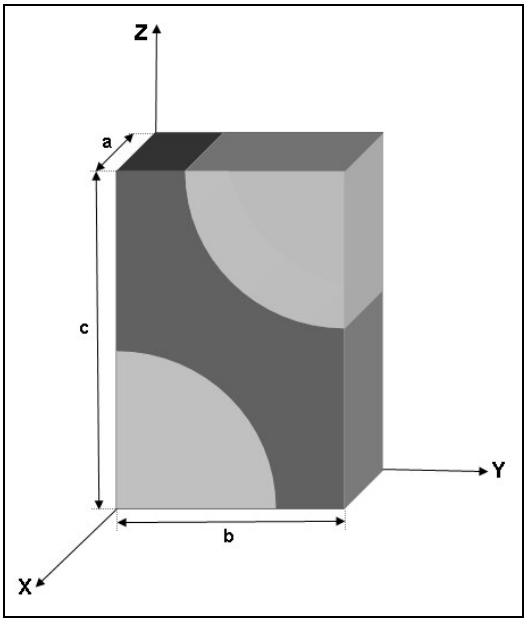

Fig. 4.2 - ¼ RVE of the hexagonal array packing.

The displacement constraints applied to the finite element model (Fig. 4.2) in order to apply normal loads are [22]:

$\boldsymbol{u_x}$ (0,y,z) = 0

$\boldsymbol{u_x}$ (a,y,z) = constant = $\boldsymbol{\delta_x}$

$\boldsymbol{u_y}$ (x,0,z) = 0

$\boldsymbol{u_y}$ (x,b,z) = constant = $\boldsymbol{\delta_y}$

$\boldsymbol{u_z}$ (x,y,0) = 0

$\boldsymbol{u_z}$ (x,y,c) = constant = $\boldsymbol{\delta_z}$

where $\boldsymbol{u_x}$, $\boldsymbol{u_y}$, $\boldsymbol{u_z}$ denote respectively displacements in the *x*-, *y*- and *z*-direction.

The meshes generated for the micro-models investigated are 20-noded hexahedral elements. The number of elements varies approximately from 6000 to 9000 depending on the V_f. Mesh sensitivity analysis suggests that the meshes are fine enough to produce accurate results compared to a mesh with twice as many elements, with a difference within 0.2% -0.5% in terms of residual stress and failure strain level depending on the fibre volume fraction.

4.2 Failure Criteria and Damage Propagation Model

In order to simulate damage, it was necessary to evaluate the current stress state at each integration point. Then by comparing the current stress state with a specific failure criterion, the material properties are reduced at each "failed" integration point to values representing the particular type of damage occurred [5, 111 and 114].

The selection of a proper failure criterion, both for matrix and fibre, represents a very important task of the modelling formulation. In particular in polymers the yield behaviour is sensitive to hydrostatic pressure and as a consequence, the yield stress in tension is different from that in compression [6-8]. Modifications of von Mises and Tresca criteria were taken into account to evaluate failure in the matrix. A common form of the von Mises failure criterion is:

$$(\sigma_1 - \sigma_2)^2 + (\sigma_2 - \sigma_3)^2 + (\sigma_3 - \sigma_1)^2 = 2\sigma_Y{}^2 \qquad (4\text{-}1)$$

where σ_1, σ_2, σ_3 are the principal stresses and σ_Y is the yield strength of material. As the von Mises criterion does not predict differences in yield stress between tension and compression, modification of this criterion have incorporated the effects of hydrostatic pressure into equation (4-1). A general form for the modified Von Mises criterion can be written in the following form [8]:

$$A(\sigma_1 + \sigma_2 + \sigma_3) + B\left[(\sigma_1 - \sigma_2)^2 + (\sigma_2 - \sigma_3)^2 + (\sigma_3 - \sigma_1)^2\right] = 1 \qquad (4\text{-}2)$$

It is possible to determine the constants A and B in terms of the simple uniaxial tensile and compressive yield stresses $\sigma_{Y,T}$ and $\sigma_{Y,C}$, respectively.

The first modified Von Mises criterion was suggested by Raghava et al.[8]:

$$2(\sigma_{Y,C} - \sigma_{Y,T})(\sigma_1 + \sigma_2 + \sigma_3) + \left[(\boldsymbol{\sigma_1} - \boldsymbol{\sigma_2})^2 + (\boldsymbol{\sigma_2} - \boldsymbol{\sigma_3})^2 + (\boldsymbol{\sigma_3} - \boldsymbol{\sigma_1})^2\right] = 2\sigma_{Y,C}\sigma_{Y,T} \qquad (4\text{-}3)$$

The second modified criterion was derived by Bauwens [8]:

$$\sqrt{2}\frac{(\sigma_{Y,C} - \sigma_{Y,T})}{(\sigma_{Y,C} + \sigma_{Y,T})}(\sigma_1 + \sigma_2 + \sigma_3) + \left[(\boldsymbol{\sigma_1} - \boldsymbol{\sigma_2})^2 + (\boldsymbol{\sigma_2} - \boldsymbol{\sigma_3})^2 + (\boldsymbol{\sigma_3} - \boldsymbol{\sigma_1})^2\right]^{1/2} = 2\sqrt{2}\frac{\sigma_{Y,C}\sigma_{Y,T}}{(\sigma_{Y,C} + \sigma_{Y,T})} \qquad (4\text{-}4)$$

If $\sigma_{Y,C} = \sigma_{Y,T}$ both the modified Von Mises criteria by Raghava and Bauwens, reduce to the Von Mises criterion, equation (4-1). The failure criterion proposed by Tresca states that failure occurs when the maximum shear stress, τ_{max} in the component being designed equals the maximum shear stress in a uniaxial tensile test at the yield stress. The criterion is:

$$\frac{1}{2}\left|\sigma_1 - \sigma_3\right| = \tau_{\max} \tag{4-5a}$$

$$\frac{1}{2}\left|\sigma_1 - \sigma_2\right| = \tau_{\max} \tag{4-5b}$$

$$\frac{1}{2}\left|\sigma_2 - \sigma_3\right| = \tau_{\max} \tag{4-5c}$$

The Tresca yield criterion can be modified to take into account the effects of the hydrostatic pressure. The critical value of the shear stress τ_{max} is expressed as function of the hydrostatic pressure:

$$\tau_{\max} = \tau_{\max}^{o} - \overline{\alpha}\left(\sigma_1 + \sigma_2 + \sigma_3\right) \tag{4-6}$$

in which $\tau_{\max}^{o}$ is the shear yield stress in absence of hydrostatic pressure and $\overline{\alpha}$ is a material constant:

$$\tau_{\max}^{o} = \frac{\left(\sigma_{y,C}\sigma_{y,T}\right)}{\left(\sigma_{y,C} + \sigma_{y,T}\right)};\ \overline{\alpha} = \frac{1}{2}\frac{\left(\sigma_{y,C} - \sigma_{y,T}\right)}{\left(\sigma_{y,C} + \sigma_{y,T}\right)} \tag{4-7}$$

The fibres adopted in the numerical models are glass fibres therefore in contrast to carbon fibres, their material properties are isotropic [1]. It was possible, in order to evaluate failure within the fibres, the use of common failure theories for isotropic materials such as the von Mises failure criterion, Maximum Principal Stress theory (Rankine, Lamè, Clapeyron) and Maximum Shear Stress theory (Tresca). The analyses were performed with the Finite Element code ABAQUS and more specifically ABAQUS/Standard Version 6.4.

It is a common practice in simulating material damage to reduce the stiffness (or stiffness in a certain direction) to a near zero value following the onset of damage. Selective and non-selective stiffness reduction schemes are often used. Selective schemes are typically applied for composites where the load-carrying nature is dependent on the damage orientation [5]. For isotropic material, damage is independent of the material orientation, so that non-selective stiffness reduction is applied. When failure is detected the degradation is applied only on the elastic moduli by multiplying them with a discount factor $\boldsymbol{d_i} \in (0, 1]$ (i designates the elastic modulus **E** or **G**). Both resin and fibre-glass are isotropic and they have the following stiffness matrix:

$$[C] = [S]^{-1} = \begin{bmatrix} \frac{1}{d_E E} & -\frac{\nu}{d_E E} & -\frac{\nu}{d_E E} & 0 & 0 & 0 \\ -\frac{\nu}{d_E E} & \frac{1}{d_E E} & -\frac{\nu}{d_E E} & 0 & 0 & 0 \\ -\frac{\nu}{d_E E} & -\frac{\nu}{d_E E} & \frac{1}{d_E E} & 0 & 0 & 0 \\ 0 & 0 & 0 & \frac{1}{d_G G} & 0 & 0 \\ 0 & 0 & 0 & 0 & \frac{1}{d_G G} & 0 \\ 0 & 0 & 0 & 0 & 0 & \frac{1}{d_G G} \end{bmatrix}^{-1} \tag{4-8}$$

The Young's modulus **E** and the shear modulus **G** were degraded independently by a discount factor d_E and d_G both initially set equal to the unity. If during the analysis the failure criteria exceed the maximum strength allowed for matrix or/and fibre, the modulus **E** is degraded to 1% of its initial value ($d_E = 0.01$) at the particular integration point. The shear modulus **G** is reduced to 20% of the initial value (($d_G = 0.2$) under the assumption that some shear stiffness remain due to the friction still present on the failure plane [5].

The non-selective stiffness degradation scheme, together with the residual stress analysis were programmed into two user-defined material subroutines, UMAT and USDFLD [97], available in

ABAQUS/Standard 6.4.. The UMAT and USDFLD subroutines allow updating the solution-dependent state variables accordingly to the solution of an analysis. In particular, solution-dependent state variables can be defined as a function of any other variables in these subroutines and evolve with the solution of the analysis [10].

4.3 Materials

The constituent materials used in this investigation are glass fibre and epoxy resin, whose properties are given in the book World-Wide Failure Exercise [10]. The properties of glass fibre are assumed to remain constant and independent of the temperature change with Young's modulus E = 80GPa and Poisson's ratio ν = 0.22, the coefficient of thermal expansion α = 4.9×10^{-6}/°C and the longitudinal tensile (σ_T) and compressive (σ_C) strength are respectively 2150MPa and 1450MPa. However, for the epoxy resin, thermal transition temperatures such as the glass transition temperature T_g strongly affect mechanical properties. In order to represent this behaviour accurately the material properties of the resin are defined as a function of temperature. The following relations are used:

(a) Poisson's ratio is assumed to be temperature independent ($\nu = 0.35$).

(b) To evaluate the variation of Young's modulus E over the temperature range from curing to room temperature, the total temperature range can be divided into three regions:

- *Region III* $\Rightarrow T_g - \Delta T \le T \le T_g + \Delta T$, in which E varies greatly.
- *Region II* $\Rightarrow T < T_g - \Delta T$, the matrix is in solid state and E changes only slightly.
- *Region I* $\Rightarrow T > T_g + \Delta T$, the matrix is in liquid or rubbery state and E has a very small value.

For each region, the modulus is obtained using the following functions [132],

$$E(T) = E(T_r)\exp\left(-k_1 \frac{T - T_r}{T_g - \Delta T - T_r}\right) \qquad T < T_g - \Delta T \tag{4-9}$$

$$E(T) = E(T_g - \Delta T)\exp\left(-k_2 \frac{T - T_g + \Delta T}{\Delta T + \Delta T}\right) \qquad T_g - \Delta T \le T \le T_g + \Delta T \tag{4-10}$$

$$E(T) = 0.01E(T_r) \qquad T > T_g + \Delta T \tag{4-11}$$

with:

$T_g = 110°C,$

$T_r = 23°C,$

$\Delta T = 35°C,$

$E(T_r) = 3.35GPa,$

$E(T_g - \Delta T) = 0.7E(T_r),$

$E(T_g + \Delta T) = 0.01E(T_r),$

$k_1 = 0.35667,$

$k_2 = 4.2485$

(c) The thermal expansion coefficient α is assumed to change linearly with the temperature:

$\alpha(T) = K(T - T_{ref}) + \alpha(T_r)$

with a slope of:

$$K = \frac{\alpha_l - \alpha(T_r)}{T_g - T_r} \tag{4-12}$$

where $\alpha(T_r) = 58\times10^{-6}$ /°C and $\alpha_l = 139\times10^{-6}$/°C.

The longitudinal tensile (σ_T) and compressive (σ_C) strength of the resin are taken to be respectively 80MPa and 120MPa.

Mechanical and thermal properties of fibre and matrix are summarized in Table 4-1.

Table 4-1 Mechanical and thermal properties of fibre and matrix [10].

Material properties	**E-Glass**	*Epoxy*
Longitudinal modulus, $\mathbf{E_x}$ (GPa)	80	***3.35***
Transverse modulus, $\mathbf{E_y}$ (GPa)	80	***3.35***
Poisson's ratio, $\boldsymbol{\nu}$	0.2	***0.35***
Shear modulus, **G** (GPa)	33.33	***1.24***
Longitudinal tensile strength, $\mathbf{X_T}$ (MPa)	2150	***80***
Longitudinal compressive strength, $\mathbf{X_C}$ (MPa)	1450	***120***
Longitudinal tensile failure strain, $\mathbf{Y_T}$ (%)	2.687	***5***
Longitudinal compressive failure strain, $\mathbf{Y_C}$ (%)	1.813	**-**
Shear strength, **S** (MPa)	1200	***70***
Thermal coefficient, $\boldsymbol{\alpha}$ (10^{-6}/°C)	4.9	***58***

The isothermal curing reaction of a thermoset resin involves dramatic changes in the properties of the resin. After heating of the initially liquid monomer, the chemical reaction commences. The molecular weight and the degree of cross-linking increase as the volume of the system decreases. As the reaction proceeds two phenomena may occur independently: gelation and vitrification. Gelation corresponds to the formation of a molecular network and can be regarded as the point after which the system can sustain stress. Vitrification occurs when the glass transition temperature T_g of the reacting system reaches the cure temperature. On vitrification the system, either a rubbery network or a viscous liquid (if vitrification precedes gelation), is transformed into a glassy state. The property change was shown to be closely related to the degree of cure of

the resin [127, 167 and 168]. Here, the properties of the resin were assumed to be independent of the degree of cure and constant at the isothermal curing temperature. Their values were obtained from the temperature-dependent functions 4-9, 4-10 and 4-11 and used for the epoxy shrinkage in residual stress analyses in the present work. This assumption was justified by the fact that the modulus was built up very quickly after resin gelation or vitrification [120]. Also stress relaxation due to the viscoelasticity of the epoxy resin [132, 169] was ignored here, and the epoxy was treated as linear elastic.

4.4 Residual Stress Analysis

Residual stress has two parts: the chemical shrinkage residual stress and the thermal cooling residual stress. In order to simulate a curing process, the analysis was performed by two discrete steps, where step *one* is the shrinkage stress analysis and step *two* is the thermal cooling stress analysis. The shrinkage residual stress was calculated by applying a given amount of resin shrinkage. For the epoxy resin considered here, the linear shrinkage strain was chosen to be 0.01%, 0.35% and 1% which corresponds to a volumetric change of circa 0.03%, 1% and 3% respectively. The thermal residual stress is due to the cooling of the system from the curing temperature, 149°C, to room temperature, 23°C. The mechanical properties of the resin, in terms of shear modulus (and Young's modulus when the resin becomes solid), increase drastically as the material evolves from a liquid state to a solid state. So in the resin, geometrically constrained within the interstices present between fibres, tensile stresses develop more easily. Moreover, during chemical shrinkage, in which resin is in a rubbery state, realistically no deformation is established along the x-direction. Strains parallel to fibres are only developed during cooling as the resin evolves from a liquid/rubbery state into a solid state.

The total induced strain of the resin due to chemical shrinkage and thermal cooling can be expressed as [170]:

$$d\varepsilon_{ij} = de_{ij} + \delta_{ij} ds + \delta_{ij} \alpha(T) dT \tag{4-13}$$

where $d\varepsilon_{ij}$ is the total strain increment, de_{ij} the elastic strain increment, ds the free shrinkage strain increment due to the chemical reaction (cross-linking) in the absence of constraint, α(T) the thermal expansion coefficient which is dependent on the temperature, dT the temperature change and δ_{ij} is the Kronecker delta. From equation (4-1), the stress-strain relationship can be derived as:

$$d\sigma_{ij} = C_{ijkl} de_{kl} = C_{ijkl} \left\{ d\varepsilon_{ij} - \delta_{ij} ds - \delta_{ij} \alpha(T) dT \right\} \tag{4-14}$$

where $d\sigma_{ij}$ are the stress increments and C_{ijkl} the stiffness components. The above stress analysis is based on linear elasticity and the stiffness components C_{ijkl} are related to the Young's modulus E and the Poisson's ratio ν of the material. Equation (4-2) was derived for the residual stress analysis in the resin. The distribution of the resin's maximum principal residual stress in the matrix, after curing and cooling is presented in Fig. 4.3.

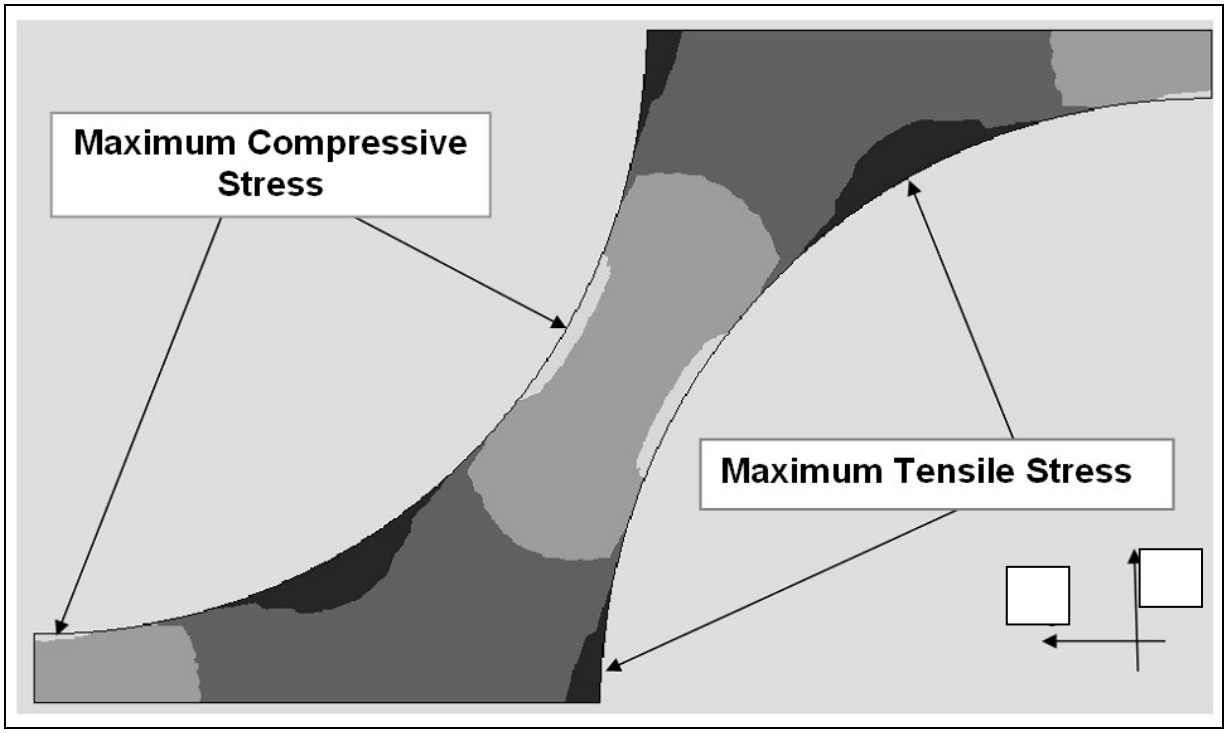

Fig.4.3 - Distribution of residual stress in the matrix after curing and cooling-down.

The mechanical properties of the resin, in terms of shear modulus (and Young's modulus when the resin becomes solid), increase drastically as the material evolves from a liquid state to a solid state. So in the resin, geometrically constrained within the interstices present between fibres, tensile stresses develop more easily. The largest values reached after chemical shrinkage and cooling are depicted in Fig. 4.4 Results from the analysis attribute the primary contribution to residual stress mainly to thermal cooling.

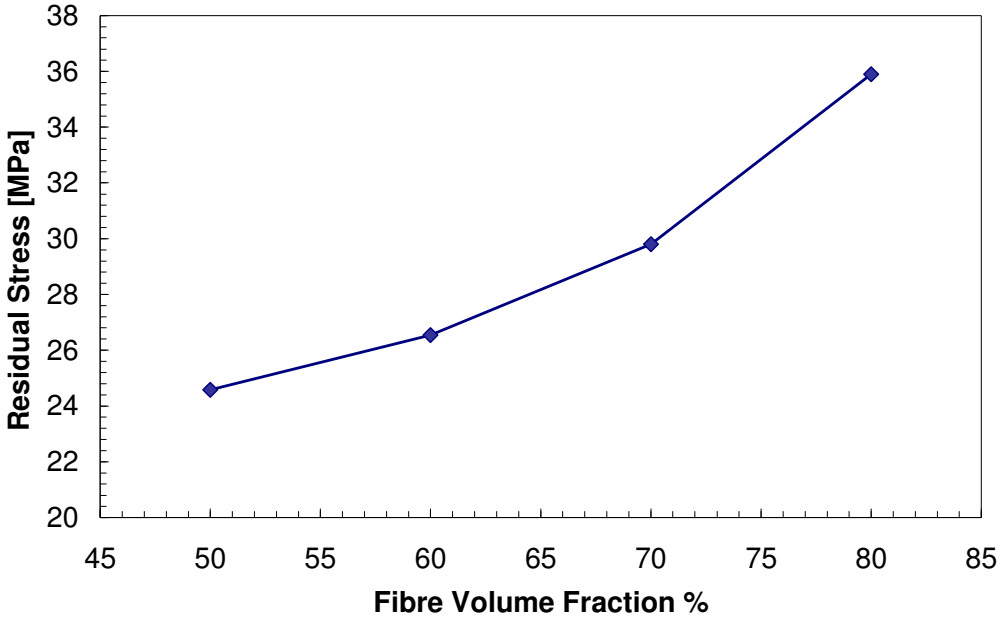

Fig. 4.4 - Trend of maximum principal residual stress (MPa) after curing and cooling-down evaluated in the area of max tensile stress at different V_f

In Fig. 4.5 the small contribution from the chemical shrinkage for four different fibre volume fractions is shown.

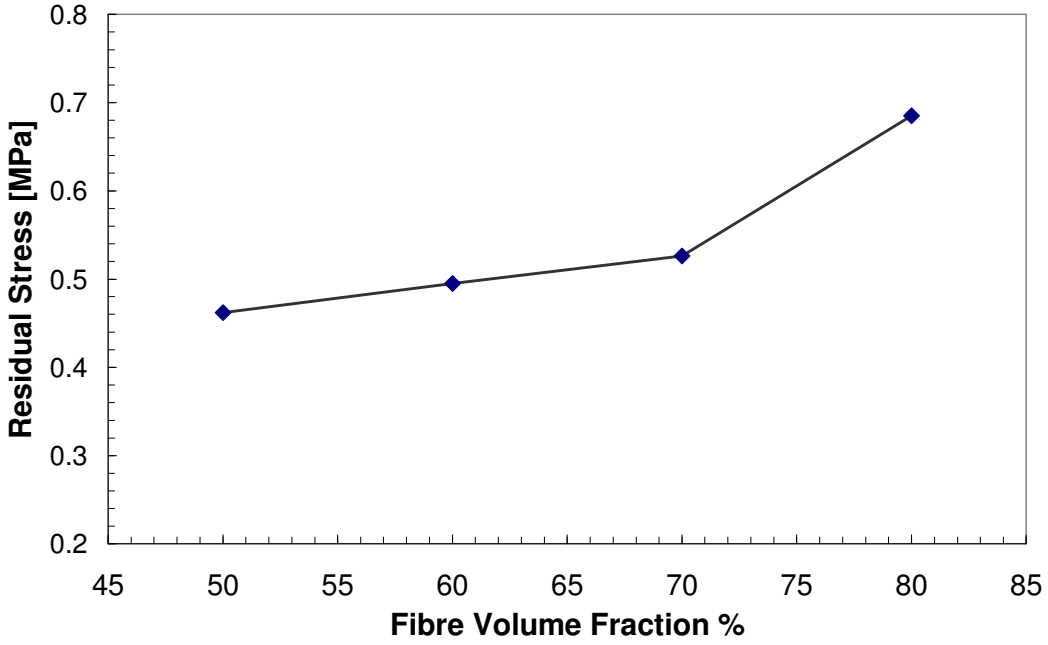

Fig. 4.5 - Trend of maximum principal residual stress (MPa) after curing evaluated in the area of max tensile stress at different V_f.

The curing stresses are small as a result of the mechanical properties of the resin during the curing process. In fact, its state is rubbery and almost liquid so the capability to interact with the fibres by transferring stresses is negligible. These results agree with most of the published work on residual stresses in which thermal cooling was evaluated as the main source of residual stress in polymer composites [120, 171].

4.5 Effect of residual stress on transverse and longitudinal failure

To study the influence of residual stress/strain on the response of the unit cell model, the damage evolution in the matrix was examined under transverse loading. After curing and thermal cooling analyses, a global strain was applied to the model which was achieved by specifying a uniform displacement at the model surfaces. At each time increment of the analysis, the damaged area in the matrix was determined using both the Maximum Principal Stress failure criterion and the von

Mises criterion modified by Raghava. Throughout the following analyses, the fibre showed no sign of damage due to its high strength, therefore, damage and failure refer to the matrix only.

4.5.1. Uniaxial longitudinal tensile loading

In UD composites the effect of the fibre is dominant, therefore during curing, in which resin is in a rubbery state, realistically no deformation is established along the *x*-direction. Strains parallel to fibres are only developed during cooling as the resin evolves from a liquid/rubbery state into a solid state. As the fibres are dominant the strength of the micro-models in the *x*-direction is of course improved if fibre volume fraction is increased.

A comparison between two different combinations of failure criteria was investigated:

1- Raghava (matrix)/von Mises (fibre)

2- Maximum Principal Stress (matrix)/ Maximum Principal Stress (fibre)

The modified von Mises criterion (Raghava) and the Maximum Principal Stress criterion were chosen in order to compare the capability to predict the damage initiation in 3D unit cells of energy based criteria (Raghava) and stress based (Maximum Principal Stress).

Both combinations show similar results in terms of ultimate strength for the fibre with residual stress (Fig. 4.6) but the Raghava criterion predicts matrix failure at a lower loading strain. In addition, the two combinations of failure criteria show a difference in the prediction of damage onset in the matrix.

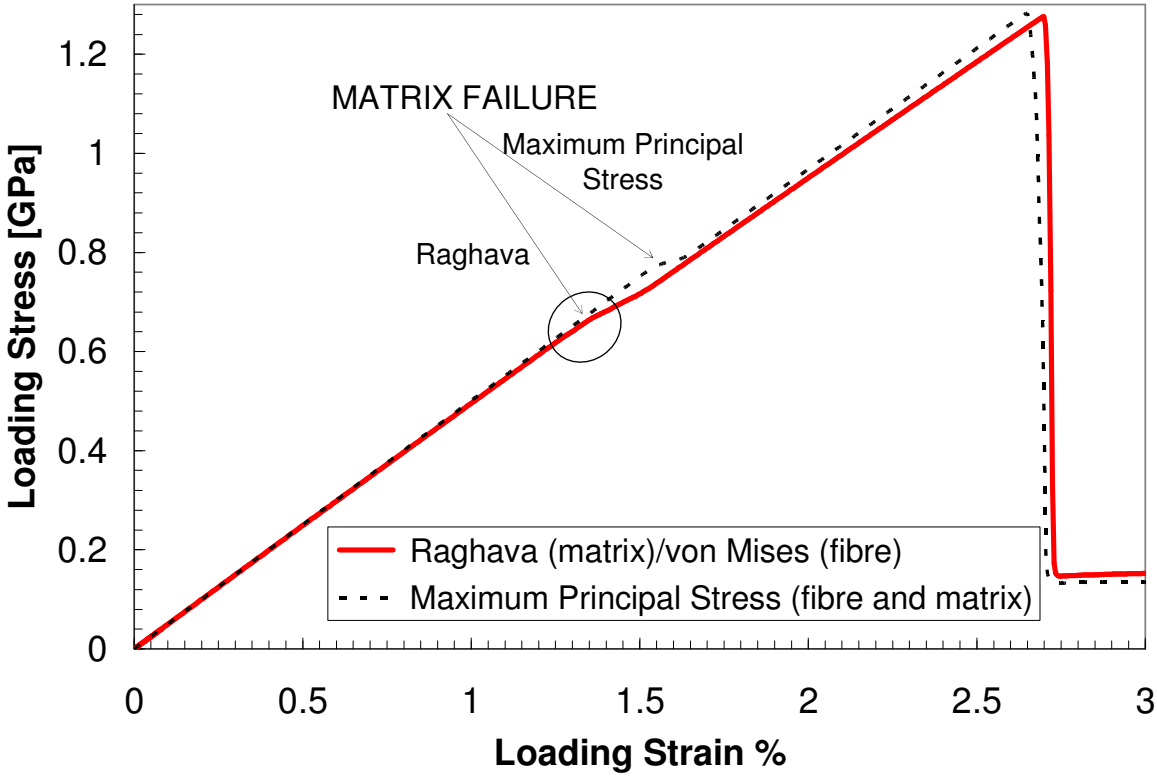

Fig. 4.6 - Global stress-strain curve in *x*-direction on uniaxial tensile loading with thermal residual stress for V_f 60.

The Maximum Principal Stress and the Raghava failure criteria predict differently the damage onset. The Maximum Principal Stress predicts the initiation of the damage in four regions (Fig. 4.7a) at the fibre/matrix interface while, according to the Raghava failure criterion the matrix undergoes a drastic failure (Fig. 4.7b). In fact on longitudinal loading the unit cell is strongly deformed in all the three directions and the energy based criterion (Raghava) results more influenced by the triaxial stress state arising at the fibre/matrix interface leading to a more conservative value if compared to the estimations determined with Maximum Stress criterion.

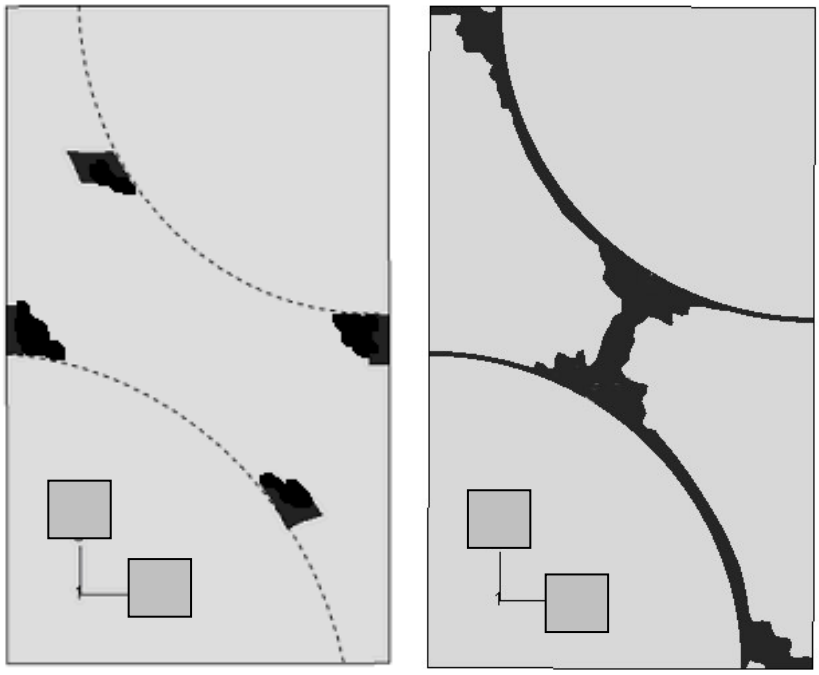

(a) (b)

Fig. 4.7 - Comparison on damage onset prediction (V_f 60%) in presence of residual stress. Maximum Principal Stress (a), Raghava failure criterion (b).

As seen in Fig.4.6, the presence of residual stresses does not modify the ultimate strength of fibres for *x*-direction loading, but for the matrix it is greatly detrimental decreasing its capability to bear loads. Comparison between stress/strain curves with and without residual stress (Fig. 4.8) shows that a premature matrix failure occurs if residual stresses are applied. Residual stresses are always detrimental for the matrix in *x*-direction longitudinal loading as shown in Fig. 4.9.

Although thermal residual stresses do not affect the ultimate strength of the micro-composites if the unit cell is biaxially or even triaxially loaded small loading strains could lead to the fibre/matrix debonding at interface and, due to the coalescence of cracks, to the catastrophic failure in the composites as demonstrated in Zhao et al [170] for a unit cell with square arrangement of the fibres.

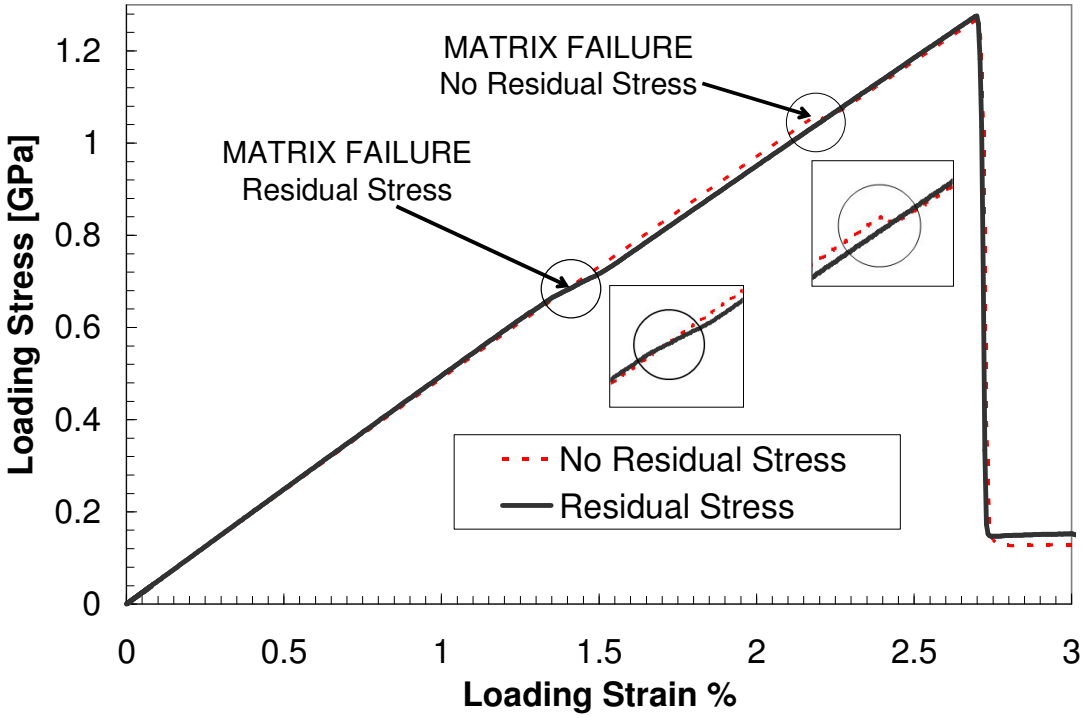

Fig. 4.8 - Global stress-strain curve in *x*-direction for uniaxial tensile loading for V_f 60. Failure criteria: von Mises for the fibre and Raghava for the matrix.

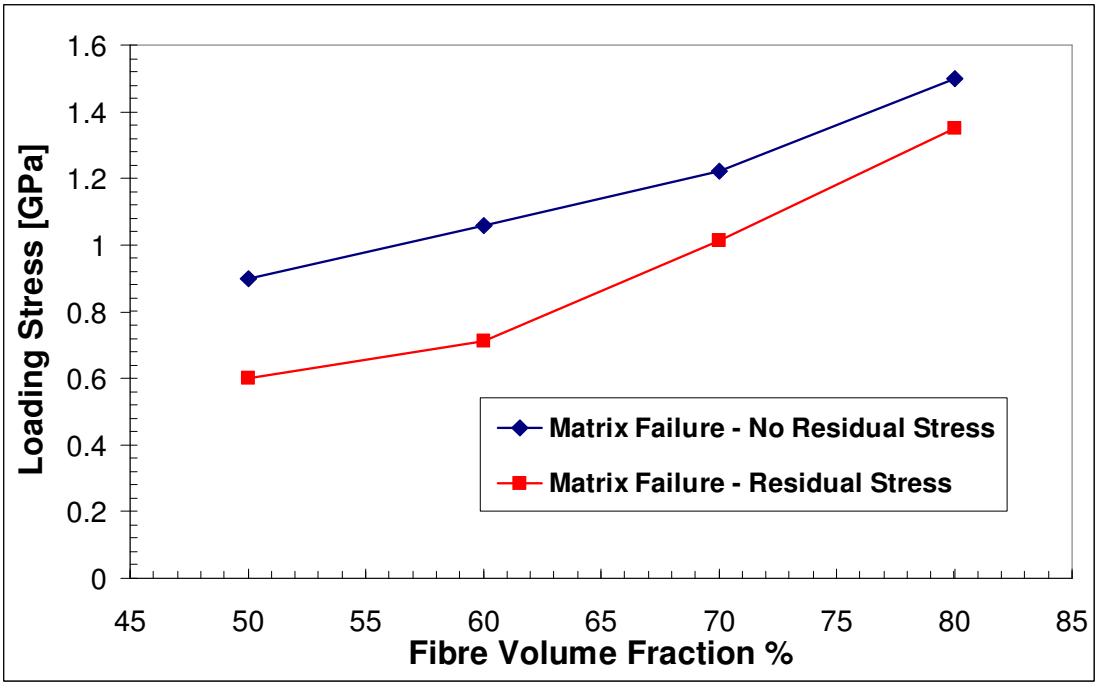

Fig. 4.9 - Comparison of ultimate strength with and without thermal residual on longitudinal (x-direction) loading by using the Raghava criterion.

4.5.2. Uniaxial transverse tensile loading

Under a *y*-direction uniaxial tensile loading and neglecting the residual stress/strain introduced during the curing process, the Maximum Principal Stress criterion predicts the damage initiation and its evolution (represented by black shading) to start from the corners of the RVE, propagating within the matrix along the edges of the micro-model (Fig.4.10).

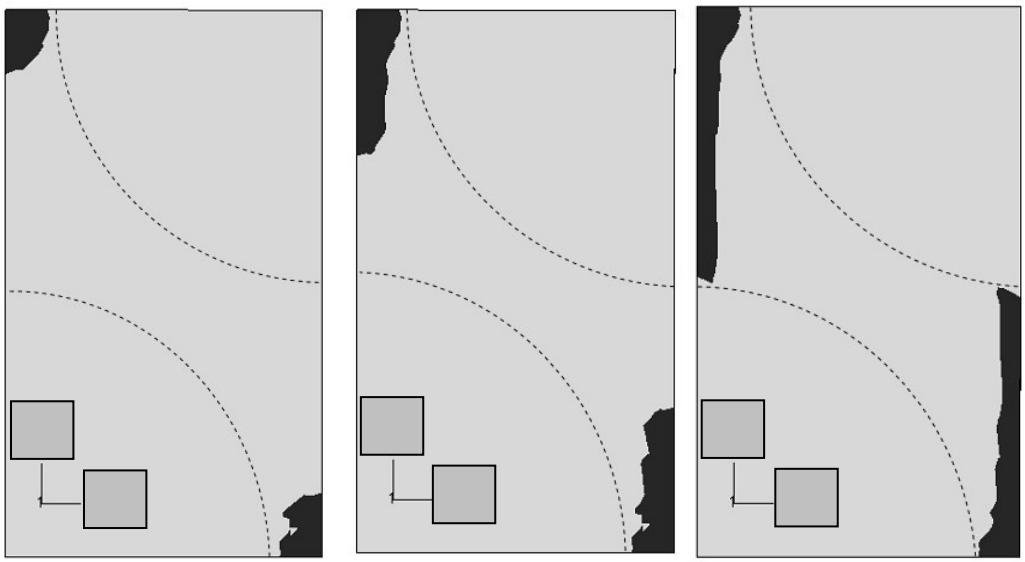

(a) (b) (c)

Fig. 4.10 - Damage initiation and evolution under uniaxial transverse tensile loading along *y*-direction evaluated by means of the Maximum Principal Stress with no residual stress (V_f 60%).

With the residual stress/strain state, the evolution of damage for uniaxial tensile loading in the *y*-direction is shown in Fig.4.11. The residual stress/strain state corresponds to the conditions of 1% shrinkage strain and 149°C curing temperature.

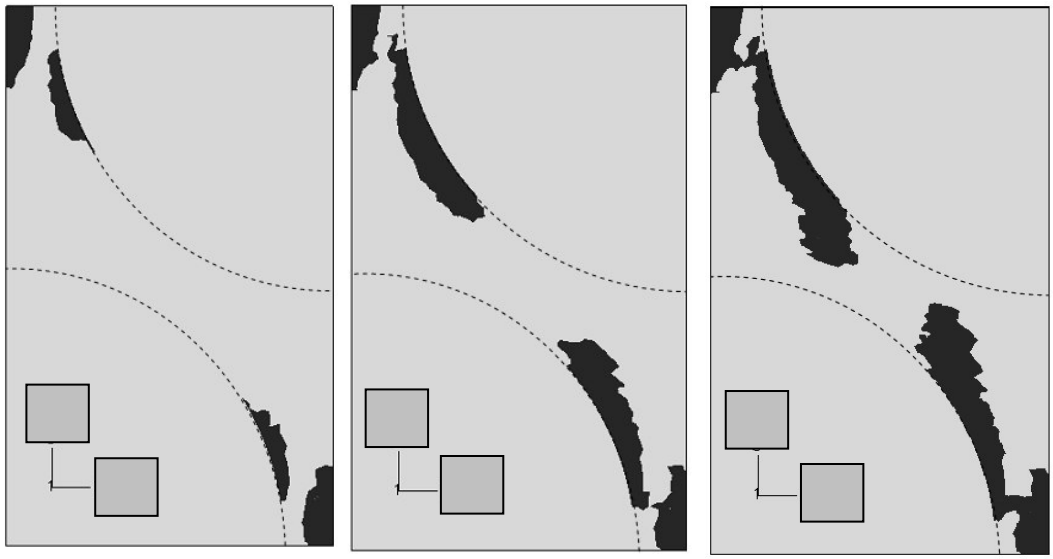

(a) (b) (c)

Fig.4.11 - Damage initiation and evolution under uniaxial transverse tensile loading along *y*-direction evaluated by means of the Maximum Principal Stress with residual stress (V_f 60%).

It can be seen that the site of damage initiation and the subsequent evolution are clearly affected by thermal residual stress. If the residual stress is included, damage initiates near the bottom of the fibre/matrix interface and evolves along the fibre/matrix interface.

The damage onset in the *z*-direction with no residual stress takes place at the fibre/matrix interface as depicted in Fig.4.12

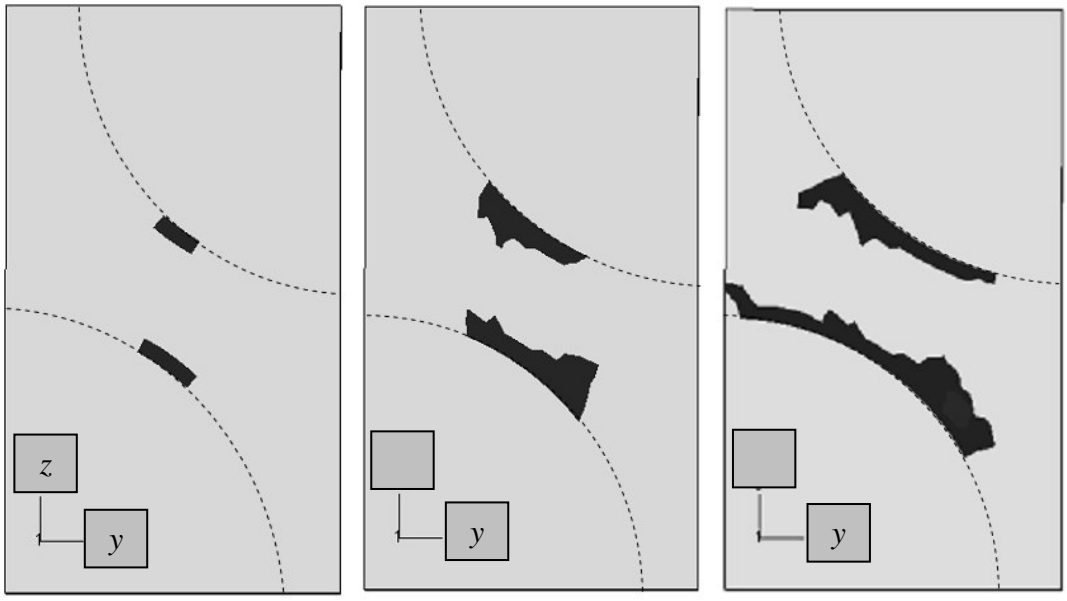

(a) (b) (c)

Fig.4.12 - Damage initiation and evolution under uniaxial transverse tensile loading along *z*-direction evaluated by means of Maximum Principal Stress criterion with residual stress (V_f 60%).

For this load case damage initiation and its evolution are not affected significantly by the presence of residual stresses. A crucial result is that the initiation of the damage depends on the mode of loading: *y*-direction or *z*-direction. As displayed in Fig. 4.10-12 the damage onset occurs within the matrix in different areas. Specifically, in the *y*-direction, damage takes place in the corners of the RVE and in the *z*-direction, at the fibre/matrix interface in the centre of the RVE. The interpretation for such a difference is due to the particular *line of symmetry* [35] in the RVE under investigation in which fibres are assembled with a hexagonal packing array (Fig.4.13). Hence the stress field, distributed symmetrically about the line of symmetry, is different than in a square packing array.

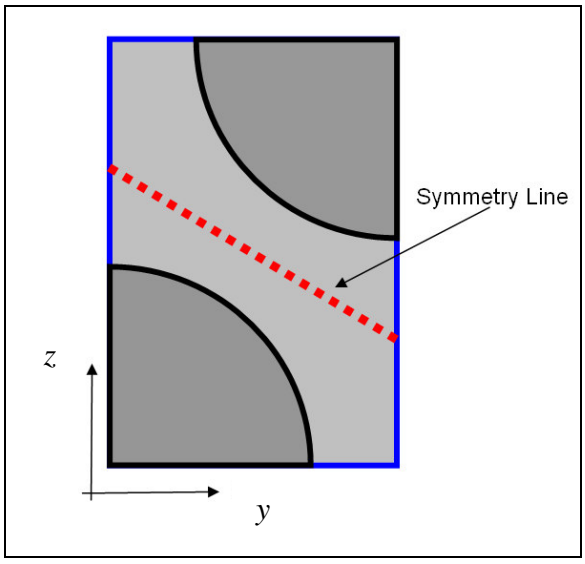

Fig. 4.13 - Line of symmetry in a RVE (hexagonal packing array).

During the damage analysis, the global stress-strain response in the loading direction was monitored and an example of results is given in Fig. 4.14 for the cases with and without residual stress.

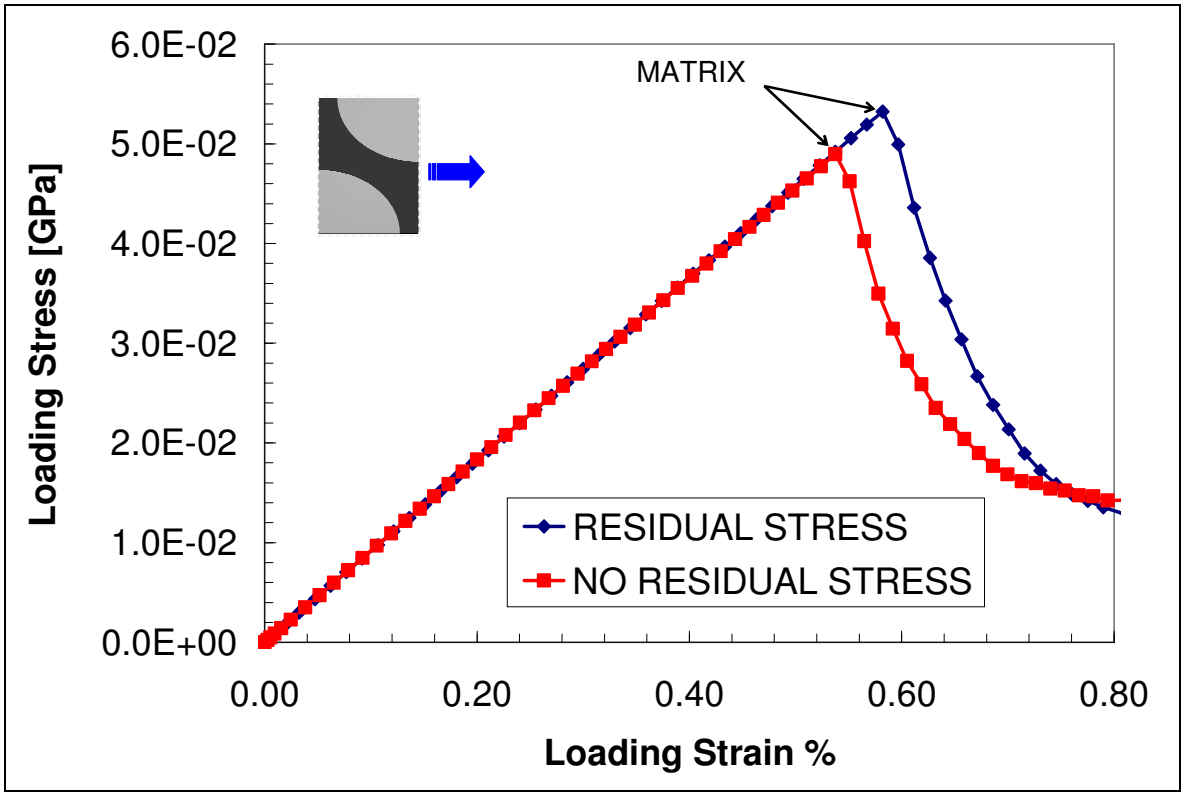

Fig. 4.14 - Global stress-strain curve in *y*-direction for uniaxial transverse tensile loading (60%).

For both cases, the carried stress starts to drop from the point of damage initiation. Once damage is initiated, the model tends to fail suddenly. Thus, the initial failure strain level is also the final failure level for transverse loading. This brittle behaviour is also observed under the *z*-direction loading. In Fig. 4.15 the dependence of ultimate strength on fibre content is displayed for these load directions in the case of no residual stress.

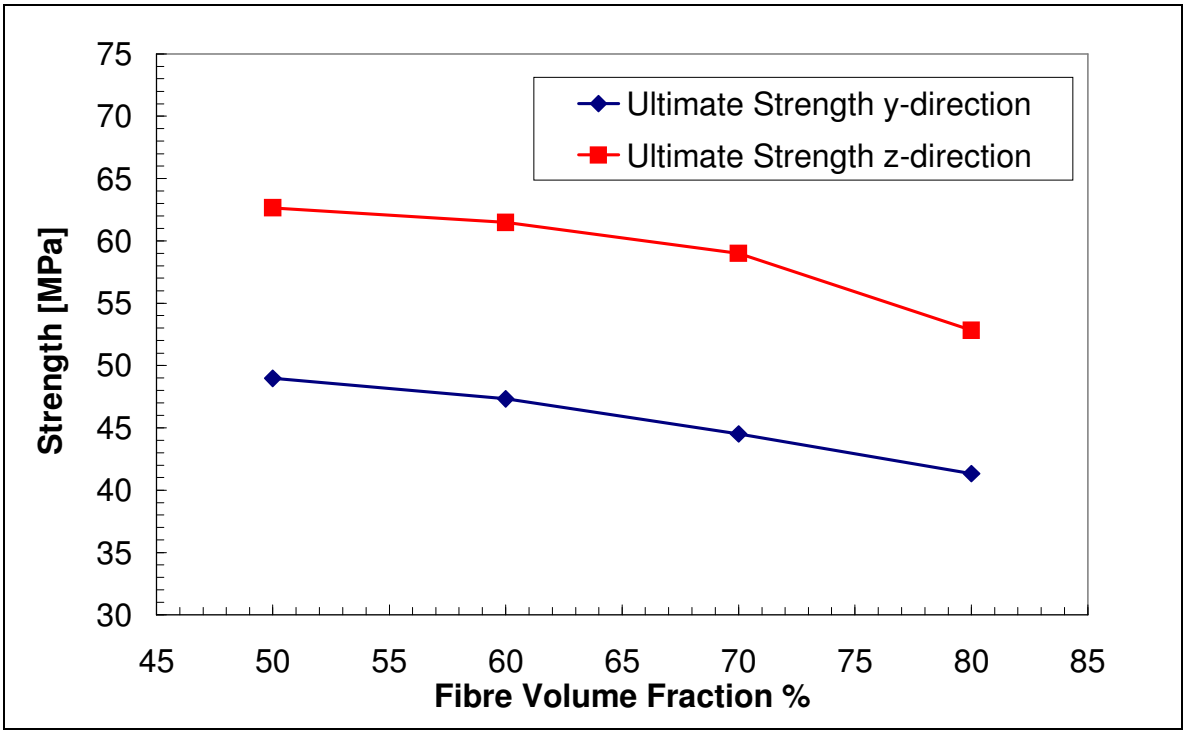

Fig. 4.15 - Comparison of ultimate strength for *y*-direction and *z*-direction loading by using the Maximum Principal Stress criterion. No residual stress applied.

The comparison between the strengths predictions using the Maximum Principal Stress and the Raghava failure criteria at different fibre content has an immediate consequence. In fact, the Raghava failure criterion shows the same location in predicting damage onset for the all cases (no-residual stress and residual stress, *y*- and *z*-direction loading state) but it is always less conservative in terms of ultimate strength (Fig. 4.16-19).

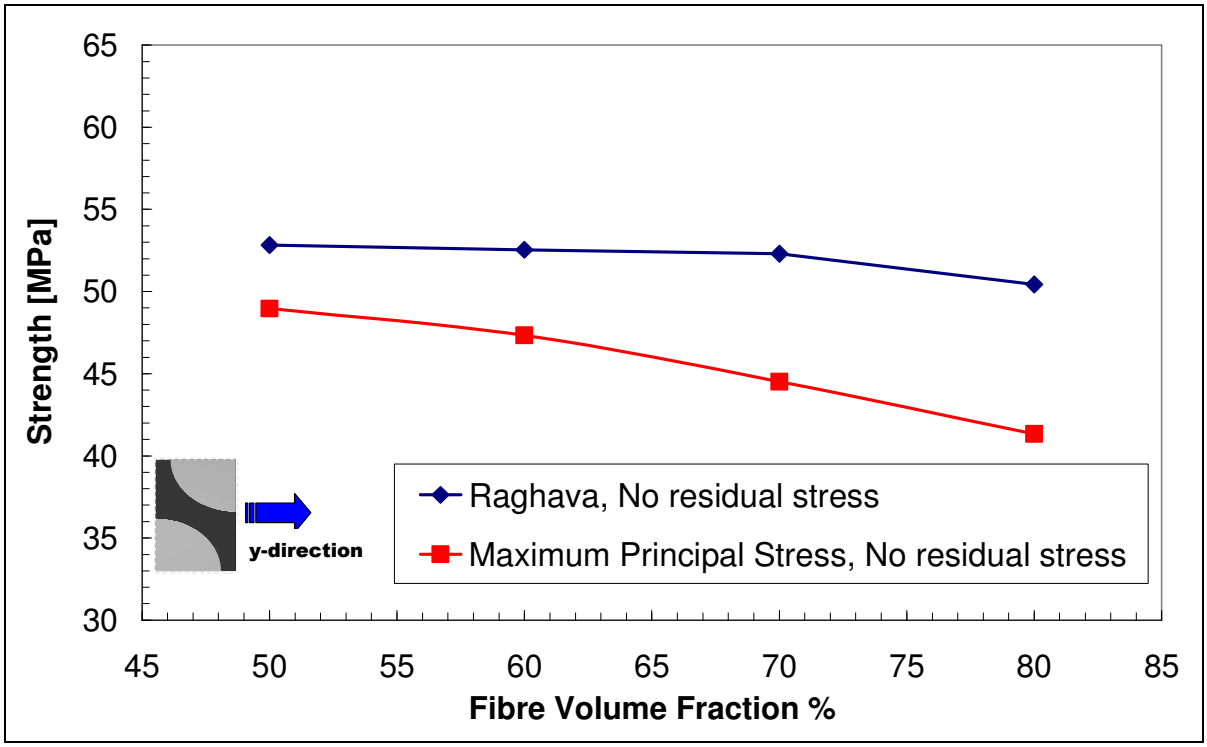

Fig. 4.16 - Trend of ultimate strength (MPa) in *y-direction* evaluated with Maximum Principal Stress and Raghava failure criteria. No residual stress.

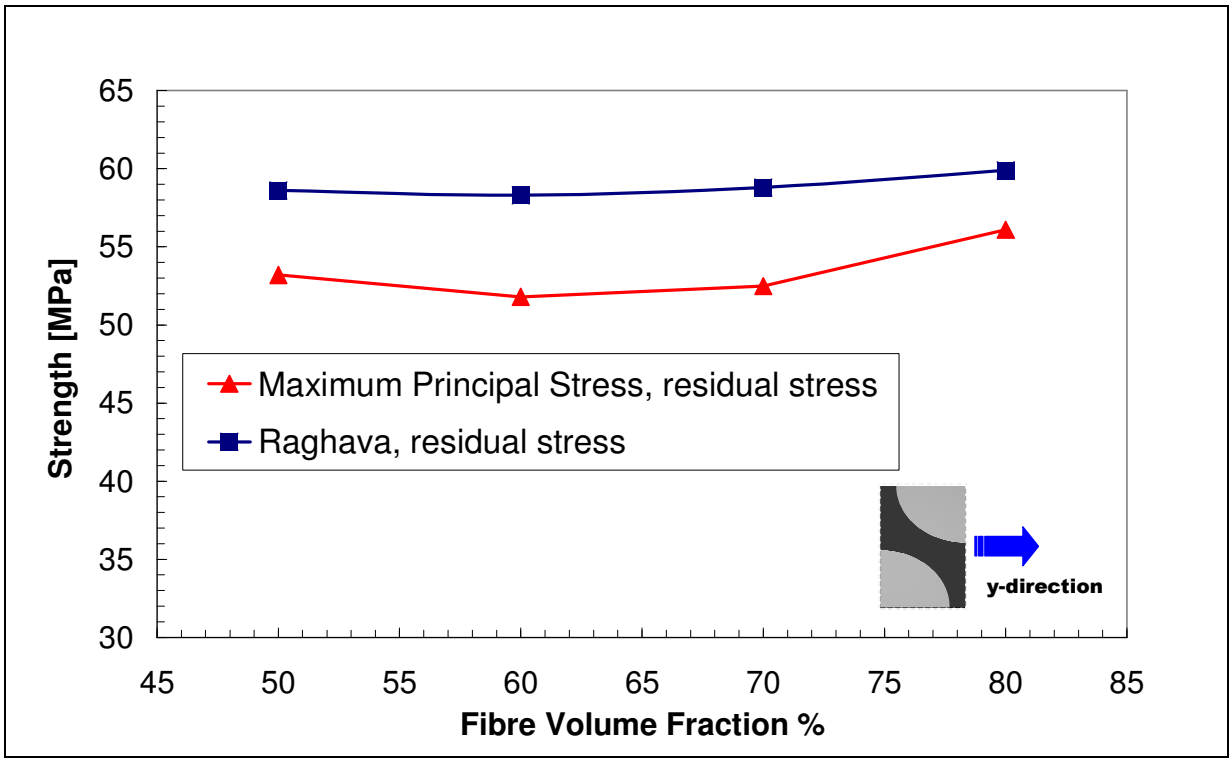

Fig. 4.17 - Trend of ultimate strength (MPa) in *y*-direction evaluated with Maximum Principal Stress and Raghava failure criteria. Effect of residual stress.

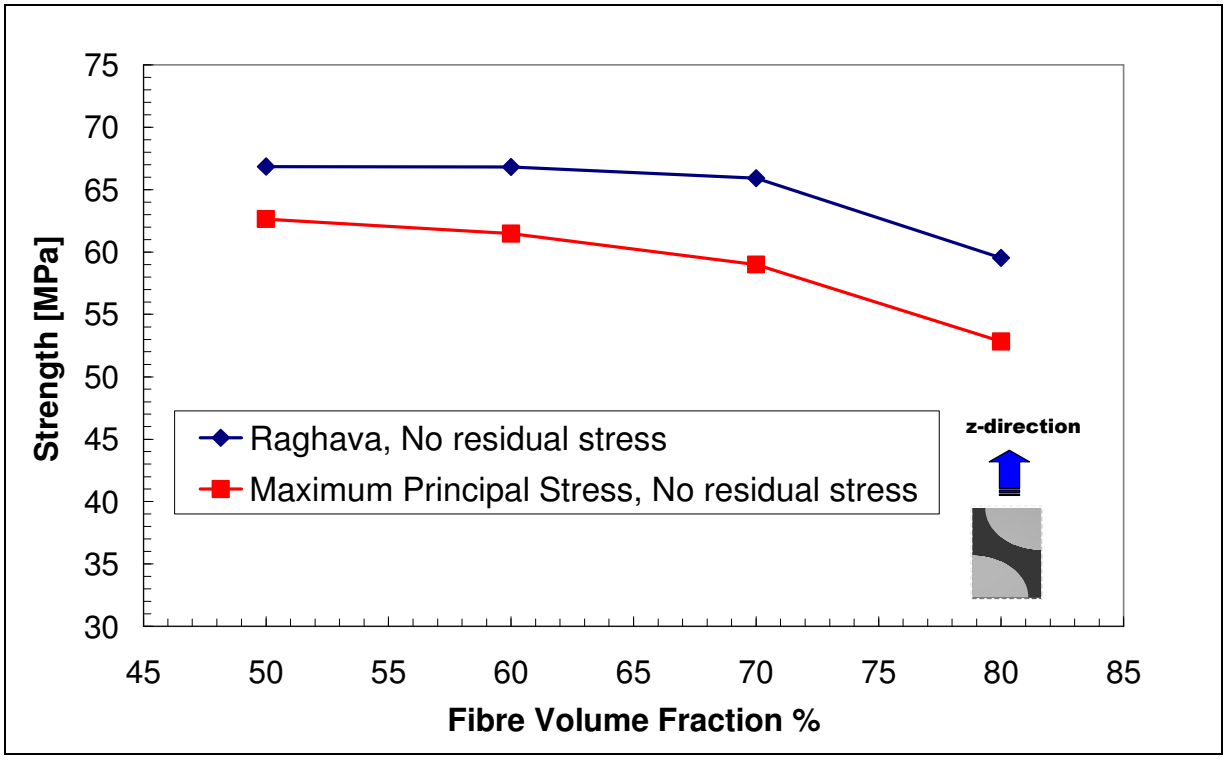

Fig. 4.18 - Trend of ultimate strength (MPa) in *z*-direction evaluated with Maximum Principal Stress and Raghava failure criteria. No residual stress.

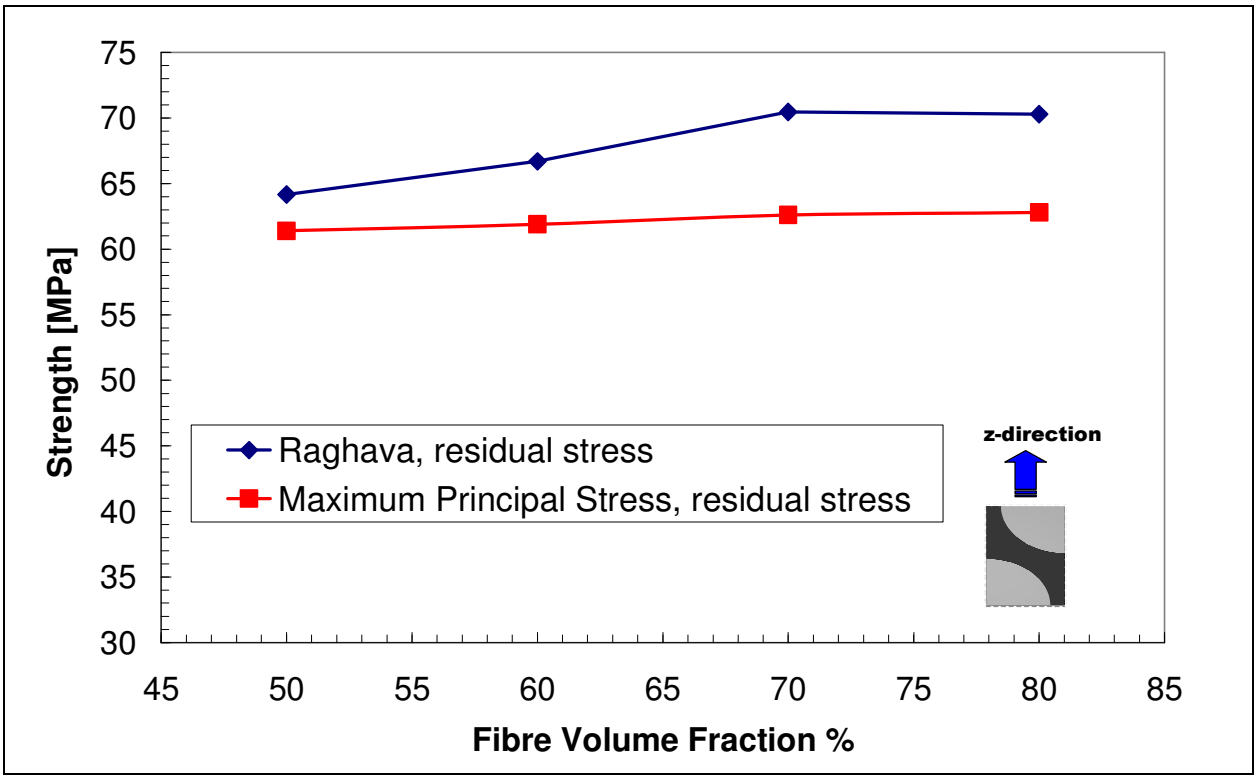

Fig. 4.19 - Trend of ultimate strength (MPa) in *z*-direction evaluated with Maximum Principal Stress and Raghava failure criteria. Effect of residual stress.

Furthermore, the presence of residual stress in *y*-direction loading above 50% fibre volume fraction is always beneficial while for *z*-direction loading residual stress is slightly detrimental for low fibre volume fractions but becomes beneficial from a V_f of 57% (Fig.4.26 and Fig.4.27).

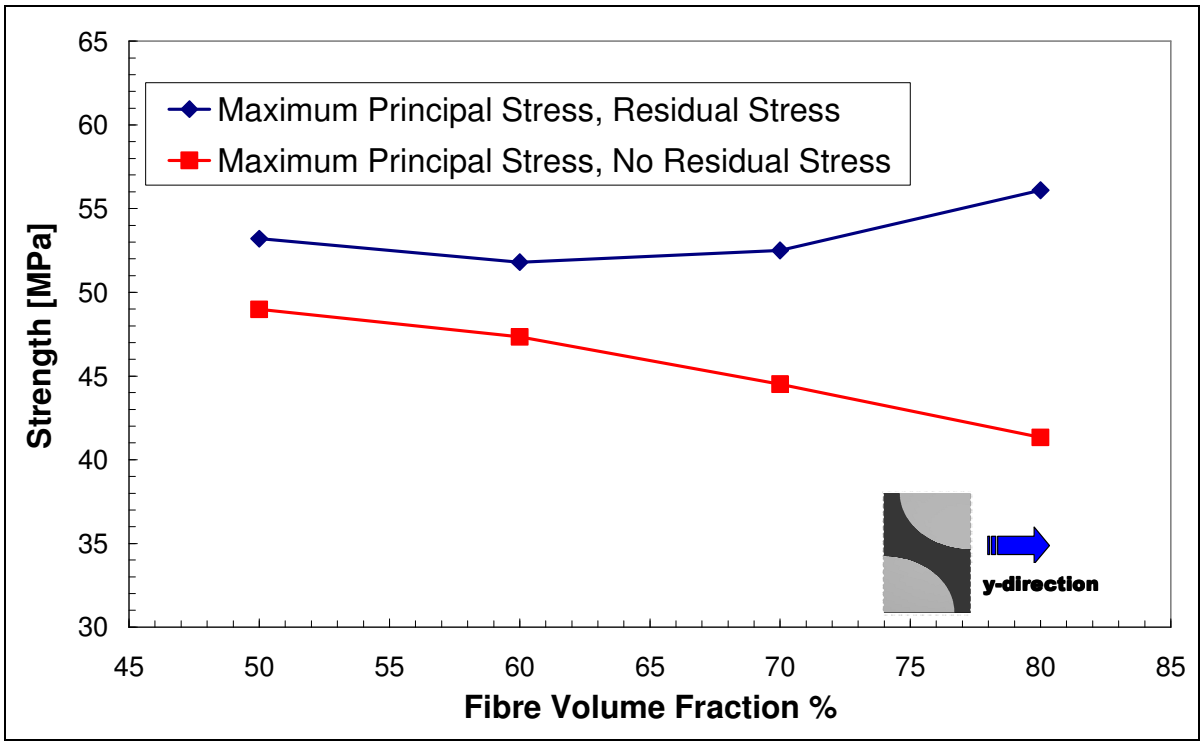

Fig.4.26 – Ultimate strength (MPa) with and without residual stress (*y*-direction).

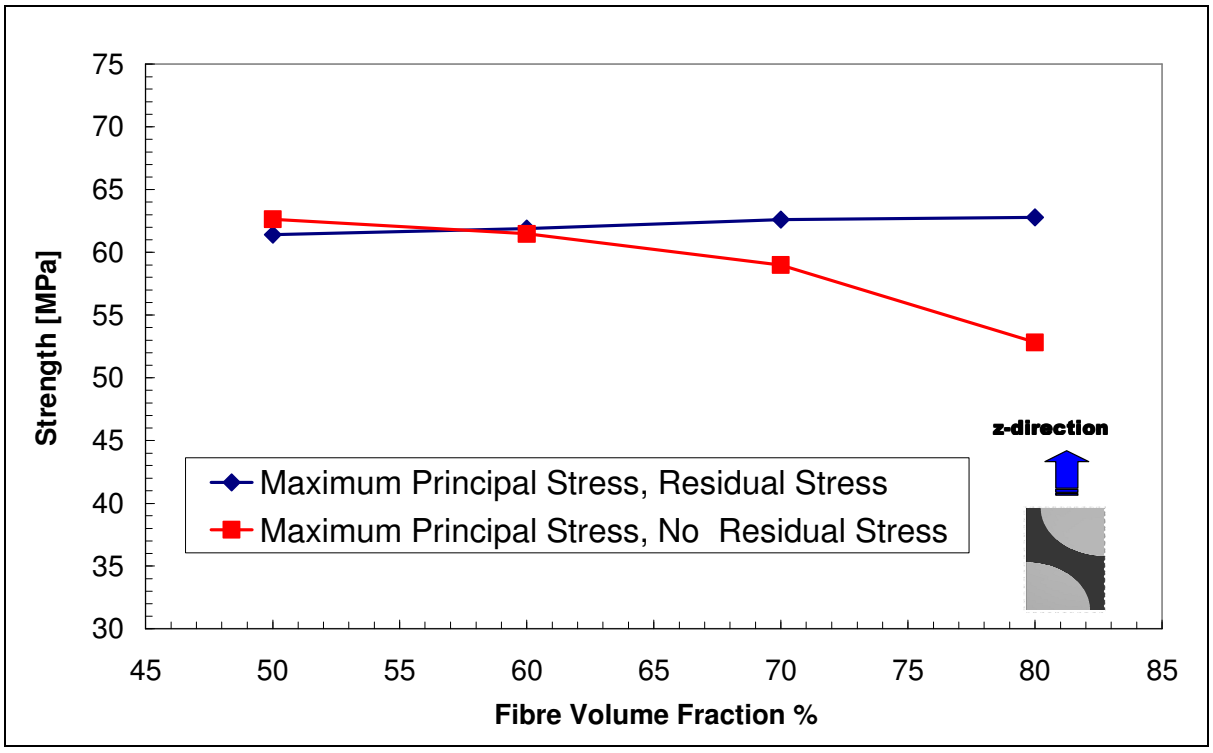

Fig.4.27 - Ultimate strength (MPa) with and without residual stress (*z*-direction).

Residual stresses after curing and cooling cause a redistribution of the internal stress field when applying loads and the positive consequence is to lower stresses in the resin, improving the ability to bear loads in the *y*- and *z*-directions. Models with low fibre volume fractions undergo a detrimental effect due to thermal residual stress when the model is loaded in the *z*-direction. After cooling the highest values of residual stresses in the matrix are concentrated along the fibre/matrix interface in particular areas but the evolution of the stress field by applying a displacement in *z*-direction is dissimilar. In fact, for high fibre volume fractions stresses tend to spread internally within the resin whilst for low fibre contents they remain highly concentrated at the interface throughout the analysis, weakening this area significantly. Hence, residual stresses could play an important role in decreasing the overall response of the composite negating the potential beneficial effects for *y*- and *z*-direction transverse loading and producing a drastic failure of the composite.

4.6 Conclusions

Residual stress and its effect on transverse and longitudinal failure of fibre-reinforced polymer matrix composites were studied using a micromechanical unit cell model and the finite element method. Results obtained with the residual stress analysis were also compared to data from a non-residual stress analysis. The overall residual stress is determined by considering two contributions: volume shrinkage of matrix resin during isothermal curing and thermal contraction of both resin and fibre as a result of cooling from the curing temperature to room temperature. Analyses confirm the isothermal residual stress during curing can be considered negligible compared to the thermal residual stress due to cooling.

A study of two different failure criteria was performed for the matrix in order to evaluate differences in the capability to predict failure. The assessment of the failure criteria investigated proves that they are capable to describe qualitatively the material behaviour of the composite

under longitudinal and transverse loading agreeing broadly with data in the literature. In particular the Raghava modified von Mises criterion results more accurate to detect the matrix failure on longitudinal (parallel to the fibres) loading. On the contrary on transverse loading, as the fibres are stiffer than the matrix, the unit cell is principally deformed in the *y*- and *z*-direction while the contraction in the *x*-direction is totally negligible and the Maximum Principal Stress failure criterion have been more conservative in the prediction of the failure.

The comparison between the residual and non- residual stress analysis has demonstrated that the predicted damage initiation and evolution are clearly influenced by the presence of residual stress. Residual stress causes a premature failure in the matrix at a lower strain than with no residual stress conditions on longitudinal loading case (*x*-direction) and it is always detrimental for the matrix while for the fibre there is no important alteration in terms of ultimate strength. In particular, the effect of residual stress on transverse tensile loading (*y*- and *z*-direction) depends on the fibre volume fraction and produces beneficial results in the *y*-direction at the fibre volume fractions studied while, in *z*-direction it is detrimental for low fibre volume fractions.

Chapter 5

Effects of Interphasial Properties on the Mechanical Behaviour of RVEs

5.1 Introduction

Recent research has showed that the local microstructure in the vicinity of fibre/matrix interface can be altered significantly by various fibre surface treatments and the presence of this interphase is critical on the final behaviour of composites. Unfortunately, experimental studies are not able to describe the "evolution" of the interphase in composites with polymeric matrix during the curing and the cooling process and moreover numerical studies neglect to take into account the distribution of micro stresses within the interphase due to the presence of residual stress occurring in the manufacturing process.

Hence, there is a need to further investigate the local response of hexagonal unit cells that undergo thermal residual stresses and in which there is the presence of an interphase.

Although results from Chapter-4 showed beneficial and detrimental effects of residual stress depending on different variables (e.g. fibre content, matrix ultimate strength), failure onset was never detected during chemical shrinkage or cooling process. This phenomenon is sometimes detected in a real curing process.

As already seen, researchers are also trying to "engineer" interphases in real composite materials at micro-scale in order to improve the overall mechanical behaviour of composites materials. Hence another important aspect in the present numerical investigations is to simulate and predict the final response of composites at the component level scale by simply varying the material properties of the interphase.

5.2 Finite Element Modelling

In the present work, three-dimensional finite element analysis has been used to study the overall behaviour, damage onset and its evolution of a simple unit cell model with a hexagonal array of fibres under transverse and longitudinal uniaxial loadings. The numerical 3D models include an interphase with a constant thickness and material properties showing **"idealised"** temperature-dependent properties over the curing a cooling process. A symmetric distribution of fibres and a constant value of the fibre volume fraction have been considered in these studies.

The initiation of microcracks in unidirectional composites at micro level is usually governed by the strength of the adhesion between fibres and matrix. The local stress concentration around the fibres due to mechanical loading, combined with the residual thermal stresses arising during the curing process, make the fibre/matrix transition region the most important constituent of a composite material. Because both terms interface and interphase are often used to refer to the fibre/matrix transition, in order to avoid confusion the definition of these terms is previously given:

1. *Interphase*: an interphase is defined as a three-dimensional region between fibre and bulk matrix, with a different morphology, chemical composition and mechanical properties, compared to both fibres and bulk matrix.
2. *Interface*: an interface is defined as a two-dimensional edge between fibre and matrix, if no inter phase is considered, or fibre and interphase.

According to these definitions, an interphase becomes an interface, if its thickness tends to zero. In this work the transition between fibre and matrix is modelled as an interphase with different properties, compared to fibre and matrix.

Despite a lot of efforts, a full characterization of the interphase, constituted during the curing process, has not been yet fully achieved. In the present work the interphase has been modelled as an isotropic layer with material properties constant over its thickness. In order to investigate the effect of residual stress the Young's modulus and Poisson's ratio of the interphase are considered temperature dependent. More precisely the Young's modulus is defined by the following relation in *Region-II* and *Region-III* described in Chaper-4 (Fig. 5.1)

$$E(T) = E_0 \exp\left[-k\left(\frac{T - T_g - \Delta T}{2\Delta T}\right)\right] \qquad (5\text{-}1)$$

$$E(T) = E_0 \exp\left[-kf(T)\right]$$

The thermal expansion coefficient α is assumed to be equal to the matrix CTE.

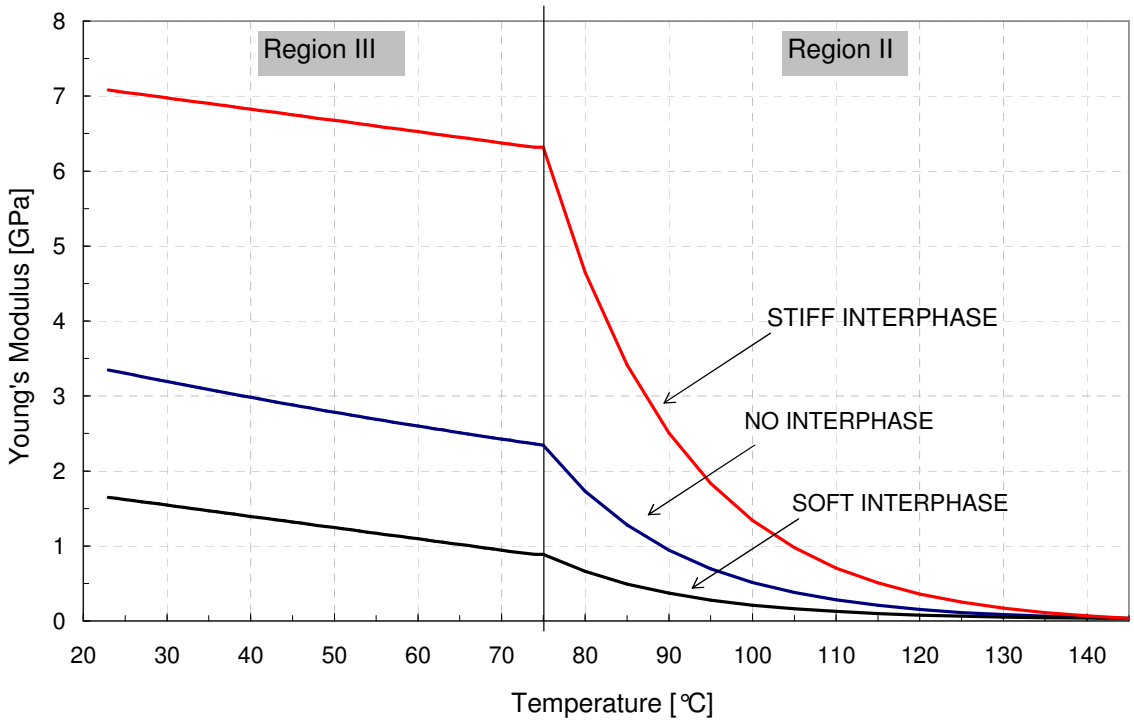

Fig.5.1 – Mechanical behaviour during the cooling and curing process.

In the micromechanical approach, the constituent fibre, matrix and interphase materials and their interaction are distinctively considered to predict the overall behaviour of the composite material

structure. The micromechanical approach allows relating stresses of each constituent in the micromodel, namely: fibre, matrix and interphase. Therefore, failure can be detected independently in each of these constituents and the appropriate property degradation can be applied. Here, the micromechanical model considers a unit cell in which fibre, matrix and interphase are assumed to be perfectly bonded at their interfaces throughout the analysis, with fibres arranged in a hexagonal cross section array by assuming the repetitive or periodic nature of the fibre and matrix materials. The unit cells are a three-dimensional solid and the fibre volume fraction is 70%.

The boundary conditions, damage and post-damage model applied for this investigation has been previously illustrated in Chapter-4. In these FEM studies only two loading conditions have been applied to the unit cell shown in Fig. 5.2, namely:

1) transverse loading on the *y*-direction,
2) transverse loading on the *z*-direction,

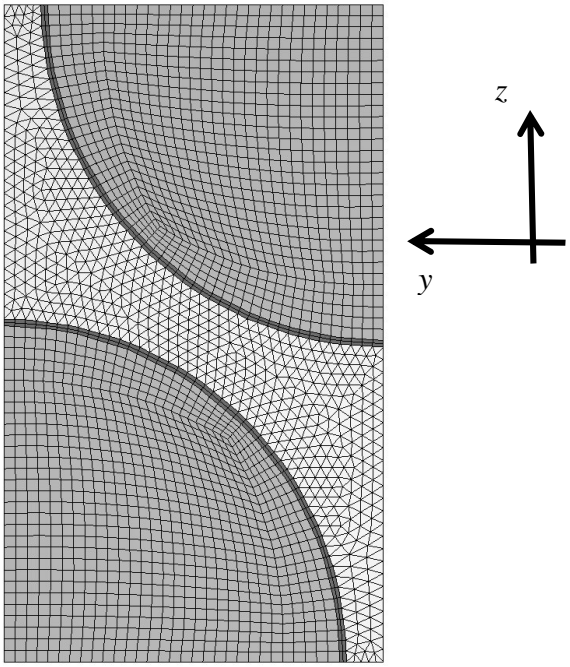

Fig.5.2 – 1/4 of the hexagonal array packing RVE used as reference model with interphase.

5.3 Finite Element Results of RVEs with Interphase

The first goal of this research was to understand whether a thin interphase can influence the mechanical behaviour of composite materials at the microscale.

A finite element study on unit cell in absence of residual stresses has been performed in order to investigate the effects of thin interphases on the overall mechanical behaviour of the micro numerical models. The ultimate strength of interphase and matrix has been assumed to be the same (80MPa) while the values of the Young's moduli $E_{interphase}$ for the interphase are:

1a) $E_{interphase\text{-}soft}$ = 1.50GPa (softer interphase);

2a) $E_{interphase\text{-}stiff}$ = 7.45GPa (stiffer interphase).

Numerical results show that the unit cell undergoes a "stiffening" or "softening" effect depending on the materials properties in the interphase on the *y*-direction and *z*-direction (Fig. 5.3 and Fig. 5.4).

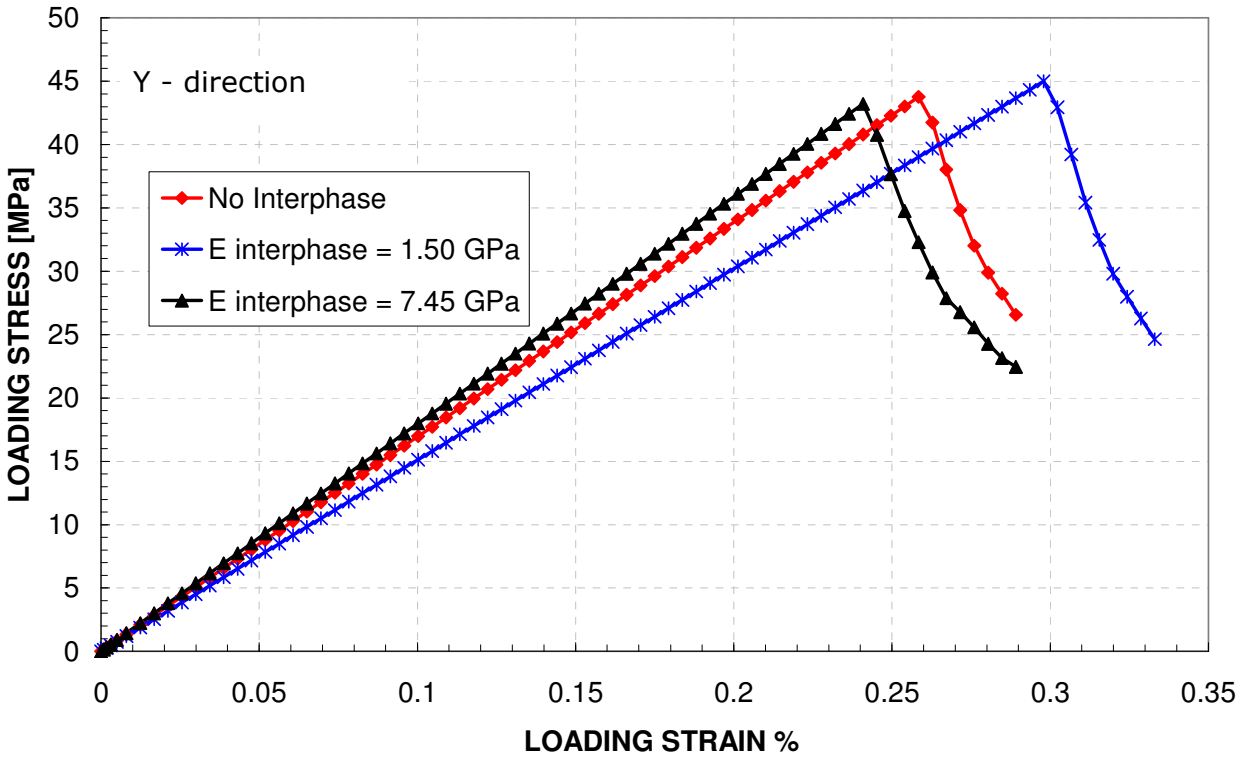

Fig 5.3 - Ultimate strength under *y*-direction loading (no residual stress).

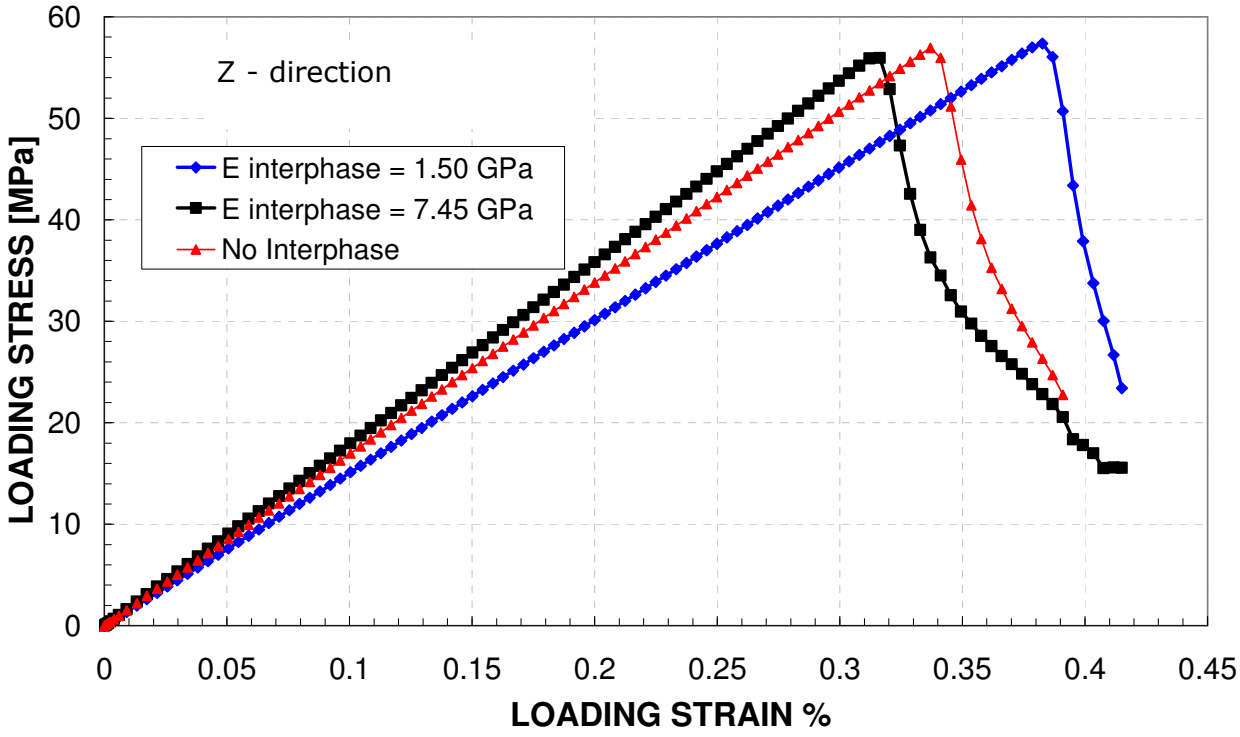

Fig.5.4 - Ultimate strength under *z*-direction loading (no residual stress).

On transverse tensile loading numerical results have shown that the ultimate strength in unit cells loaded in the *y*-direction and with a softer interphase is circa 4% greater than the ultimate strength in the micromodel with a stiffer interphase. The ultimate strength in unit cells with a soft interphase and loaded in the *z*-direction is circa 2.5% greater than the ultimate strength evaluated in the stiffer interphase. The magnitude of the ultimate strain in the unit cell with a softer interphase is even larger if compared to the ultimate strain of the unit cell with a stiffer interphase, namely: 20% in the *y*-direction and 22.5% in the *z*-direction.

Although the interphase (0.1μm) is only 1/100 of the fibre diameter it plays a significant effect on the overall elastic response of the micromodels. In fact, by adding a thin interphase with a Young's modulus of nearly 50% lower than the matrix Young's modulus, the elastic properties of the micromodel display a beneficial effect in terms of transverse ultimate stress and transverse

ultimate strain while, the stiffer interphase (E=7.45GPa) tends to reduce the capability of the micro-composite to bear transverse loads.

5.3.1 Effect of elastic interphasial properties and thermal residual stresses

Preliminary analyses have been performed on unit cells with different combinations of Young's moduli and Poisson's ratios in order to investigate both the distribution and the magnitude of thermal residual stresses within the micromodels.

The overall contraction of the resin has to be attributed to chemical shrinkage and thermal cooling and it can be expressed as:

$$d\varepsilon_{ij} = de_{ij} + \delta_{ij} ds + \delta_{ij} \alpha(T) dT \tag{5-2}$$

where $d\varepsilon_{ij}$ is the total strain increment, de_{ij} the elastic strain increment, ds the shrinkage strain increment due to the chemical reaction (cross-linking) in the absence of constraint, α(T) the thermal expansion coefficient which is dependent on the temperature, dT the temperature increment and δ_{ij} is the Kronecker delta. The stress-strain relationship can be derived as:

$$d\sigma_{ij} = C_{ijkl} de_{kl} = C_{ijkl} \{ d\varepsilon_{ij} - \delta_{ij} ds - \delta_{ij} \alpha(T) dT \} \tag{5-3}$$

where $d\sigma_{ij}$ are the stress increments and C_{ijkl} the stiffness components. The stress analysis is based on linear elasticity and the stiffness components C_{ijkl} are related to the Young's modulus E and the Poisson's ratio ν of the material. In order to simulate the curing process, the analysis was performed by two discrete steps, where step *one* is the shrinkage stress analysis and step *two* is the thermal cooling stress analysis.

The shrinkage residual stress was calculated by applying a given amount of resin shrinkage. For the epoxy resin considered here, the linear shrinkage strain was chosen to be 0.35% which

corresponds to a volumetric change of circa 1%. The overall thermal residual stresses are due to the cooling of the system from the curing temperature, 149°C, to room temperature, 23°C.

The mechanical properties of the resin, in terms of shear modulus (and Young's modulus when the resin becomes solid), increase drastically as the material evolves from a liquid state to a solid state. Hence in the resin, geometrically constrained within the interstices present between fibres, tensile stresses develop more easily. Moreover, during chemical shrinkage, in which resin is in a rubbery state, realistically no deformation is established along the *x*-direction. Strains parallel to fibres are only developed during cooling as the resin evolves from a liquid/rubbery state into a solid state. The amount of residual stresses within the matrix and interphase also strongly depend on the material properties of interphase e.g. Young's moduli and Poisson's ratio and thickness.

Preliminary analyses have been carried out to evaluate the amount of residual stresses after the processes of curing and cooling in order to understand the effects of the residual stresses in unit cells with an interphase and different mechanical characteristics. The material properties of the interphase and the matrix have been assumed the same in *Region-I* in which the matrix I s in liquid or rubbery state and E has a very small value. In *Region-II* and *Region-III* the evolution of the material properties for the interphase are expressed with equation (5-1) and it is shown in Fig.5.1. The final values of the Young's moduli are:

1a) E = 1.50GPa (softer interphase);
2a) E = 3.35 GPa (equal to matrix's modulus);
3a) E = 7.45GPa (stiffer interphase).

The values of Poisson's ratio have been considered constant throughout the numerical simulation of curing and cooling process. Three values have been chosen and they are here summarized:

Poisson's Ratio

1b) $\nu = 0.3$;
2b) $\nu = 0.35$;
3b) $\nu = 0.4$.

The Poisson's ratio ν = 0.35 derives from the material properties of the epoxy matrix while the other two values have been chosen arbitrarily. The interphase has a thickness is 0.1µm (fibre diameter is 11µm) and it has been considered as homogeneous. Hence it has been assumed that material properties in the interphase undergo spatially the same behaviour during the chemical shrinkage and cooling process. The elements used to mesh the interphase are quadratic solid brick elements. The dimension of these elements is the smallest dimension allowed by ABAQUS for this geometry.

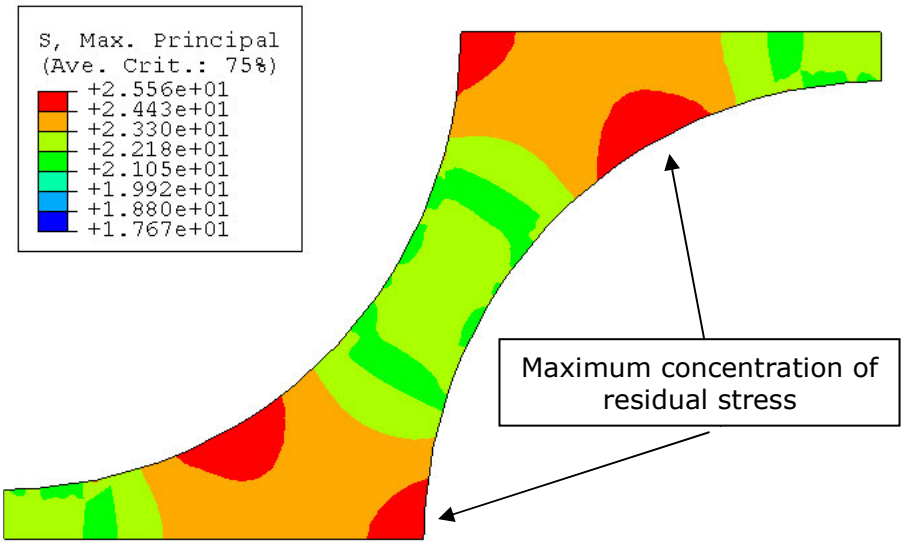

Fig. 5.5 - Maximum Principal Stress [MPa] in the matrix - SOFT INTERPHASE (ν=0.3)

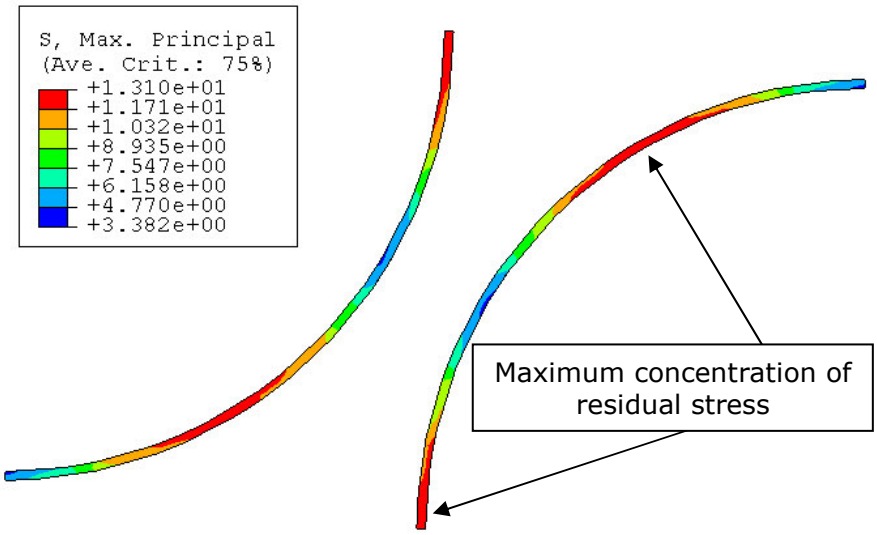

Fig. 5.6 - Maximum Principal Stress in the interphase - SOFT INTERPHASE (ν=0.3)

The distribution of stresses after chemical shrinkage and cooling is shown in Fig.5.5 and Fig.5.6 Residual stresses for different combinations of elastic properties has been summarised in Table 5-1. Estimated residual stresses have been calculated with the Maximum Principal Stress criterion.

Table 5-1 – Values of residual stresses in the matrix and interphase for different material properties of the interphase

Interphase Properties		Residual Stress after cooling [MPa]	
Young's Modulus [GPa]	Poisson's Ratio (constant value)	Matrix	Interphase
1.50	0.3	25.5	12
1.50	0.35	25.5	13
1.50	0.4	25.5	14.5
7.45	0.3	27	57
7.45	0.35	27	59
7.45	0.4	27	67

From the results presented in Table 5-1 it is clearly shown that the material properties of a thin interphase influence the magnitude of the residual stresses within the matrix and interphase. Although residual stresses in unit cells with "soft" interphase display higher values of stresses in the matrix, the magnitude of these stresses is less than 50% of the values reached in unit cells with a "stiffer" interphase. In unit cells with a stiff interphase (E= 7.45GPa), residual stress are totally concentrated within the interphase.

5.4 Strength Study

The high value of thermal residual stresses evaluated at the interphase of unit cells with stiffer interphase highlight the importance to further investigations on the effects of the overall mechanical behaviour and especially the damage onset and evolution in the numerical micromodels under different unidirectional tensile loadings.

In the analyses that account for the presence of residual stresses, the material characteristics of the interphase as well as the matrix undergo profound modification throughout the analysis. The value of the ultimate strength has been assumed constant over the curing and the cooling process. But while for the matrix the value of the ultimate strength is known (80MPa) as for the interphase, this parameter remain unknown and it has been chose arbitrarily in order to carry out parametric studies on the effect of different ultimate strengths on damage formation and evolution.

5.4.1 Effect of a stiff interphase on the transverse loading

Different values of interphase ultimate strengths have been investigated to study the effects of thermal residual stress on failure and damage onset and evolution. Finite element analyses have been carried out on unit cell of 70% in fibre volume fraction with and without residual stress to compare the overall mechanical behaviour on tensile uniaxial loading. The values of ultimate strengths attributed to the interphase ($\sigma_{U,interphase)}$ for the parametric study vary from 20MPa to 140MPa.

Moreover the Poisson's ratio has been assumed equal to ν=0.35 both for the matrix and the interphase throughout the curing and cooling process.

Fig.5.7-12 display the damage onset and the following propagation within the unit cells with the stiff interphase (E=7.45GPa) on transverse loading along the *y*-direction.

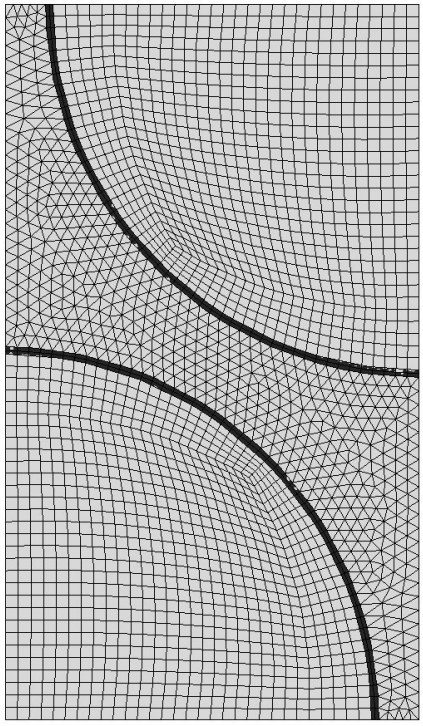

Fig.5.7 – Damage onset in unit cells with ultimate strength $\sigma_{U,interphase}$ 40 MPa (residual stress analysis).

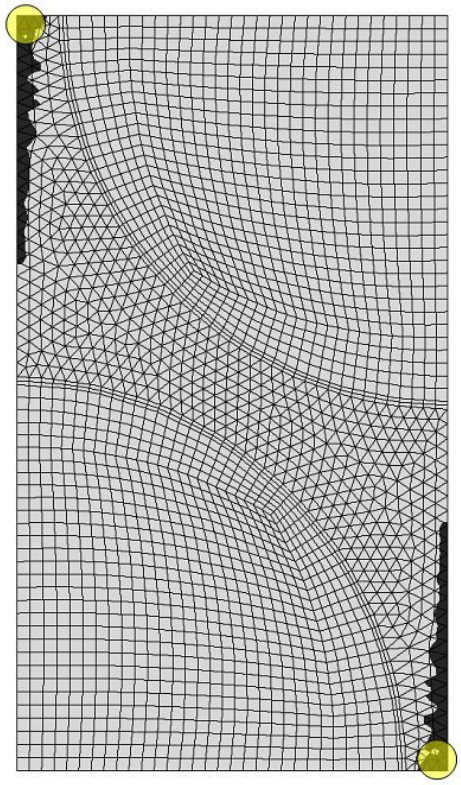

Fig. 5.8 - Damage onset and evolution in unit cells with $\sigma_{U,interphase}$ 80 MPa (no residual stress analysis). Yellow circles show the location of damage onset.

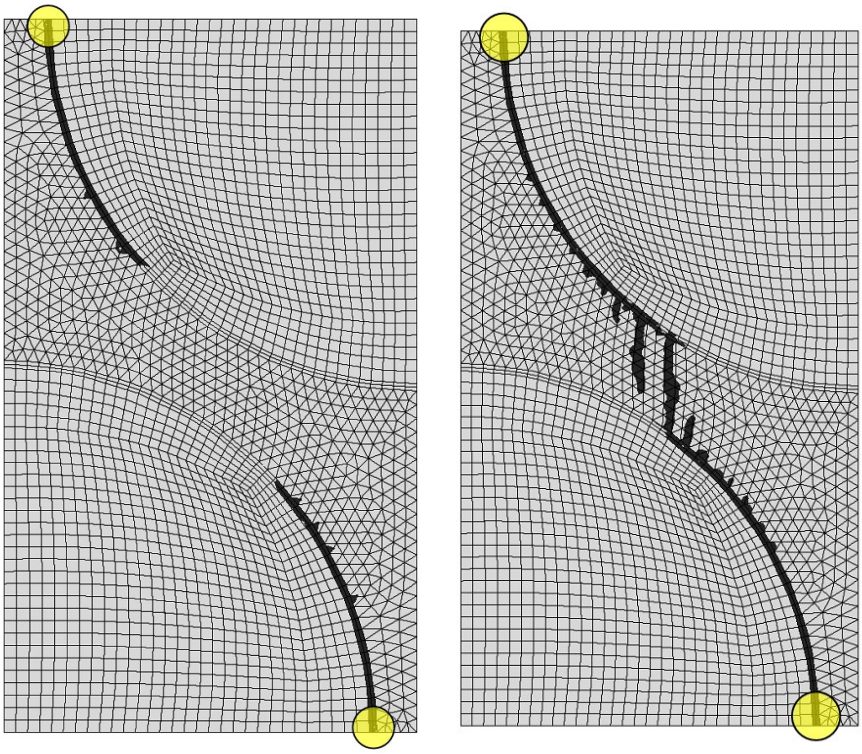

Fig. 5.9 - Damage onset and evolution in unit cells with $\sigma_{U\text{-}interphase}$ 80 MPa (residual stress analysis).

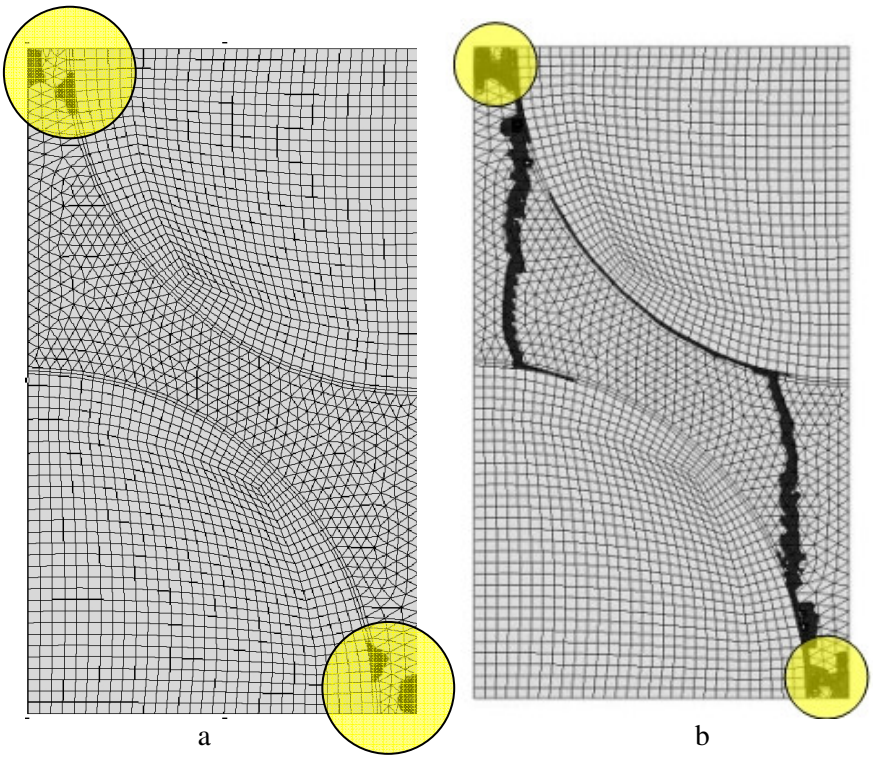

a b

Fig. 5.10 – Damage onset and evolution in unit cells with $\sigma_{U\text{-}interphase}$ 100 MPa (residual stress analysis). Yellow circles show the location of damage onset.

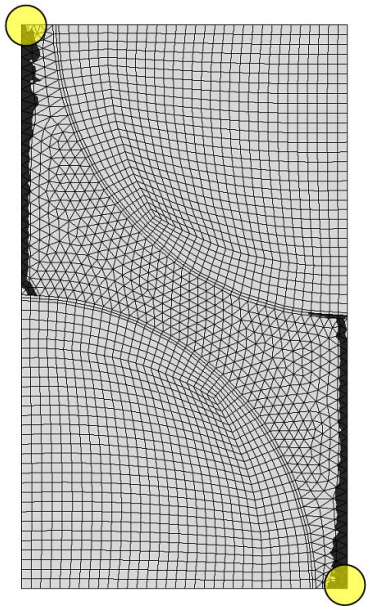

Fig.5.11 – Damage onset and evolution in unit cells with $\sigma_{U,interphase}$ 120 MPa (no residual stress analysis).

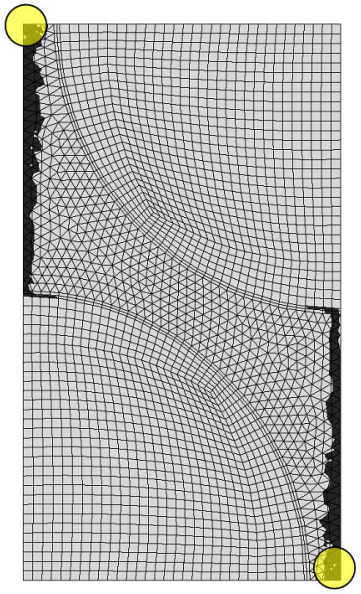

Fig. 5.12 – Damage onset and evolution in unit cells with $\sigma_{U,interphase}$ 120 MPa (residual stress analysis).

A relevant result of the finite element study has been that for values of the $\sigma_{U,interphase}$ below 60MPa strength the failure is detected during the cooling process (Fig.5.7) in which the amount of thermal residual stress, after the curing process, is higher than 60MPa.

Fig.5.7 shows the drastic failure of the interphase during the cooling process.

The unit cells in Fig. 5.8 and Fig. 5.9 show that the presence of residual stresses also greatly influence the location of damage onset. In fact, damage, depicted with black areas, starts in the matrix and/or in the interphase depending on the magnitude of the ultimate strength of the interphase. In general in unit cells with a stiffer interphase (E=7.45GPa) failure has been detected within the matrix in absence of thermal residual stress, for values of $\sigma_{U,interphase}$ above 60MPa (no residual stress) and finally for values of the interphase $\sigma_{U,interphase}$ greater than 100MPa in presence of residual stresses.

Damage initiation in numerical micromodels with an $\sigma_{U,interphase}$ lower than 60MPa (no residual stress) and in unit cells with thermal residual stress and the interphase ultimate strength lower than 100MPa has been localized within the interphase.

A particular case is represented by the unit cell in which the ultimate strength of the interphase is 100MPa. Due to the redistribution of the internal stress during the loading after the whole curing process, the micromodel fails both in the interphase and in the matrix (Fig. 5.10). The damage initiation points are always highlighted by means of a circle in Fig. 5.8-12.

All set of the results related to unit cells with a stiffer interphase are briefly summarized in Table 5-2.

Table 5-2 – Numerical results for a unit cell with a stiff interphase with different ultimate strengths.

	STIFF INTERPHASE - Transverse y-direction			
	No Residual Stress	Residual Stress	No Residual Stress	Residual Stress
$\sigma_{u,INTERPHASE}$ **[MPa]**	RVE Ultimate Strength [MPa]		RVE Failure onset	
20	23.0	**COOLING**	INTERPHASE	INTERPHASE
40	23.0	**COOLING**	INTERPHASE	INTERPHASE
60	33.0	4.3	INTERPHASE	INTERPHASE
80	43.0	31.5	MATRIX	INTERPHASE
100	43.0	51.0	MATRIX	MATRIX/INTERPHASE
120	43.0	51.0	MATRIX	MATRIX
140	43.0	51.0	MATRIX	MATRIX

A further consequence of the residual stress is the detrimental or beneficial effects on the mechanical properties of the micro-composites. Finite element investigation has shown that for values of the interphase ultimate strength below 80MPa, the high values of thermal residual stress has a significant negative effect for the interphase. In particular, thermal residual stress leads to a complete failure of the interphase itself during the cooling process for values of $\sigma_{U,interphase}$ lower than 60MPa. The failure of the entire interphase simulates the complete "debonding" between fibre and matrix. This kind of failure in real composites at micro-scale represents the most likely mode of failure either during the complete curing process or during loading. Under these circumstances the capability of the micro-composite to bear loads under transverse tensile loading are negatively altered.

Nevertheless, the effect of residual stresses starts to produce a beneficial effect in unit cells with the interphase ultimate strength greater than 80MPa. In these unit cells failure has been mainly

localized in the matrix and the damage evolution in general involves partially (Fig 5.10a) or at the last stage of its development (Fig 5.10b) the interphase. Hence fibre/matrix debonding is avoided.

Although the symmetry from the hexagonal distribution of fibres over the cross-section implies the same elastic response both on the *z*-direction and *y*-direction, the effect of damage onset and evolution could display significant differences.

Under the *z*-direction of loading, the weakest area in the unit cell appears to be the region indicated in Fig. 5.13, in which inter-fibre distance has the minimum magnitude. Failure can be detected in the interphase or matrix depending on the value of the interphase ultimate strength.

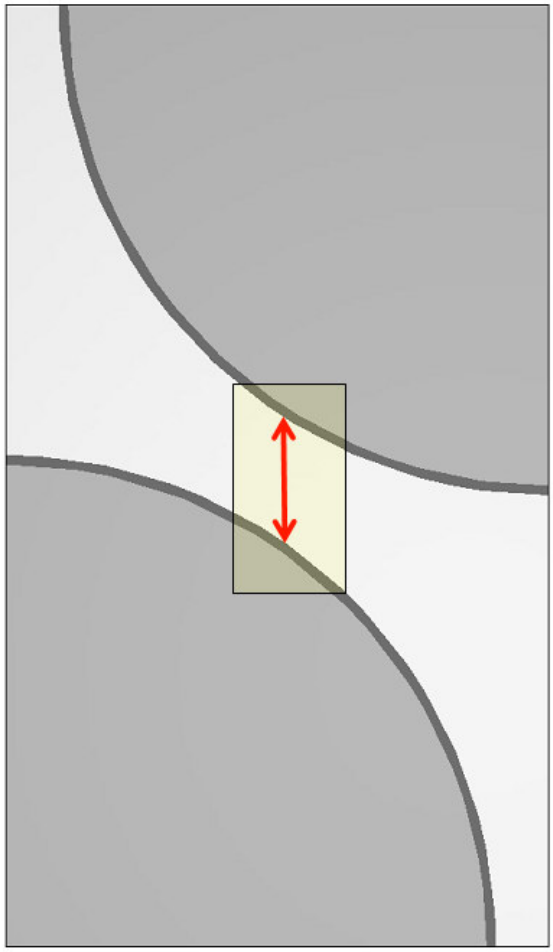

Fig. 5.13 – Location of damage onset in unit cells under transverse loading on the *z*-direction.

The presence of residual stresses, it has been already seen, leads to a failure in micro-composites with a particular weak interphase ($\sigma_{U,interphase}$<60MPa). The micromodel with an interphase $\sigma_{U,interphase}$ = 60MPa represent an interesting case. In fact, damage onset is located in the areas in which residual stresses after cooling are mostly concentrated (Fig. 5.5 and Fig. 5.6). Numerical analyses have shown that in unit cells with a stiffer interphase (E=7.45GPa) residual stresses tend to remain mainly localized within the interphase. Hence, unlike the non-residual stress analysis, the concentration of stress in the interphase leads to the complete failure of interphase without involving matrix failure.

The damage evolution for micromodels with $\sigma_{U,interphase} \geq$ 60MPa and $\sigma_{U,interphase} \leq$ 100MPa is also greatly influenced by residual stress as it is displayed in Fig.5.14-16.

Finite element studies show that the damage initiation and evolution do not undergo particular modification in the local distribution within the composite. Damage onset for $\sigma_{U,interphase}$ > 60MPa starts at the interphase in the region marked with a square in Fig. 5.16 and progresses principally within the interphase due to the internal redistribution of stresses within the interphase itself and at the last stage failure involves the matrix.

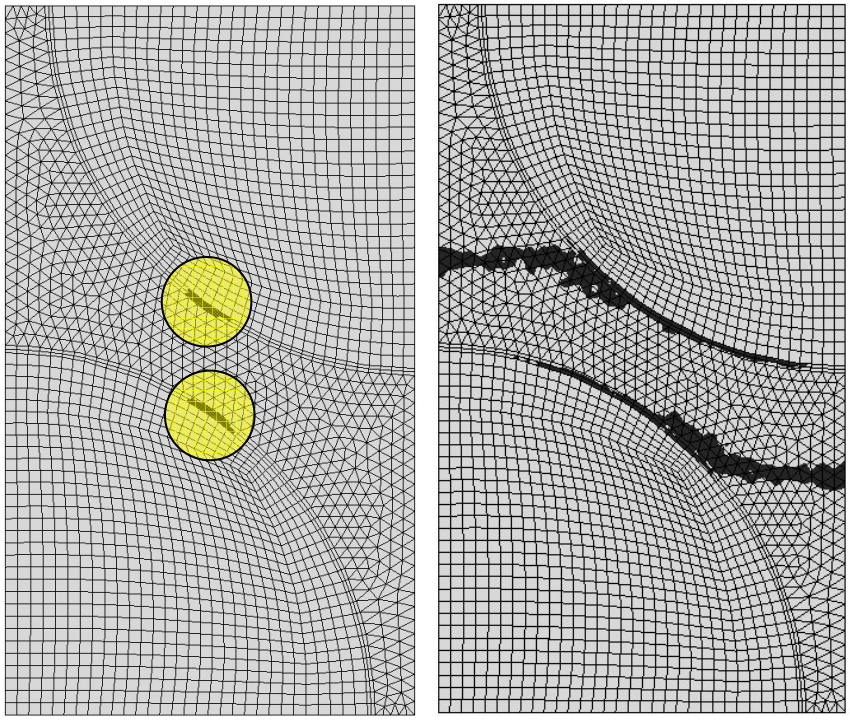

a **b**

Fig. 5.14 – Damage onset and evolution in unit cells with $\sigma_{U,interphase}$ 60MPa, 80MPa and 100MPa (No residual stress analysis).

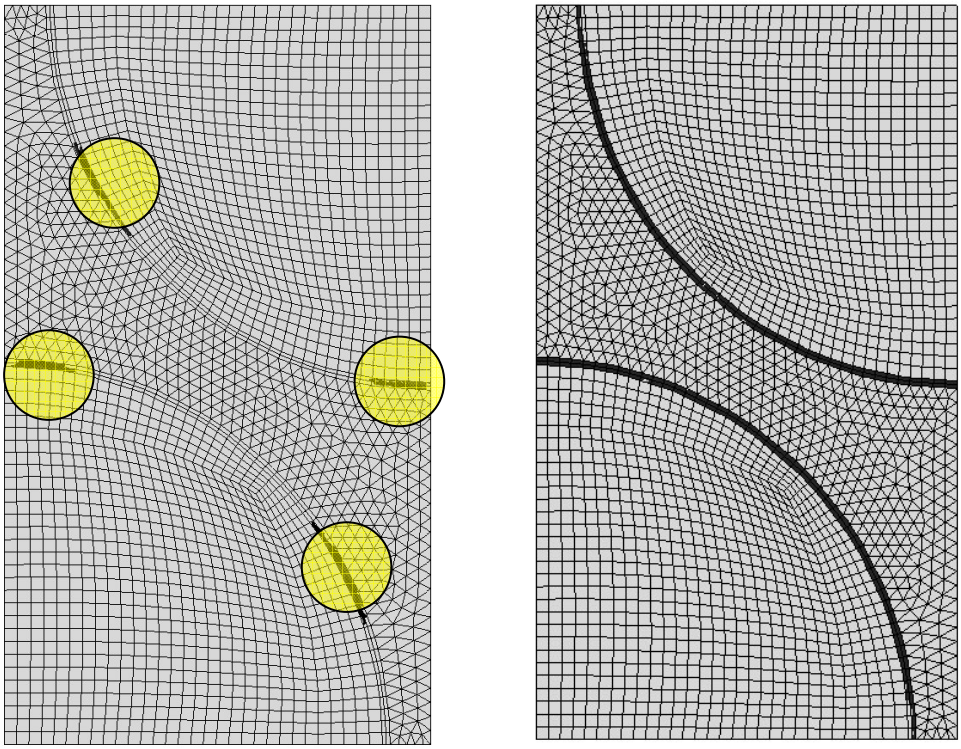

Fig. 5.15 Damage onset and evolution in unit cells with $\sigma_{U,interphase}$ 60MPa (residual stress analysis).

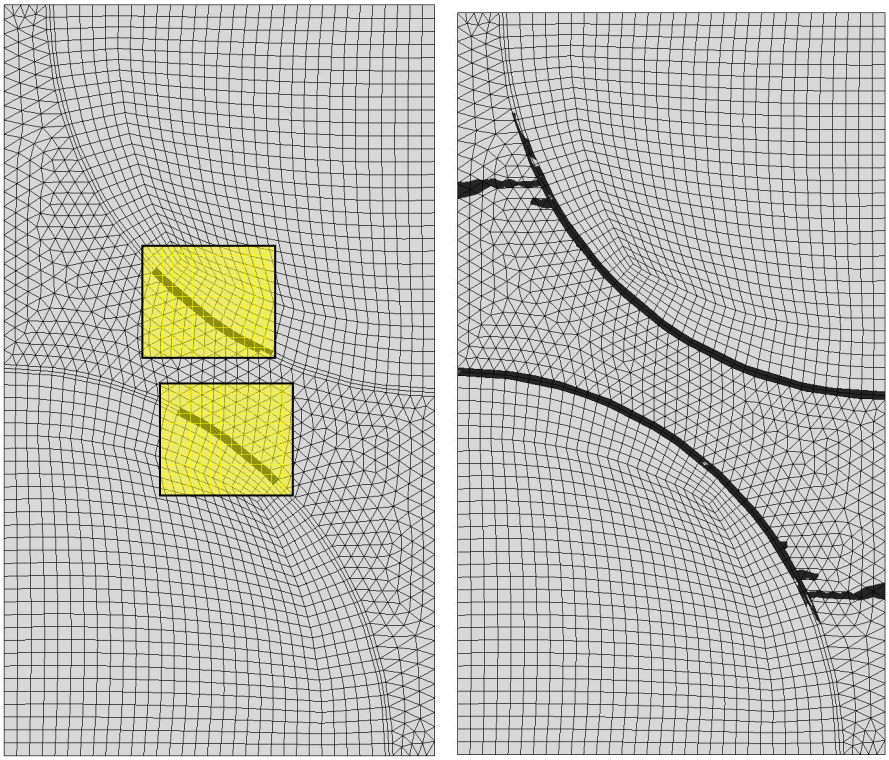

a **b**

Fig. 5.16 – Damage onset and evolution in unit cells with $\sigma_{U,interphase}$ 80MPa and 100MPa (residual stress analysis).

Few analyses have been performed on unit cells with a particular strong interphase ($\sigma_{U,interphase}$>100MPa). Although for high values of the ultimate strength of the interphase under transverse loading in the *z*-direction failure has still been detected in the weakest area (minimum distance in the *z*-direction), damage onset (Fig. 5.17) and damage evolution are now totally located within the matrix.

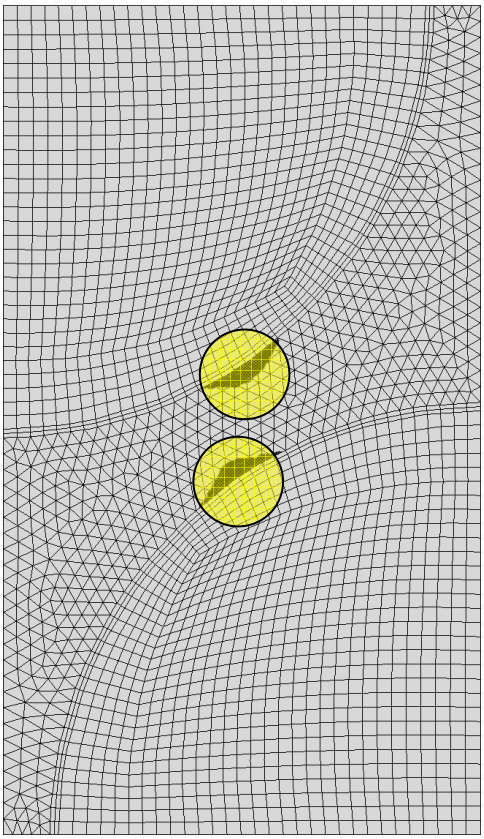

Fig.5.17 – Damage onset and evolution in unit cells
with $\sigma_{U,interphase}$ 120MPa and 140MPa (residual stress analysis).

In Table 5-3 the ultimate strengths of the unit cells and the location of initial failure in presence and absence of residual stresses are summarised.

In general, for this configuration of micromodels in which the Young's modulus is E=7.45GPa and the Poisson's ratio is ν=0.35, effect of thermal residual stress can be considered detrimental for interphase ultimate strengths below 60MPa due to the weakening action of the residual stresses on stiff interphases. Finite element analyses have demonstrated in fact that the stiff interphase tends to accumulate stresses and to avoid the redistribution of thermal residual stresses within the matrix. Although the hexagonal packing array displays the same elastic stiffness both in the *z*- and *y*-direction, the results without residual stress show that under transverse uniaxial loading on the *z*-direction gives higher values for the ultimate strengths in comparison with

results from the analyses in the *y*-direction. This trend is also repeated if residual stress due to the curing and cooling process is applied in the numerical calculations.

Table 5-3 – Numerical results for a unit cell with a stiff interphase with different ultimate strengths.

	STIFF INTERPHASE - Transverse *z*-direction			
	No Residual Stress	Residual Stress	No Residual Stress	Residual Stress
$\sigma_{u,INTERPHASE}$ **[MPa]**	RVE Ultimate Strength [MPa]		RVE Failure onset	
20	15.0	**COOLING**	INTERPHASE	INTERPHASE
40	15.0	**COOLING**	INTERPHASE	INTERPHASE
60	42.0	7.6	INTERPHASE	INTERPHASE
80	56.0	40.0	INTERPHASE	INTERPHASE
100	57.7	62.4	MATRIX/INTERPHASE INTERFACE	INTERPHASE
120	57.7	62.4	MATRIX/INTERPHASE INTERFACE	MATRIX/INTERPHASE INTERFACE
140	57.7	62.4	MATRIX/INTERPHASE INTERFACE	MATRIX/INTERPHASE INTERFACE

5.4.2 Effect of a soft interphase on the transverse loading

On transverse loading along the *y*-direction the RVE with a "soft" interphase (E=1.5GPa) the mechanical properties are improved in terms of ultimate strength and strain. Numerical studies including thermal residual stress arising during the curing process have shown that the magnitude of these residual stresses is greatly smaller than residual stresses in stiffer interphases. This result avoids the drawback of a possible failure within the interphase and/or in the matrix while the curing process is taking place ever for small values of the interphase ultimate strength (e.g. $\sigma_{U,interphase}$=20MPa).

Although for small values of the interphase strength, no failure at interphase has been detected during the curing and cooling process. Nevertheless, thermal residual stresses produce a severe

reduction of material properties leading to a drastic total failure of the interphase at low levels of loading stresses. Failure occurs at interphase in the regions of the unit cell highlighted with a circle (Fig. 5.18).

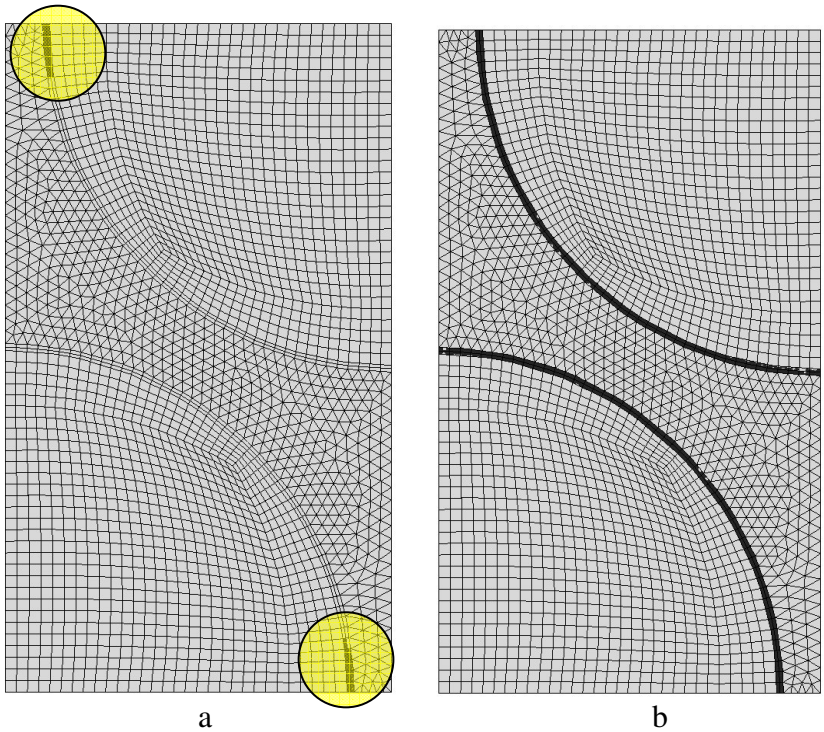

a b

Fig. 5.18 - Comparison of damage onset in unit cells with $\sigma_{U,interphase}$ 20MPa with no residual stress (a) and residual stress (b).

Fig. 5.19 depicts damage onset relative to micromodels with an $\sigma_{U,interphase}$ below 80MPa with and without residual stresses. Analyses have demonstrated that damage in the numerical models occurs in the areas of the interphase in which the amount of residual stress reachs its maximum magnitude (Fig. 5.6-7).

Although the presence of residual stress slightly modifies the location in which failure is detected the overall behaviour of the unit cell undergoes an advantage in terms of ultimate strength.

A comparison of the effect of residual stress on transverse loading (*y*-direction) for two unit cells with different ultimate strengths displayed in Fig. 5.20 clearly shows the beneficial effect of residual stresses.

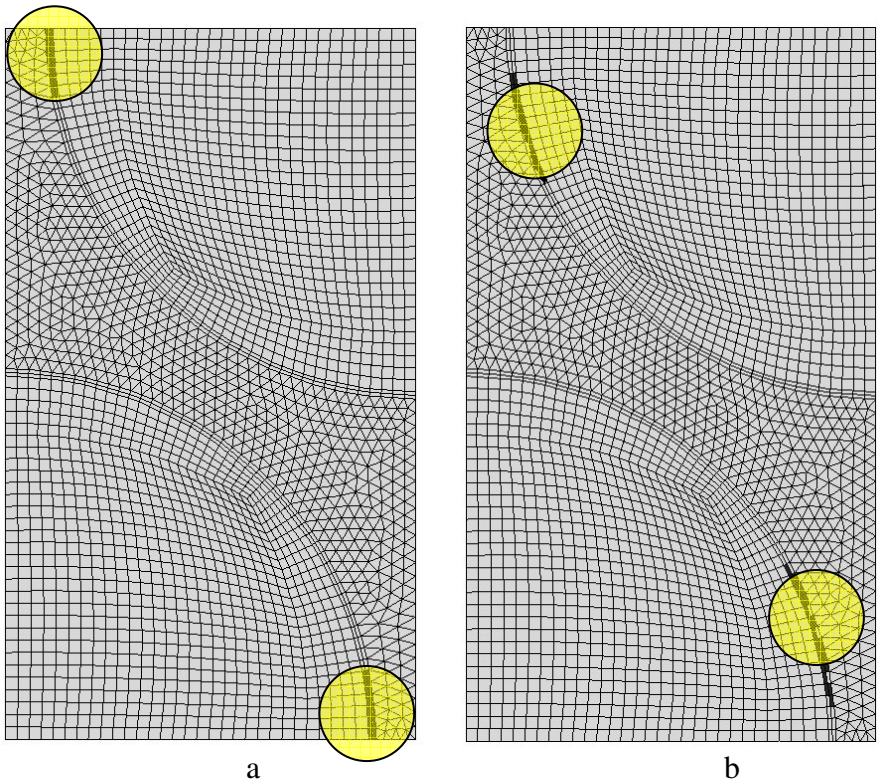

a b

Fig. 5.19 - Comparison of damage onset in unit cells with $\sigma_{U,interphase}$ 20MPa, 40MPa and 60MPa with no residual stress (a) and residual stress (b).

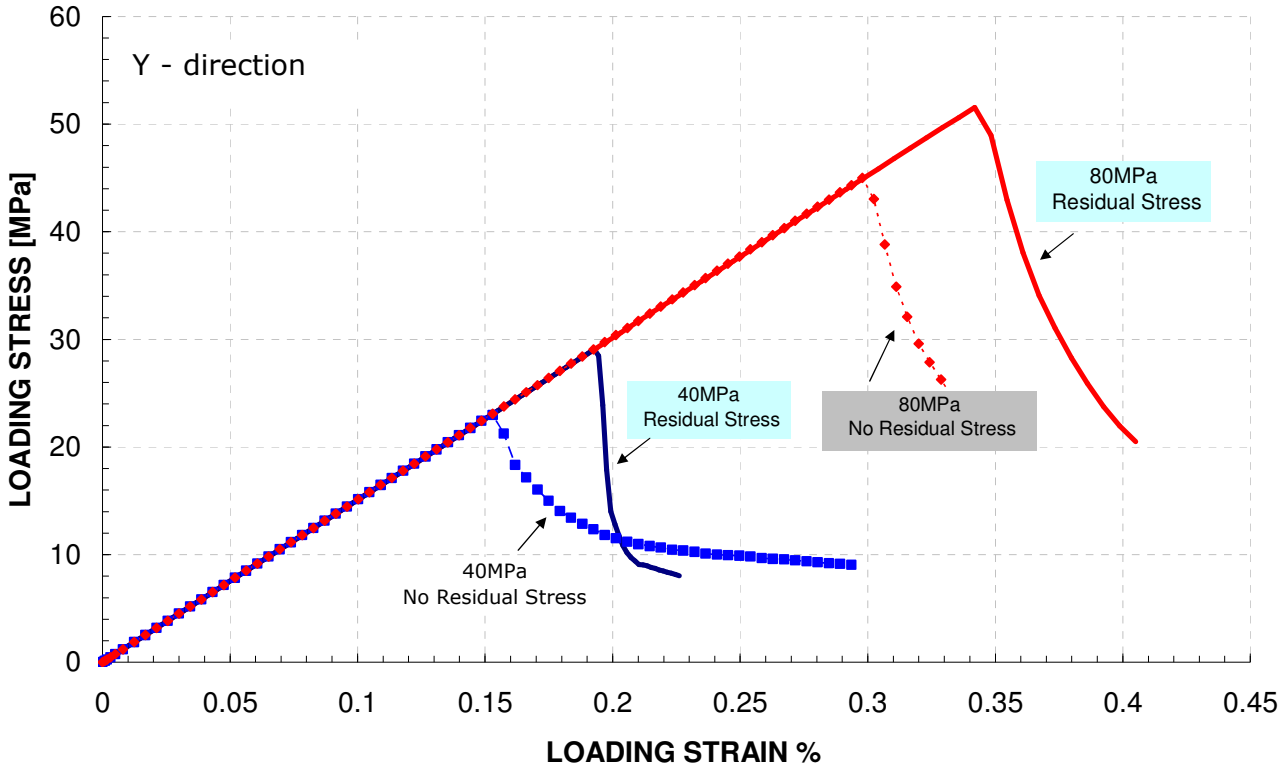

Fig. 5.20 – Comparison of global stress-strain curves on transverse loading (*y*-direction) for residual and non-residual stress analyses.

It is clearly visible that the presence of residual stresses plays a beneficial role by improving the material toughness. The data are summarized in Table 5-4.

The studies has shown that in unit cells with softer interphases damage onset is detected in the interphase for $\sigma_{U,interphase}$ lower than 80MPa both in presence and absence of residual stress, in the matrix for values of $\sigma_{U,interphase}$ higher than 80MPa (Fig. 5.21) with or without residual stresses while, in case of $\sigma_{U,interphase}$=80MPa (Fig. 5.22) both interphase and matrix are involved. Moreover for ultimate strengths of the interphase above 20MPa residual stresses improve the capability of micro-composites to bear transverse load on the *y*-direction.

Numerical analysis with residual stress has shown that the soft interphase (E=1.5GPa) during the complete curing process works as a ”damper”. It is seen to transfer gradually the stresses due to shrinkage from the interphase to the matrix.

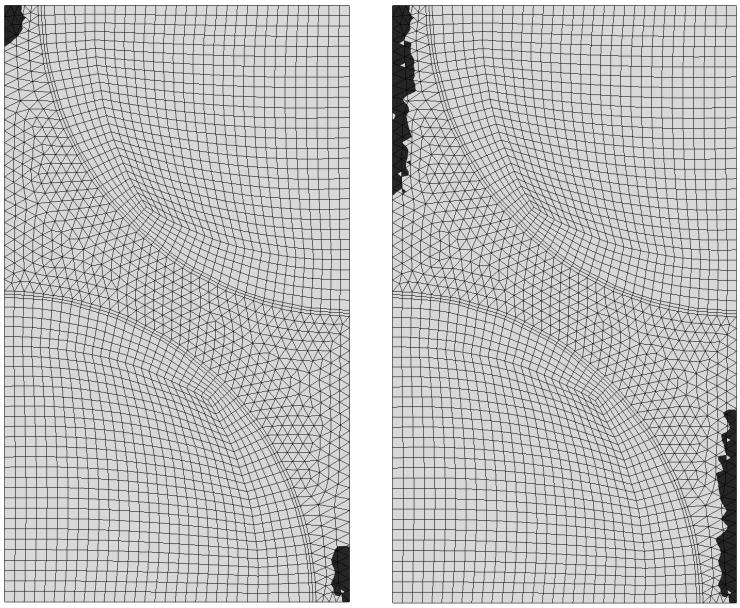

Fig.5.21 – Damage onset and evolution in a unit cell
with $\sigma_{U,interphase}$>80MPa (residual and non-residual stress analysis)

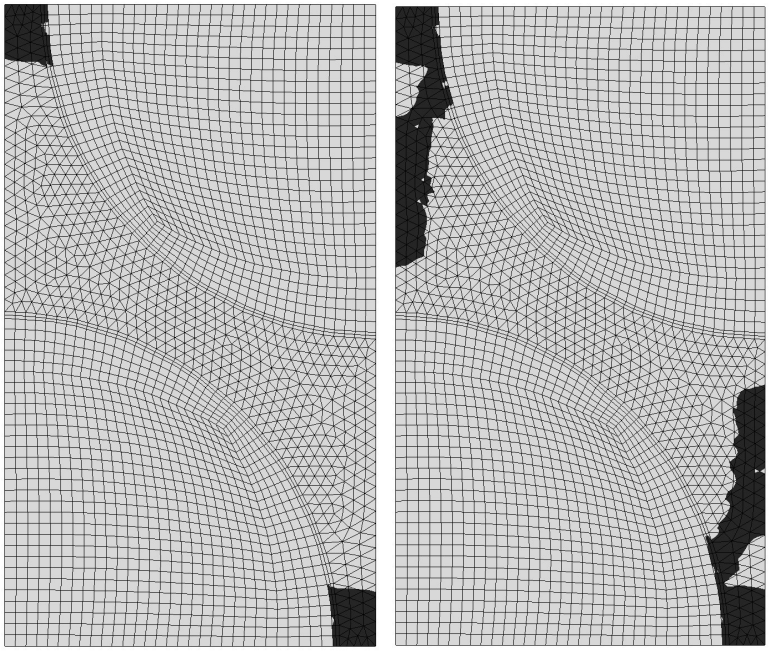

Fig.5.22 – Damage onset and evolution in a unit cell
with $\sigma_{U,interphase}$=80MPa (residual stress analysis)

In this case therefore stresses, should not reach critical values that could lead to the drastic interphase failure with fibre and debonding.

Table 5-4 – Numerical results for a unit cell with a soft interphase under transverse loading (*y*-direction).

	SOFT INTERPHASE - Transverse *y*-direction			
	No Residual Stress	Residual Stress	No Residual Stress	Residual Stress
$\sigma_{u,INTERPHASE}$ [MPa]	RVE Ultimate Strength [MPa]		RVE Failure onset	
20	11.8	7.8	INTERPHASE	INTERPHASE
40	23.0	29.0	INTERPHASE	INTERPHASE
60	34.0	41.0	INTERPHASE	INTERPHASE
80	45.0	51.5	MATRIX	MATRIX/INTERPHASE
100	45.0	51.5	MATRIX	MATRIX
120	45.0	51.5	MATRIX	MATRIX

Finite element investigations have already proved the positive action of soft interphase in terms of ultimate strength and ultimate strain of the micro-composites undergoing transverse loading in the *y*- and *z*-direction in absence of residual stresses arising throughout the manufacturing process.

Numerical models with a soft interphase have shown similar behaviour to the stiff interphase studies even in analyses including the effects of thermal residual stress. Examples of damage initiation points for these cases are shown in Fig. 5.23.

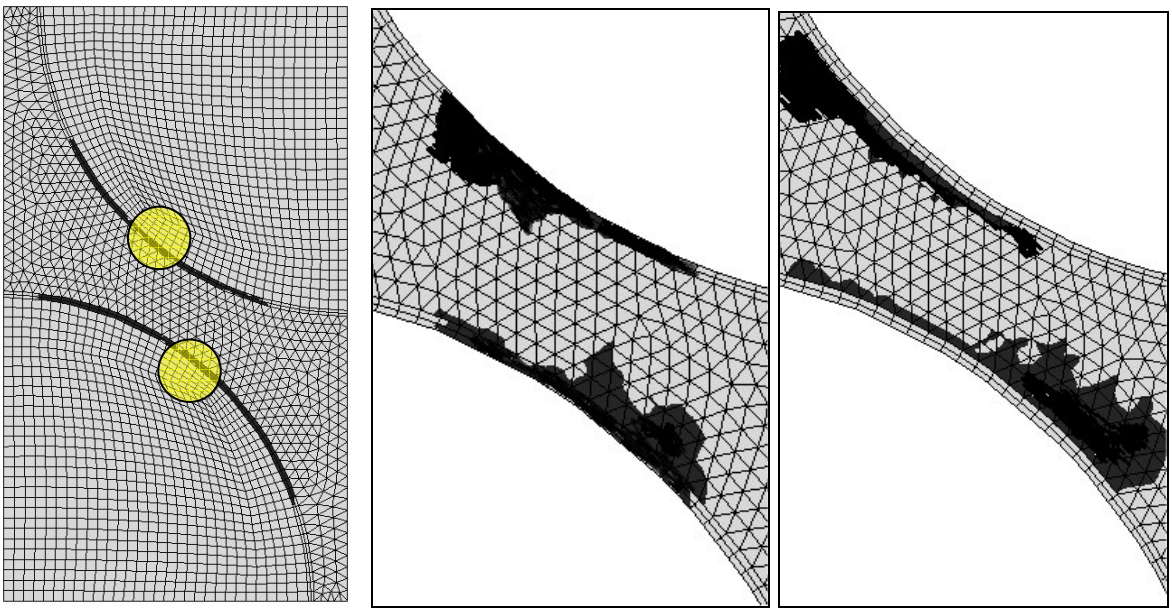

Fig. 5.23 – Damage onset and evolution in a unit cells with $\sigma_{U,interphase}$=40MPa (a), $\sigma_{U,interphase}$=80MPa, $\sigma_{U,interphase}$=100MPa (c) in residual stress analyses.

Results of finite element calculations on unit cell with soft interphase under transverse uniaxial loading on the *z*-direction are presented in Table 5-5.

Table 5-5 – Numerical results for a unit cell with a soft interphase under transverse loading (*z*-direction).

.	**SOFT INTERPHASE - Transverse *z*-direction**			
	No Residual Stress	Residual Stress	No Residual Stress	Residual Stress
$\sigma_{u,INTERPHASE}$ **[MPa]**	RVE Ultimate Strength [MPa]		RVE Failure onset	
20	15.0	11.0	INTERPHASE	INTERPHASE
40	30.0	35.0	INTERPHASE	INTERPHASE
60	44.7	50.6	INTERPHASE	INTERPHASE
80	57.8	64.0	INTERPHASE	MATRIX/INTERPHASE
100	60.0	64.0	MATRIX/INTERPHASE INTERFACE	MATRIX/INTERPHASE INTERFACE
120	60.0	64.0	MATRIX/INTERPHASE INTERFACE	MATRIX/INTERPHASE INTERFACE

It can be seen that the presence of residual stresses generally produce a beneficial action and for interphases in which $\sigma_{U,interphase}$ >20MPa the ultimate strength of the unit cell improves of circa 15%.

Soft interphases are able to redistribute the stresses along the interphase and to transmit part of the loading stress within the matrix. For values of the ultimate strength of interphase equal and below 20MPa, thermal residual stresses play a more severe role on the overall material response of unit cells in fact, as clearly depicted in Fig. 5.24 they tend to reduce the material properties of the interphase and hence to influence, as already shown for the stiff interphase case, the location of damage initiation points that appears to take place in regions, indicated with the circles in Fig. 5.24, in which residual stress are more concentrated after curing and cooling.

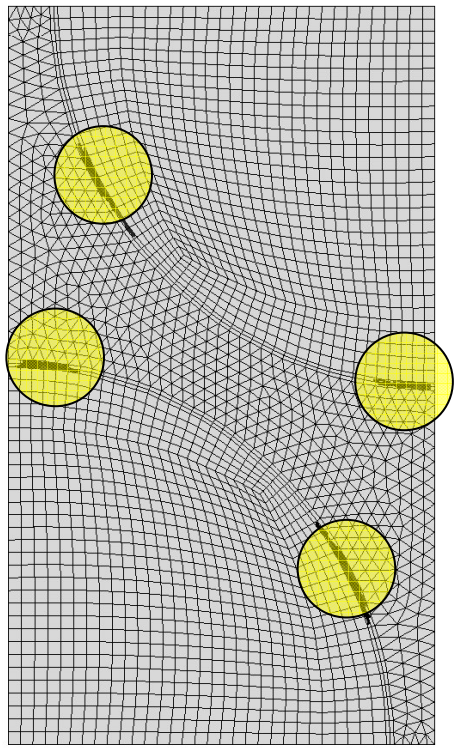

Fig.5.24 – Damage onset and evolution in a unit cells with $\sigma_{U,interphase}$=20MPa (residual stress analysis)

5.5 Poisson's Ratio Study

Due to a lack of data in the literature, a parametric finite element study on the effect of interphases with different material properties and various ultimate strengths has been carried out. The Poisson's ratio of the interphase and the matrix have been assumed to be temperature independent and equal to ν=0.35 throughout the numerical analysis. Further investigation have been performed on representative volume elements (RVE) by modifying the magnitude of Poisson's ratio in order to better understand the role they play on the overall behaviour of micro-composites on transverse uniaxial loading.

Preliminary finite element analyses have been carried out on RVEs without considering the presence of thermal residual stresses. The ultimate strength of the interphase for these set of analyses has been assumed to be equal to the ultimate strength of the matrix:

$\sigma_{U,matrix} = \sigma_{U,interphase} = 80MPa$

In analyses accounting for the effect of residual stresses the Poisson's ratio of the interphase has been assumed temperature dependent. To evaluate the variation of Young's modulus *E* over the temperature range from curing to room temperature, the total temperature range has been be divided into three regions described in Chapter 4, namely:

- *Region I* $\Rightarrow T > T_g + \Delta T$, in which the Poisson's ratio for matrix and interphase has been still assumed ν=0.35.

- *Region II* $\Rightarrow T_g - \Delta T \leq T \leq T_g + \Delta T$, in which the Poisson's ratio for the interphase has been still considered temperature dependent and the behaviour has been described by a simple linear relation:

$$\nu = \nu_o \pm m(T-T_o)$$

where ν_o=0.35, T_o = 149°C (curing temperature) and m is a fitting parameter.

- *Region III* $\Rightarrow T < T_g - \Delta T$, in which the Poisson' ratio in *Region III* for the interphase has been assumed constant and equal to the its final value reached at the end of *Region II*, namely:

  1) if $\nu = \nu_o - m(T-T_o) \Rightarrow \nu$=0.3

  2) if $\nu = \nu_o + m(T-T_o) \Rightarrow \nu$=0.4

The behaviour of the Young's moduli over the range of temperatures and the values of the glass transition temperature T_g and ΔT have been already described previously in section 5.2.

The hypothetical linear behaviour of the Poisson's ratio in *Region II* is mainly to attribute to the lack of experimental data on the interphase properties during the manufacturing process. The aim is to investigate numerically the effect of different Poisson's ratios both in presence and absence

of residual stress on the mechanical ability to bear uniaxial loads in which the linear modifications of the Poisson's ratio ν during the cooling process could be considered as an upper and lower bound of a real case.

Moreover, as the majority of the chemical reactions that modify the material properties of the resin take place during the cooling within *Region II*, it has been decided to impose the hypothetical linear change of the ν only in this region from 149°C to the room temperature.

5.5.1 Effect of a stiff interphase on the transverse loading

Numerical studies on unit cells with stiff ($E_{interphase}$=7.45GPa) interphase and different Poisson's ratios have proved that the micromechanical models are still influenced by the different elastic properties of the interphase. In particular, in the micromodels investigated under uniaxial transverse loading (*y*-direction), the damage onset in presence of residual stresses has been detected in different areas of the unit cell as can be seen by comparing Fig. 5.25 and Fig. 5.26 in which the damage onset is highlighted by circles and its evolution is represented by the shadowed area.

It is clearly visible that the effect of residual stresses is to weaken the interphase especially in the regions of the unit cell in which thermal stress reaches the maximum value. Hence failure, as it is more likely to occur in real micro-composites, takes place at the fibre/interphase and/or matrix/interphase "interfaces" that, in general, represent the most vulnerable areas in real composites at micro-scale.

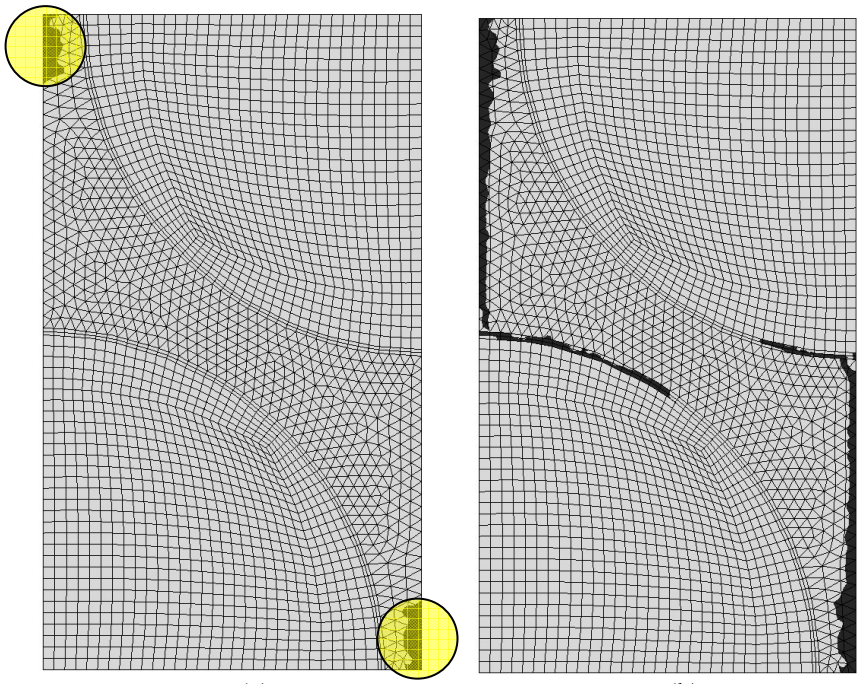

(a) (b)

Fig. 5.25 – Damage onset (a) and evolution (b) in unit cells with Poisson's ratios of ν=0.3 and ν=0.4 in a non-residual stress analysis.

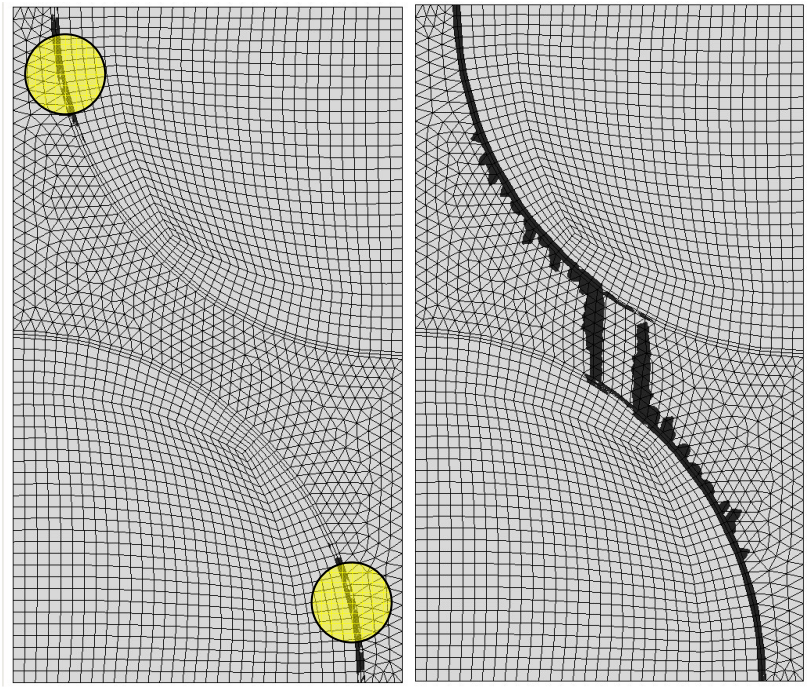

(a) (b)

Fig. 5.26 – Damage onset (a) and evolution (b) in unit cells with Poisson's ratios of ν=0.3 and ν=0.4 in a residual stress analysis.

Results of numerical analyses on a unit cell with a stiff interphase and different values of the Poisson's ratio are presented in Table 5-6.

A comparison between the analysis that do not account for residual stress and the numerical analysis in which the curing and cooling process has been simulated shows that thermal stress play a key role in the distribution of the damage initiation and moreover they introduce detrimental effects on the capability of the micromodels to bear transverse load on the *y*-direction.

Table 5-6 – Numerical results for a unit cell with a stiff interphase at various Poisson's ratios under transverse loading (*y*-direction).

	STIFF INTERPHASE - Transverse *y*-direction			
	No Residual Stress	Residual Stress	No Residual Stress	Residual Stress
Poisson's Ratio	RVE Ultimate Strength [MPa]		RVE Failure onset	
0.3	44.0	42.0	MATRIX	INTERPHASE
0.35*	43.0	31.5	MATRIX	INTERPHASE
0.4	42.5	21.0	MATRIX	INTERPHASE

Nevertheless, different values in the Poisson's ratio affect only marginally (Fig. 5.26) the elastic stiffness of RVE with the Young's modulus $E_{interphase}$=7.45GPa and the difference between the Young's modulus evaluated at ν=0.4 and ν=0.3 has been estimated circa 1%.

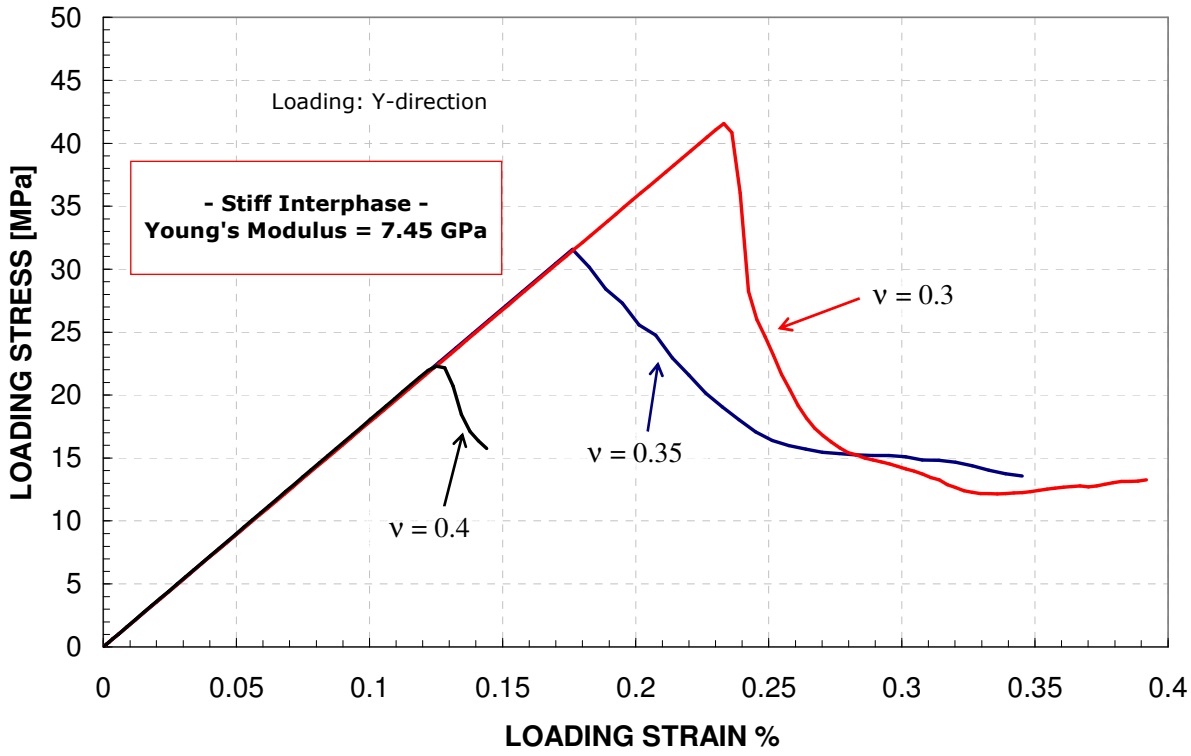

Fig. 5.26 – Comparison of global stress-strain curves with different Poisson's ratios and stiff interphase on transverse loading (*y*-direction).

.

Finite element analysis accounting for thermal residual stress on unit cell with $E_{interphase}$=7.45GPa confirms the decreasing ultimate strength of the micromodels under investigation whilst the magnitude of the Poisson's ratio is increased as shown in Table 5-7.

Numerical analyses also make evident the severe weakening effect of thermal residual stress on the mechanical properties of the interphase. In particular, in the RVE with the Poisson's ratio ν=0.4 the reduction of the ultimate strength has been estimated nearly 50% less than the ultimate strength in micromodels that do not include thermal residual stress.

Damage onset has been primarily detected at interphase in the regions already described previously for the strength study and depicted in Fig. 5.13.

Moreover under uniaxial transverse loading in the *z*-direction, the ultimate strength is higher than the ultimate strength in the *y*-direction.

Table 5-7 – Numerical results for a unit cell with a stiff interphase at various Poisson's ratios under transverse loading (z-direction).

	STIFF INTERPHASE - Transverse z-direction			
	No Residual Stress	Residual Stress	No Residual Stress	Residual Stress
Poisson's Ratio	RVE Ultimate Strength [MPa]		RVE Failure onset	
0.3	56.5	45.0	INTERPHASE	INTERPHASE
0.35	56.25	40.0	INTERPHASE	INTERPHASE
0.4	53.5	27.5	INTERPHASE	INTERPHASE

5.5.2 Effect of a soft interphase on transverse loading

Micromodels with soft interphase appear sensitive to the Poisson's ratio values as can be seen in Fig. 5.27. Despite the thickness of the interphase is about 1/100 of the fibre diameter different values of the Poisson's ratio imply a difference of circa 4% in the elastic stiffness. On the contrary, different values in the Poisson's ratio play only a negligible role on overall material properties in the unit cells with a stiff interphase.

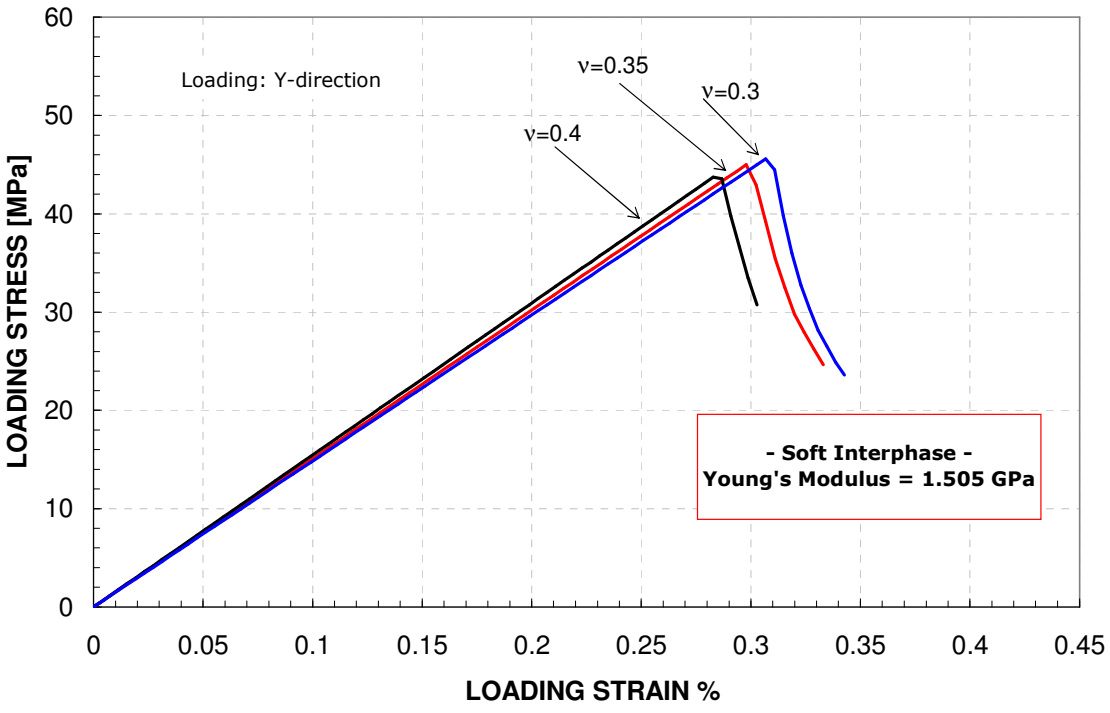

Fig. 5.27 – Comparison of global stress-strain curves with different Poisson's ratios and soft interphase on transverse loading (*y*-direction).

Unlike the different configurations of unit cells with a stiff interphase, finite element study with residual stresses has proved that micromodels including soft interphases undergo slightly beneficial effects in terms of ultimate strength and strain in the unit cells that have been investigated (Table 5-8). A comparison with data (Table 5-8) obtained from analyses that simulate curing and cooling show the thermal residual stress enhances the material properties (ultimate strength and strain) of the micro-composites of circa 14-16%

Table 5-8 – Numerical results for a unit cell with a soft interphase at various Poisson's ratios under transverse loading (*y*-direction).

	SOFT INTERPHASE - Transverse *y*-direction			
	No Residual Stress	Residual Stress	No Residual Stress	Residual Stress
Poisson's Ratio	RVE Ultimate Strength [MPa]		RVE Failure onset	
0.3	45.5	52.0	MATRIX	MATRIX
0.35	45.0	51.5	MATRIX	MATRIX/INTERPHASE
0.4	43.5	51.0	MATRIX	MATRIX/INTERPHASE

Initial failure has been detected in the areas indicated with the circles in Fig. 5.28 in the analysis without residual stress. It can be noticed that damage onset is not influenced by different values of the Poisson' ratio. Nevertheless damage evolution within the RVE is slightly modified by the presence of residual stress. In particular the unit cells with interphasial Poisson's ratios above ν=0.3 undergo a stiffening effect as depicted in Fig. 5.27. These slightly stiffer interphases appear less able to dissipate thermal stress arising during curing and cooling within the interphase and the matrix. Hence on transverse loading along the *y*-direction damage occurs both in the matrix and the interphase and as it can be seen in Fig. 5.29 the location of the initial failure in the interphase remains in the region of maximum concentration of thermal stresses.

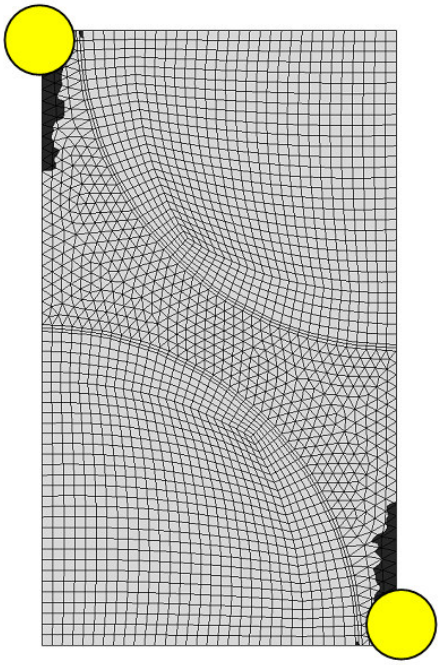

Fig. 5.28 – Damage onset (yellow circles) and damage evolution (shadowed area) in unit cells with Poisson's ratios of ν=0.3 and ν=0.4 in a non-residual stress analysis

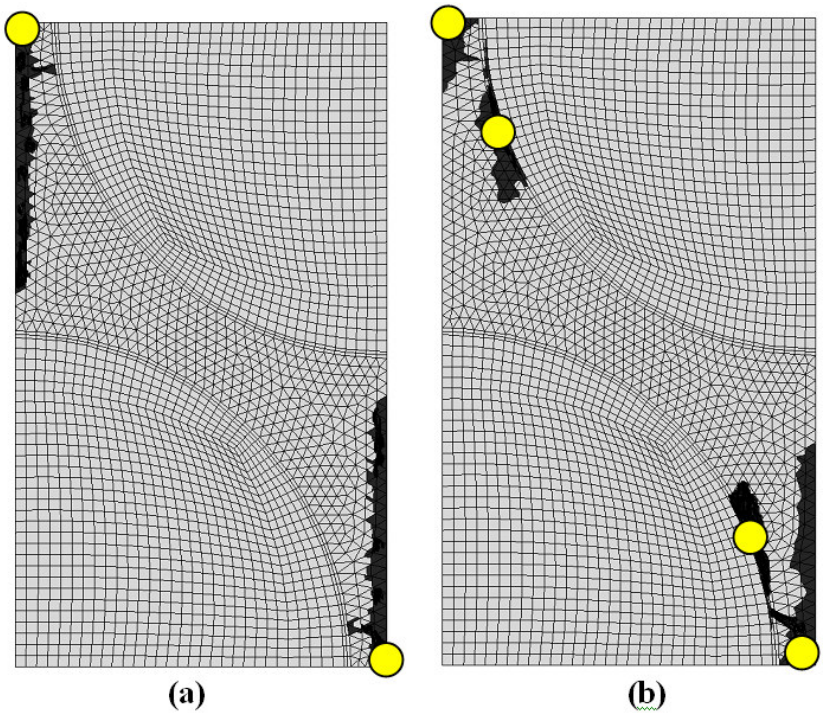

Fig. 5.29 – Damage onset (yellow circles) and damage evolution (shadowed area) in unit cells with Poisson's ratios of ν=0.3 (a) and ν=0.4 (b) in a residual stress analysis

Numerical analyses have demonstrated that unit cells loaded transversely along the z-direction show the location of damage onset is located in the narrow region between the fibres as shown in Fig. 5.30.

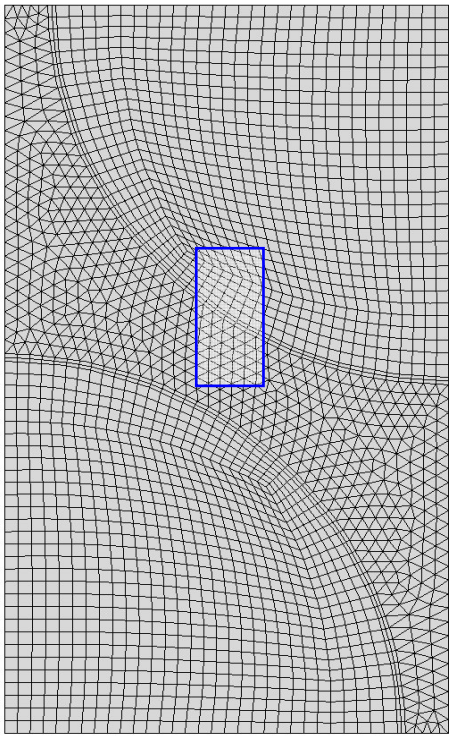

Fig. 5.30 – Region of damage onset under transverse loading on the z-direction.

These set of investigations on unit cells with a thin soft interphase under uniaxial loading along the z-direction confirmed the increasing capability of bearing loads whilst decreasing the magnitude of the Poisson's ratio (Fig. 5.31)

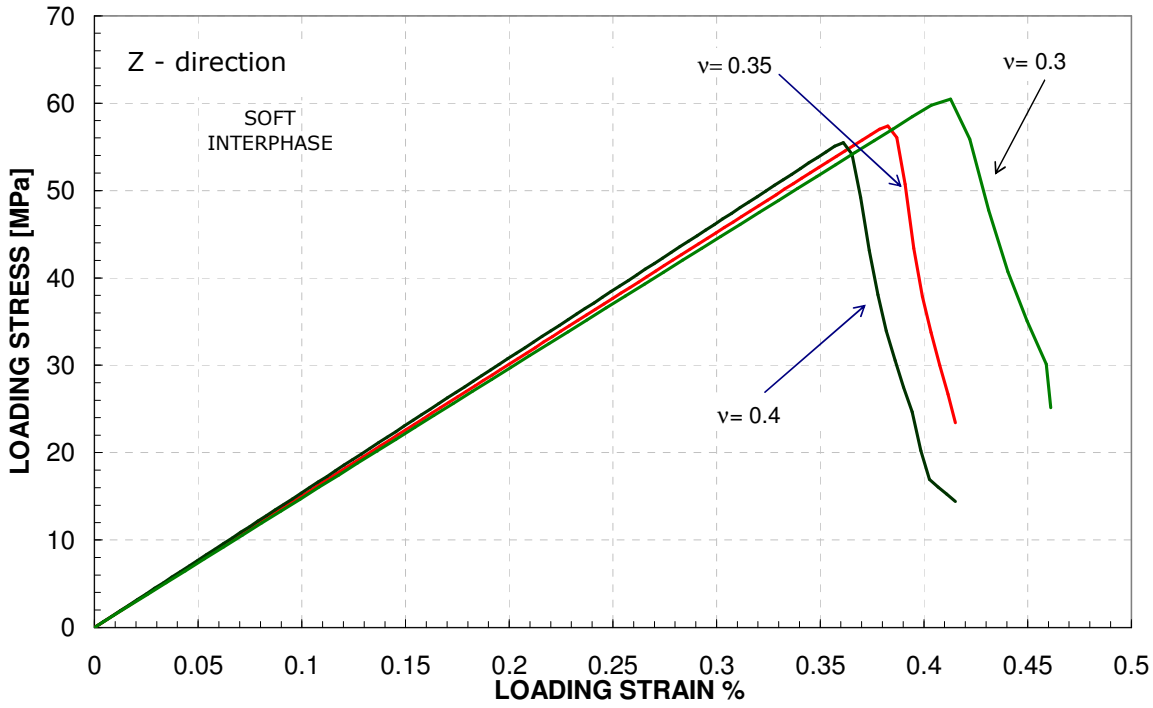

Fig. 5.31 – Comparison of global stress-strain curves with different Poisson's ratios and soft interphase on transverse loading (*z*-direction).

The ability of the softer (E=1.50GPa) interphases to redistribute stresses arising during the whole curing process over the interphase and within the matrix are clearly visible in the results presented in Table 5-9. Although, damage onset in the softer interphase can take place either within the interphase or in the matrix located at the matrix/interphase interface, the ultimate strength undergos a beneficial improvement and their values increase of circa 5-9%.

Table 5-9 – Numerical results for a unit cell with a soft interphase at various Poisson's ratios under transverse loading (*z*-direction).

	SOFT INTERPHASE - Transverse *z*-direction			
	No Residual Stress	Residual Stress	No Residual Stress	Residual Stress
Poisson's Ratio	RVE Ultimate Strength [MPa]		RVE Failure onset	
0.3	60.0	64.0	INTERPHASE	MATRIX/INTERPHASE INTERFACE
0.35*	57.0	64.0	INTERPHASE	MATRIX/INTERPHASE INTERFACE
0.4	56.0	61.5	INTERPHASE	INTERPHASE

5.6 Conclusion

Finite element analyses have been performed in order to investigate the overall mechanical response of unit cells including the presence of hypothetical thin soft and hard interphases under uniaxial transverse tensile loading. The effect of residual stress has been also analysed by simulating the manufacturing process (curing and cooling) by means a user-defined subroutine (UMAT) available in ABAQUS. Results obtained with the residual stress analysis were also compared to numerical results from a non-residual stress analysis. Numerical analyses have proved that the thin interphase is able to modify slightly the elastic stiffness of the micromodels. "Softened" unit cells have displayed a significant improvement in terms of ultimate strength and strain in comparison to the unit cells with a harder interphase both on the *z*- and *y*-direction.

More interestingly, finite element analyses that simulate a hypothetical behaviour of the interphasial properties during curing and cooling process have demonstrated that the magnitude of thermal residual stress within the interphase and the matrix is strongly influenced by the material properties of the interphase leading to severe high values within the stiff interphase. The soft interphase appears to work as a "shock absorber" by redistributing thermal residual stresses within the interphase itself and transferring part of them onto the matrix. On the contrary the stiff interphase tends to concentrate the total amount of the stresses that are particularly elevated, especially in some internal region of the interphase. In fact, numerical simulations have demonstrated that for ultimate strengths of the stiff interphase equal and/or lower to the magnitude of residual stress the interphase appears utterly weakened by the presence of residual stresses and failure occurs during the cooling process leading to the total fibre/matrix debonding if uniaxial transverse loading is eventually applied.

Nevertheless, finite element results, for higher values of the interphasial ultimate strengths, have proved that thermal residual stresses enable an improvement in the overall mechanical response

of the micromodels undergoing uniaxial transverse loading both for the stiff and the soft interphase. In these cases the presence of residual stress, especially in the soft interphase, contributes to delay the action of the transverse loading stress on the regions of the unit cells that are more likely to fail as described in the investigations in which the curing and cooling process has not been simulated.

In conclusion, finite element analyses indicate that unit cells with soft interphases show superior characteristics in terms of ultimate strength and strain under transverse loadings and reduce significantly the amount of stresses if the manufacturing process is included in the numerical simulations, and finally improve the mechanical response even for low values of the interphasial ultimate strength when residual stress is included. On the other hand, the micromechanics based damage model in combination with the residual stress analyses have demonstrated that the failure onset could also take place during the cooling process within the stiff interphase for particular values of the interphasial mechanical properties.

Chapter 6

Effect of fibre packing geometry on the Mechanical Behaviour of RVEs

6.1 Introduction

Most of the investigations described previously in the literature review related to the effect of constituents are based on multi-fibre RVEs and are unable to describe accurately and locally damage onset and its evolution that usually requires a fine mesh refinement around the fibre/matrix interface. Moreover, they account rarely for the effect of residual stresses arising during the curing process. In fact the local stress distributions after chemical shrinkage and the following cooling could influence the onset of micro-cracks in the matrix especially in presence of a random distribution of the fibre over the cross-section [134]. In order to investigate the effects of non-uniform unit cells with a hexagonal packing array of fibres, a robust numerical investigation that includes a damage model has been undertaken to evaluate the local response. The effect thermal residual stresses have been also accounted for.

6.2 Finite Element Results

In order to investigate the effect of inter-fibre spacing on damage evolution, micromechanical unit cell models have been constructed by shifting the central fibre in Fig. 6.1 along the z-direction of the "translation" factor Γ (in ηm).

In the micromodel investigated the central fibre has been translated by the following Γ:

0.0ηm; 0.25ηm;0.45ηm; 0.90ηm; 1.35ηm; 1.55ηm; 1.7ηm.

To each Γ corresponds a single micromodel, namely:

Γ=0.25 $\rightarrow$ RVE/0.25ηm;

Γ=0.45 → RVE/0.45ηm;

Γ=0.90 → RVE/0.90ηm;

Γ=1.35 → RVE/1.35ηm;

Γ=1.55 → RVE/1.55ηm;

Γ=1.70 → RVE/1.70ηm.

RVE/0.0ηm (reference model); RVE/0.25ηm; RVE/0.45ηm; RVE/0.90ηm; RVE/1.35ηm; RVE/1.55ηm; RVE/1.70ηm.

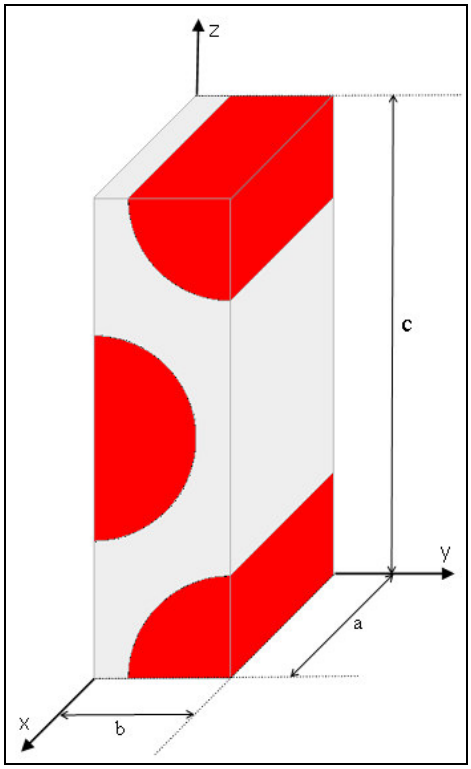

Fig. 6.1 - ½ of the hexagonal array packing RVE used as a reference model.

This solution also allows applying correct periodic boundary conditions and moreover to keep a constant fibre content (70%). A comparison between a uniform and non-uniforms unit cells is shown in Fig. 6.2. The displacement constraints applied to the finite element model (Fig.6.1) in order to apply normal loads are [3]:

$\boldsymbol{u_x}$ (0, y, z) = 0

$\boldsymbol{u_x}$ (a, y, z) = constant = $\boldsymbol{\delta_x}$

$\boldsymbol{u_y}$ (x, 0, z) = 0

$\boldsymbol{u_y}$ (x, b, z) = constant = $\boldsymbol{\delta_y}$

$\boldsymbol{u_z}$ (x, y, -c) = 0

$\boldsymbol{u_z}$ (x, y , c) = constant = $\boldsymbol{\delta_z}$

where $\boldsymbol{u_x}$, $\boldsymbol{u_y}$, $\boldsymbol{u_z}$ denote respectively displacements in the *x*, *y* and *z* direction.

The damage and post-damage model applied for this investigation has been already described in Chapter 4 and three different loading conditions have been applied to the unit cell shown in Fig. 6.1 namely:

3) transverse loading in the *y*-direction,

4) transverse loading in the *z*-direction,

5) longitudinal loading in the *x*-direction (parallel to the fibres).

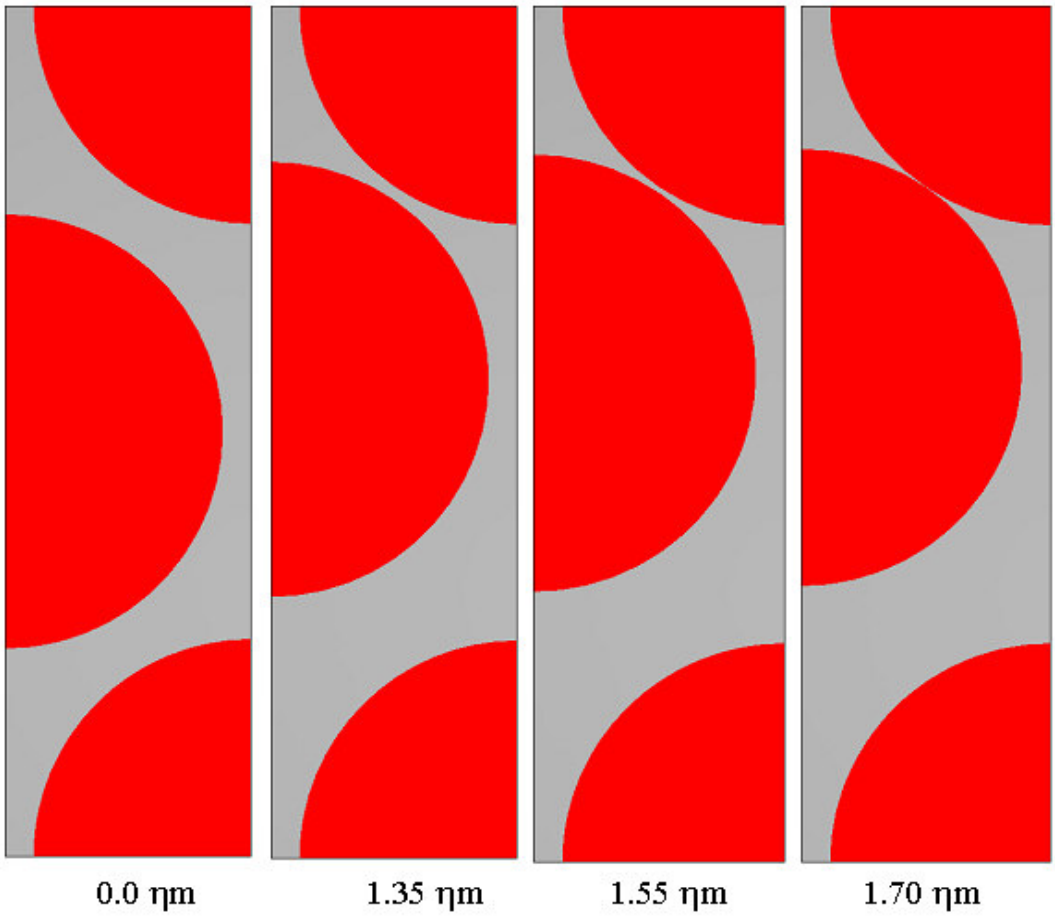

Fig. 6.2 – Range of fibre positions.

6.2.1 Transverse loading

As already mentioned, the purpose of this study is to investigate the effect of local damage evolution under transverse and longitudinal loading. A previous analysis on a uniform RVE (perfect symmetry) under *x*, *y* and *z*-direction loading has been performed to compare results with data from non-uniform unit cells. Details of damage onset and evolution for non-uniform unit cells that undergo *y*-direction loading are illustrated in Fig. 6.3-7, where RVE/0.0ηm denotes the reference representative volume element. Damage contour is represented by means of a black area and the damage onset has been indicated in the figures with capital letters (A, B and C).. Interestingly, it has been noticed that for the RVE/0.0ηm and for relatively small shifting factors the damage is due to micro-crack in the resin.

Initiation of damage in unit cell RVE/1.35ηm (Fig. 6.5) is still similar but the damage in the region C in Fig. 6.3 but it has been detected at lower strains. Micromodels with a higher **Γ** (Fig. 6.5-7) exhibit a different location of damage onset. In particular damage, due to fibre/matrix debonding, starts in the region A (Fig.6.5-7)

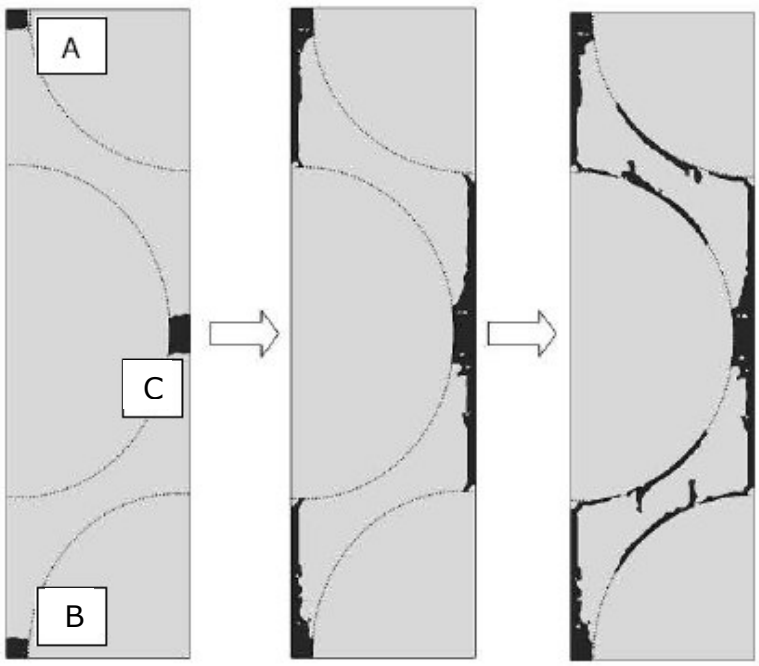

Fig. 6.3 – Damage onset and evolution in **RVE/0.0ηm** under *y*-direction loading condition.

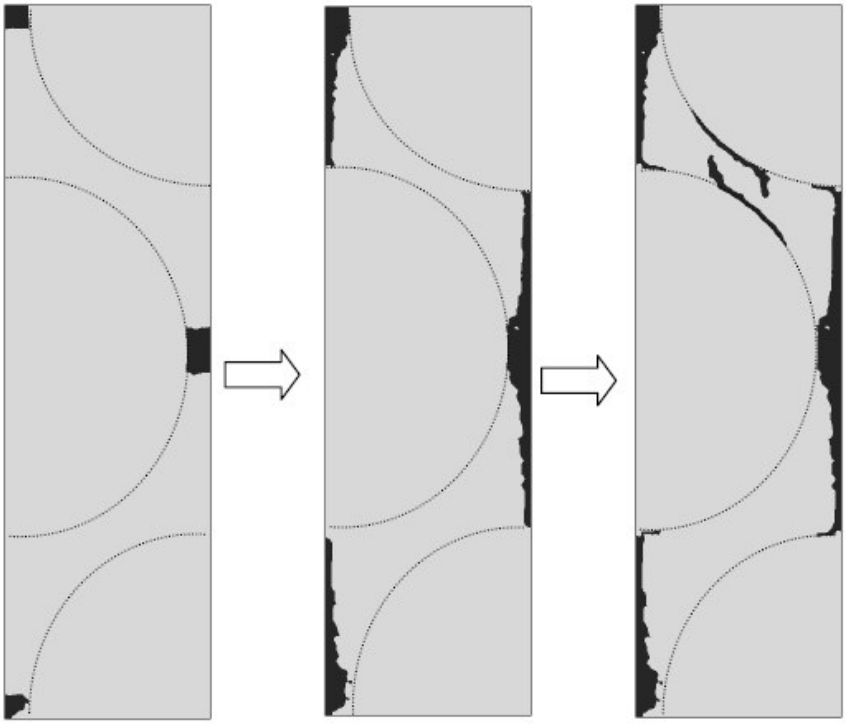

Fig. 6.4 – Damage onset and evolution in **RVE/0.25ηm** under *y*-direction loading condition.

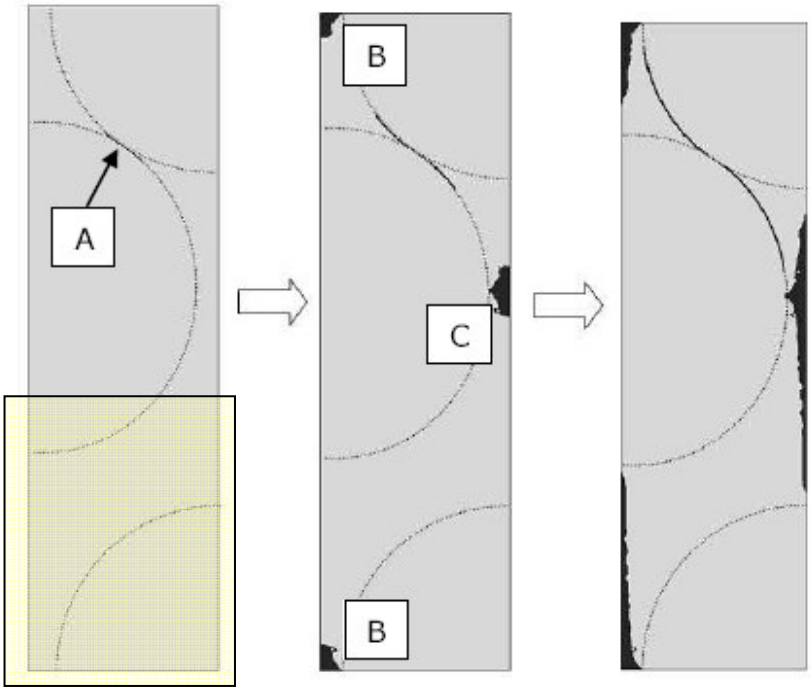

Fig.6.5 – Damage onset and evolution in **RVE/1.35ηm** under *y*-direction loading condition. The yellow square indicate the non-damaged region of the unit cell at failure onset.

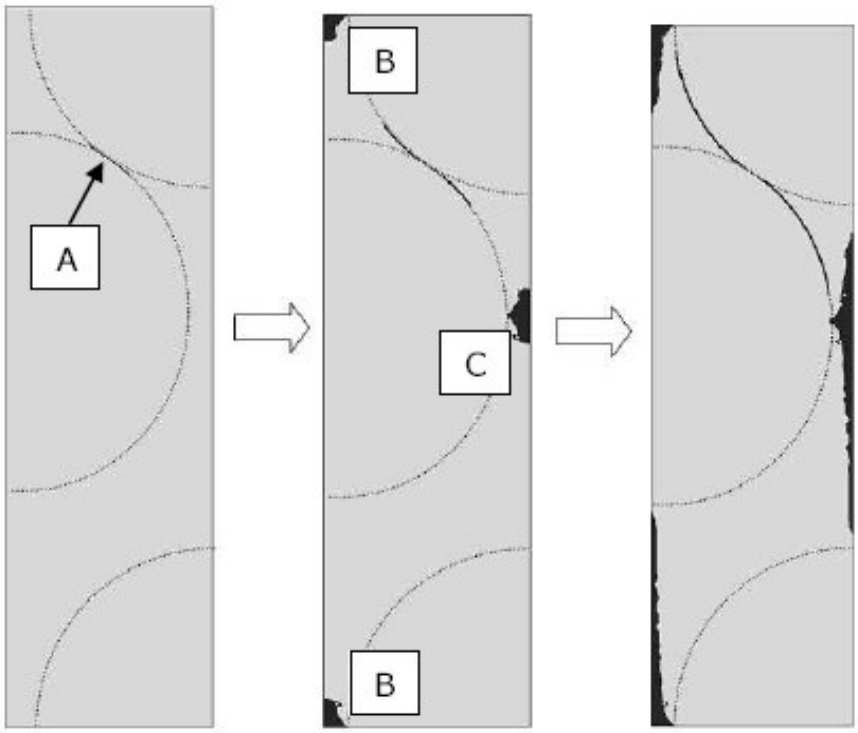

Fig. 6.6 – Damage onset and evolution in **RVE/1.55ηm** under *y*-direction loading condition.

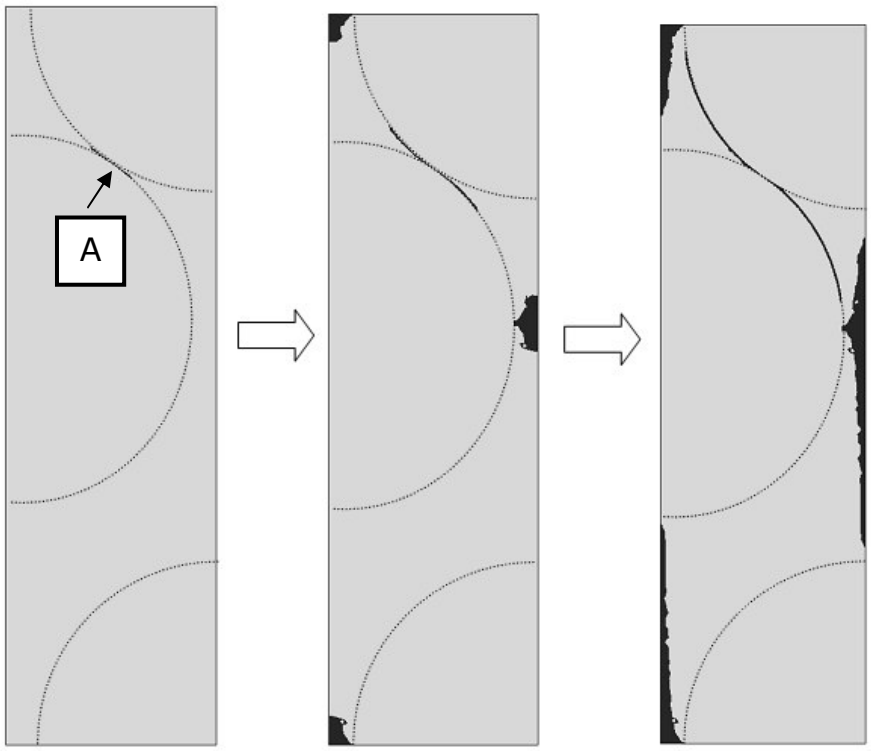

Fig. 6.7 – Damage onset and evolution in **RVE/1.70ηm** under *y*-direction loading condition.

Global stress-strain curves (Fig. 6.8) indicate interesting results on the overall response of the unit cells that undergo transverse loading along the *y*-direction. Under the *y*-direction loading condition, the ultimate strength and strain manifests a slightly beneficial effect. This improvement in the ultimate strength could be explained with the non-symmetric damage progression in non-uniform RVEs (Fig.6.5-7) in which a remarkable result is represented by a less damaged area on the inferior site of the unit cell (yellow square in Fig. 6.5) when decrementing the inter-fibre spacing on the upper region of the unit cells.

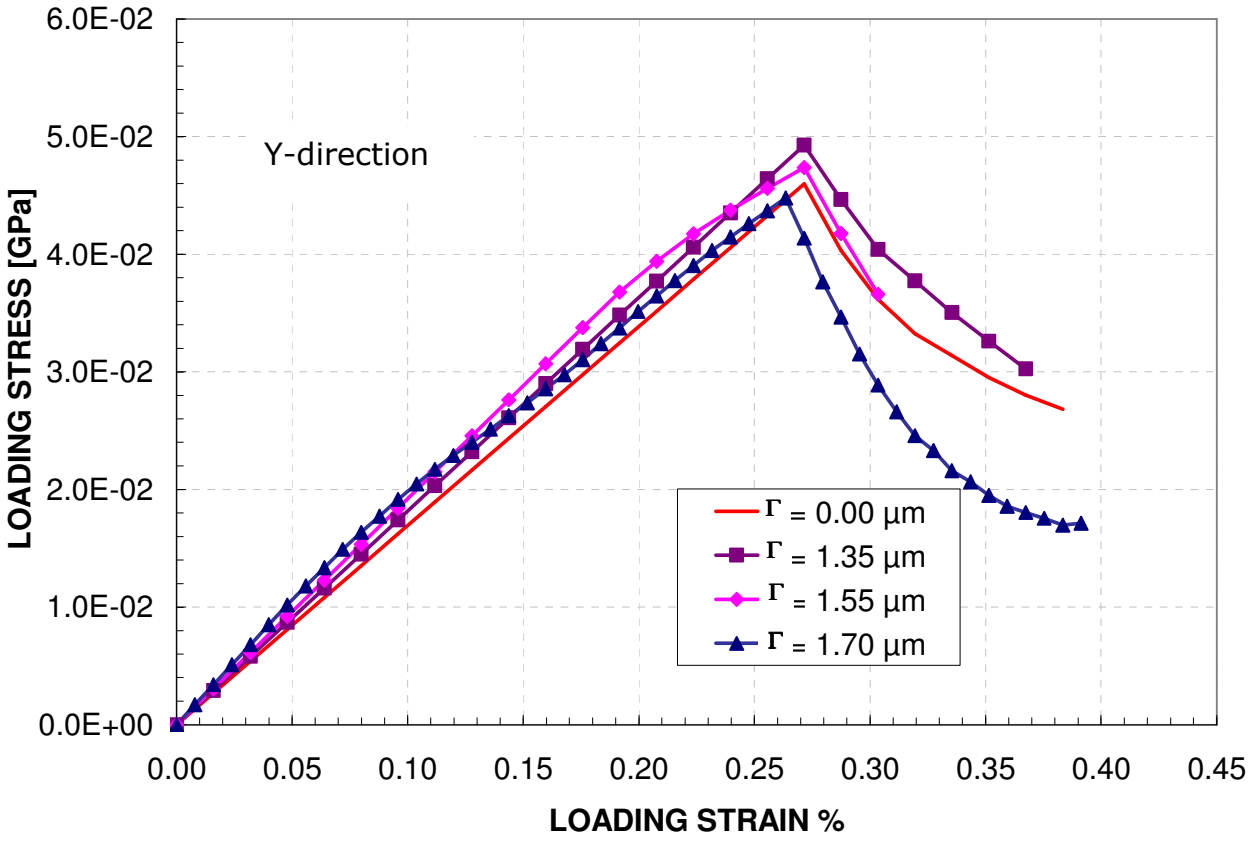

Fig. 6.8 – Global stress-strain curve in *y*-direction for uniaxial transverse tensile loading.

The micromodel RVE/1.70ηm displays a different response due to the minimum distance between fibres. The plot in Fig. 6.9 shows an initial and drastic matrix failure at very low strains leading to a consistent modification of elastic stiffness. This tendency to a premature matrix failure can be also noticed in Fig. 6.8 for the curve related to the micromodel RVE/1.55ηm.

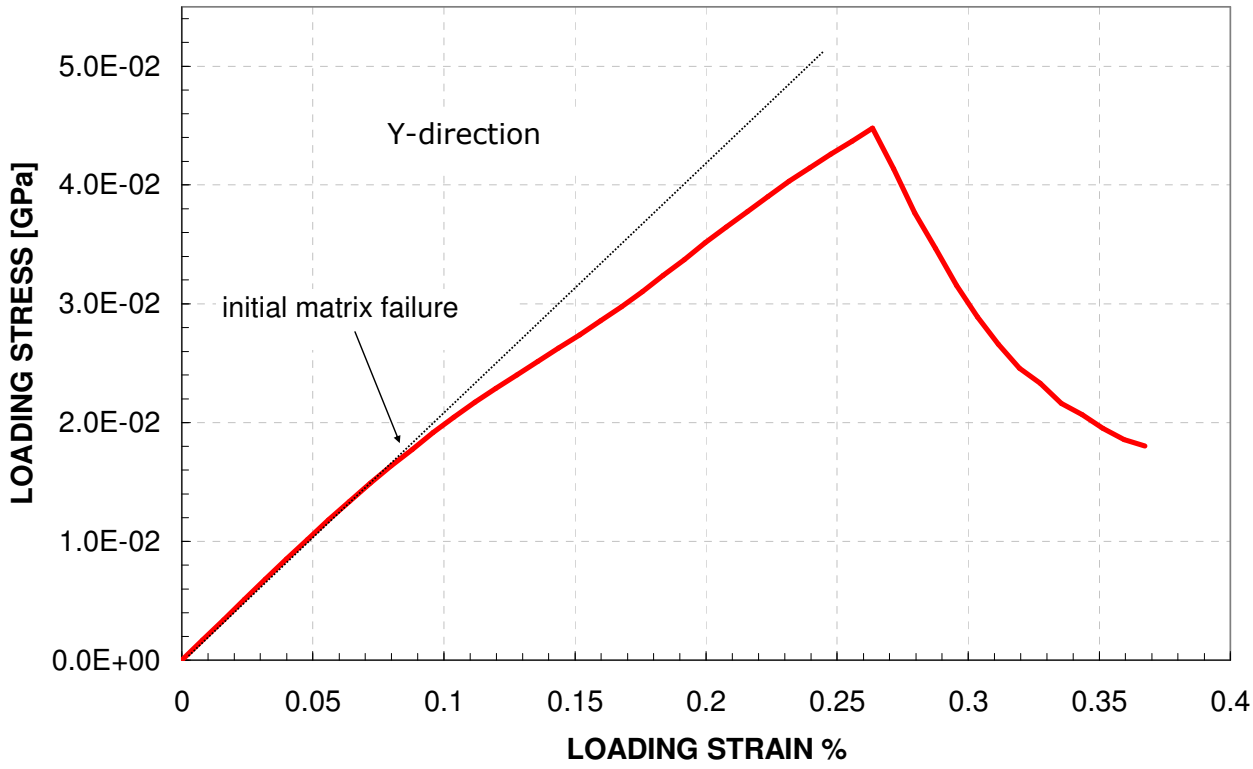

Fig. 6.9 – Global stress-strain curve in *y*-direction for uniaxial transverse tensile loading related to RVE/1.70ηm.

Damage onset and evolution for the reference micromodel under z-direction is shown in Fig. 6.10. The weakest region is represented by the fibre/matrix interfaces (region A and B) and damage can be principally attributed to the fibre/matrix debonding that propagates along the interfaces.

Non-uniform micromodels such as RVE/1.70ηm in Fig. 6.11 show that only the region A of the micro model has been involved in the failure but, this result has no beneficial effect on the micromodel in terms of ultimate strength as shown in the stress/strain curves in Fig. 6.12 in which it can be seen the detrimental effect of a decreasing inter-fibre distance.

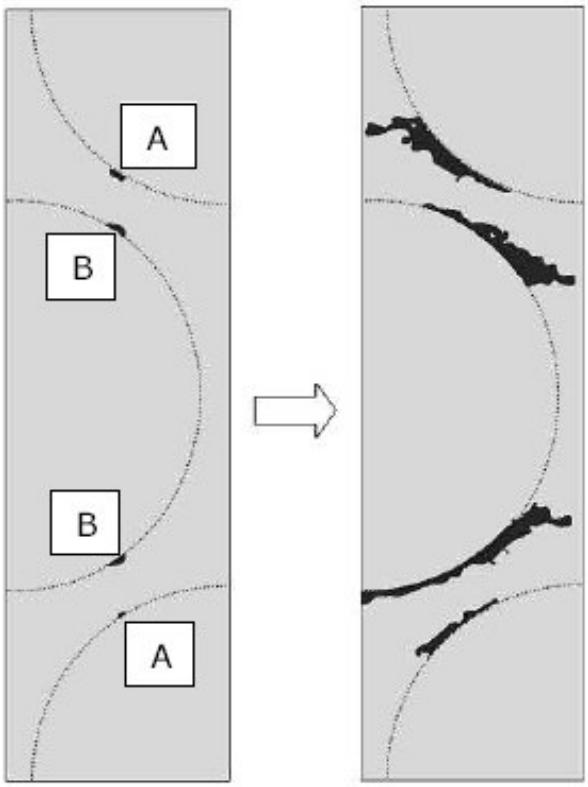

Fig. 6.10 – Damage onset and evolution in **RVE/0.0ηm** under *z*-direction loading condition.

Model RVE/1.70ηm exhibits a high ultimate strain despite a very poor ultimate strength and this can be presumably attributed to the very small area involved in the damage and its slow progression by debonding along the fibre/matrix interface. The stress/strain curve related to model RVE/1.70ηm in Fig. 6.12 gives evidence of a premature matrix failure at very low loading stress and strain that modify greatly the overall mechanical response. No premature matrix failure has been detected for other micromodels.

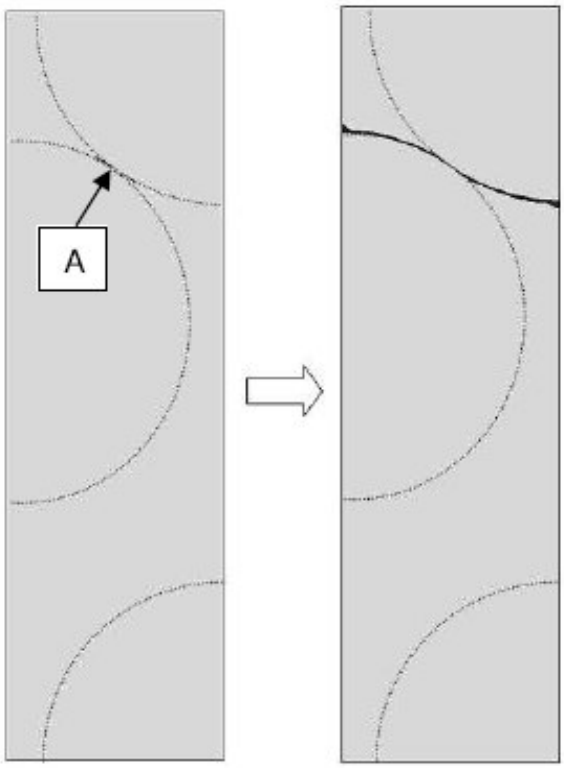

Fig. 6.11 – Damage onset and evolution in **RVE/1.70ηm** under *z*-direction loading condition.

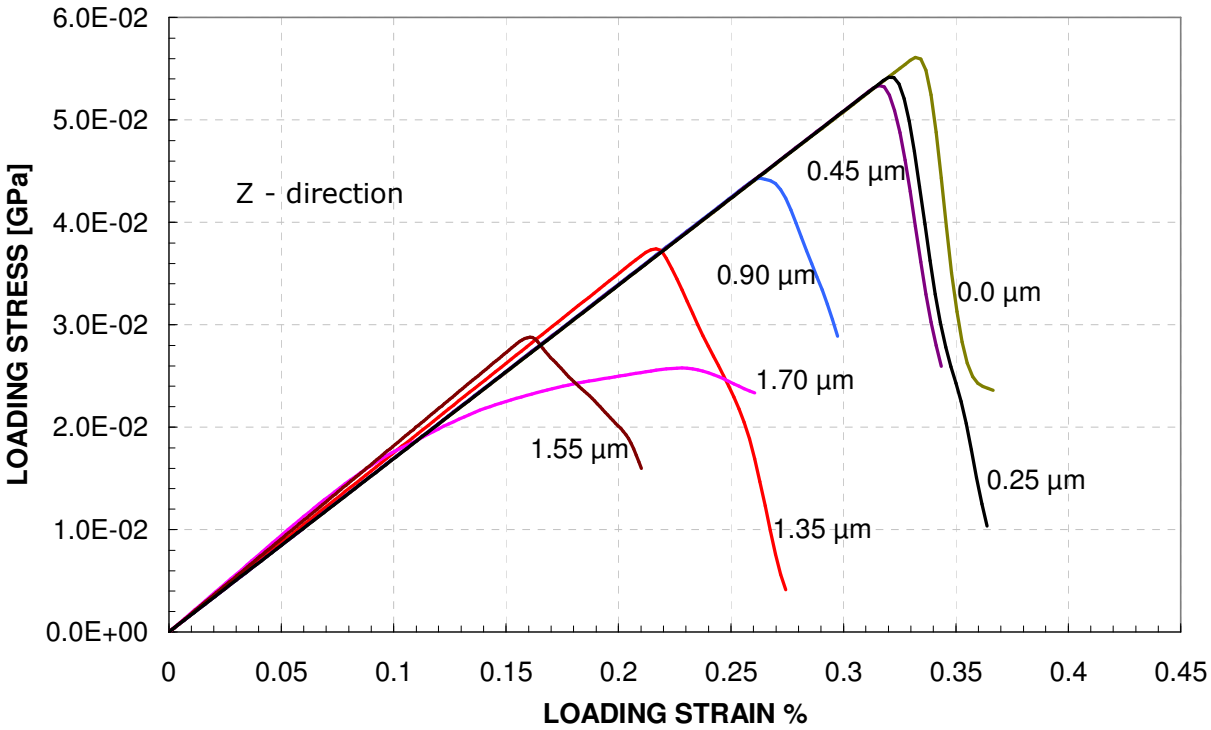

Fig. 6.12 – Global stress-strain curve in *z*-direction for uniaxial transverse tensile loading.

A peculiar effect in non-symmetric unit cells is an increasing elastic stiffness when incrementing the central fibre translation along the *z*-direction as can be seen in Fig. 6.13. The Young's modulus presents a visible increase of its value above a central fibre translation of 0.9ηm while it is moderately constant under this value. In a previous investigation [172] it was found that the elastic stiffness depends on the fibre content and it augments by increasing the fibre volume fraction. Hence, the stiffening effect in non-uniform RVEs with a decreasing inter-fibres spacing can be attributed to a more dominant effect of fibres. In fact, the decreasing inter-fibre distance allows only negligible transverse strains.

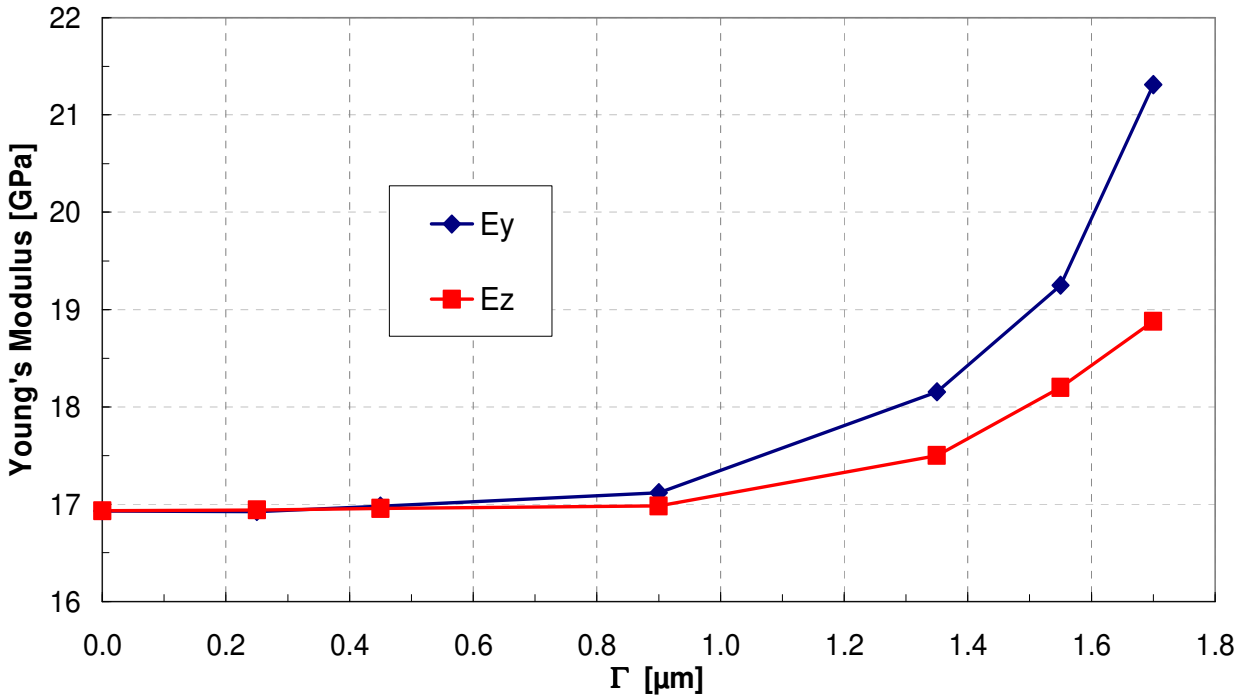

Fig. 6.13 – Trend of Young's modulus on transverse loading at different translation factors (**Γ**).

.

6.2.2 Longitudinal loading

In UD composites that are loaded along the longitudinal direction (*x*-direction, parallel to the fibres), the fibres are predominantly involved in bearing the loads. In this study the fibre content has been kept constant and the only variable is the position on the *z*-axis of the fibre.

A comparison of damage onset sites (Fig. 6.14) displays different results in non-uniform RVEs. These unit cells exhibit different regions of the damage onset that in general depends on the shifting factor Γ. In particular the reference model exhibits four entirely failed regions symmetrically distributed within the unit cell. While non-uniform unit cells show a non-symmetric distribution of failed areas (Fig. 6.14). Hence, as fibres are dominant no change in terms of ultimate strength and strain of the micromodel is expected. In fact as shown in Fig. 6.15 the stress/strain curves for the highest values of Γ and the reference model exhibit a perfect superposition.

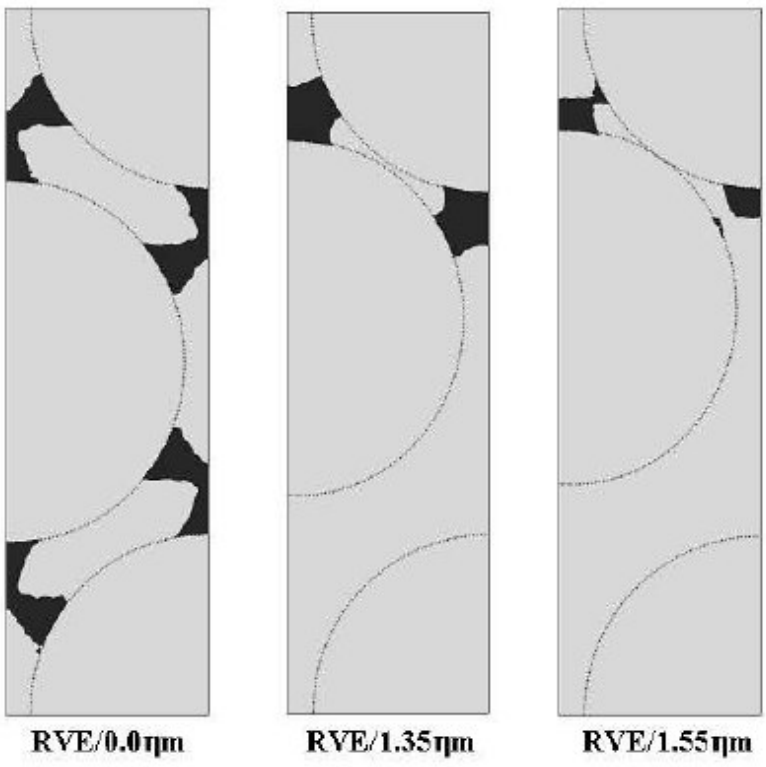

Fig. 6.14 – Damage onset under *x*-direction loading condition.

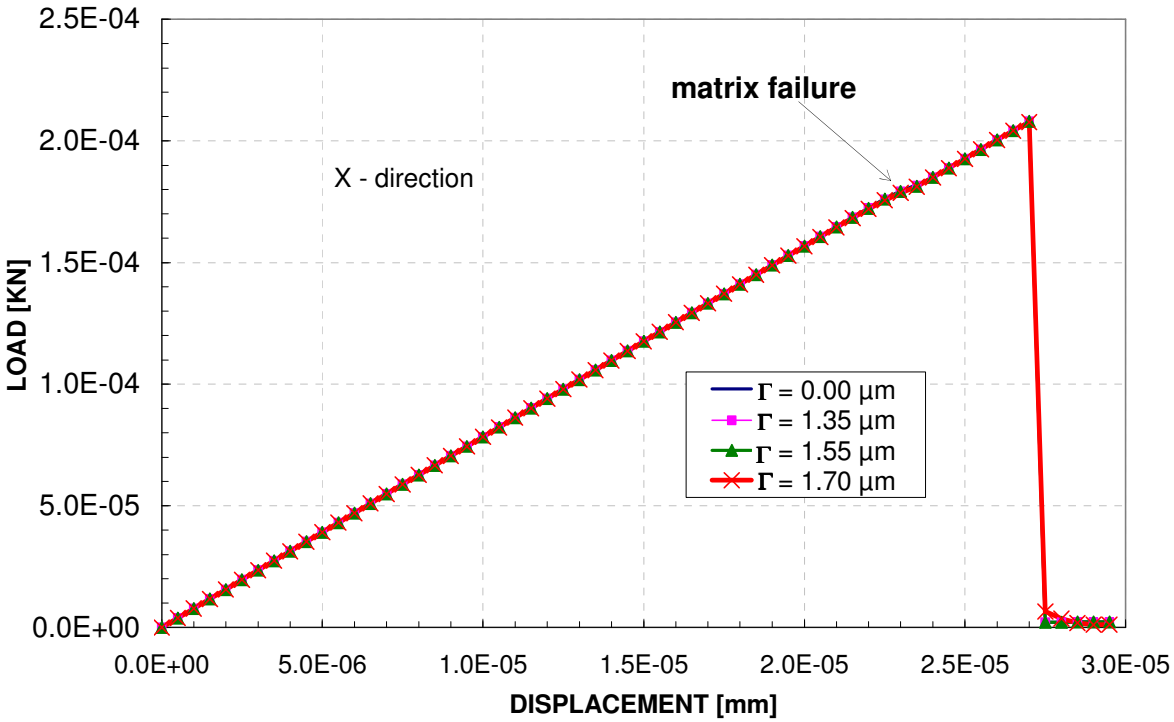

Fig. 6.15 – Global load-displacement curve in *x*-direction for uniaxial transverse tensile loading.

6.3 Residual Stress Analysis

6.3.1 Effect of residual stress on transverse loading

To study the influence of residual stress/strain on the response of non-uniform unit cells after curing and thermal cooling analyses a global strain has been applied to the unit cells. The global strain was achieved by specifying a uniform displacement at the model surfaces, At each time increment of the analysis, the damaged area in the matrix or in the fibre has been determined using the Maximum Principal Stress failure criterion. Throughout the following analyses, the fibre showed no sign of damage due to its high strength, therefore, damage and failure refer to the matrix only.

Micromodels RVE/0.25ηm, RVE/0.45ηm, RVE/0.90ηm, RVE/1.35ηm and RVE/1.55ηm, that present an inter-fibre spacing greater than ~0.15ηm do not indicate any sign of failure during the whole curing process for the three different linear chemical shrinkages (0.01%, 0.35% and 1%).

The most important result can be seen for the unit cell RVE/1.70ηm (Fig. 6.16) that presents a minimum inter-fibre distance of ~0.05ηm. In fact, this unit cell fails during the cooling process in the whole set of linear chemical shrinkages that has been examined. Matrix failure is detected in the narrow gap between fibres and should be attributed to a high compressive stress (Fig. 6.17) arising in this particular site during the contraction along the *y*-direction, *z*-direction and *x*-direction due to the cooling process.

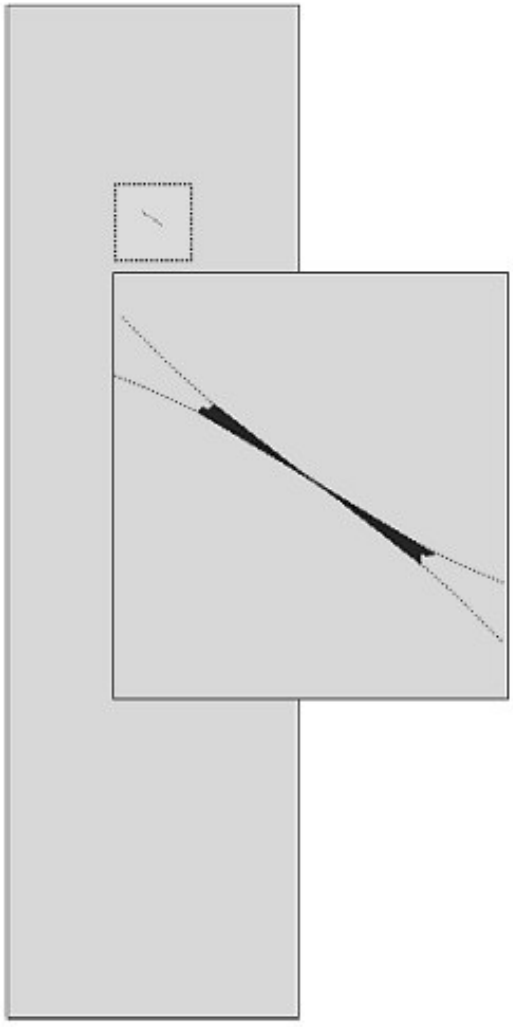

Fig. 6.16 – Damage onset in **RVE/1.70ηm** during the cooling process.

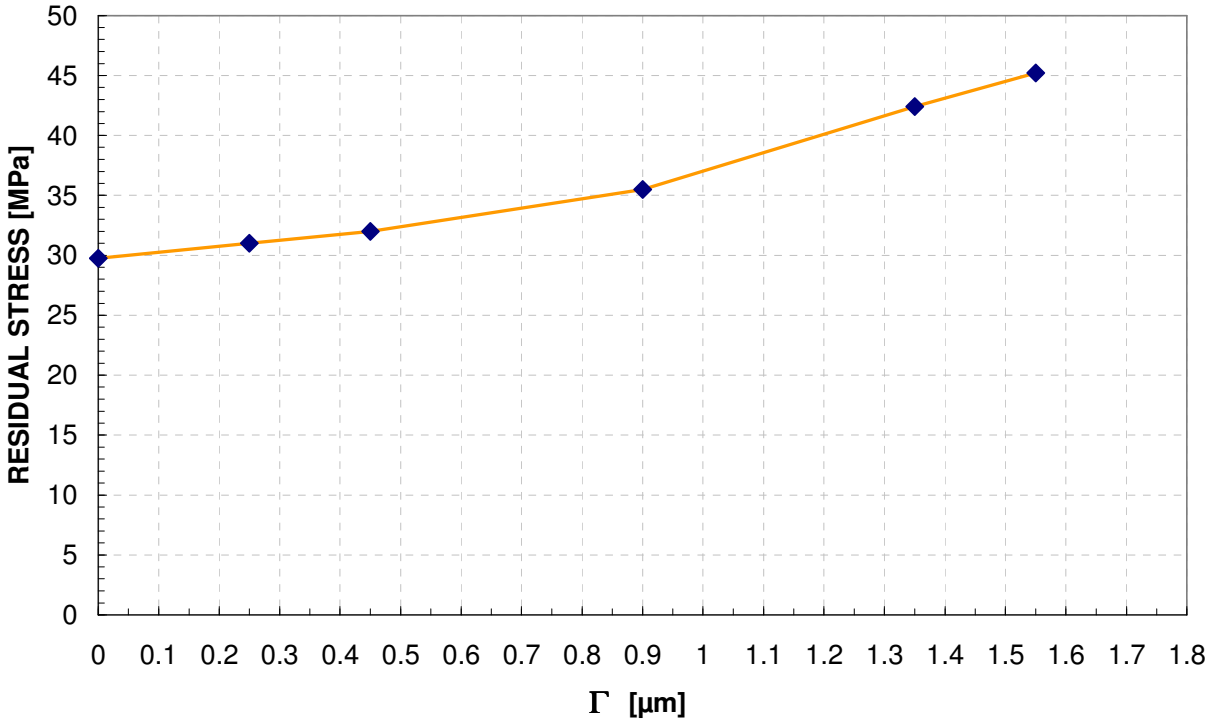

Fig 6.17 - Trend Maximum Principal Stress during the cooling process.
The abscissas indicates the position of the central fibre centre for various translation factors Γ.

In the *y*-direction loading case the reference model (Fig. 6.3) and micromodels with a shifting factor equal or less than 1.35ηm display a damage onset still located in the same regions named A and B but its progression strongly depends on the fibre packing geometry. For instance, in the reference model (Fig. 6.18) damage is likely to spread within the matrix from the region A and B while without residual stress its evolution is mainly located along the edge and eventually progresses toward fibre/matrix interfaces. Residual stresses completely modify damage onset in Model RVE/1.55ηm now localized in the region A and B in Fig. 6.19.

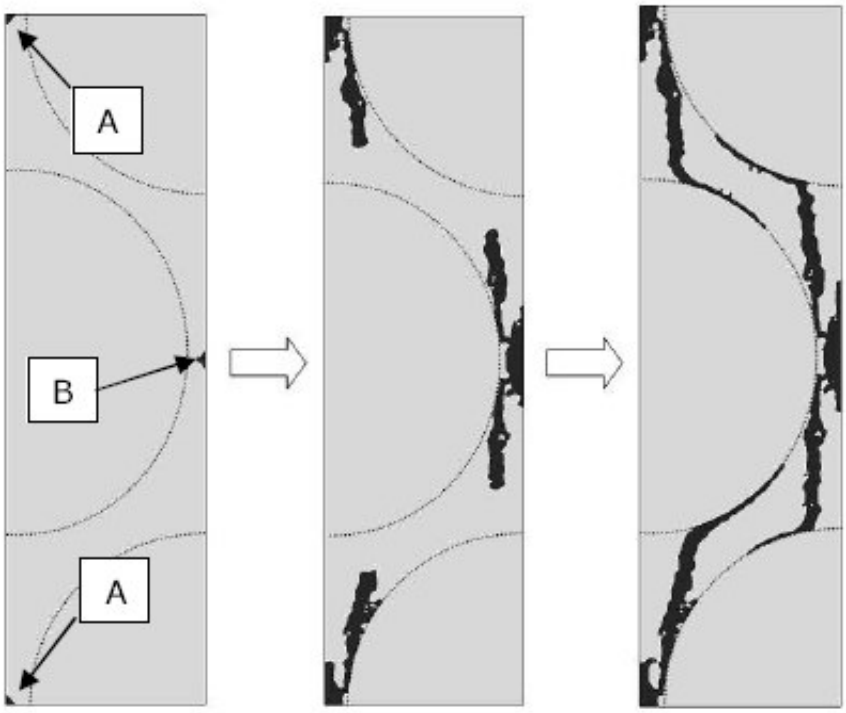

Fig. 6.18 – Damage onset and evolution in **RVE/0.00ηm** under *y*-direction loading condition with residual stress.

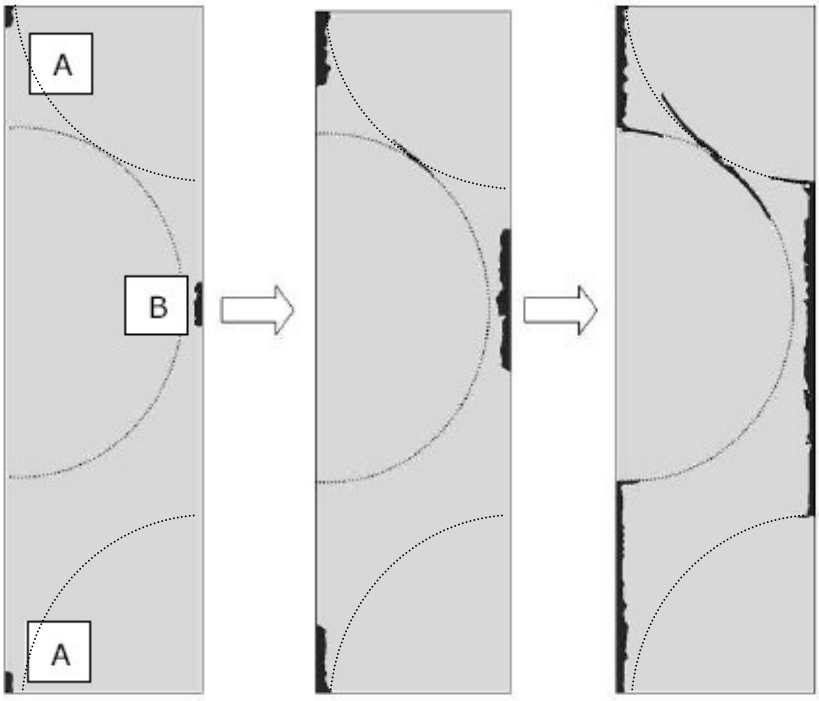

Fig. 6.19 – Damage onset and evolution in **RVE/1.55ηm** under *y*-direction loading condition with residual stress.

Results regarding the *z*-direction loading conditions show there are no relevant differences in the damage onset and its evolution. The unit cell RVE/1.70ηm displayed in Fig. 6.20 shows an initiation site of damage in region A both in case of *y*-direction and *z*-direction loading. Failure in this area "must" be completely attributed to the high compressive stress during the cooling process after chemical shrinkage that causes matrix rupture. Nevertheless the initiation points of the failure are not significantly affected by the presence of residual stress especially in the *z*-direction, monitoring the global stress-strain response during the damage analysis results indicates in general a beneficial effect of residual stress as shown in Fig. 6.21 and Fig. 6.22.

A particular effect of residual stress can be seen in the stress/strain curves related to the micromodel RVE/1.70ηm in Fig. 6.23 and Fig. 6.24 in which failure is detected during the cooling process. In this case, by applying the load after the curing process, it can be seen a slightly modification of elastic stiffness (more evident in Fig. 6.24). This change of the stiffness is caused by the damage and the detrimental effect of residual stress on the *z*-direction loading.

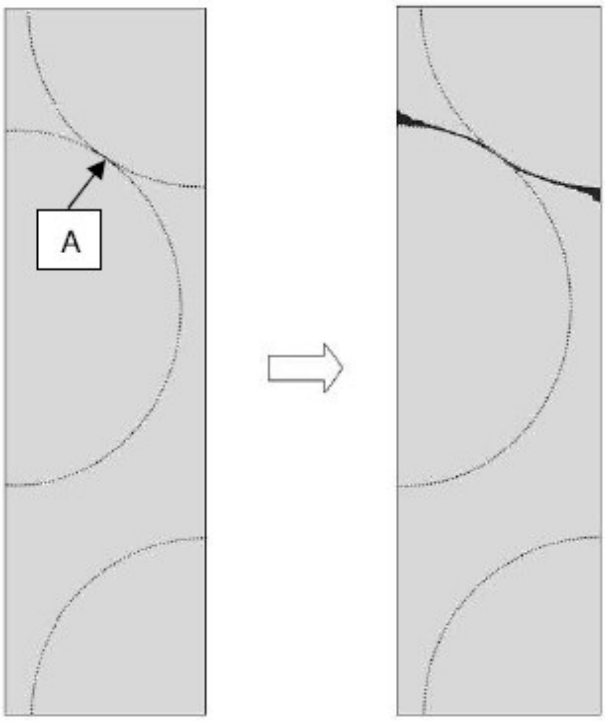

Fig. 6.20 – Damage onset and evolution in **RVE/1.70ηm** under *z*-direction loading condition with residual stress.

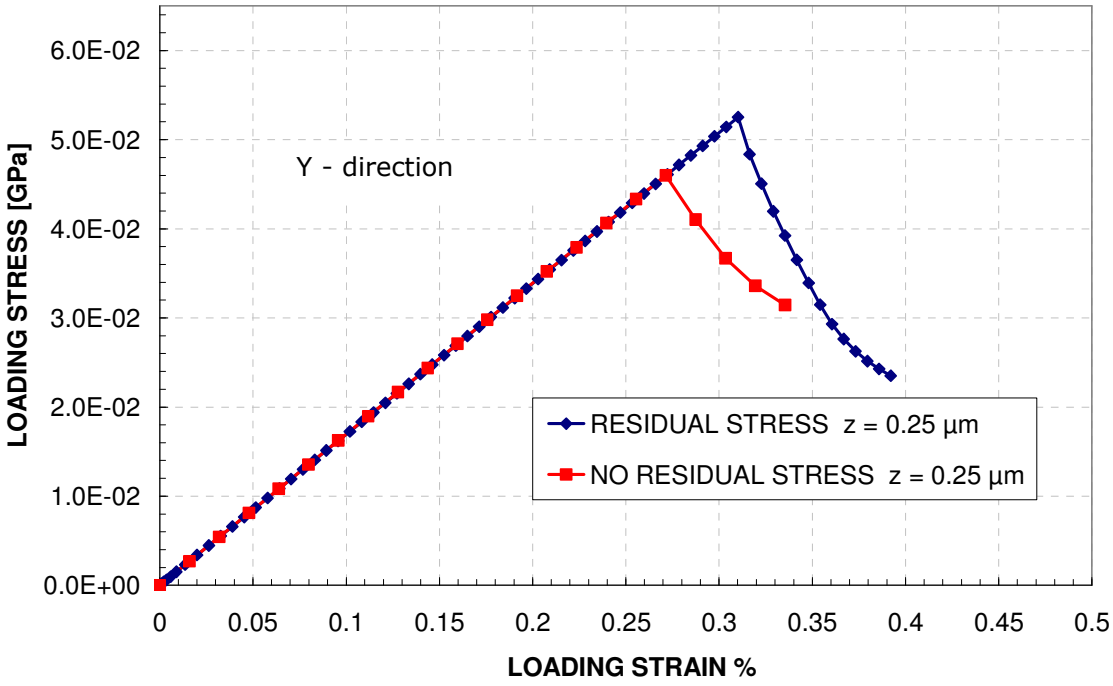

Fig. 6.21 – Global stress-strain curve in *y*-direction for uniaxial transverse tensile loading related to RVE/0.25ηm.

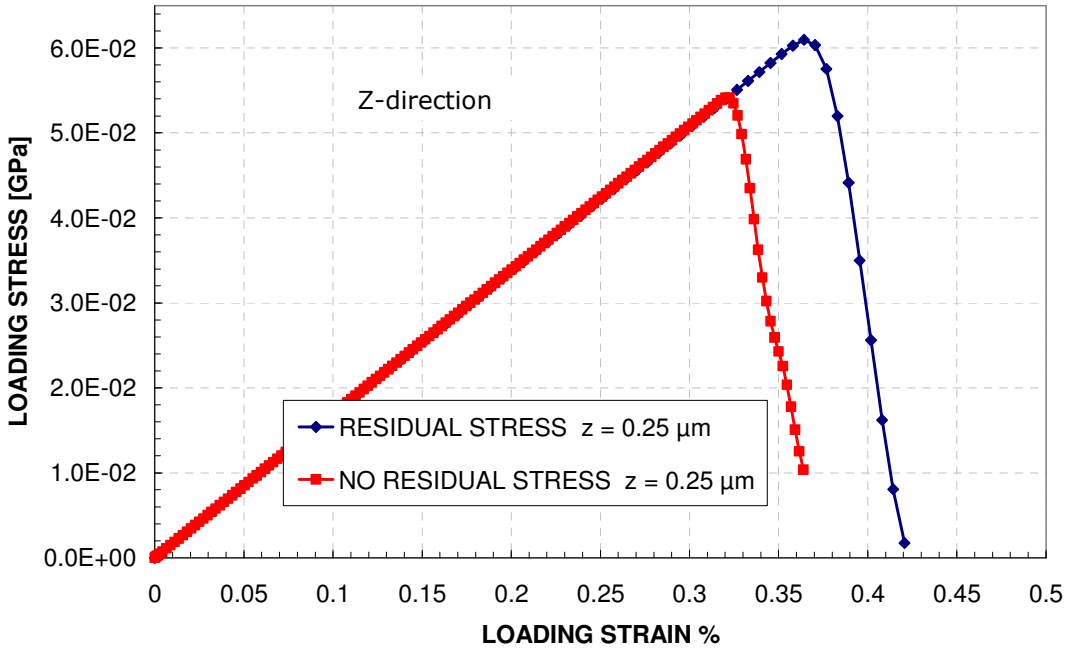

Fig. 6.22 – Global stress-strain curve in *z*-direction for uniaxial transverse tensile loading related to RVE/0.25ηm.

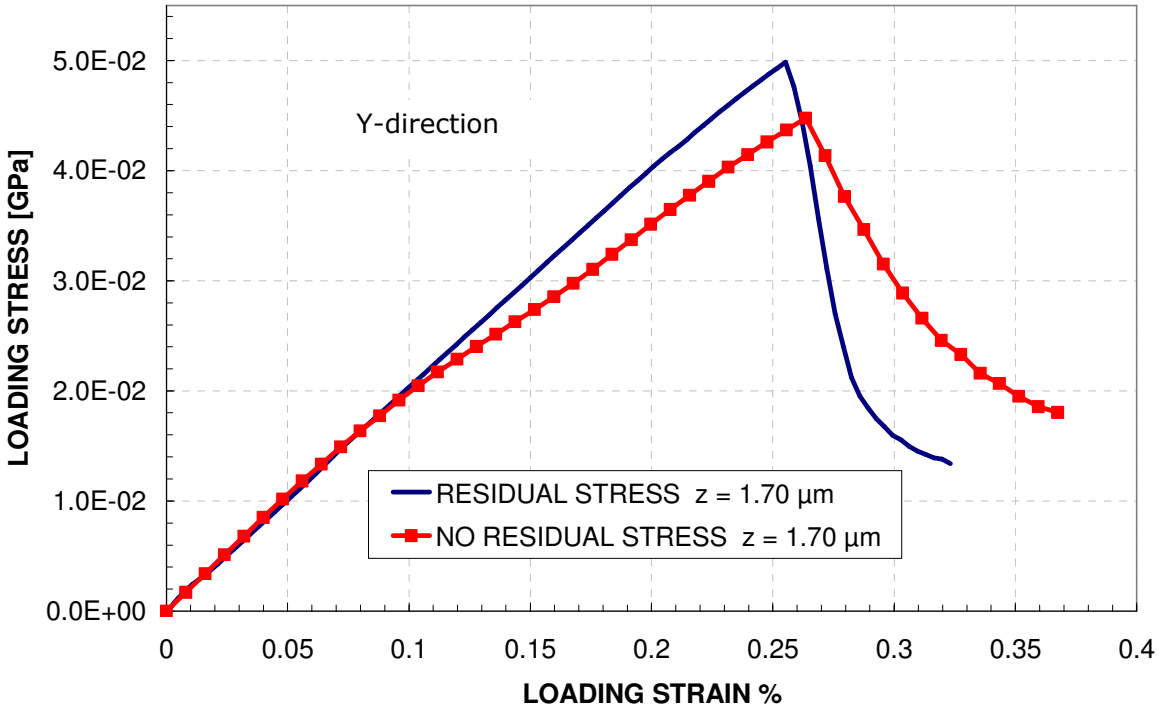

Fig. 6.23 – Global stress-strain curve in *y*-direction for uniaxial transverse tensile loading related to RVE/1.70ηm.

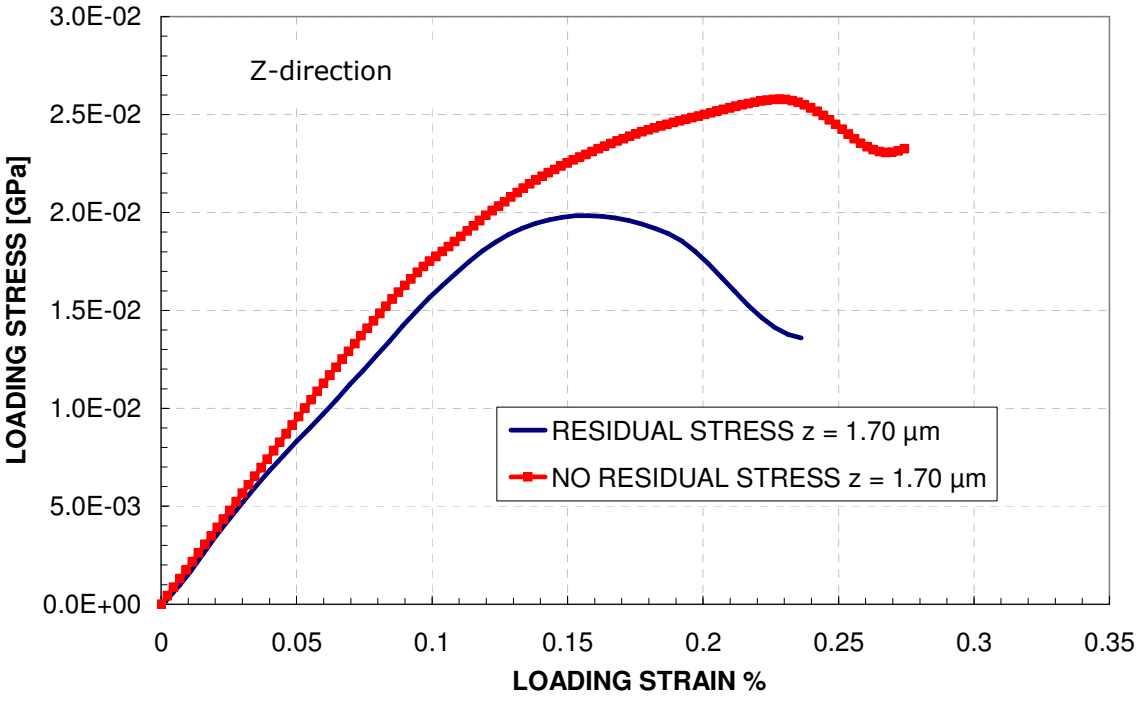

Fig. 6.24 – Global stress-strain curve in *z*-direction for uniaxial transverse tensile loading related to RVE/1.70ηm.

Residual stresses after curing and cooling cause a redistribution of the internal stress field and the positive consequence is to lower stresses within the resin in the weakest regions (e.g. corners, interfaces) of the micromodel, improving the ability to bear loads in the *y*- and *z*-direction. In particular, it can be observed that residual stresses tend to delay the growth of high concentrated tensile stresses in these regions. Fig. 6.25, for example, displays the highest values of Maximum Principal Stress at the end of the cooling process and during the loading. When loading is applied, e.g. in *y*-direction, high stresses start decreasing from the position after cooling, shown in Fig 6.25(a), and keep "migrating" toward the corners and the central area of the unit cell as depicted in Fig. 6.25(b).

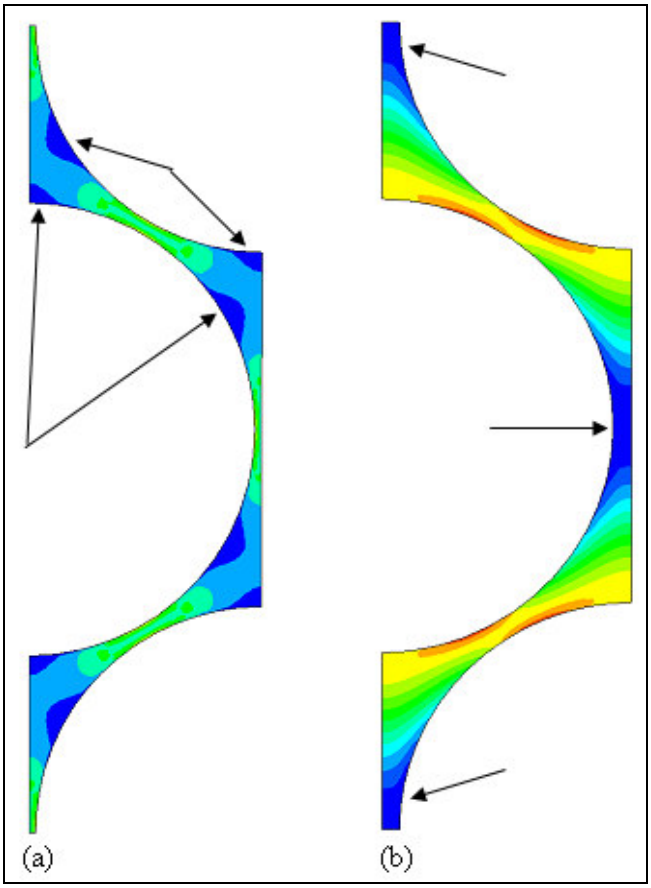

Fig. 6.25 – Maximum Principal Stress distribution (RVE/0.0ηm) after cooling (a) and before failure (b) under a transverse (*y*-direction) loading. Arrows indicate the highest tensile stress distribution.

Numerical results show that for high shifting factors initial and final failure of micromodels are not coincident especially for high **Γ.**

In addition matrix failure could occur during the cooling process. In Table 6-1 and Table 6-2 results are summarized for transverse loading and in particular strains in which failure is detected (initial failure) and the strains in which the mechanical properties of the matrix undergo an abrupt drop (final failure).

Table 6-1 Failure strains data for transverse loading along the *y*-direction.

	Transverse *y*-direction			
	No Residual Stress initial failure	No Residual Stress final failure	Residual Stress initial failure	Residual Stress final failure
Γ	ε_{matrix} (%)		ε_{matrix} (%)	
0	0.27	0.27	0.31	0.31
0.25	0.27	0.27	0.31	0.31
0.45	0.27	0.27	0.31	0.31
0.90	0.27	0.27	0.31	0.31
1.35	0.27	0.27	0.29	0.29
1.55	0.19	0.27	0.28	0.28
1.70	0.11	0.26	cooling	0.25

Table 6-2 Failure strains data for transverse loading along the *z*-direction

	Transverse *z*-direction			
	No Residual Stress initial failure	No Residual Stress final failure	Residual Stress initial failure	Residual Stress final failure
Γ	ε_{matrix} (%)		ε_{matrix} (%)	
0	0.33	0.33	0.37	0.37
0.25	0.32	0.32	0.36	0.36
0.45	0.31	0.31	0.35	0.35
0.90	0.26	0.26	0.32	0.32
1.35	0.22	0.22	0.27	0.27
1.55	0.16	0.16	0.19	0.19
1.70	0.08	0.23	cooling	0.16

6.3.2 Effect of residual stress on longitudinal loading

In UD composites during the curing process the resin is in a rubbery state and realistically no deformation is established along the *x*-direction. Strains parallel to fibres are only developed during cooling as the resin evolves from a liquid/rubbery state into a solid state. If residual stresses are included on the *x*-direction loading, numerical analyses show that the damage onset tends to be more localized at fibre/matrix interface (Fig. 6.26). Although residual stresses do not affect the ultimate strength of the unit cells but most importantly, they are greatly detrimental for the matrix causing failure at lower loading strains as can be seen in Fig. 6.27 and Table 6-3.

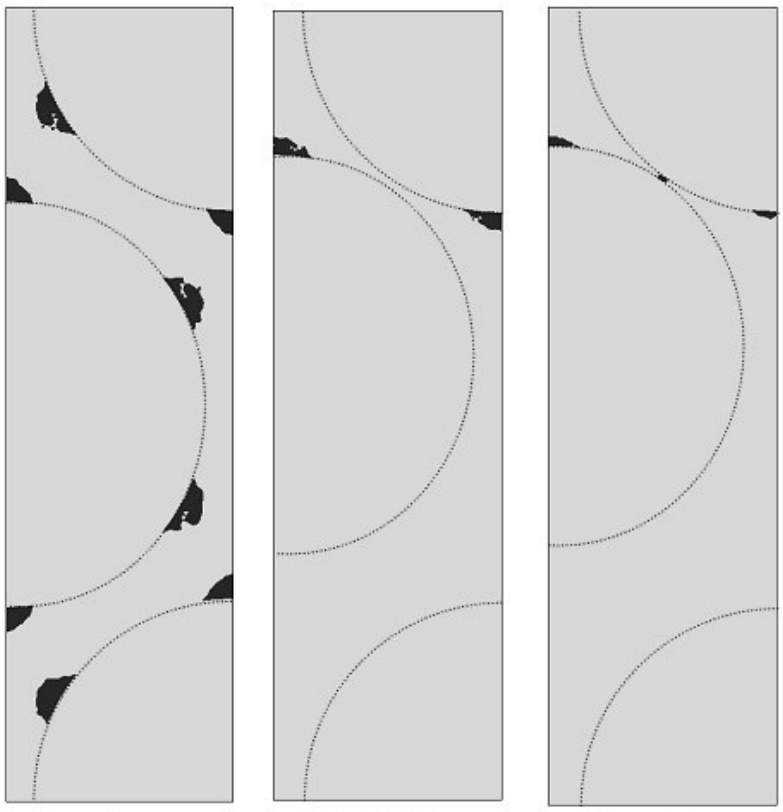

Fig. 6.26 – Damage onset under *x*-direction loading condition with residual stress.

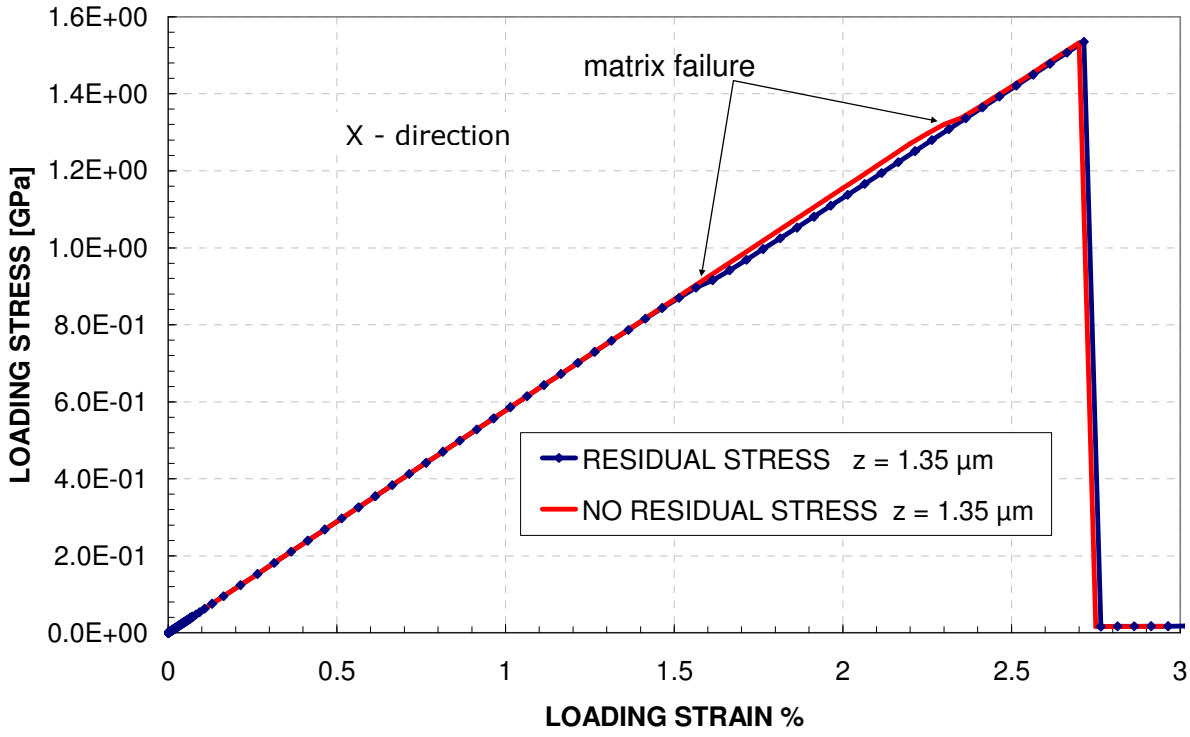

Fig. 6.27 – Global stress-strain curve in *x*-direction for uniaxial transverse tensile loading with a without residual stress related to RVE/1.35ηm.

Table 6-3 Failure strains data for longitudinal loading along the *x*-direction

	Longitudinal *x*-direction			
	No Residual Stress	Residual Stress	No Residual Stress	Residual Stress
Γ	ε_{fibre} (%)	ε_{fibre} (%)	ε_{matrix} (%)	ε_{matrix} (%)
0	2.70	2.71	2.50	1.65
0.25	2.70	2.71	2.50	1.65
0.45	2.70	2.71	2.50	1.65
0.90	2.70	2.71	2.50	1.65
1.35	2.70	2.71	2.50	1.65
1.55	2.70	2.71	2.50	1.55
1.70	2.70	2.71	2.50	cooling

A full understanding of this detrimental effect can be highlighted in Fig. 6.25a and Fig.6.28. Unlike transverse loading conditions, in which the residual stress is redistributed from the position at the end of the cooling process along the fibre/matrix interface and within the matrix, for the longitudinal (*x*-direction) loading condition the already high values of residual stresses

remain concentrated at fibre/matrix interface in the same position as after cooling process. Hence thermal residual stresses tend to weaken this area furthermore and moreover they promote its premature failure.

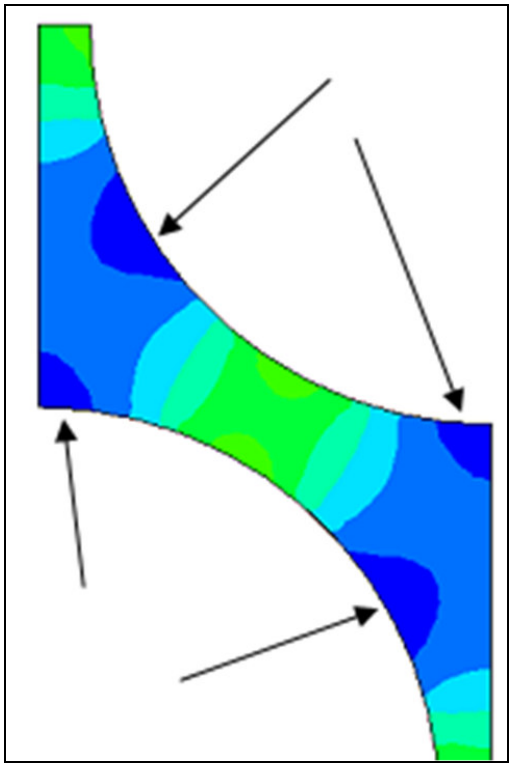

Fig. 6.28 – Maximum Principal Stress distribution (RVE/0.0ηm) before failure under longitudinal (*x*-direction) loading. Arrows indicate the highest tensile stress distribution.

6.4 Conclusion

Effects of inter-fibre spacing on transverse and longitudinal failure of fibre-reinforced polymer matrix composites have been studied using a micromechanical non-uniform unit cell model and the finite element method. Predicted damage initiation and evolution as well as mechanical properties are clearly influenced by different inter-fibre spacing.

A further investigation accounting for residual stress shows that residual stress and inter-fibre spacing play an important role during the curing process and in presence of micro- gaps between fibres (~0.05ηm). Matrix failure has been detected for all three different values of the linear

chemical shrinkage (0.01%, 0.35% and 1%) that have been investigated. The presence of residual stresses also affects damage initiation sites especially in unit cells in which inter-fibre spacing is of the order of few micro-meters (0.08-0.05).

Finally the FEM investigations have proved that thermal residual stresses are highly detrimental for the matrix in the longitudinal loading while in the transverse loading the unit cells see in general beneficial effects.

Chapter 7

Conclusion and Discussion

7.1 Introduction

Thermoset composite materials are becoming a viable alternative to more conventional materials (e.g. aluminium) in a wide range of industrial applications but their use remains still limited due to the limitations in the current understanding of the damage behaviour and lack of fully validated modelling tools. Moreover the overall ultimate properties, at macroscale, depend on the manufacturing process of fibre reinforced thermosetting resins that appears particularly influenced by the microstructure (e.g. fibre architecture, fibre content) of the composite material. Hence, it appears evident that a better understanding of the processes arising during the curing and cooling phases at the constituent level could suggest strategies to improve the ultimate mechanical properties at the macroscale.

7.2 Finite Element Analysis

The aim of this research has been the development of a micromechanics-based damage model and the implementation of this damage model into the FEM code ABAQUS. The damage model used to simulate the failure onset and damage progression is based on the work of Blacketter [5] and represents a powerful tool to simulate physically observed damage such as fibre-matrix debonding and micro-cracks within the matrix. It has been implemented into ABAQUS via the user's subroutines UMAT and USDFLD.

Two different kinds of numerical analyses have been carried out in order to identify the characteristics of the micromodels investigated, namely:

A) Non residual stress analyses.

B) Residual stress analyses.

Numerical results obtained with the "non-residual" stress analyses have been used as a benchmark in order to compare the effects of thermal residual stresses on the overall mechanical properties of the UD composites at their microscale. Although other researchers [3, 8, 147, 170] have investigated the mechanical characteristics of UD composites at their microscale, in general only two-dimensional unit cells have been adopted for their studies.

In the present work, three-dimensional RVEs have been employed. The main difficulty of 3D unit cells is represented by the set of boundary conditions. In fact, these boundary conditions must be applied accurately on the faces of the micromodel in order to achieve a more realistic stress state that is generated from the different loading conditions.

Moreover, although the computational implementation of the damage models via subroutines in FORTRAN represents a well established methodology, the realistic simulation of the manufacturing process (curing and cooling) with the subroutines UMAT and USDFLD, coupled to the micromechanics-based damage model, can be considered as an innovative computational technique. This new computational methodology that takes into account temperature dependant material properties was successfully implemented for the evaluation of local distribution and magnitude of thermal residual stresses introduced during the manufacturing process for different fibre volume fractions.

7.2.1 Micromechanical stiffness

An important factor of this research was to identify the proper boundary conditions to apply to the faces of each numerical model in order to demonstrate their potential to describe accurately the material properties of unidirectional composite materials at microscale. The applied boundary conditions are based on the research of Sun et al [3] and have been used in FE analyses resulting in a good agreement with experimental and the semi-empirical expressions such as the Rule of Mixtures.

7.2.2 Micromechanical strength

The mechanical strength of the unit cells was investigated in order to characterize the mechanical response of the numerical models under tensile loading. The novel computational method that includes the damage model and the thermal residual stresses was employed to establish the relationship between damage behaviour and fibre content using 3D unit cells with a hexagonal packing array. The user subroutines have also included different failure criteria developed to detect failure in polymers taking into account their different behaviour in tension and compression. Preliminary analyses without the residual stress have been initially carried out and the results have been used as a benchmark for the residual stress analyses.

These analyses have shown the strong dependence on the fibre volume fraction especially under transverse loading. The mechanical response of the unit cells has been significantly affected by the presence of residual stresses. Ultimate strength was increased under transverse tensile loading due to the redistribution of stresses within the matrix. On the contrary under longitudinal loading conditions, the residual tensile stress remained concentrated at the fibre/matrix interface and caused weakening of the matrix in that area. The analyses (with and without residual stress) have contributed to the description of the mechanical behaviour of the composite at the constituent level under unidirectional tensile loading.

7.2.3 Effects of Interphasial Properties on the Mechanical Behaviour of RVEs

Numerical investigations have been performed on unit cells incorporating a third phase (interphase) in order to approach more realistically the structure of composites at microscale. In fact, composite materials in general show a third phase in the vicinity of the fibres that arises either via unexpected modifications of the matrix during the manufacturing process or via accurate engineering, by modifying the nature of the fibre surfaces (sizing) to affect the curing kinetics and cross-link density of the nearby matrix.

The most innovative aspect of these investigations is represented by the characterization of the interphases in the analyses with residual stress. The third phase arises during the simulated manufacturing process by assigning “idealised” temperature dependant properties (different from the matrix properties) to some elements of the mesh at the fibre/matrix interface.

This numerical approach, in combination with the already described damage-residual stress computational model, represents a valuable instrument to evaluate the distribution and magnitude of residual stress after the curing and cooling process. Moreover the comparison with the results from non-residual stress analyses has permitted evaluation the effects of thermal stresses and interphasial properties on the damage behaviour.

Non-residual and residual stress analyses have shown peculiar results. Firstly they have proved that the interphase is able to modify slightly the elastic stiffness of the micro-models. RVEs with soft interphase have displayed a significant improvement in terms of ultimate strength and strain in comparison to the unit cells with a stiffer interphase.

More interestingly, finite element analyses that simulate an idealised behaviour of the interphase curing and cooling processes have indicated that the magnitude of thermal residual stress within the interphase and the matrix has been strongly influenced by the material properties of the interphase with significantly high values in the hard interphase. The soft interphase appears to work as a “damper” by redistributing stresses within the interphase and the matrix while hard interphases lead to accumulated high stresses in the interphasial region.

In conclusion, numerical investigations have indicated that unit cells with soft interphases have shown increased characteristics in terms of ultimate strength and strain under transverse loadings and reduce significantly the amount of stresses if the manufacturing process is considered in the numerical simulations, and finally improve the mechanical response even for low values of the interphasial ultimate strength when thermal residual stresses are included.

On the other hand, unit cells with hard interphases have displayed significantly reduced mechanical properties and residual stress analyses applied to these 3D unit cells have indicated the onset of failure during the cooling process within the interphase.

7.2.4 Effects of Fibre Packing Geometry the Mechanical Behaviour of RVEs

Most research related to microstructural properties of composite materials has been investigated by assuming a uniform periodic distribution of fibres within the unit cells.

In the present work a new approach has been used to investigate the effects of the non-uniform fibre distribution on the local damage behaviour. The novel approach is based on a "single-fibre" 3D unit cell in which the central fibre is shifted along one of the transverse axes (the *z*-direction in these work).

The innovative computational methodology (coupled damage-residual stress analysis) has also been adopted to study the effect of manufacturing induced stresses in order to determine the effect of the fibre position on damage onset and the modification of the residual stress distribution in the RVE. A single-fibre approach has been considered particularly suitable for the numerical investigations. In fact, the computational damage model implemented in ABAQUS follows a "local damage" criterion and, therefore it requires a high quality mesh refinement all over the unit cell, with special emphasis at the fibre/matrix interface, to achieve reliable results. Hence, two kinds of analyses have been performed namely: non-residual and residual stress analyses.

The simple fibre shifting along one of the transverse axes has allowed a good awareness of the crucial mechanisms that regulate local damage onset with and without residual stress for a non-symmetric position of the reinforcement within the RVE and, in addition, has made possible the determination of a critical inter-fibre distance. Below that distance, it is likely that fibre/matrix debonding will occur during the manufacturing process.

7.3 Future work

FE studies, with and without residual stress, on various combinations of unit cells under uniaxial loading have been extensively carried out in the present research.

Numerical analyses have shown that the mechanical behaviour of the microstructure of composite materials is significantly influenced by thermal residual stresses. In particular the present study has demonstrated that thermal residual stresses play a key role on the damage onset and damage progression in unit cells under uniaxial tensile loading. In addition, the mechanical properties of the composites are also determined by other factors such as fibre volume fraction, fibre arrangement, properties of interphase.

In order to improve the understanding of the mechanical behaviour of unit cells with various configurations the following directions of future effort are suggested:

1. Apply biaxial loadings in analyses with and without residuals stresses on the unit cells investigated in the present work. Draw failure envelopes for biaxial loading.

2. Include additional sources of material variability for the interphase such as thickness.

3. Include a 3D interphase in “non-uniform” unit cells and repeat the set of uniaxial and biaxial loadings in FE analyses with and without residual stress.

In addition, few researchers such as Chen et al [172] have investigated the effect of viscoelasticity of matrix material on the evolution of residual stresses induced during the manufacturing process in glass fibre/epoxy composites with finite element micromechanical analyses. The epoxy matrix has been represented by a nonlinear viscoelastic model. The finite

element residual stress analysis has indicated that higher cooling rate results in higher initial residual stresses in the laminate. However, the residual stress relaxes with time and tends to an asymptotic small value independent of the cooling rate. Although these results have been applied at the mesoscale of composite materials, they suggest that the implementation of more advanced constitutive models (e.g. viscoelastic model) for the epoxy matrix could estimate more accurately the magnitude of the manufacturing induced residual stresses within the unit cells after the cooling process.

7.4 Conclusion

After a review of the current literature on the microstructure of composite materials, the area related to the effects of residual stress on the overall mechanical response of composite materials at the microscale was identified as requiring further research.

The review of literature related to the modelling of RVE to be implemented into finite element codes has suggested the use of the unit cells proposed by Sun et al [3] in their investigations to simulate the periodic distributions of fibres within the matrix.
These unit cells are particularly suitable to be used in numerical analyses, in fact, due to their simple geometry, boundary conditions and loads can be imposed with particular accuracy.

The damage model implemented into the finite element calculations has indicated that, unidirectional composite materials are not particularly able to bear transverse stresses especially in presence of a non-uniform position of the fibres, as physically observed, and the presence of a "stiff interphases". Although residual stresses in general improve the strength of composites under transverse uniaxial loading, RVEs undergoing more realistic loading conditions are

unlikely to show these beneficial effects as already demonstrated by Liguo et al [170] for 2D unit cells.

The non-uniform distribution of the fibres in real composites coupled with the effects of the manufacturing process can trigger both fibre/matrix debonding and microcracks in the matrix as indicated by the numerical analyses in Chapter-6. Thus, in order to improve the transverse strength of unidirectional composites at microscale, more effort must be done to minimize the effect or residual stress arising during the curing and cooling phases in the proximity of the fibre/matrix interface. FE analyses on unit cells with different interphasial properties have suggested that properly engineered interphases can overcome this problem.

Appendix

The appendix contains listings of the subroutines written for this research. User subroutines are part of the commercial FEM code ABAQUS and are designed to offer more functionality to the code in cases where the standard options are insufficient to describe a particular mechanical constitutive behaviour of a material. To describe specific material characteristics, UMAT subroutines are called at all material calculation points of elements for which the material definition includes a user-defined material behaviour. The UMAT subroutines update the stresses and solution-dependent state variables to their values at the end of the increment for which it is called and finally must provide the material Jacobian matrix, $\partial\Delta\sigma/\partial\Delta\varepsilon$, for the mechanical constitutive model. In addition the UMAT subroutine can be used in conjunction with user subroutine `USDFLD`.

The USDFLD subroutine will be called at all material points of elements for which the material definition includes user-defined field variables and can be used to introduce solution-dependent material properties since such properties can easily be defined as functions of field variables.

UMAT Subroutine

Two different UMAT subroutines have been implemented into the code. The first subroutine includes the damage model for epoxy matrix and the E-glass fibres. The second UMAT includes the temperature dependant material properties for the epoxy matrix to simulate the curing and cooling processes for the residual stress analysis.

```
C*************************************************************
C  This UMAT was developed for:
C    1.  ANY ELEMENT TYPE WITH 3 NORMAL STRESS
C        COMPONENTS (NDI=3).  Note that the
C        Order of stresses in ABAQUS: 11,22,33,12,13,23
C    2.  Isotropic Elastic
C
C             * DAMAGE MODEL WITH NO RESIDUAL STRESS*
C
C*************************************************************
C Parameters which MUST be defined in ABAQUS input file:C
C
C   PROPS(1)   = E11
```

```
C  PROPS(2)   = E22
C  PROPS(3)   = E33
C  PROPS(4)   = v12
C  PROPS(5)   = v13
C  PROPS(6)   = v23
C  PROPS(7)   = G12
C  PROPS(8)   = G13
C  PROPS(9)   = G23
      SUBROUTINE UMAT (STRESS,STATEV,DDSDDE,SSE,SPD,
     +   SCD,RPL,DDSDDT,DRPLDE,DRPLDT,STRAN,DSTRAN,
     +   TIME,DTIME,TEMP,DTEMP,PREDEF,DPRED,CMNAME,NDI,
     +   NSHR,NTENS,NSTATV,PROPS,NPROPS,COORDS,DROT,
     +   PNEWDT,CELENT,DFGRD0,DFGRD1,NOEL,NPT,LAYER,KSPT,
     +   KSTEP,KINC)

      INCLUDE 'ABA_PARAM.INC'

      CHARACTER*80 CMNAME

      DIMENSION STRESS(NTENS),STATEV(NSTATV),
     +   DDSDDE(NTENS,NTENS),DDSDDT(NTENS),
     +   DRPLDE(NTENS),STRAN(NTENS),DSTRAN(NTENS),
     +   TIME(2),PREDEF(1),DPRED(1),PROPS(NPROPS),
     +   COORDS(3),DROT(3,3),DFGRD0(3,3),DFGRD1(3,3)
C*************************************************************C
C
C  SELECT WHICH UMAT TO BE USED
C
C
C*************************************************************C
C*************************************************************C
C       MATERIAL 1
C*************************************************************C

      IF(CMNAME.EQ.'MATERIAL-1') THEN
            CALL UMAT_MAT1(STRESS,STATEV,DDSDDE,SSE,SPD,
     +   SCD,RPL,DDSDDT,DRPLDE,DRPLDT,STRAN,DSTRAN,
     +   TIME,DTIME,TEMP,DTEMP,PREDEF,DPRED,CMNAME,NDI,
     +   NSHR,NTENS,NSTATV,PROPS,NPROPS,COORDS,DROT,
     +   PNEWDT,CELENT,DFGRD0,DFGRD1,NOEL,NPT,LAYER,KSPT,
     +   KSTEP,KINC)
      END IF

C*************************************************************C
C       MATERIAL 2
C*************************************************************C

      IF(CMNAME.EQ.'MATERIAL-2') THEN
            CALL UMAT_MAT2(STRESS,STATEV,DDSDDE,SSE,SPD,
     +   SCD,RPL,DDSDDT,DRPLDE,DRPLDT,STRAN,DSTRAN,
     +   TIME,DTIME,TEMP,DTEMP,PREDEF,DPRED,CMNAME,NDI,
     +   NSHR,NTENS,NSTATV,PROPS,NPROPS,COORDS,DROT,
     +   PNEWDT,CELENT,DFGRD0,DFGRD1,NOEL,NPT,LAYER,KSPT,
     +   KSTEP,KINC)
      END IF

      RETURN
           END

C*************************************************************C
C      UMAT FOR MATERIAL 1
C*************************************************************C

      SUBROUTINE UMAT_MAT1 (STRESS,STATEV,DDSDDE,SSE,SPD,
     +   SCD,RPL,DDSDDT,DRPLDE,DRPLDT,STRAN,DSTRAN,
     +   TIME,DTIME,TEMP,DTEMP,PREDEF,DPRED,CMNAME,NDI,
     +   NSHR,NTENS,NSTATV,PROPS,NPROPS,COORDS,DROT,
     +   PNEWDT,CELENT,DFGRD0,DFGRD1,NOEL,NPT,LAYER,KSPT,
     +   KSTEP,KINC)

      INCLUDE 'ABA_PARAM.INC'
```

```
      CHARACTER*80 CMNAME

      DIMENSION STRESS(NTENS),STATEV(NSTATV),
     +   DDSDDE(NTENS,NTENS),DDSDDT(NTENS),
     +   DRPLDE(NTENS),STRAN(NTENS),DSTRAN(NTENS),
     +   TIME(2),PREDEF(1),DPRED(1),PROPS(NPROPS),
     +   COORDS(3),DROT(3,3),DFGRD0(3,3),DFGRD1(3,3)
           DIMENSION C(6,6),DSTRESS(6)

C-----------------------------------------------------------C
C B.1 Check for consistency between the specified and
C     required number of input parameters
C-----------------------------------------------------------C
      IF (NPROPS.LT.2) THEN
        WRITE(7,*) '** ERROR: UMAT REQUIRES *NPROPS= 2'
        STOP
      ENDIF
C-----------------------------------------------------------C
C B.2 Initialise flags
C-----------------------------------------------------------C
      E11   = PROPS(1)
      E22   = PROPS(1)
      E33   = PROPS(1)
      V12   = PROPS(2)
      V13   = PROPS(2)
      V23   = PROPS(2)
      G12   = PROPS(1)/2.0/(1.0+PROPS(2))
      G13   = PROPS(1)/2.0/(1.0+PROPS(2))
      G23   = PROPS(1)/2.0/(1.0+PROPS(2))
           IF(STATEV(1).GT.0.99)THEN
             E11=0.01*E11
             E22=0.01*E22
             E33=0.01*E33
             G12=0.2*G12
             G13=0.2*G13
             G23=0.2*G23
           END IF
           IF(STATEV(2).GT.0.99)THEN
             E11=0.01*E11
             E22=0.01*E22
             E33=0.01*E33
             G12=0.2*G12
             G13=0.2*G13
             G23=0.2*G23
           END IF
           IF(STATEV(3).GT.0.99)THEN
             E11=0.01*E11
             E22=0.01*E22
             E33=0.01*E33
             G12=0.2*G12
             G13=0.2*G13
             G23=0.2*G23
           END IF
           IF(STATEV(4).GT.0.99)THEN
             E11=0.01*E11
             E22=0.01*E22
             E33=0.01*E33
             G12=0.2*G12
             G13=0.2*G13
             G23=0.2*G23
           END IF
           IF(STATEV(5).GT.0.99)THEN
             E11=0.01*E11
             E22=0.01*E22
             E33=0.01*E33
             G12=0.2*G12
             G13=0.2*G13
             G23=0.2*G23
           END IF
           IF(STATEV(6).GT.0.99)THEN
```

```
            E11=0.01*E11
            E22=0.01*E22
            E33=0.01*E33
            G12=0.2*G12
            G13=0.2*G13
            G23=0.2*G23
          END IF
          IF(STATEV(7).GT.0.99)THEN
            E11=0.01*E11
            E22=0.01*E22
            E33=0.01*E33
            G12=0.2*G12
            G13=0.2*G13
            G23=0.2*G23
          END IF
          IF(STATEV(8).GT.0.99)THEN
            E11=0.01*E11
            E22=0.01*E22
            E33=0.01*E33
            G12=0.2*G12
            G13=0.2*G13
            G23=0.2*G23
          END IF
          IF(STATEV(9).GT.0.99)THEN
            E11=0.01*E11
            E22=0.01*E22
            E33=0.01*E33
            G12=0.2*G12
            G13=0.2*G13
            G23=0.2*G23
          END IF
C         write(7,*)time(1),time(2)

C-------------------------------------------------------C
C B.3 MATERAIL COMPLIANCE AND STIFFNESS MATRIX
C-------------------------------------------------------C
     S11   = 1.0/E11
     S21   = -V12/E11
     S31   = -V13/E11
     S12   = S21
     S22   = 1.0/E22
     S32   = -V23/E22
     S13   = S31
     S23   = S32
     S33   = 1.0/E33
          S44   = 1.0/G12
          S55   = 1.0/G13
          S66   = 1.0/G23
          S     = S11*S22*S33-S11*S23**2-S22*S13**2
    &             -S33*S12**2+2.0*S12*S23*S13
          C(1,1)= (S22*S33-S23**2)/S
          C(1,2)= (S13*S23-S12*S33)/S
          C(1,3)= (S12*S23-S13*S22)/S
          C(2,1)= C(1,2)
     C(2,2)= (S33*S11-S13**2)/S
          C(2,3)= (S12*S13-S23*S11)/S
          C(3,1)= C(1,3)
          C(3,2)= C(2,3)
          C(3,3)= (S11*S22-S12**2)/S
          C(4,4)= 1.0/S44
          C(4,5)= 0.0
          C(4,6)= 0.0
          C(5,4)= 0.0
          C(5,5)= 1.0/S55
     C(5,6)= 0.0
          C(6,4)= 0.0
          C(6,5)= 0.0
          C(6,6)= 1.0/S66

C-------------------------------------------------------C
C C.1. Calculate the current stress increments
```

```
C-------------------------------------------------------C
     DO K1=1,NDI
          TERM1=0.0
          TERM2=0.0
            DO K2=1,NDI
              TERM1=TERM1+C(K1,K2)*DSTRAN(K2)
              TERM2=TERM2+C(K1,K2)*(DSTRAN(K2)+STRAN(K2))
            END DO
            DSTRESS(K1)=TERM1

            STRESS(K1)=TERM2
     END DO
     I1=NDI
          DO K1=1,NSHR
            I1=I1+1
            DSTRESS(I1)=C(I1,I1)*DSTRAN(I1)

            STRESS(I1)=C(I1,I1)*(DSTRAN(I1)+STRAN(I1))
     END DO


C-------------------------------------------------------C
C D.1. CREATE NEW JACOBIAN
C-------------------------------------------------------C
     DO K1=1,NTENS
           DO K2=1,NTENS
             DDSDDE(K2,K1)=0.0
           END DO
     END DO
          DO K1=1,NDI
            DDSDDE(K1,K1)=C(K1,K1)
          END DO
          DO K1=2,NDI
            N2=K1-1
            DO K2=1,N2
              DDSDDE(K2,K1)=C(K2,K1)
              DDSDDE(K1,K2)=C(K1,K2)
            END DO
          END DO
          I1=NDI
          DO K1=1,NSHR
            I1=I1+1
            DDSDDE(I1,I1)=C(I1,I1)
          END DO


C-------------------------------------------------------C
C  SPECIFIC ELASTIC ENERGY
C-------------------------------------------------------C
     TDE=0.0
          DO K1=1,NTENS
            TDE=TDE+(STRESS(K1)+0.5*DSTRESS(K1))*DSTRAN(K1)
          END DO
     DEE=0.0
          DO K1=1,NDI
            TERM1=0.0
            TERM2=0.0
            DO K2=1,NDI
              TERM1=TERM1+C(K1,K2)*STRAN(K2)
              TERM2=TERM2+C(K1,K2)*DSTRAN(K2)
            END DO
            DEE=DEE+(TERM1+0.5*TERM2)*DSTRAN(K1)
          END DO
          I1=NDI
          DO K1=1,NSHR
            I1=I1+1
            DEE=DEE+C(I1,I1)*(STRAN(I1)+0.5*DSTRAN(I1))
     &           *DSTRAN(I1)
          END DO
          SSE=SSE+DEE
```

```
      RETURN
      END
```

USDFLD Subroutine

These subroutines have been employed to modify the damage variables state depending on the stress level detected by the failure criteria during the analysis. The Maximum Principal Stress criterion has been used for the subroutine described here.

```
      SUBROUTINE USDFLD(FIELD,STATEV,PNEWDT,DIRECT,T,CELENT,
      & TIME,DTIME,CMNAME,ORNAME,NFIELD,NSTATV,NOEL,NPT,LAYER,
      & KSPT,KSTEP,KINC,NDI,NSHR,COORD,JMAC,JMATYP,MATLAYO,
      & LACCFLA)

       INCLUDE 'ABA_PARAM.INC'

       CHARACTER*80 CMNAME,ORNAME
       CHARACTER*8  FLGRAY(15)

       DIMENSION FIELD(NFIELD),STATEV(NSTATV),DIRECT(3,3),
      &  T(3,3),TIME(2)
       DIMENSION ARRAY(15),JARRAY(15),JMAC(*),JMATYP(*),COORD(*)
            DIMENSION BSTRESS(6), ROOT(3)
ccccccccccccccccccccccccccccccccccccccccccccccccccccccccccccccccccccc
c
c Get the solution dependent variables
c
ccccccccccccccccccccccccccccccccccccccccccccccccccccccccccccccccccccc

       CALL GETVRM('S',ARRAY,JARRAY,FLGRAY,JRCD,JMAC,JMATYP,
      &       MATLAYO,LACCFLA)
        SS11= ARRAY(1)
        SS22= ARRAY(2)
        SS33= ARRAY(3)
        SS12= ARRAY(4)
             SS13= ARRAY(5)
             SS23= ARRAY(6)

ccccccccccccccccccccccccccccccccccccccccccccccccccccccccccccccccccccc
c
c Get principle stress components & maximum shear stress
c [MATERIAL 1 - eglass 21xK43 GEVETEX]
ccccccccccccccccccccccccccccccccccccccccccccccccccccccccccccccccccccc

             IF(CMNAME.EQ.'MATERIAL-1') THEN
               BSTRESS(1)=SS11
               BSTRESS(2)=SS22
               BSTRESS(3)=SS33
               BSTRESS(4)=SS12
               BSTRESS(5)=SS13
               BSTRESS(6)=SS23
          CALL PRINCIPLE(ROOT,BSTRESS)
               IF(ROOT(1).GT.0.0.AND.ROOT(1).GT. 2.150)THEN
                 FIELD(1)=1.0
           STATEV(1)=1.0
           STATEV(10)=1.0
               END IF
               IF(ROOT(1).LT.0.0.AND.ROOT(1).LT. -1.450)THEN
                 FIELD(2)=1.0
```

```
        STATEV(2)=1.0
        STATEV(10)=1.0
           END IF
           IF(ROOT(2).GT.0.0.AND.ROOT(2).GT. 2.150)THEN
             FIELD(3)=1.0
        STATEV(3)=1.0
        STATEV(10)=1.0
           END IF
           IF(ROOT(2).LT.0.0.AND.ROOT(2).LT. -1.450)THEN
             FIELD(4)=1.0
        STATEV(4)=1.0
        STATEV(10)=1.0
           END IF
           IF(ROOT(3).GT.0.0.AND.ROOT(3).GT. 2.150)THEN
             FIELD(5)=1.0
        STATEV(5)=1.0
        STATEV(10)=1.0
           END IF
           IF(ROOT(3).LT.0.0.AND.ROOT(3).LT. -1.450)THEN
             FIELD(6)=1.0
        STATEV(6)=1.0
        STATEV(10)=1.0
           END IF
           IF(DABS(ROOT(1)-ROOT(3))/2.0.GT. 1.200)THEN
             FIELD(7)=1.0
        STATEV(7)=1.0
        STATEV(10)=1.0
           END IF
           IF(DABS(ROOT(2)-ROOT(3))/2.0.GT. 1.200)THEN
             FIELD(8)=1.0
        STATEV(8)=1.0
        STATEV(10)=1.0
           END IF
           IF(DABS(ROOT(1)-ROOT(2))/2.0.GT. 1.200)THEN
             FIELD(9)=1.0
        STATEV(9)=1.0
        STATEV(10)=1.0
           END IF
         END IF
RETURN
END
```

References

[1] D. Hull, T.W. Clyne "An Introduction to Composite Materials", Cambridge University Press, Cambridge, (second edition).

[2] M.W. Hyer, A.M. Waas "Micromechanics of Linear Elastic Continuous Fiber Composites", Reference Works, Comprehensive Composite Materials, Elsevier 2000.

[3] C. T. Sun, R.S. Vaidya, "Prediction of composite properties from a representative volume element", Composites Science and Technology 56 (1996), pp.171-179.

[4] ABAQUS/Standard User's Manual, Version 6.4, Vol.3.

[5] D. Blackketter, D. E. Walrath, and A. C. Hansen, "Modelling Damage in a Plain Weave Fabric Reinforced Composite Materials", Journal of Composites Technology and Research 15 (1993), pp. 136-142.

[6] H. Altenbach , K. Tushtev "A New Static Failure Criterion for Isotropic Polymers", Mechanics of Composite Materials, 37 (2001), Nos. 5/6.

[7] H. Altenbach "A unified phenomenological limit state criterion for ductile and brittle materials", published in Plasticity and Impact Mechanics, ed. by N.K. Gupta; New Dehli, Phoenix (2003), pp. 180-120.

[8] L.E. Asp, L.A. Berglund, R. Talreja, "A Criterion for Crack Initiation in Glassy Polymers Subjected to a Composite Like Stress State", Composite Science and Technology, 56 (1996), pp. 1089-1301.

[9] Handbook of Composites. Vol.3 Failure Mechanics of Composites. New-York: Elsevier Science Publishers B.V., 1985,

[10] M.J. Hinton, P D Soden, A S Kaddour, "Failure Criteria in Fibre Reinforced Polymer Composites - The World-Wide Failure Exercise", Elsevier Science Publishers (2004).

[11] P.A. Zinoviev, O.V. Lebedeva, L.V. Tairova, "A coupled analysis of experimental and theoretical results on the deformation and failure of composite laminates under a state of plane stress", Composites Science and Technology 62 (2002), pp.1711-1723

[12] F. París "A Study of Failure Criteria of Fibrous Composite Materials", NASA/CR-2001-210661, March 2001.

[13] K.S. Liu, S.W. Tsai, "A progressive quadratic failure criterion for a laminate", Composites Science and Technology 58 (1998), pp.1023-1032.

[14] S.W. Tsai, A. Kuraishi, K.S. Liu, “A progressive quadratic failure criterion, part B”, Composites Science and Technology 62 (2002), pp.1683-1695.

[15] H. Thom, “A review of the biaxial strength of fibre-reinforced plastics”, Composites Part-A 29 (1998), pp.869-886.

[16] G. Caligiana, F. Cesari, “I Materiali Compositi”, Pitagora Editrice Bologna, Ed.2002.

[17] Z. Hashin, BW. Rosen, “The elastic moduli of fibre-reinforced materials”, ASME, Journal Applied Mechanics 31 (1964), pp. 223-32.

[18] S. Li “On the unit cell for micromechanical analysis of fibre-reinforced composites”, Proceedings Royal Society London A 455 (1999), pp. 815-38.

[19] D.F. Adams, D.A. Crane, “Finite element micromechanical analysis of a unidirectional composite including longitudinal shear loading”, Computers and Structures 18 (1984), pp.1153-65.

[20] D.F. Adams, D.R. Doner, “Longitudinal shear loading of a unidirectional composite”, Journal Compoite Materials 1 (1967), pp. 4-17.

[21] D.F. Adams, D.R. Doner, “Transverse normal loading of a unidirectional composite”, Journal Compos. Mater., 1 (1967), pp. 152-64.

[22] S. Li, “General unit cell for micromechanical analyses of unidirectional composites”, Composites Part-A 32 (2000), PP. 815-816.

[23] D.S. Li, M.R. Wisnom, “Finite element micromechanical modelling of unidirectional fibre-reinforced metal-matrix composites”, Compos Sci Technol 51 (1994), pp. 545-63.

[24] D. Zahl, S. Schmauder, R. McMeeking, “Transverse strength of metal matrix composites reinforced with strongly bonded continuous fibres in regular arrangement”, Acta Metall Mater 42 (1994), pp. 2983-97.

[25] M.R. Nedele, M.R. Wisnom, “Finite element micromechanical modelling of a unidirectional composite subject to axial shear loading”, Composites 25 (1994), pp. 263-72.

[26] G.J. Dvorak, Y.A. Bahei-El-Din, Y. Macheret, C.H. Liu, “An experimental study of elastic-plastic behaviour of a fibrous boron-aluminum composite”, Journal Mech. Phys Solids 36 (1988), pp. 655-87.

[27] S.C. Cowin, M. Mehrabad, “Anisotropic symmetries of linear elasticity”, ASME Appl. Mech. Rev. 48 (1995), pp. 247-285.

[28] A. Love, “A treatise on the mathematical theory of elasticity”, 4th edn, ch. 6. Cambridge University Press (1927).

[29] J. Echaabi, F. Trochu, R. Gauvin, “Review of failure criteria of fibrous composite Materials”, Polymer Composites 17 (1996), pp.786–798.

[30] C.H. Chen, S. Cheng, “Mechanical properties of fibre reinforced composites”, Journal of Composite Materials 1 (1967), pp. 30-40.

[31] L. E Govaert, H. Schellens, J.M. De Kok, “Micromechanical modelling of time dependent failure in transversely loaded composites” Proc. 3rd Int. Conf. on deformation and fracture of composites”, University of Surrey, Guildford, Surrey, UK, 27-29 March 1995, pp.77-85. The Institute of Materials.

[32] Ahuja N, Schachter BJ., “Pattern models“, New York: Wiley, 1983.

[33] J. R. Yeh, “Effect of interface on the transverse properties of composites. International Journal Solids Structures 29 (1992), pp. 2493-2502.

[34] Crookston J.J, Long A.C., Jones I.A., “Modelling effects of reinforcement deformation during manufacture on elastic properties of textile composites”; Plastics, Rubber and Composites 31 (2000), pp.58-64.

[35] Wolfenden A., Wolla J.M. “Mechanical damping and dynamic modulus measurements in alumina and tungsten fibre reinforced aluminium”, Journal of Materials Science 24 (1989), pp.3205-3212.

[36] Wilczyński A.P., “A basic theory of reinforcement for unidirectional fibrous composites”, Composites Science and Technology 38 (1990), pp.327-337.

[37] Wilczyński A.P., Lewiński J., “Predicting the properties of unidirectional fibrous composites with monotropic reinforcement”, Composites Science Technology 55 (1995), pp.139-143.

[38] Huang Z.M., “Micromechanical prediction of ultimate strength of transversely isotropic fibrous composites”, Materials Letters 40 (1999), pp. 164-169.

[39] Taliercio A., Coruzzi R. “Mechanical behaviour of brittle matrix composites: a homogenization approach”, International Journal of Solids and Structures 36 (1999), pp.3591-3615.

[40] P. Labossiere, K.W. Neal, “Macroscopic failure criteria for fiber-reinforced composite materials”, Solid Mechanics 12 (1987), pp. 439–450.

[41] J. Echaabi, F. Trochu, R. Gauvin, “Review of failure criteria of fibrous composite materials”, Polymer Composites 17 (1996), pp.786–798.

[42] W.A. Curtin, “Ultimate strengths of fiber-reinforced ceramics and metals”, Composites 24 (1993), pp.98–102.

[43] M.J. Pindera, “Micromechanical aspects of yielding and failure criteria of composites”, J.P. Boehler Ed., Failure Criteria of Structured Media, Balkema, Rotterdam, Netherlands, 1993, pp.121- 141.

[44] De Kok, J.M.M., Meijer H.E.H. “Deformation, yield and fracture of unidirectional composites in transverse loading 1: Influence of fibre volume fraction and test-temperature”, Composites Part-A 30 (1999), pp.905-916.

[45] Adams D.F., Tsai S.W. “The influence of random filament packing on the transverse stiffness of unidirectional composites”, Journal of Composite Materials 3 (1969), pp.368-381.

[46] S.W. Tsai, H.T. Hahn “Introduction to composite materials “Micromechanics”, Technomic Publishing, Lancaster, Basel, 1980, pp. 377–431, Chapter 9.

[47] S. Y. Fu and B. Lauke, “Elastic modulus of misaligned short-fiber-reinforced polymers” Composites Science Technology 58 (1998), pp. 389-400.

[48] M. Xia, H. Hamada and Z. Maekawa, “Flexural Stiffness of Injection Molded Glass Fiber Reinforced Thermoplastics”, International Polymer Process. 10 (1995).

[49] J. C. Halpin and S. W. Tsai, U.S. Air Force Materials Laboratory Rept, AFML TR 67–423 (1967).

[50] J. C. Halpin,” Stiffness and expansion estimates for oriented short fiber composites” Journal Composites Materials 3 (1969) pp.732.

[51] J . C. Halpin and J . L. Kardos, “Halpin-Tsai equations: A review”, Polymer Engineering Science 16 (1976), pp. 344.

[52] B. W. Shaffer, “Stress-strain relations of reinforced plastics parallel and normal to their internal filaments”, American Institute of Aeronautics and Astronautics Journal 2 (1964), pp.348.

[53] S. W. Tsai, NASA Report CR-71 (1964).

[54] Shao-Yun Fu et alii, “A new model for the transverse modulus of unidirectional fiber composites”, Journal Materials Science 33 (1998), pp. 4953-4960.

[55] Shi, N., Wilner, B. & Arsenault, R. J., "An FEM study of the plastic deformation process of whisker reinforced SIC/Al composites", Acta Metallurgica Materialia., 40 (1992), pp. 2841-54.

[56] Foye, R. L., "An evaluation of various engineering estimates of the transverse properties of unidirectional composites", SAMPE, 10 (1966) 31.

[57] Brockenbrough, J. R., Suresh, S. & Wienecke, H. A., "Deformation of metal-matrix composites with continuous fibers: Geometrical effects of fiber distribution and shape", Acta Metallurgica Materialia, 5 (1991), pp. 735-52.

[58] Naik, R. A. & Crews Jr, J. H., "Micromechanical analysis of fiber-matrix interface stresses under thermomechanical loadings", Composite Materials: Testing and Design (Vol. II), ASTM STP 1206, ed. E. T. Camponeschi Jr. American Society for Testing and Materials, Philadelphia, PA, 1993, pp. 205-19.

[59] Caruso, J. J., "Application of finite element substructuring to composite micromechanics". NASA TM-83729, NASA Lewis Research Center, Cleveland, OH, 1984.

[60] Crookston J.J., Robitaille F., Long A.C., Jones I.A., Ooi J. "A systematic study of the mechanical properties of textile composite unit cells based on geometric modelling", Proceedings of the Fourteenth International Conference on Composite Materials, ICCM-14, San Diego, USA, 2003, pp.1303-1312

[61] Carvelli V., Taliercio A. "A micromechanical model for the analysis of unidirectional elastoplastic composites subjected to 3D stresses", Mechanics Research Communications 26 (1999), pp. 547-553.

[62] M.K. Chati, A.K. Mitra, "Prediction of elastic properties of fiber-reinforced unidirectional composite", Engineering Analysis with Boundary Element Vol. 21 (1998), pp. 235-244.

[63] Eischen, J. W. and Torquato, S., "Determining elastic behaviour of composites by the boundary element method", Journal Applied Physics 74 (1991), pp. 159-170.

[64] Asp L.E., Berglund L.A., Talreja R. "Prediction of matrix-initiated transverse failure in polymer composites", Composites Science and Technology 56 (1996), pp.1089-1097.

[65] Hashin Z. "Analysis of cracked laminates: A variational approach", Mechanics of Materials 4 (1985), pp.121-136.

[66] K. Benzarti, L. Cangemi, F. Dal Maso "Transverse properties of unidirectional glass/epoxy composites: influence of fibre surface treatments", Composites Part-A 32 (2001), pp. 197–206.

[67] Christensen RM, Rinde J.A., “Transverse tensile characteristic of fiber composites with flexible resins: theory and test results”, Polymer Engineering and Science 19 (1979), pp.506–11.

[68] Briancon C, Sigety P, G’sell C., “In situ study of matrix strain in carbon/resin composite materials”, Composite Science and Technology 56 (1996), pp. 835–40.

[69] Asp LE, Berglund LA, Gudmundson P., “Effect of a composite-like stress state on the fracture of epoxies”, Composite Science and Technology 53 (1995), pp. 27–37.

[70] De Buhan P, Taliercio A., “A homogenisation approach to the yield strength of composite materials”, European Journal of Mechanics 10 (1991), pp. 129–54.

[71] Tryson LD, Kardos JL., “The use of ductile innerlayers in glass fiber reinforced epoxies”, 36th Annual Conference Reinforced Plastics/Composite Institute, February 16–20 1998.

[72] Podgaiz RH, Williams RJJ., “Effect of fiber coating on mechanical properties of unidirectional glass reinforced composites”, Composite Science and Technology 57 (1997), pp. 1071–6.

[73] Gatward C, Hull D., “Effect of flexible interface on transverse properties of polyester-glass composite materials”, Proceedings of the Reinforced Plastic Group Meeting on Interfaces in Composites Materials. Plastic and Rubber Institute 1981.

[74] R. S. Kody and A. J. Lesser, “Deformation and yield of epoxy networks in constrained states of stress,” Journal Material Science 32 (1997), pp. 5637-5643.

[75] A. J. Lesser and R. S. Kody, “A generalised model for the yield behaviour of epoxy networks in multi-axial stress states,” Journal Polymer Science 35 (1997), pp. 1611-1619.

[76] N. R. Karttunen and A. J. Lesser, “Yield behaviour and failure response of an aliphatic polyketone terpolymer subjectedto multi-axial stress states,” Journal Material Science 35 (2000), pp. 2507-2515.

[77] S. Rabinowitz, I. M. Ward, and J. S. C. Parry, “The effect of hydrostatic pressure on the shear yield behaviour of polymers,” Journal Material Science 5 (1970), pp. 29-39.

[78] A. S. Wronski and M. Pick, “Pyramidal yield criteria for epoxides,” Journal Material Science 12 (1977), pp. 28-34.

[79] H. L. D. Pugh, E. F. Chandler, L. Holliday, and J. Mann, “The effect of hydrostatic pressure on the tensile properties of plastics,” Polymer Engineering Science 11 (1971), pp. 463-473.

[80] K. D. Pae and D. R. Mears, “The effect of high pressure on mechanical behaviour and properties of polytetrafluoroethylene and polyethylene,” Polymer Letters 6 (1968), pp. 269-273.

[81] P. B. Bowden and J. A. Jukes, “The plastic flow of isotropic polymers,” Journal Material Science 7 (1972), pp. 52-63.

[82] R. Quinson, J. Perez, M. Rink, and A. Pavan, “Yield criteria for amorphous glassy polymers,” Journal Material Science 32 (1997), pp. 1371-1379.

[83] J. C. Bauwens, “Yield condition and propagation of Lüders’ lines in tension-torsion experiments on poly(vinyl Chloride),” Journal Polymer Science 8 (1970), pp. 893-901.

[84] R. S. Raghava, R. M. Caddell, and G. Yeh, “The macroscopic yield behavior of polymers,” Journal Materelia Science 8 (1973), pp. 225-232.

[85] R. S. Raghava, and R. M. Caddell, “A macroscopic yield criterion for crystalline polymers,” Int. J. Mech. Sci., 15, 967-974 (1973).

[86] R. M. Caddell, R. S. Raghava, and A. G. Atkins, “Pressure-dependent yield criteria for polymers,” Material Science Engineering 13 (1974), pp. 113-120

[87] P. B. Bowden, “The yield behavior of glassy polymers,” in: The Physics of Glassy Polymers, Ch.5, Wiley, New York, pp. 279-389.

[88] B. Fiedler, M. Hojo, S. Ochiai, K. Schulte, M. Andoc ” Failure behavior of an epoxy matrix under different kinds of static loading”, Composites Science and Technology 61 (2001), pp. 1615–1624.

[89] D. Bigoni, A. Piccolroaz “Yield criteria for quasibrittle and frictional materials”, International Journal of Solids and Structures 41 (2004), pp. 2855–2878.

[90] P.S. Theocaris “Failure Criteria for Isotropic Bodies Revisited”, Engineering Fracture Mechanics 51 (1995) No. 2, pp. 239-264.

[91] McClintock FA., “A criterion for ductile fracture by the growth of holes”, Journal Applied Mechanics 35 (1968), pp.363–71.

[92] Gurson AL., “Continuum theory of ductile rupture by void nucleation and growth”, Part I: Yield criteria and flow rules for porous ductile materials. Journal Engineering Material Technology 99 (1977), pp. 2-15.

[93] Naik RA., “Failure analysis of woven and braided fabric reinforced composites” Journal Composite Materials 29 (1995), pp. 2334–63.

[94] Kawada H, Watanabe T, Honda T., “Fracture behavior of aramid/epoxy composite with a circular hole subjected to compressive load”, Material Science Research International 2 (1996), pp. 66–72.

[95] Whitcomb J, Kondagunta G, Woo K., “Boundary effects in woven composites”, Journal Composite Materials 29 (1995), pp. 507–24.

[96] Chapman C, Whitcomb J., “Effect of assumed tow architecture on predicted moduli and stresses in plain weave composites”, Journal Composite Materials 29 (1995), pp.2134–59.

[98] Tan P, Tong L, Steven GP., ”A flexible 3D FEA modelling approach for predicting the mechanical properties of plain weave unit cell”, Proc ICCM-11 1997; V:67–76.

[99] Kollegal MG, Sridharan S. “Compressive behavior of plain weave lamina”, Journal Composite Materilias 32 (1998), pp.1334-55.

[100] Dasgupta A, Bhandarkar SM., “Effective thermomechanical behaviour of plain-weave fabric-reinforced composites using homogenization theory”, Journal Enginerring Materials Technology (1994), pp. 116:99–105.

[101] Woo K, Whitcomb J., “Three-dimensional failure analysis of plain weave textile composites using a global/local finite element method” Journal Composites Materials 30 (1996), pp. 984-1003.

[102] Carvelli V, Poggi C. A., “homogenization procedure for the numerical analysis of woven fabric composites”. Composites Part-A 32 (2001), pp. 1425–32.

[103] Whitcomb J, Srirengan K., “Effect of various approximations on predicted progressive failure in plain weave composites”, Composites Structures 34 (1996), pp. 13-20.

[104] Zako M, Takano N, Tsumura T. Numerical prediction of strength of notched UD laminates by analyzing the propagation of Intra-and Inter-laminar damage. Journal Materials Science 2 (1996), pp.117-22.

[105] Zako M, Takano N, Uetsuji Y., “Prediction of strength for fibrous composites based on damage mechanics”, In: Proceedings 3rd International Symposium Textile Composites, 1996, pp. 1-9.

[106] Uetsuji Y, Zako M, Takano N. Simulation for mechanical behaviours of laminated composites based on damage mechanics. In: Proceedings International Conference Computational Engineering Science, 1997, pp. 1287–92.

[107] Zako M, Uetsuji Y., Kurashiki T., "Finite element analysis of damaged woven fabric composite materials", Composites Science and Technology 63 (2003), pp. 507-516.

[108] Hashin Z, Rotem A., "A fatigue failure criterion for fiber reinforced materials", Journal Composite Materials 7 (1973), pp, 448-64.

[109] Murakami S., "Mechanical modeling of material damage", Journal Applied Mechanics 55 (1988), pp. 55:2 80.

[110] J. G. Bakuckas, A. C. W. Lau, T. M. Tan, "Computational methology to predict damage growth in unidirectional composites-I. Theoretical formulation and numerical implementation", Engineering Fracture Mechanics 52 (1995), pp. 937-951.

[111] A. Tabiei, G. Song, Y. Jiang, "Strength simulation of woven fabric composite materials with material non-linearity using micromechanics based model", Journal Thermoplastic Composites 16 (2003), pp. 5-20.

[112] I. Ivanov, A. Tabiei, "Three-dimensional computational micro-mechanical model for woven fabric composites", Composites Structures 54 (4) (2001), pp. 489-496.

[113] A. Tabiei, I. Ivanov, "Fiber reorientation in unidirectional and woven composites for 'nite element simulation", Composite Science Technolology (2001), submitted for publication.

[114] A. Tabiei, I. Ivanov, "Materially and geometrically non-linear woven composite micro-mechanical model with failure for finite element simulations", International Journal of Non-Linear Mechanics 39 (2004), pp. 175-188.

[115] Y. W. Kwon and J. M. Berner, "Micromechanics model for damage and failure analyses of laminated fibrous composites", Engineering Fracture Mechanics 52 (1995), pp. 231-242.

[116] H. Ismar, F. Schroter, F. Streicher, "Modeling and numerical simulation of the mechanical behavior of woven SiC/SiC regarding a three-dimensional unit cell", Computational Materials Science 19 (2000), pp. 320-328.

[117] R.A. Schapery, "Thermal expansion coefficients of composite materials based on energy principles", Journal Composite Materials 2 (1968), pp. 380–404.

[118] Huang Z.M., "Strength formulae of unidirectional composites including thermal residual stresses", Materials Letters, Vol.43, 2000, pp. 36-42.

[119] Ifju, P.G., Niu, X., Kilday, B.C., Liu, S.C., Ettinger, S.M., “Residual stress measurement in composite using the cure-referencing method”, Experimental Mechanics 40 (2000), pp. 22-30.

[120] Lange, J., Toll, S., Månson, J-A.E., “Residual stress build-up in thermoset films cured above their ultimate glass transition temperature”, Polymer 36 (1995), pp. 3135-3141.

[121] Rendler, N.J., Vigness, I., “Hole-drilling strain gauge method of measuring residual stress”, Experimental Mechanics 6 (1996), pp. 577-586.

[122] Gascoigne, H.E., “Residual surface stress in laminated cross-ply fibre-epoxy composite materials”, Experimental Mechanics 34 (1994), pp. 27-36.

[123] Kim, R.Y., Hahn, H.T., “Effect of curing stress on the first ply-failure in composite laminates”, Journal of Composite Materials 13 (1979), pp. 2-16.

[124] Dannenberg, H., “Determination of stresses in cured epoxy resins”, SPE Journal 1965, pp. 669-675.

[125] Kesler, O., Matejicek, J., Sampath, S., Suresh, S., Gnaeupel-Herold, T., Brand, P.C., Prask, H.J., “Measurement of residual stress in plasma-sprayed metallic, ceramic and composite coatings”, Materials Science and Engineering 257 (1998), pp. 215-224.

[126] Benedikt, B., Kumosa, M., Predecki, P.K., Kumosa, L., Castelli, M.G., Sutter, J.K., “An analysis of residual thermal stress in a unidirectional graphite/PMR-15 composite based on X-ray diffraction measurements”, Composites Science and Technology 61 (2001), pp. 1977-1994.

[127] Stone, M.A., Schwartz, I.F., Chandler, H.D., “Residual stress associated with post-cure shrinkage in GRP tubes”, Composites Science and Technology 57 (1997), pp. 47-54

[128] Olivier, P., Cottu, J.P., “Optimisation of the co-curing of two different composites with the aim of minimising residual curing stress levels”, Composites Science and Technology 58 (1998), pp. 645-651.

[129] Gopal, A., Adali, S., Verijenko, V.E., “Optimal temperature profiles for minimum residual stress in the cure process of polymer composites”, Composite Structures 48 (2000), 99-106.

[130] Andersson, B., Sjögren A., Berglund, L., „Micro- and meso-level residual stresses in glass-fibre/vinyl-ester composites”, Composites Science and Technology 60 (2000), pp. 2011-2028.

[131] Sweeting, R.D., Thomson, R.S.,”The effect of thermal mismatch on Z-pinned laminated composite structures”, Composite Structures 66 (2004), pp. 189-195.

[132] Zhang, Y., Xia, Z., Ellyin, F., "Evolution and influence of residual stress/strains of fiber reinforced laminates" Composites Science and Technology 64 (2004), pp. 1613-1621.

[133] Nimmer, R.P., "Fibre-matrix interface effect in presence of thermally induced residual stresses" Journal of Composites Technology and Research. 12 (1990), pp. 65-75.

[134] Gentz, M., Armentrout, D., Rupnowski, P., Kumosa, L., Shin, E., Sutter, J.K., Kumosa, M.,"In-pane shear testing of medium and high modulus woven graphite fiber reinforced/polyimide composites", Composites Science and Technology 64 (2004), pp. 203-220.

[135] Gentz, M., Benedikt, B., Sutter, J.K., Kumosa, M., "Residual stress in unidirectional graphite fiber/polyimide composites as a function of aging", Composites Science and Technology 64 (2004), pp. 1671-1677.

[136] Fiedler B, Klisch A, Schulte K. Thermal residual stresses in fibre reinforced polymers. Proceedings of Asian Conference of Composite Materials-I, Osaka, Japan; October 7–9, 1998. pp. 604-1–604-4.

[137] Fiedler B, Hojo M, Ochiai S, Schulte K, Ochi M., "Finite-element modeling of the initial matrix failure in CFRP under static transverse tensile load", Compos Sci Technol 61 (2001), pp.95–105.

[138] S.L Gao, E. Mader, "Characterisation of interphase nanoscale property variation in glass fibre reinforced polypropylene and epoxy resin composites", Composites Part-A 33 (2002); pp 559-576

[139] S.L Gao, E. Mader, R. Plonka, "Enhancing the properties of composites by controlling their interphase parameters", Advanced Material Engineering 6 (2004).

[140] S. Kobayashi, A. Nakai, H. Hamada, "Suppression of microscopic damage in epoxy-based composites using flexible interphase", Journal of Materials Science Letters **22**, 2003, 1315 – 1318.

[141] M. Tanoglu, S.H. McKnight, G.R. Palmese, J.W. Gillespie, "The effects of glass-fiber sizings on the strength and energy absorption of the fiber/matrix interphase under high loading rates", Composites Science and Technology 61 (2001), pp. 205-220.

[142] A. Matzenmiller, S. Gerlach, "Parameter identification of elastic interphase properties in fiber composites", Composites Part-B 37 (2006), pp. 117-126.

[143] Asp LE, Berglund LA, Talreja R. Effects of fiber and interphase on matrix initiated transverse failure in polymer composites. Composite Science and Technology 56 (1996), pp. 657–65.

[144] Podgaiz RH, Williams RJJ. Effect of fiber coating on mechanical properties of unidirectional glass reinforced composites. Composite Science and Technology 57 (1997), pp. 1071–6.

[145] K. Benzarti, L. Cangemi, F. Dal Maso, "Transverse properties of unidirectional glass/epoxy composites: influence of fibre surface treatments", Composites Part-A 32 (2001), pp.197–206.

[146] M.E. Foley, A. Abu Obaid, X. Huang, M. Tanoglu, T.A. Bogetti, S.H. McKnight, J.W. Gillespie, "Fiber/matrix interphase characterization using the dynamic interphase loading apparatus", Composites Part-A 33 (2002), pp. 1345–1348.

[147] M.M. Aghdam, S.R. Falahatgar, "Micromechanical modeling of interface damage of metal matrix composites subjected to transverse loading", Composite Structures 66 (2004), pp. 415–420.

[148] Jianlin Wang, Steven L. Crouch, Sonia G. Mogilevskaya, "Numerical modeling of the elastic behavior of fiber-reinforced composites with inhomogeneous interphases", Composites Science and Technology 66 (2006), pp. 1-18.

[149] Mogilevskaya SG, Crouch SL., "A Galerkin boundary integral method for multiple circular elastic inclusions with uniform interphase layers", International Journal Solids Structures 41 (2004), pp. 1285–311.

[150] F.T. Fisher, L.C. Brinson, "Viscoelastic interphases in polymer–matrix composites: theoretical models and finite-element analysis", Composites Science and Technology 61 (2001), pp. 731–748.

[151] Benveniste Y., "A new approach to the application of Mori–Tanaka's theory in composite materials", Mechanics of Materials 6 (1987), pp. 147–57.

[152] A. Wongsto, S. Li, "Micromechanical FE analysis of UD fibre reinforced composites with fibres distributed at random over the transverse cross-section", Composites Part-A 36 (2005), pp. 1246–1266.

[153] M.M. Aghdam , A. Dezhsetan," Micromechanics based analysis of randomly distributed fiber reinforced composites using simplified unit cell model", Composite Structures 71 (2005), pp. 327–332.

[154] Daining Fang, Tieqi Liu," Transverse plastic deformation of metal-matrix with randomly arranged continuous fibers", Computational Materials Science 7 (1997), pp. 343-350.

[155] V.N. Bulsara, R. Talreja, J. Qu, “Damage initiation under transverse loading of unidirectional composites with arbitrarily distributed fibers”, Composites Science and Technology 59 (1999), pp. 673-682.

[156] A. A. Gusev, P. J. Hine, I. M. Ward, “Fiber packing and elastic properties of a transversely random unidirectional glass/epoxy composite”, Composites Science and Technology 60 (2000), pp. 535-541.

[157] A. Rossoll, B. Moser, A. Mortensen, “Longitudinal deformation of fibre reinforced metals: influence of fibre distribution on stiffness and flow stress”, Mechanics of Materials (2004) - In press.

[158] M.G. Knight, L.C. Wrobel, J.L. Henshall, “Micromechanical response of fibre-reinforced materials using the boundary element technique”, Composite Structures 62 (2003), pp. 341–352.

[159] S. C. Baxter, L. L. Graham-Brady, X. F. Xu, “Modeling the effects of material non-linearity using moving window micromechanics”, International Journal of Non-Linear Mechanics 40 (2005),pp. 351–359.

[160] L. Zhang a, L.J. Ernst , H.R. Brouwer, ”Transverse behaviour of a unidirectional composite (glass fibre reinforced unsaturated polyester). Part I. Influence of fibre packing geometry”, Mechanics of Materials 27 (1998), pp. 13-36.

[161] L. Zhang a, L.J. Ernst , H.R. Brouwer, “Transverse behavior of a unidirectional composite (glass fibre reinforced unsaturated polyester). Part II. Influence of shrinkage strains”, Mechanics of Materials 27 (1998), pp. 37-61.

[162] K. K. Jin, J. H. Oh, S.K.U Ha, “Effect of Fiber Arrangement on Residual Thermal Stress Distributions in a Unidirectional Composite”, Journal of Composite Materials OnlineFirst, May 19, 2006.

[163] Oh, J.H., Jin, K.K. and Ha, S.K., “Interfacial Strain Distribution of a Unidirectional Composite with Randomly Distributed Fibers under Transverse Loading”, Journal of Composite Materials 40 (2005), pp. 759–778.

[164] Yang, S., Tewari, A. and Gokhale, M.A., “Modeling of Non-uniform Spatial Arrangement of Fibers in a Ceramic Matrix Composite”, Acta Materialia 45 (1997), pp. 3059–3069.

[165] Louis, P. and Gokhale, A.M., “Computer Simulation of Spatial Arrangement and Connectivity of Particles in Three-dimensional Microstructure: Application to Model Electrical Conductivity of Polymer Matrix Composite”, Acta Materialia 44 (1996), pp. 1519–1528.

[166] M.R. Garnich, G. Karami "Finite Element Micromechanics for Stiffness and Strength of Wavy Fiber Composites", Journal of Composite Materials, Vol.38 (2004).

[167] Flores, F., Gillespie, J.W., Bogetti, T.A., "Experimental investigation of the cure-dependent response of vinyl ester resin", Polymer Engineering and Science 42 (2002.), pp. 582-590.

[168] Stone, M.A., Fink, B.K., Bogetti, T.A., "Thermal-chemical response of vinyl-ester resin", Polymer Engineering and Science 40 (2000), pp. 2489-2497.

[169] Kim, Y.K., White, S.R., "Cure-dependent viscoealstic residual stress analysis of filament-wound composite cylinders", Mechanics of Composite Materials and Structures 5 (1998), pp. 327-354.

[170] Zhao L.G., Warrior N.A., Long A.C., "A Micromechanical Study of Residual Stress and its Effect on Transverse Failure in Polymer-Matrix Composites", International Journal of Solids and Structures, 2005 in press.

[171] Eom Y., Boogh L., Michaud V., Sunderland P., Manson, J., "A Stress-initiated void formation during cure of a three-dimensionally constrained thermoset resin", Polymer Engineering and Science, March, 41 (2001), pp. 492-503.

[172] Chen Y, Xia Z., Ellyn F, "Evolution of Residual Stresses Induced during Curing Processing Using a Viscoelastic Micromechanical Model", Journal of Composite Materials, Vol. 35, No. 06 (2001).